DYNAMIC ROUTING WITH CROSS-LAYER ADAPTATIONS FOR MULTI-HOP WIRELESS NETWORKS

by

Amitangshu Pal

A dissertation submitted to the faculty of
The University of North Carolina at Charlotte
in partial fulfillment of the requirements
for the degree of Doctor of Philosophy in
Electrical Engineering

Charlotte

2013

Approved by:

Dr. Asis Nasipuri

Dr. Jiang (Linda) Xie

Dr. Yasin Raja

Dr. Yu Wang

Dr. Ehab Al-Shaer

ABSTRACT

AMITANGSHU PAL. Dynamic routing with cross-layer adaptations for multi-hop wireless networks.
(Under the direction of DR. ASIS NASIPURI)

In recent years there has been a proliferation of research on a number of wireless multi-hop networks that include mobile ad-hoc networks, wireless mesh networks, and wireless sensor networks (WSNs). Routing protocols in such networks are often required to meet design objectives that include a combination of factors such as throughput, delay, energy consumption, network lifetime etc. In addition, many modern wireless networks are equipped with multi-channel radios, where channel selection plays an important role in achieving the same design objectives. Consequently, addressing the routing problem together with *cross-layer* adaptations such as channel selection is an important issue in such networks. In this work, we study the joint routing and channel selection problem that spans two domains of wireless networks. The first is a cost-effective and scalable wireless-optical access networks which is a combination of high-capacity optical access and unethered wireless access. The joint routing and channel selection problem in this case is addressed under an anycasting paradigm. In addition, we address two other problems in the context of wireless-optical access networks. The first is on optimal gateway placement and network planning for serving a given set of users. And the second is the development of an analytical model to evaluate the performance of the IEEE 802.11 DCF in radio-over-fiber wireless LANs. The second domain involves resource constrained WSNs where we focus on route and channel selection for network lifetime maximization. Here, the problem is further exacerbated by distributed power control, that introduces additional design considerations. Both problems involve cross-layer adaptations that must be solved together with routing. Finally, we present an analytical model for lifetime calculation in multi-channel, asynchronous WSNs under optimal power control.

ACKNOWLEDGMENTS

During my PhD study, I have been helped, encouraged, and supported by many people whom I would like to acknowledge my deepest gratitude.

My sincere thanks to my adviser Professor Asis Nasipuri for his guidance, suggestions, and invaluable encouragement throughout the development of this dissertation. His creativity, insightful discussions, and passion for research provided a productive atmosphere for my work. Without him, I would not be where I am now. I consider myself a fortunate person to have him as my Ph.D. advisor. Not only as an independent researcher, but also as a socially mature person, I have learned a lot from him.

I am very grateful to my committee members: Dr. Linda Xie, Dr. Yu Wang, Dr. Yasin Raja and Dr. Ehab Al-Shaer for their time and advice. I owe special thanks to Dr. Aravind Kailas, Dr. Robert Cox and Dr. James Conrad for their suggestions and help at various phases of my PhD study. Also I would like to thank our Department Chair Dr. Ian Ferguson for his help and encouragement throughout my PhD.

I am very fortunate to have a close circle of friends from my undergraduate days: Khan, Sayan, Shibu, Avishek, Arghyadip and Dhrubo. Specifically thanks to Subhra, Kushal, Manisha, Bonee, Kushalda, Reshmidi, Chuku, Harish, Bhargavi, Sandeep, Rajib, Juma, Yi, Haopeng, Weiyi and many others who became good friends, and made life at Charlotte enjoyable for me. Special thanks to Yi Song, who always helped me as a friend during the course of my PhD. My sincere and deepest gratitude to Sarbani Madam for always being my well-wisher.

Last but not least, my family, relatives, and cousins. I would have had no chance to complete my studies without the love, support, and encouragement of my parents (Anil Kumar Pal and Basanti Pal), brothers (Anirban Pal and Angshuman Pal) and sister-in-laws (Pragna Roy and Sudipta Ghosh): acknowledging them is never enough. At the same time I am very grateful to my uncle (Nirapada Pal), aunt (Sima Pal) and

my cousins (Susmita Pal and Nabarun Pal) for their love and support. This work is *dedicated* to my beloved parents and family members who always gave me strength when I am down.

This research was sponsored in part by the NSF grant CNS-1117790 and the Electric Power Research Institute (EPRI).

TABLE OF CONTENTS

LIST OF TABLES

LIST OF FIGURES

LIST OF ABBREVIATIONS

WOBAN	wireless-optical broadband-access networks
ONU	optical network unit
OLT	optical line terminal
CO	central office
PON	passive optical network
NIC	network interface card
DCF	distributed coordination function
RoF	radio over fiber
MAC	medium access control
RAU	remote antenna unit
CAR	carrier access ratio
CSR	carrier sensing range
POS	probability of success
SNR	signal to noise ratio
RTS	request to send
CTS	clear to send
SINR	signal to interference and noise ratio
IDAR	interference and delay aware routing
GSQAR	gateway selection and quality aware routing
JRCA	joint routing and channel assignment
WSN	wireless sensor network
ETX	expected transmission count
DRCS	distributed routing and channel selection

CHAPTER 1: INTRODUCTION

The aim of this dissertation is to address a set of design challenges on adaptive routing in multi-hop wireless networks. Specifically, we explore design issues in which routing is associated with other distributed algorithms such as channel selection and power control in order to achieve a global performance objective. In the first part of this dissertation we focus on multi-channel wireless-optical access networks, where route and channel selection must be performed to achieve desired quality of service objectives. Access networks are the last mile of the communication networks that connects the telecom central office (CO) to the residential or business users. Optical (such as passive optical networks) and wireless networks (such as wireless mesh networks) are initially deployed as the access networks. Optical networks are mainly used for high-bandwidth and long distance communications, whereas wireless technologies are used for flexibility and low bandwidth uses. The tremendous growth of Internet users in recent past (shown in Figure 1.1) propels the necessity of modifying the Internet access architecture in a cost effective and efficient way to extend the reach of Internet. The present growing demands for bandwidth-intensive services and at the same time the flexibility (anytime-anywhere service) of the users are accelerating the research on efficient and cost-effective access infrastructures where optical-wireless combinations are seen as a promising approach. This new network architecture brought new research challenges, ranging from establishing the energy-efficient optical backbone, optical-wireless integration to efficiently using network resources to maximize the network traffic quality to meet the customers, using the low-bandwidth wireless multi-hop access networks. Our research focuses on developing different quality aware routing features mainly in the wireless access part of the *Wireless-Optical Broadband-*

Access Networks (WOBAN), along with exploring the channel assignment capabilities of multi-radio mesh routers as well as load balancing and traffic optimizations using the advantages of multiple gateways in a WOBAN.

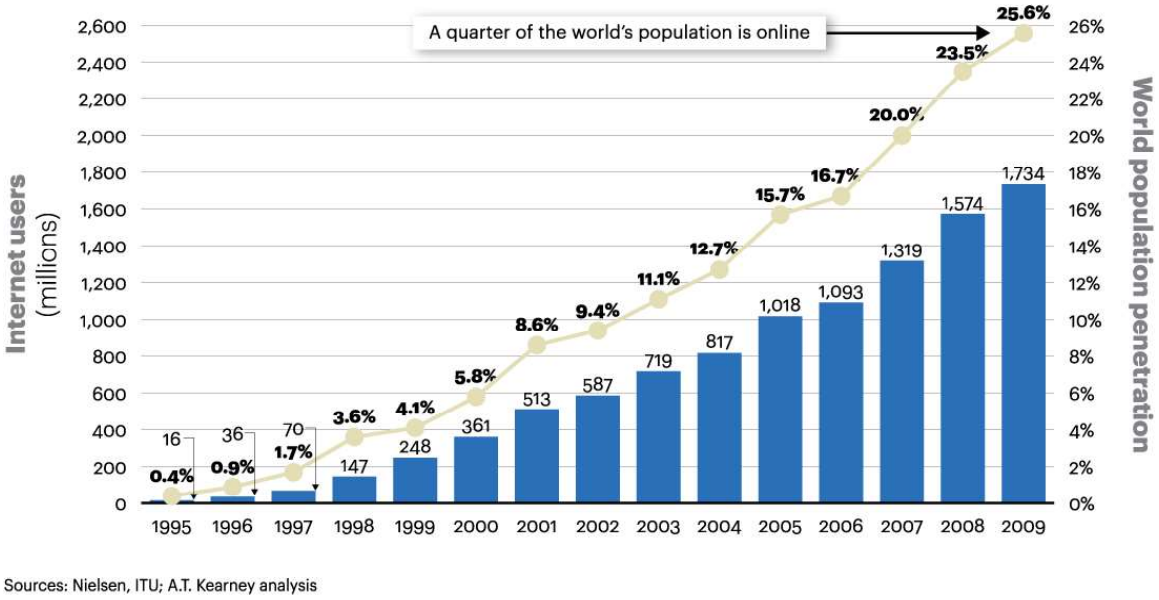

Figure 1.1: Global Internet users and penetration rate (1995-2009).

The second part of this dissertation is devoted to several design challenges for routing in wireless sensor networks (WSNs), where route selection is to be performed jointly with channel selection and/or transmission power level adaptation for energy management. In addition to energy conservation issues to maximize battery life, we also focus on design issues of rechargeable WSNs, which have emerged as an alternative to alleviate the problem of limited time operation of traditional battery-powered systems. Even if rechargeable WSNs enjoy energy scavenging from environmental resources, due to the high variation of spatial and temporal availability of these resources, achieving perpetual or long lasting network operation still remain challenging. To address these challenges, physical layer issues such as adaptive transmit power control or radio channel selection as well as route adaptation in network layer need to interact with one another, and so the cross-layer optimization is not only desirable, but also necessary. The key difference between the multi-channel WSNs and

multi-channel WOBAN lies in the fact that in WSNs, nodes typically has single radio that needs to switch between different channels; whereas nodes in wireless mesh of a WOBAN use multiple radios. At the same time the routing and channel assignment in a WOBAN tries to fulfill the primary objective of route quality enhancement to meet customers demands, whereas the adaptive features in WSNs are mainly towards lifetime enhancements, keeping the quality as the secondary concern.

1.1 Quality Aware Routing and Channel Assignment Problem in Multi-Channel Wireless Optical Access Networks

We explore new methods for improving the quality of communications in wireless optical broadband access networks (WOBAN), which is a novel hybrid access network paradigm with the combination of high-capacity optical backhaul and highly flexible wireless front-end that can provide higher bandwidth in a cost effective manner. In WOBAN architecture, optical fibers are provided as far as possible from the CO to the end users and then wireless access is provided in the front end. Because of it's excellent compromise, this WOBAN architecture reduces deployment costs because of lower fiber costs in comparison to traditional passive optical networks. To provide Internet access in a cost-effective and efficient manner, proper network planning and setup is essential. Especially the placement of the ONUs across the network plays an important role in determining the network performance. We address the ONU placement scheme and propose a clustering technique [2] to distribute the ONUs across the network, given the distribution of wireless mesh routers. As the same time the fiber layout schemes to connect the ONUs and the OLT is important to make the network setup cost-effective. This dissertation addresses different fiber-layout schemes as well as their cost comparison.

A WOBAN consists of a passive optical networks (PON) at the back end and a multi-hop wireless mesh networks at the front end as shown in Figure 1.2. At the back end, optical line terminal (OLT) resides in the CO and feed to multiple optical

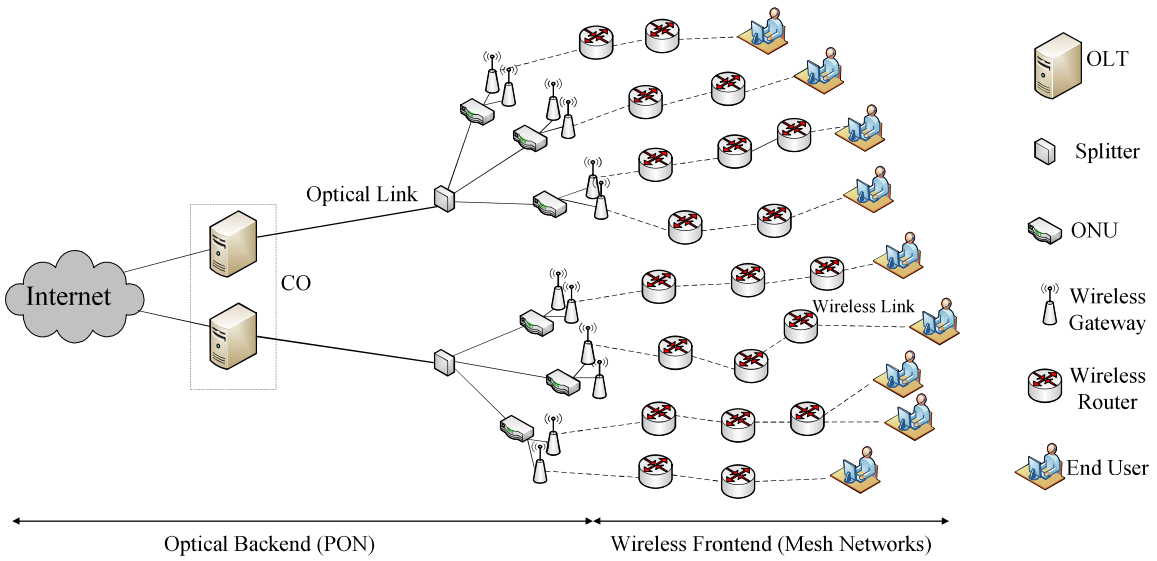

Figure 1.2: A typical WOBAN architecture.

network units (ONUs) through a traditional fiber network. At the front end, wireless mesh routers form a multi-hop wireless mesh network; and a few of the mesh routers are called gateways that are attached to the ONUs. Thus if a mesh router needs to send a packet to the Internet, it has to send it to any one of the gateways and after that the packet is sent through the optical part of the WOBAN. In the upstream direction (from wireless routers to gateways), WOBAN is an *anycast* network. In the downstream (from gateway to mesh router), a gateway send a packet to a specific wireless router, thus in downstream, WOBAN is a *unicast* network. Our interest in this dissertation is to develop routing protocols in the upstream direction. We first develop an *interference and delay aware routing protocol (IDAR)* [3], [4] for single gateway WOBAN. Since interference is a key factor that affects data transmissions in multi-hop wireless networks, there is a need for investigating mechanisms by which routing decisions are based on interference considerations in addition to the path length, which is often the primary factor considered for routing in dynamic multi-hop wireless networks. The proposed scheme IDAR tries to optimize the end-to-end POS and delay in all active routes in the network by using a novel quality based routing

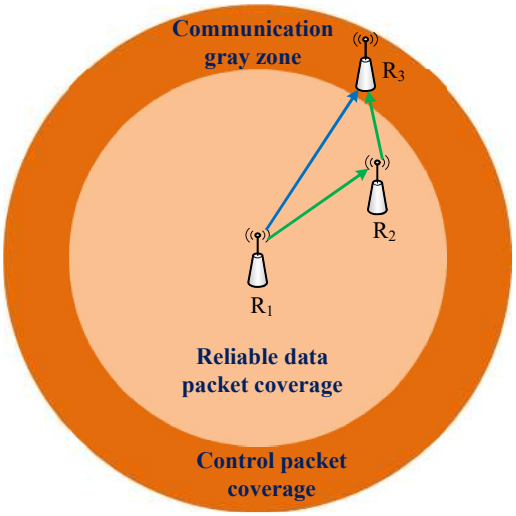

Figure 1.3: Communication Gray Zone problem in wireless networks.

metric. Although a lot of work has been reported on quality based routing for multi-hop wireless networks, most existing approaches rely on the usage of control packets to estimate the route quality. But control (broadcast) packets differ from actual data packets as they are smaller in size and are sent at a lower transmission rate than data packets. Consequently, the data transmission performance using routing protocols that estimate route quality from control packets only may be poorer than expected. This phenomenon, known as *communication gray zone* problem [5] is depicted in Figure 1.3 where the link between R_1 and R_3 is considered as a reliable link based on control packet transmissions, but unreliable for data packet transmissions. Thus while transmitting data packets, R_1 may need to hop through R_2 to reach R_3. To avoid this problem, we propose a scheme that tries to obtain the *predicted route quality* by applying interference models that are obtained using offline measurements of actual *data packet transmissions*. The proposed quality based routing protocol uses control packets to determine relevant parameters of candidate routes, such as hop count and node IDs, which are utilized by the routing metric to provide accurate estimates of the route quality. It is assumed that all communication requests are directed towards the gateway, which serves as the centralized manager for all routing decisions based

on global knowledge of node locations and activities.

To avoid the network *bottleneck* on a single gateway, we extend routing scheme for multiple gateways, named *gateway selection and quality aware routing protocol (GSQAR)* [6], [7]. Multi-gateway WOBANs with anycast routing has several features that can be utilized for improving the quality of service of wireless connections. Firstly, multiple gateways provide redundancy, which help in reducing congestion on any single gateway. In addition, the possibility for cooperative selection of gateways for all active users and their corresponding routes enables better utilization of resources in the network. However, this leads to a joint gateway selection and routing problem, which is computationally hard. In addition, the network parameters may vary with time, which increases the complexity of the problem. We consider a centralized approach to address this issue, where the gateways collaborate with each others through the optical backbone, and collaborate with each other for determining the optimum gateway and route selections for all active nodes in the network.

The co-channel interference is the main factor that reduces the network throughput in the wireless networks. To cope for this, the IEEE 802.11 standards provide multiple overlapping frequency channels to support multiple simultaneous transmissions in the same interference region. For example, IEEE 802.11b/g offers 3 non-overlapping channels, while IEEE 802.11a offers 12 non-overlapping channels. By exploring the advantage of multiple channels and multiple radios, the system performance of the mesh networks can be improved significantly compared to the single-channel wireless access networks. However, all these benefits can only be achieved by applying a carefully designed channel assignment scheme so as to utilize these multiple channels and radios effectively.

In addition to effective channel assignment and management of usage of radios or network interface cards (NICs) at the nodes, a key factor that determines the end-to-end communication quality in wireless mesh networks is the routing protocol. Due to

the fact that co-channel interference at a node is determined by the assignments of channels to the neighboring nodes as well as their traffic pattern, an ideal approach for this problem is to consider both channel assignment and routing simultaneously. Thus, we develop a centralized *joint routing and channel assignment (JRCA)* [8] protocol, that includes multiple channels on top of our anycast quality based routing model.

In the context of WOBAN, we analyze the performance of the IEEE 802.11 DCF in RoF networks using an analytical model. We consider non-saturated traffic conditions for both the basic and the optional RTS/CTS access mechanisms. In wireless networks, a packet transmission is affected by two types of nodes around the sender and the receiver. The first ones are contending nodes, i.e. nodes contending to gain access to the channel at the same time as the source node. The second ones are the hidden terminals, which might disrupt the reception of a packet if they commence transmission at any time during the receiver's vulnerable period. To accurate capture the network parameters, the effects of both contending and hidden terminals need to be considered. We also assume the effects of large buffer sizes, to capture the accurate computation of the total packet delay (MAC plus queuing delay). This mathematical model is validated using simulations.

1.2 Dynamic Routing, Channel Selection and Power Control Schemes for WSNs

Development of new approaches for optimizing energy usage is a key issue for achieving reliable and long-term operation of wireless sensor networks (WSNs). Since batteries are hard to replenish, energy optimization is a critical design requirement for all protocols and algorithms for WSNs. Much of the work on energy optimization in WSNs are focused on development of methods for minimizing the number of radio transmissions and/or receptions, which is the largest contributor to energy usage in sensor nodes. The complexity of this energy optimization problem in sensor networks arises due to the fact that it has to be addressed by *network wide* adaptations as

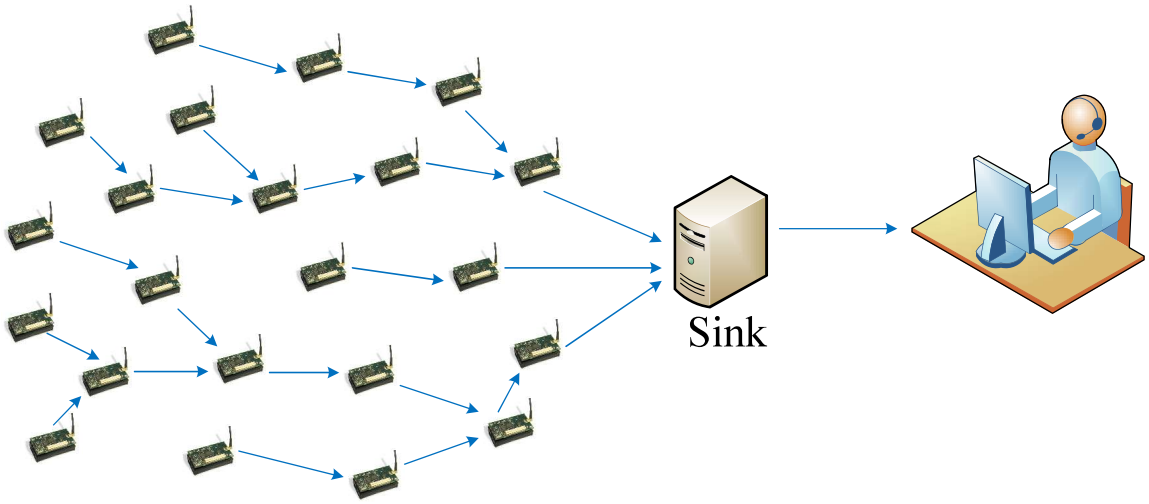

Figure 1.4: A typical data collection WSN.

opposed to independent adaptations at the nodes.

We consider large-scale WSNs for data collection applications (shown in Figure 1.4), where implementation of network-wide time synchronization is a significant challenge. Hence, it is difficult to apply synchronized duty cycling and scheduled transmissions in such networks, which are critical for avoiding energy wastage from *overhearing*. In this work, we propose the use of multiple orthogonal channels to alleviate the overhearing problem and thereby improve the network lifetime. Current WSN platforms such as MICAz and Telos that use CC2420 radio can operate on multiple channels, which are traditionally used to address interference problems. On the contrary, we propose quality and battery-health aware routing and channel selection schemes that dynamically choose channels and routes to optimize network lifetime and performance. We propose two types of channel selection schemes. The first one is known as *flow based channel assignment* [9], where all nodes on a flow have the same channel. Even if this scheme reduces overhearing throughout the network, it does not consider dynamic channel selection with respect to the *varying energy resources* of the individual resources. To achieve this, we propose another type of channel selection scheme, know as *receiver based channel assignment* [10], [11] with the objective

of dynamically equalizing the remaining lifetimes of nodes as estimated from their current battery capacity and usage. An analytical model of compare the network lifetime using these two types of channel assignment schemes is also developed and discussed [12].

In addition to multi-channel routing, another way to reduce overhearing and thus increasing network lifetime is transmission power control. In the recent past, a significant amount of efforts have been devoted towards using harvesting energy from different renewable sources which includes sunlight, wind, vibrations, heat etc. Due to the high degree of spatial and temporal variations of these energy sources, some nodes receive sufficient renewable energy to sustain their normal operations, whereas some nodes that are placed in challenged regions (such as under shadow in case of sunlight) suffer from quick battery drainage and ultimately form network partitioning. To prolong the operation of these challenged nodes, we develop a *power control and routing scheme (PCOR)* [13], [14] that performs quality aware route selection while reducing the energy consumption in sensor nodes that have low remaining battery life through cooperative and network-wide adaptations of transmit power levels and parent selection. Performance evaluations are presented from extensive simulation studies as well as from an experimental testbed.

In addition to these, we also present a theoretical model for lifetime calculation in asynchronous sensor networks under optimal power control. This is derived under a node energy consumption model that assumes asynchronous sleep and wake cycle and a data collection tree structure. This model is then extended further to consider multi-channel operation where nodes are assumed to dynamically select channels with optimal power control to balance the nodes remaining lifetimes. Figure1.5 shows the overview of the proposed schemes discussed in this dissertation.

1.3 Organization

The rest of the dissertation is organized as follows.

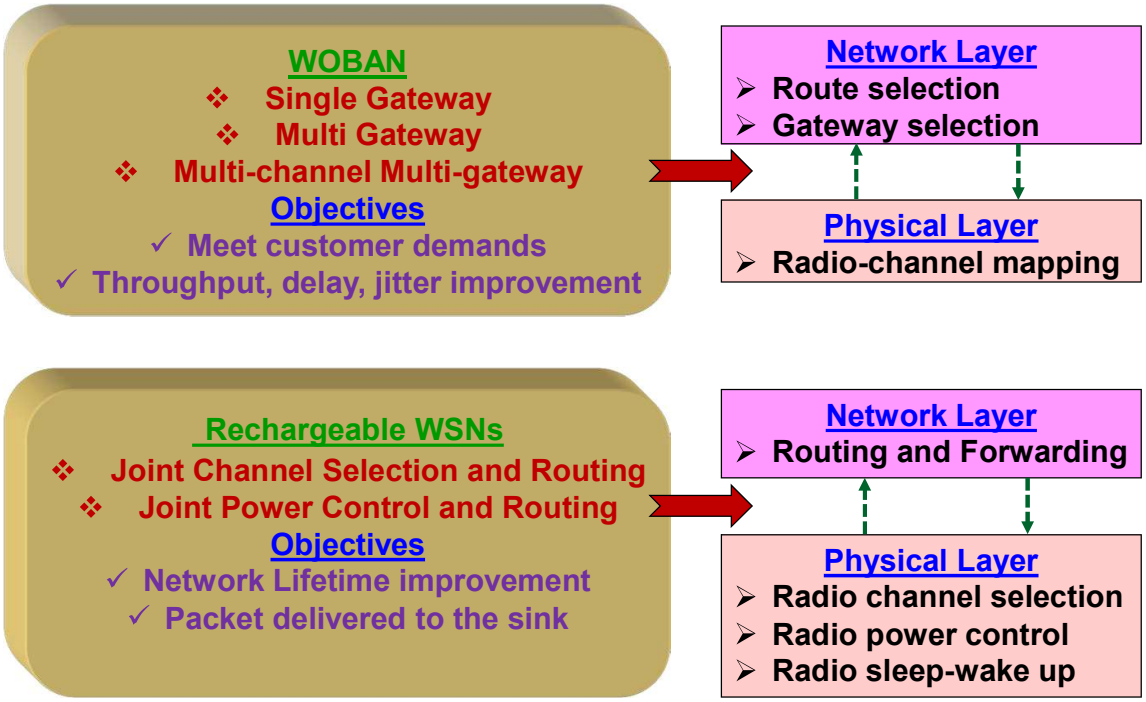

Figure 1.5: The overview of the proposed routing schemes with different cross-layer optimizations.

1. Chapter 2 describes a brief description of WOBAN architecture and the benefits of WOBAN compared to PON and wireless mesh networks. We also discuss a detailed survey of different quality aware routing and channel assignment schemes in wireless mesh networks.
2. Chapter 3 describes the planning and setup of an WOBAN. In this chapter, we address the problem ONU placement in a WOBAN. Different fiber layout schemes are also discussed in this chapter.
3. In Chapter 4, we propose a quality aware routing IDAR for single-gateway WOBAN. Here we also describe our quality metric that consists of end-to-end probability of success and delay of a transmitted packet.
4. Chapter 5 describes a quality aware anycast routing protocol named GSQAR for multi-gateway WOBAN. The optimal gateway selection problem is turned out to be a NP-hard problem, so we propose two heuristics to solve this problem.
5. In Chapter 6, we describe a joint routing and channel selection scheme JRCA

for multi-gateway multi-channel WOBAN. We present a novel backtracking and genetic algorithm based channel assignment and quality aware route selection scheme to maximize the overall performance of communications while reducing the computational complexity.

6. In Chapter 7, we present an analytical model to evaluate the performance of the IEEE 802.11 Distributed Coordination Function (DCF) in radio-over-fiber (RoF) wireless LANs. The model captures the effects of contending nodes as well as hidden terminals under non-saturated traffic conditions assuming large buffer sizes. The effect of fiber propagation delay is also considered.
7. Chapter 8 discusses the motivation for developing our distributed, multi-channel selection schemes for WSNs. A survey of related literature is also discussed.
8. Chapter 9 addresses a number of flow-based channel assignment schemes for multi-channel sensor networks for overhearing minimization. Performance evaluations form simulations are also presented to compare different proposed channel assignment schemes.
9. In Chapter 10, we propose a distributed receiver based multi-channel routing scheme for WSNs for lifetime maximization. The proposed scheme achieves lifetime improvement by reducing the energy consumed by overhearing and also by dynamically balancing the lifetimes of nodes.
10. Chapter 11 proposes a distributed and cooperative power control and routing scheme for rechargeable WSNs that achieves lifetime improvement by reducing transmission power of the nodes that are neighbors to the challenged nodes, which effectively reduces overhearing on those nodes. Extensive simulations as well as experimental evaluations are also discussed in this chapter.
11. Chapter 12 describes a mathematical model to calculate the network lifetime with dynamic channel selection and power control for reducing the effect of overhearing in asynchronous wireless sensor networks.
12. Conclusions and future works are presented in Chapter 13.

CHAPTER 2: SYSTEM OVERVIEW AND RESEARCH DIRECTIONS IN WOBAN

2.1 Current Trends in Access Networks

The current access networks are broadly divided into high-bandwidth optical access networks and wireless access networks. The dominant broadband optical access technology is *Passive Optical Network (PON)* (shown in Figure 2.1). A PON connects the telecom central office (CO) to businesses and residential users by using one wavelength channel in the downstream direction [from Optical Line Terminal (OLT) at CO to Optical Network Units (ONU)], and another wavelength channel in the upstream direction [from ONUs to OLT]. The PON interior elements are basically passive combiners, couplers and splitters. Since no active elements exist between the OLTs and the ONUs, PONs are robust networks that are cost and power efficient as well. In single wavelength PONs, the number of ONUs are limited 16 ONUs at a maximum distance of 20 km from the OLT and 32 ONUs at a maximum distance of 10 km. To increase the network bandwidth, some upgraded versions of PON architectures, such as Ethernet PON (EPON), Gigabit PON (GPON)1, Broadband PON (BPON) are proposed in the literature that support multiple wavelengths over the same fiber infrastructure. The main idea behind WDM-PON is to increase the bandwidth by employing WDM multiplexing, such as multiple wavelengths are supported in both upstream and downstream directions of the access network.

On the other hand the promising technologies for wireless access networks are WiFi and WiMAX. WiFi (standard: IEEE 802.11) technology is mainly used in local-area networks and offers low bit rate (max 54/11/54 Mbps for 802.11a/b/g respectively) and limited range (typically 100 meters) communications. WiMAX (standard: IEEE 802.16) is particularly suitable for wireless metropolitan-area networks (WMAN),

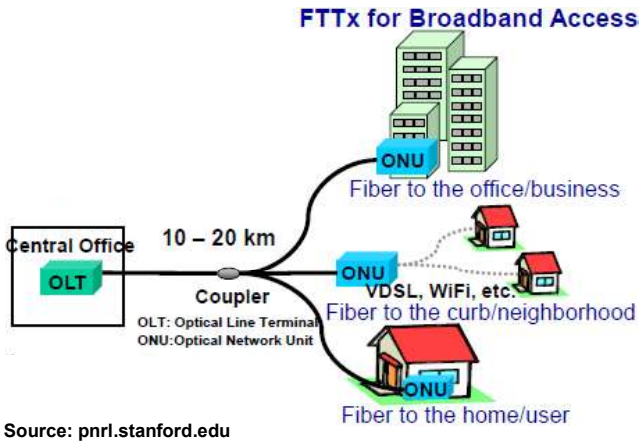

Figure 2.1: A PON architecture for optical access.

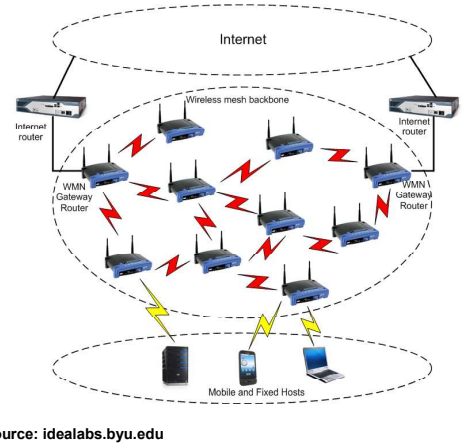

Figure 2.2: A typical wireless mesh network for wireless access.

because of its offers high bit rate and long range communications. WiMAX supports data rates upto 75 Mbps in a range of 3-5 km, and typically 20-30 Mbps over longer ranges. Popular use of wireless access networks is in wireless mesh newtorks (shown in Figure 2.2), where the mesh routers forwards their traffic to the gateway using multi-hop communications. The WOBAN architecture, described in the next section, is a good compromise between the high-bandwidth optical access and unethered wireless access networks to extend the reach of Internet in a cost-effective and efficient manner.

2.2 WOBAN Architecture and the Motivation Behind WOBAN

A WOBAN consists of a multi-hop multi-radio wireless mesh network at the front end and an optical access network at the back end that provides connection to the Internet. At the back end the dominant technology is the passive optical network (PON) having optical line terminals (OLTs) located at the CO and optical network units (ONUs) that are connected to the wireless gateways routers.

In the wireless infrastructure, standard WiFi and WiMAX technology can be used for wireless mesh networks. The subscribers, i.e. the end-users (also known as mesh clients) send packets to their neighborhood mesh routers. The mesh routers inject packets to the wireless mesh of the WOBAN. The mesh routers can reach any of the

gateways/ONUs through multi-hop routing. Thus in the upstream direction(mesh routers to ONUs), it involves anycast routing and in the downstream direction (ONUs to mesh routers), it requires unicast routing as traffic is sent from an ONU to a particular mesh router. The gateways/ONUs can be strategically placed over a geographic region to better serve the wireless users. Based on these, a generalized model for the WOBAN architecture is depicted in Figure 2.3.

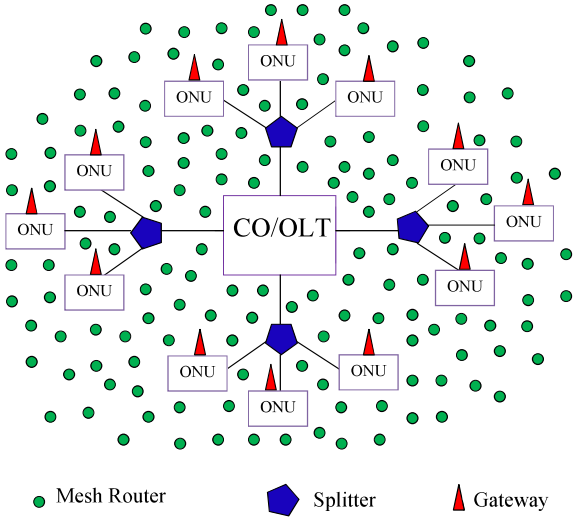

Figure 2.3: Architecture of a WOBAN.

The advantages of using a WOBAN as opposed to a purely optical network infrastructure can be summarized as follows:

- A WOBAN can be very cost efficient as compared to PON since a WOBAN does not require fibers to be deployed up to every subscriber's homes, premises or offices.
- The wireless mesh architecture provides more flexible wireless access to the users compared to optical access networks. It is often difficult to deploy optical fibers and equipments in highly populated areas as well as in rugged environments. In these environments the wireless front-end can provide easy coverage and connectivity in a cost-effective manner.
- The self-healing nature of the wireless front end makes WOBAN more robust

and fault tolerant than traditional PON. In traditional PON, a fiber cut between the splitter and an ONU or between the splitter and the OLT makes some or all of the ONUs disconnected from OLT. In WOBAN, the traffic disrupted by any failure or fiber cut can still be forwarded through the mesh routers using multi-hop routing to other ONUs and then to the OLT.

- WOBAN enjoys the advantages of anycast routing. If one gateway is congested, a wireless router can route it's traffic through other gateways. This reduces load and congestion on one gateway and gives WOBAN a better load-balancing capability.
- WOBAN has much higher bandwidth capacity compared to the low capacity wireless networks, which reduces the traffic congestion, packet loss rate as well as end-to-end packet delay.

2.3 Overview of Research on WOBAN

Proper network planning is important for optimizing both network performance as well as deployment cost, which has received considerable attention in published literature. Other than network planning, the key challenge is to design network protocols for achieving adequate quality of service, in terms of throughput and delay, in the wireless domain of the WOBAN. The system model considers that the wireless access network is a mesh network comprising of a fixed set of wireless mesh nodes or routers, which employ multihop routing to convey wireless data packets between user stations to ONUs. Since communication is assumed to be between mobile stations and an external destination that can be reached through any ONU using the optical backbone, this involves *quality aware anycast* routing between each user and any ONU. In addition, to improve throughput performance, wireless mesh networks have been considered to use multi-channel radios, usually employing multiple network interface cards (NICs). Optimizing the performance of multi-channel mesh networks involves optimum channel selection at the mesh nodes, which is coupled with the rout-

ing problem. As this dissertation captures a number of dimensions of routing and channel assignment problems, we classify the related works in following categories: routing metrics and quality based routing schemes, anycast based routing schemes and channel assignment schemes along with the planning and setup strategies of an WOBAN.

2.3.1 Network Planning and Deployment

Much of the work on network planning has been directed towards development of optimal placement of ONUs across an WOBAN to optimize a performance metric. In [15], the authors propose a greedy algorithm where a number of predefined points are considered as initial candidates to place the ONUs. Then each user identifies the primary ONU which is the closest and then the locations of the primary ONUs are calculated as the center of the users. An improvement of this greedy algorithm by using *simulated annealing* and *hill climbing* is described in [16]. In [17], the authors propose a *mixed-integer-programming* approach to solve the problem of ONU placement.

2.3.2 Routing Metrics and Quality Based Routing

A review of research on the development of different routing metrics for QoS guarantees in mesh networks can be summarized as follows.

2.3.2.1 Routing Metrics

A number of routing metrics have been proposed for achieving quality based routing in wireless mesh networks. In [18] the authors propose a metric named *expected transmission count (ETX)* that uses the expected number of transmissions a node requires to successfully transmit a packet to a neighbor. The *minimum loss (ML)* metric proposed in [19] computes the delivery ratio with the objective of choosing the route with the lowest end-to-end loss probability. The *expected transmission time (ETT)* metric proposed in [18] is based on the time a data packet requires to be transmitted successfully to each neighbor. In [20], the *modified ETX (mETX)*

metric is proposed that computes the bit error probability using the position of the corrupted bit in the probe and the dependence of these bit errors throughout successive transmissions. The *interference aware (iAWARE)* metric in [21] uses *signal to noise ratio (SNR)* and *signal to interference and noise ratio (SINR)* to continuously reproduce neighboring interference variations onto routing metrics.

2.3.2.2 Interference Aware Routing

Several routing protocols have been proposed that try to improve *QoS* by estimating parameters related to wireless interference. In [22], the authors propose an interference aware *QoS* routing protocol MARIA, where nodes involved in a route discovery estimate the residual bandwidth in its neighborhood and forwards the information over the route request packet (RREQ). MARIA uses conflict graphs to characterize interference. The destination selects the route based on the highest minimum residual bandwidth, i.e. the least interference. An algorithm that chooses the route that has minimum commitment period of the bottleneck node is presented in [23]. Commitment period is defined as the sum of the time the node spends in transmission/reception and the time a node has to reserve to be idle for enabling the flow of interfering traffic. Thus reducing the commitment period results in reduced interference. In the *DARE* protocol [24], all nodes in a path reserve time slots for flows and all nodes near the reserved path abstain from transmissions during the reserved time slots, thus minimizing the possibility of interference. In [25], the authors propose an algorithm where each mesh router periodically measures the *RSSI*, average *SINR*, average number of transmission rounds, average residual block error rate and the actual spectral efficiency of the transport channel. For any path, the algorithm uses this information to meet minimum tolerable levels of a set of metrics.

2.3.2.3 Other Approaches for QOS Routing

Other approaches to *QoS* routing have also been proposed. In [26], a *Genetic Algorithm (GA)* for *QoS* multicast routing has been defined. Every route has to

guarantee the bandwidth and delay requirements. Among all the routes satisfying the *QoS* requirements, the algorithm chooses the route that has the minimum hop count. *QUORUM* [27] uses reactive route discovery and reservation based *QoS* provisioning. It estimates route robustness by counting the frequent *HELLO* packets that are received during a given time. It makes an estimation of end-to-end delay by sending *DUMMY-RREP* packets, which have the same size, priority and data rate as the actual data packets. This helps in emulating real data traffic on a data path. The source selects the route for which the average delay of the *DUMMY* packets is within acceptable bounds and starts transmitting data traffic. *Wireless Mesh Routing (WMR)* [28] uses a novel bandwidth estimation algorithm where the required bandwidth and delay constraints are embedded in the route discovery message by the source. This information is used by nodes propagating the route discovery packets to help in determining the shortest-path route to mesh router. In [29], the authors propose an *Integrated Qos Routing (IQoSR)* procedure, where each intermediate node averages previous one-hop delay, link throughput and packet error rate measurements and piggybacks these information in the request packet. After getting the reply from destination, the source chooses the best route by calculating the integrated *QoS* performance metric. In [30], the authors propose and investigate the characteristics of *Delay-Aware Routing Algorithm (DARA)* that minimizes the average packet delay in the wireless front end of a *WOBAN*. A *Capacity and Delay Aware Routing (CaDAR)* is proposed in [31] that routes packets in wireless mesh to reduce the average packet delay using optimal capacity assignment on the links.

2.3.3 Anycasting Based Routing

In [32], the authors propose a *multi-gateway wireless mesh network routing protocol (MAMSR)* based on the *Dynamic source routing (DSR)* protocol. The routing metric used in *MAMSR* is hop count, where gateway and route selection is performed on the basis of the first RREP packet received by the source. A hybrid anycast routing

is proposed in [33] where the network is divided into two regions: proactive and reactive. Nodes that are very close to any gateway are in the proactive region and send packets to this gateway only. Nodes that are not in the proactive region are part of the reactive region; these nodes choose gateways that carry minimum load. Another multi-gateway association scheme is proposed in [34], where the shortest paths from any node to each gateway and the available bandwidth in all the paths are computed. The path that has the largest available bandwidth is selected in a greedy manner. In [35], the authors propose a scheme where each source keeps track of its nearest gateway as the primary and other gateways as secondary gateways. All nodes generally send traffic to their primary gateways. If the primary gateway is congested, sources with high traffic are notified by the gateway to switch their traffic to some other gateways.

2.3.4 Channel Assignment Schemes for wireless-optical access networks

Prior work on channel assignment schemes can be broadly classified into three categories: static assignment, dynamic assignment and hybrid assignment.

2.3.4.1 Static Channel Assignment

Static assignment strategies assign a channel to each interface for permanent use. In [36], the authors formulate the channel assignment problem as a topology control problem. They develop a greedy algorithm that minimizes the maximum link conflict weight and simultaneously preserves the connectivity of the connectivity graph. Another tabu search based centralized scheme is proposed in [37]. In [38], the authors propose two algorithms that also use the link conflict graph to model interference. The first algorithm minimizes the average link conflict weight, while the second minimizes the maximum link conflict weight. Both algorithms are based on an approximation algorithm for the *MAX k-CUT problem*. Authors in [39] propose two integer linear-programming models. The objective is to maximize the number of simultaneous transmissions in the network, subject to connectivity restrictions. In [40], the au-

thors present a multi-commodity network flow model used to find an upper bound of the achievable throughput for a given set of flows. In [41], the authors propose a *joint radio and channel assignment scheme (JRCA)* that first uses a maximum flow based centralized channel assignment to obtain an initial assignment of channel. Then the residual demand, i.e. actual link demand minus the allocated demand is calculated for each link. Finally, the links are visited in decreasing order of residual demands and the least used channels are assigned one by one.

2.3.4.2 Dynamic Channel Assignment

Dynamic protocols enforce nodes to switch their interfaces dynamically from one channel to another between successive data transmission. In [42] a centralized architecture for channel assignment and routing is presented. Given the node placement and the traffic load between each pair of nodes, the channel assignment algorithm binds each interface to a channel such that the available bandwidth on each link is proportional to its expected load. If the loads change over time, the algorithm can perform channel reassignments. In [43] a distributed architecture for routing and channel assignment is discussed. In this scheme, when a node finds a channel with a lower usage, it can perform a reassignment to that channel. A genetic algorithm based channel assignment scheme is proposed in [44] where a central unit invokes the genetic algorithm based channel selection procedure periodically and sent back that assignment to the mesh routers. In [45], the authors model the traffic flows among the mesh routers as linear programming problem, targeting to find the fair flow of each mesh router. Based on the fair flows, a weighted flow-based conflict graph is constructed and then channels are assigned to each vertex of the conflict graph based on vertex coloring scheme. The channels are reassigned after a certain time period because of the change in traffic demands.

2.3.4.3 Hybrid Channel Assignment

Another set of strategies [46], [47] known as hybrid approaches apply a static or semi-dynamic assignment to the fixed interfaces and a dynamic assignment to the switching interfaces. In [46], the authors present a scheme where at least one interface of the receiver is assigned to a channel statically or semi-dynamically, while interfaces of the senders are dynamically switched to one of the assigned channel of the receiver. In [47], the authors propose a scheme where one radio on each mesh router operates on a *default channel* to preserve network connectivity. The authors introduce the concept of *multi-radio conflict graph* and then use a *breadth-first search* from the gateway to assign channel such that the interference is minimized.

In the context of WOBAN, our research addresses three major problems. First, we address the network planning of a WOBAN from the perspective of optimum ONU placement for serving a given set of users that are characterized by fixed locations of wireless mesh routers. We develop a clustering scheme for placement of the ONUs across the network in Chapter 3. Different fiber layout schemes to connect ONUs and the OLT is also discussed in this chapter.

Second, we address the routing and channel selection problem in the wireless mesh network for a given set of ONUs and wireless mesh routers, and their locations. We address this problem by first developing a route quality metric that takes into account wireless interference and channel contention. This is first applied to an interference and delay aware routing protocol for a WOBAN operating on a single channel and a single gateway/ONU. The effectiveness of the proposed quality aware routing metric is demonstrated through extensive simulation experiments in this specified WOBAN framework in Chapter 4. Next, we address the anycasting problem by considering a single channel WOBAN with multiple gateways. We propose two gateway selection and quality aware routing protocols that tries to optimize wireless interference using route and gateway selection. This is presented in Chapter 5. Finally, we consider the

scenario of a WOBAN with multiple gateways where the wireless mesh routers are equipped with multi-channel radios with multiple NICs. The multi-channel scheme proposed in this dissertation falls in the hybrid category, where we assume a dedicated control channel on which all nodes assign a NIC. This is the *default channel* which is mainly used to send request and reply packets. Other interfaces are switched between different data channels for data transmission. We explore the problem of *joint routing and channel assignment* scheme in this type of WOBAN architecture, that significantly reduces the co-channel interference and channel contention. This is presented in Chapter 6.

Third, we address the performance modelling of the IEEE 802.11 Distributed Coordination Function (DCF) in radio-over-fiber (RoF) wireless LANs. The model captures the effects of contending nodes as well as hidden terminals under non-saturated traffic conditions assuming large buffer sizes. Comprehensive performance evaluations of RoF networks obtained from the proposed model as well as simulations are presented in Chapter 7.

CHAPTER 3: NETWORK PLANNING AND SETUP FOR WOBAN

This chapter is devoted to the issue of network planning and deployment of a WOBAN. The approach to network deployment should capture the design interplay between various aspects, ranging from the *optical network unit (ONU)* placement across the network, their effects for various network performance to different fiber layout schemes as well as their cost comparison. In a WOBAN, the ONUs modulate the upstream data that are received from the wireless mesh routers to optical signals and transmit them to the optical line terminal (OLT). In the downstream direction, the optical signal is demodulated into wireless and transmitted to the mesh routers. Due to the broadcast nature of the wireless transmission, the network throughput of a WOBAN in the upstream direction is limited by wireless interference. Wireless interference can be minimized by selecting appropriate quality aware routing [3], [6], [4], [7] as well as effective channel assignment schemes [8]. Besides channel selection and routing, the placement of ONUs [15], [16], [17] in the network plays an important role in determining the performance of the network. In practice, the placements of wireless access points and routers are dictated by the need, as determined by the density and usage patterns of users in different regions of a deployment area. Here, we consider the problem of optimizing the placement of ONUs to serve a fixed set of mesh routers to minimize a performance cost metric. Developing a proper ONU placement scheme is important as it is hard to move the ONUs and connected fibers after deployment. While planning for a network setup, the network architects need to know the peak demands of the customers in a geographic area. A typical example is an academic campus (shown in Fig 3.1), where office buildings, living areas and lobby areas will be crowded by users for getting Internet access. The ONU

placement scheme needs to be developed based on the peak demands and the known distribution of corresponding mesh routers to meet the demands. To achieve this, we propose a *cluster-based* scheme for ONU placement where ONUs are the cluster-heads and performance cost depends on the average distance between the mesh routers and their corresponding ONUs. Extensive simulations are conducted to evaluate the performance of the proposed clustering scheme in comparison with uniform-random ONU placement.

A key aspect of designing a WOBAN includes fiber deployment from OLT to the ONUs to form the optical backend. The planning for fiber deployment depends on the *passive optical networks* (PON) architecture, which can be based on a tree or ring topology. We also compare schemes for laying out fiber for tree and ring PON topologies and evaluate their cost comparison.

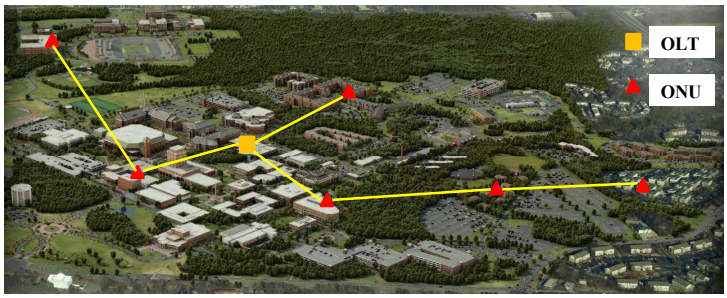

Figure 3.1: A hypothetical example of a WOBAN architecture in a campus network (UNC Charlotte campus).

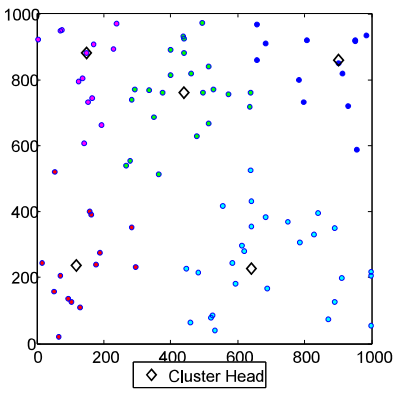

Figure 3.2: The placement of ONUs in a random distribution of mesh routers.

3.1 ONU Placement Scheme

Our objective is to place the ONUs in a geographic area (such as in a college campus or in a residential area) with the assumption that the location of the wireless mesh routers $(MR_1, MR_2, ..., MR_V)$ are known. Let us assume that the locations of the ONUs are given by (X_i, Y_i), $i \in (1, 2, ..., U)$, and the locations of all the routers are

given by (x_j, y_j), $j \in (1, 2, ..., V)$. We develop a clustering scheme for ONU placement which is described as follows.

The ONU placement problem is to divide the network into U clusters and place the ONUs in the centroid of the cluster routers so that the distance between each ONU and its corresponding routers is minimized. This problem is basically same as *minimum sum-of-squares clustering (MSSC) problem.* The MSSC problem is to partition a given set of n entities into k clusters in order to minimize the sum of squared distances from the entities to the centroid of their clusters. A mathematical programming formulation of MSSC is as follows:

$$Minimize \sum_{i=1}^{V} \sum_{j=1}^{U} w_{ij}\{(X_i - x_j)^2 + (Y_i - y_j)^2\} \tag{3.1}$$

subject to

$$\sum_{j=1}^{U} w_{ij} = 1 (1 \leq i \leq V) \tag{3.2}$$

$$w_{ij} = 0 \text{ or } 1 \ (1 \leq i \leq V) \ (1 \leq j \leq U) \tag{3.3}$$

where w_{ij} is a binary variable which is 1 if ONU_i is assigned to cluster j and 0 otherwise. The MSSC problem is shown to be a *NP-hard* problem in [48]. A number of approximation algorithms for MSSC are reported in [49]. Here, we propose a heuristic to solve this problem.

★ Proposed clustering scheme for ONU Placement: In this section we discuss our propose clustering scheme for ONU placement. First, we need to find how many ONUs are required to satisfy the demands of all users. If the peak demand of the whole network is D and each ONU can serve a demand of d then the number of ONU required is $U = \frac{D}{d}$. Now, we propose a greedy algorithm to place these U ONUs. We describe this with the help of Figure 3.2. In Figure 3.2, there are $V = 100$ routers

and $U = 5$ ONUs. Our idea of choosing ONU locations is mainly based on *k-means clustering* technique. At first, an initial set of U locations are generate randomly, these points are denoted by $m_1^{(1)}, m_2^{(1)}, ..., m_U^{(1)}$ (the superscripts (1) corresponds to initial position). The algorithm consists of two steps:

- Assignment phase: In this phase, the routers are assigned to their closest ONUs, i.e. an ONU and its corresponding routers are in one cluster (this is basically partition the routers according to the *Voronoi diagram* generated by the ONUs. Mathematically, if a router V_j (the position of V_j is denoted by vector x_j) is in cluster $S_i^{(t)}$ in the t-th iteration then

$$S_i^{(t)} = \{x_j : \|x_j - m_i^{(t)}\| \leq \|x_j - m_{i^*}^{(t)}\| \quad \forall i^* = 1, 2, ..., U\} \tag{3.4}$$

- Update phase: In this stage, the new ONU position of cluster i are calculated by taking the mean of all the router-positions, i.e.

$$m_i^{(t+1)} = \frac{1}{|S_i^{(t)}|} \sum_{x_j \in S_i^{(t)}} x_j \tag{3.5}$$

  The *Assignment* and *Update* phase is repeated until the solution converged, i.e. the coordinates of the ONUs no longer change.

  The algorithm is repeated a large number of times with different random ONU positions and the best solution is taken at last. A pseudocode is shown in Algorithm 1.

★ Fiber deployment from OLT to the ONUs: After the positions of the ONUs are identified, the OLT and the ONUs need to be connected using optical fiber. Depending on the network planning, in the optical backend the OLT and the ONUs can be connected using a tree topology or a ring topology. In case of a tree topology, a *minimum spanning tree* is constructed to connect the OLT and the ONUs. The

Algorithm 1. ONU placement scheme

1: INPUT : ONU=set of ONUs; MR=set of mesh routers; (x_j, y_j)=position of the j-th mesh router
2: OUTPUT : the placement of the ONUs
3: Generate U ONU locations randomly
4: **while** Solution does not converge **do**
5: Assign the routers to the nearest ONU // Assignment phase
6: Put ONUs at the mean of all router-positions // Update phase
7: **end while**
8: Repeat step 3-7 for a large number of time and take the best solution

reason behind using the minimum spanning tree is to minimize the length of the fiber needed, thus the cost of deployment is also minimized. In case of a ring architecture, the laying out of fiber with minimum length can be modeled as a *travelling salesman problem (TSP)*. TSP can be defined as follows: given a list of cities and the distances between each pair of cities, we need to find the shortest possible route that visits each city exactly once and returns to the origin city. TSP is typical NP-hard problem. In our case the position of the OLT and the ONUs can be thought as the cities and the shortest possible route gives the minimum fiber needed.

3.2 Performance Study

In this section we compare the performance of our ONU placement scheme along with the random placement scheme using *network simulator–2 (ns2)* [50] simulator with IEEE 802.11 MAC, with substantial modifications in the physical and the MAC layers, to model the cumulative interference calculations and also include the physical carrier sensing based on cumulative received power at the transmitter. The *DataCapture* is also modeled in our modified *ns-2* version. Next we extend *ns-2* to support multiple channels and multiple radios as described in [51]. We also compare the effects of these ONU placement schemes on minimum hop-count routing in the upstream direction of the WOBAN. The effects and benefits of using multiple channels are also explored. The amount of total fiber required for designing the PON backend is also calculated. We consider two different network topologies based on the distribution of mesh routers. In the first case, we distribute the mesh routers uniformly in an area of 1000×1000 square meters as shown in Figure 3.3. In the second case, we simulate

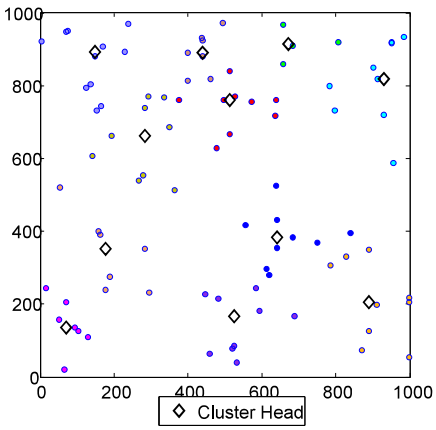

Figure 3.3: The placement of eleven ONUs with cluster-heads where mesh routers are uniformly distributed.

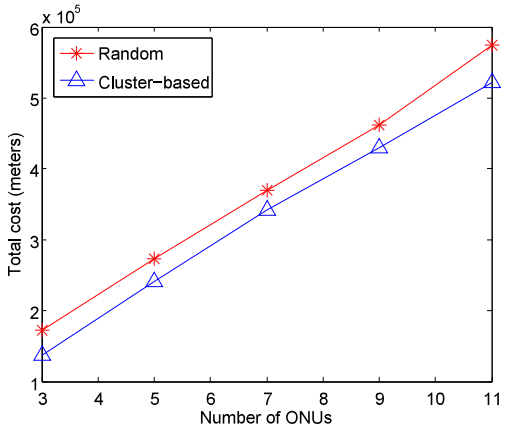

Figure 3.4: Comparison of overall cost for random placement and clustering-based schemes for uniform distribution of mesh routers.

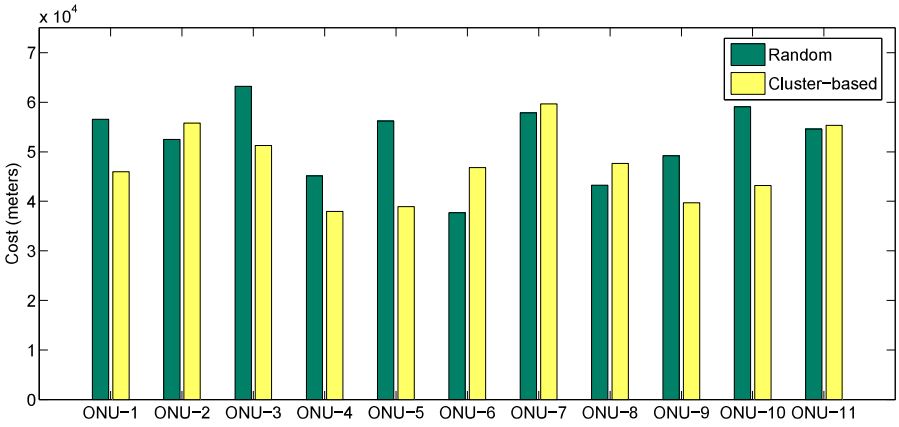

Figure 3.5: Costs of different ONUs for random placement and clustering-based schemes where mesh routers are uniformly distributed.

our ONU placement, routing and channel assignment scheme where the distribution of the mesh routers is non-uniform. This is modeled by considering a bivariate Gaussian distribution of routers that are centered at four specific locations in the region, as depicted in Figure 3.8. The transmission power is assumed to be 20 dBm for all cases. All the mesh routes generate traffic at a rate of 15 KBps which are carried to the ONUs using multi-hop communications based on shortest hop-count routes. Each flow runs UDP and is alive for 140 seconds. The parameters used in the simulations are listed in Table 3.1.

- Performance evaluation on uniformly distributed mesh routers: Figure 3.3 shows

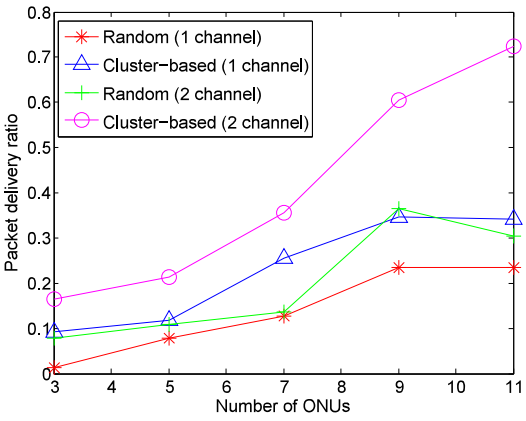

Figure 3.6: Comparison of delivery ratio with different number of ONUs for random placement and clustering-based schemes for uniform distribution of mesh routers.

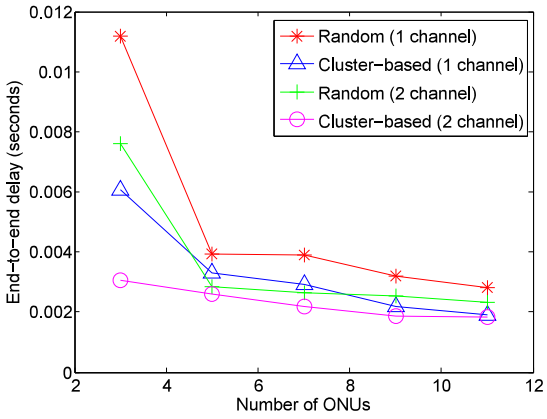

Figure 3.7: Comparison of end-to-end delay with different number of ONUs for random placement and clustering-based schemes for uniform distribution of mesh routers.

Table 3.1: Simulation environment

Parameter	**Values**	**Parameter**	**Values**
Max queue length	200	Data packets size	1000 bytes
Propagation Model	Two Ray Ground	Traffic Generation	Exponential
Antenna gain	0 dB	Transmit power	20 dBm
Noise floor	-101 dBm	SINRDatacapture	10 dB
Bandwidth	6 Mbps	PowerMonitor Thresh	-86.77 dBm
Modulation scheme	BPSK	Traffic Generation	Exponential

the placement of eleven ONUs in a geographic area comprising of uniformly distributed mesh routers. Figure 3.5 shows the costs of the ONUs in case of random (uniformly) ONU placement scheme and clustering scheme. The cost of the ONU_i is defined as follows:

$$C_{ONU_i} = \sum_{j=1}^{V} \sqrt{(X_i - x_j)^2 + (Y_i - y_j)^2} \tag{3.6}$$

From Figure 3.5, we can observe that the clustering scheme improves the cost of most of the ONUs, compared to random placement scheme. Figure 3.4 shows the variation of overall cost with the number of ONUs for both random placement and clustering schemes. It is observed that the clustering scheme generates a significantly lower cost

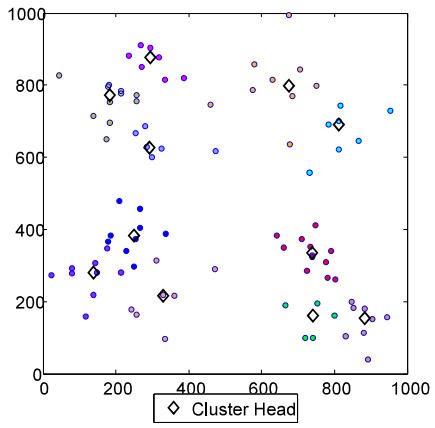

Figure 3.8: The placement of eleven ONUs with cluster-heads where mesh routers are non-uniformly distributed.

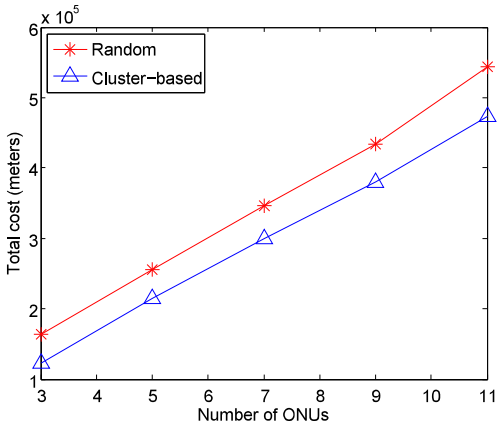

Figure 3.9: Comparison of overall cost for random placement and clustering-based schemes for non-uniform distribution of mesh routers.

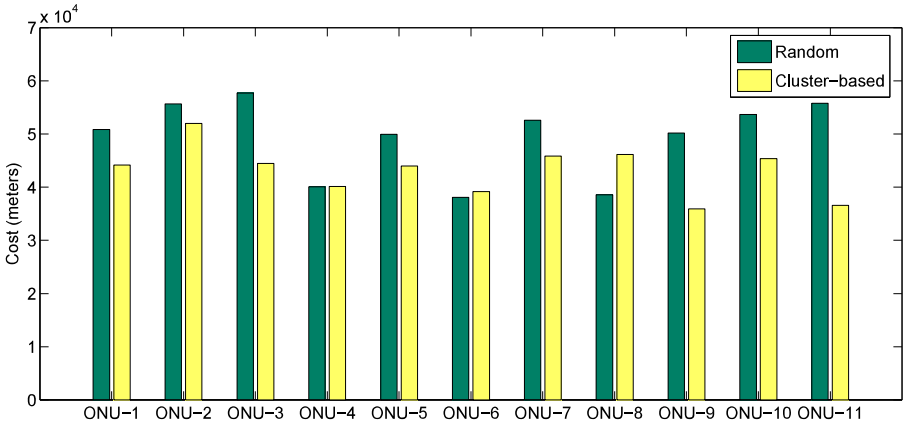

Figure 3.10: Costs of different ONUs for random placement and clustering-based schemes where mesh routers are non-uniformly distributed.

in comparison to the random placement scheme.

We also compare the effects of ONU placement on routing when multiple orthogonal channels are used. Here we consider routing in upstream direction, i.e. from the mesh router to any one of the ONUs (anycast routing). We consider minimum hop-count based routing. The minimum hop-count routes are calculated from each mesh router to all the ONUs. Then the ONU with the minimum hop is chosen as the best ONU for that mesh router as well as the corresponding route. We use Dijkstra's shortest path algorithm for deciding the minimum hop-count path. After the routes are decided, the channels are assigned to the links as follows. The links are sorted in

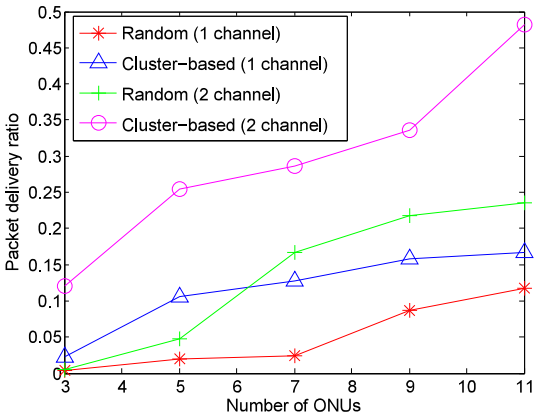

Figure 3.11: Comparison of delivery ratio with different number of ONUs for random placement and clustering-based schemes for non-uniform distribution of mesh routers.

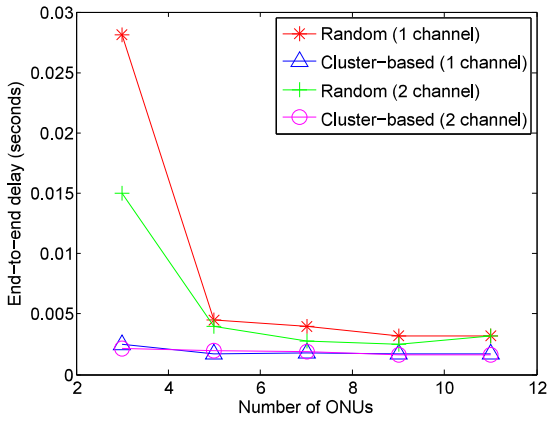

Figure 3.12: Comparison of end-to-end delay with different number of ONUs for random placement and clustering-based schemes for non-uniform distribution of mesh routers.

the decreasing order of their interfering load. Then channels are assigned to the links one-by-one as the least used channel in their interfering neighborhood. In case of a tie, a random channel is chosen among the channels that make the tie. Figure 3.6 shows the variation of packet delivery ratio with the number of ONUs. From this figure we can observe that the delivery ratio increases with the increase in number of ONUs. This is because the increase in ONUs results in reduced route length as well as traffic load on each link, which results in better route quality as well as delivery ratio. Figure 3.7 shows variation of end-to-end delay with the number of ONUs. We can observe that the delay decreases with the increase in ONUs due to reduced route length and less channel access delay due to less traffic load on each link. We can also observe that the clustering scheme performs better compared to the random ONU placement scheme, which shows the effectiveness of our proposed scheme. Also we can observe that the delivery ratio is improved in case of two channels because of reduced interference due to the presence of multiple channels, whereas the reduction in delay is mainly due to reduction in channel access delay from using multiple channels in neighbouring transmitting nodes.

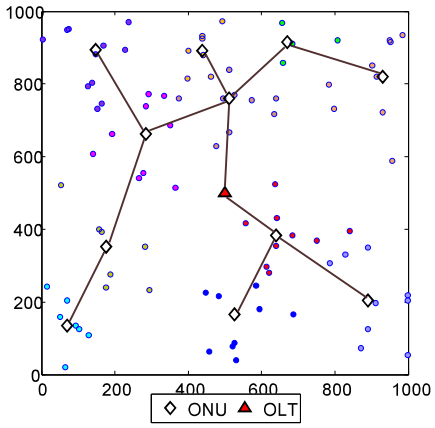

Figure 3.13: Fiber layout using minimum spanning tree for uniform distribution of mesh routers.

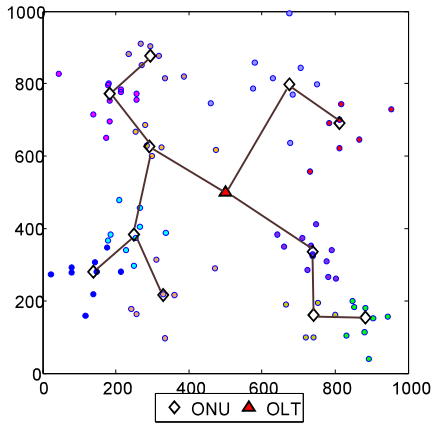

Figure 3.14: Fiber layout using minimum spanning tree for non-uniform distribution of mesh routers.

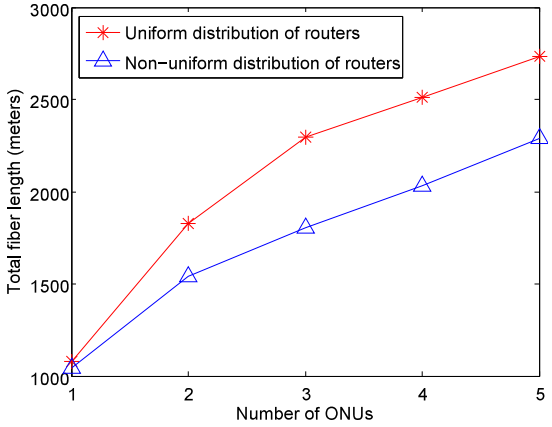

Figure 3.15: Comparison of total fiber length required for tree PON architecture for uniform and non-uniform distribution of mesh routers.

• Performance evaluation on non-uniformly distributed mesh routers: Now we consider the case of ONU placement on a more realistic scenario, where the mesh routers are non-uniformly distributed as shown in Figure 3.8. Figure 3.10 and Figure 3.9 show the improvement of cost in case of clustering scheme compared to the random placement scheme. The performance of packet delivery ratio and end-to-end delay are shown in Figure 3.11 and Figure 3.12, respectively. Comparing Figure 3.6-3.7 and Figure 3.11- 3.12, we observe that the delivery ratio as well as the end-to-end delay experience higher improvements under uniform distributions of routers in comparison to the non-uniform case. This is because, in case of non-uniform distribution,

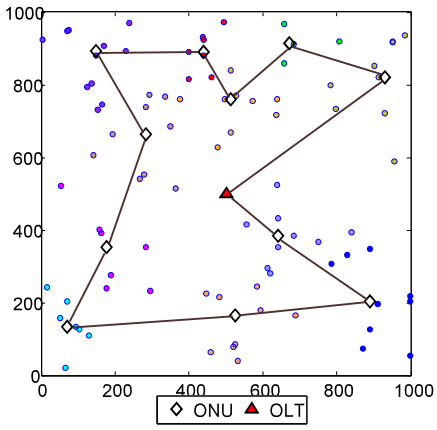

Figure 3.16: Fiber layout by solving the travelling salesman problem for uniform distribution of mesh routers.

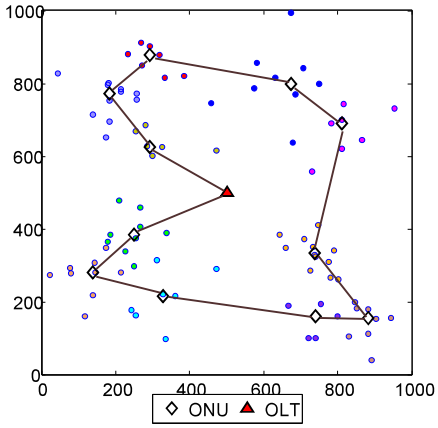

Figure 3.17: Fiber layout by solving the travelling salesman problem for non-uniform distribution of mesh routers.

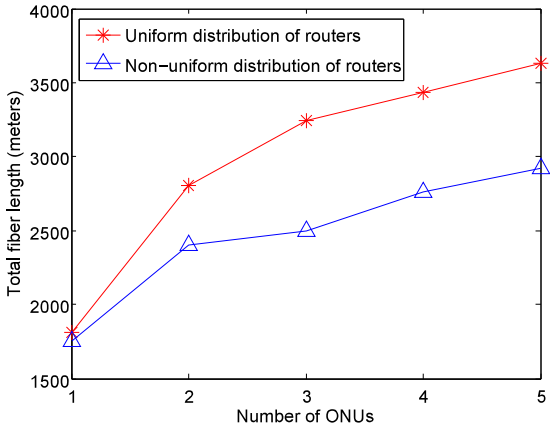

Figure 3.18: Comparison of total fiber length required for ring PON architecture for uniform and non-uniform distribution of mesh routers.

the mesh routers are confined in few areas. This makes those areas more congested which results in more interference and access delay, which in turn reduces delivery ratio and increases the end-to-end packet delay. On the other hand in case of uniform distribution of mesh routers, the traffic is uniformly distributed, which results in improved delivery ratio and end-to-end delay.

- Comparison of total required fiber for tree and ring topology at the optical backend: Depending on how the OLT and the ONUs are connected using optical fiber, the required fiber length will be different as well as the total deployment cost. Figure 3.13- 3.14 show the network topology for uniform and non-uniform distribution

of mesh routers respectively, where the minimum spanning tree is constructed joining the OLT and the ONUs to ensure the minimum fiber cost. The position of the OLT is assumed to be (500, 500). Figure 3.16- 3.17 depict of case of a ring topology where the fiber layout is done by solving the travelling salesman problem. For solving the TSP, we derive all the possible *Hamiltonian cycles* of the graph constructed by OLT and the ONUs and then choose the shortest cycle to minimize the fiber deployment cost. Figure 3.15 and Figure 3.18 show the total fiber required for both tree and ring topology with different distribution of mesh routers. These figures clearly show the amount of extra fiber required for the ring topology compared to the tree PON architecture.

3.3 Discussions

In this chapter, we study the ONU placement problem in WOBAN which aims to minimize some cost function. We propose a clustering technique to solve the problem of ONU placement and compare its benefits compared to the random ONU placement scheme in improving the network quality. We also studied the effects of number of ONUs as well as well as the effects of routing and multiple channels on the overall network packet delivery ratio and end-to-end packet delay. We also explain different PON architectures and their corresponding fiber layout schemes along with their deployment cost comparison.

CHAPTER 4: INTERFERENCE AND DELAY AWARE ROUTING IN SINGLE GATEWAY WOBAN

In this chapter, we address the routing problem in WOBANs that have a single gateway. Here, the wireless mesh routers try to determine routes to the gateway that maximize the end-to-end network performance. We consider an on-demand framework for routing, where a source node S broadcasts a route request packet when it requires a route to the gateway. The route request packet reaches the gateway node via various routes, and carries relevant parameters of each of the paths traced. The gateway node considers these inputs and existing traffic conditions from all active nodes in the network to determine the best route for S. Note that all communications are directed to the same gateway node, and hence it is practically possible to implement a centralized routing solution under the assumed network model. Although technically any ad hoc routing protocol can be applied here, such routing protocols usually try to minimize path lengths, which does not necessarily give the best quality. The problem here is to determine the route that provides the best *communication quality*, in terms of the end-to-end *POS* and delay. Hence, the main problem addressed in this work is to determine a suitable routing metric that accurately captures the quality of communication over a candidate route.

4.1 Quality Based Routing in Wireless Mesh Networks

Our approach for solving the above problem is to develop accurate models for the POS and delay in multi-hop wireless networks using a simple set of measurable parameters, and incorporating these models into a route quality metric. Our goal is to implement an on-demand routing scheme that evaluates various routes based on the quality metric and selects the best. The proposed routing scheme is structured similar to AODV except that the control packets collect essential information to evaluate the

quality metric, which forms the basis for route selection.

In order to develop a route quality metric, we start with extensive performance evaluations of a wireless link in a multi-hop network to determine important parameters that affect the characteristics of a link. We assume IEEE 802.11 as the underlying MAC protocol, and develop its performance models with and without the RTS/CTS option. Our objective here is to develop a performance model that is suitable for incorporating into a route quality metric, which can be evaluated for routing decisions by the gateway node. In particular, we show that when the 802.11 MAC is used without the RTS/CTS and ACK options, the primary factors influencing the throughput and delay in a test link at a given offered load can be effectively captured by two measurable quantities: (a) the number of active neighbors of the transmitter, and (b) the number of interferers of the receiver, along with a number of other parameters such as locations and interplay of neighboring nodes. These parameters can be easily obtained by the gateway node to evaluate the communication qualities of candidate routes. The evaluation is somewhat more complex when the RTS/CTS and ACK packets are enabled, since it involves more parameters. However, we obtain appropriate models for capturing the link performance using a measurable set of parameters for this case as well.

4.2 Development of the Route Quality Metric

We now present the characterization of wireless transmissions in multi-hop networks leading to the development of the proposed route quality metric. These are obtained from simulation experiments using the *network simulator–2 (ns2)* [50]. For sake of explanations and performance evaluations, we consider a network where the nodes are placed in an uniform grid, as shown in Figure 4.2. However, our analysis applies to any deployment scenario. The parameters used in the simulations are listed in Table 4.1. As stated before, we assume the IEEE 802.11 CSMA/CA MAC with and without the RTS/CTS option. We focus on the key link-level performance

issues, which include the (a) channel access ratio (CAR), i.e. the ratio of the offered load that is actually transmitted, (b) the link-level probability of success, i.e. the probability that a transmitted packet is successfully received by the receiver, and (c) the average transmission delay of a packet in the MAC layer.

Table 4.1: Simulation environment

Parameter	**Values**	**Parameter**	**Values**
Max queue length	200	Data packets size	1000 bytes
Propagation Model	Two Ray Ground	Trans antenna gain	0 dB
Recv antenna gain	0 dB	Transmit power	20 dBm
Noise floor	-101 dBm	SINRDatacapture	10 dB
Modulation scheme	BPSK	PowerMonitor Thresh	-86.77 dBm
Traffic Generation	Exponential	SINRPreamblecapture	4 dB

4.2.1 Channel Access Ratio

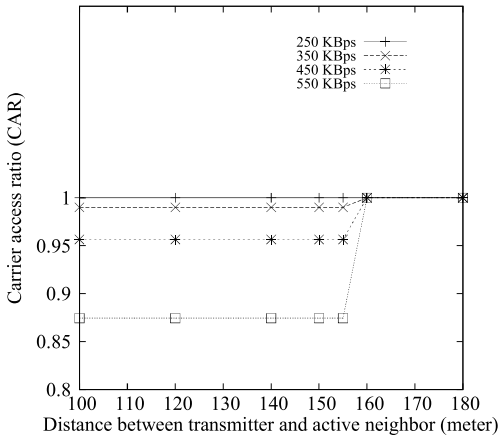

Figure 4.1: Variation of CAR with respect to distance from an active neighbor.

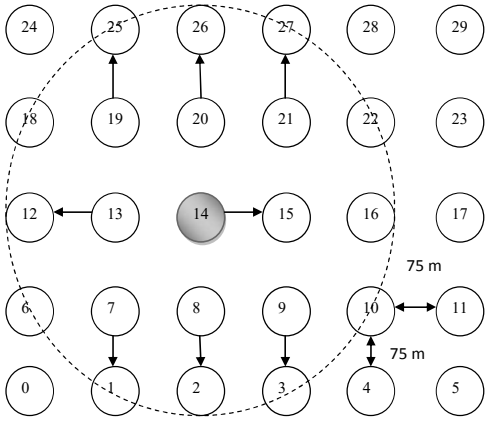

Figure 4.2: Simulation environment to evaluate the effect of active neighbors on the test link 14→15. The dotted line shows the carrier sensing range.

A transmitting node has to contend with its active neighbors to gain access to the channel. Consequently, the CAR for a transmitter depends on the number of active neighbors and their level of activity, which is dependent on the traffic load. It does not depend on the distance from the active neighbors as long as they are within the carrier sensing range. These observations are validated in Figure 4.1, which depicts

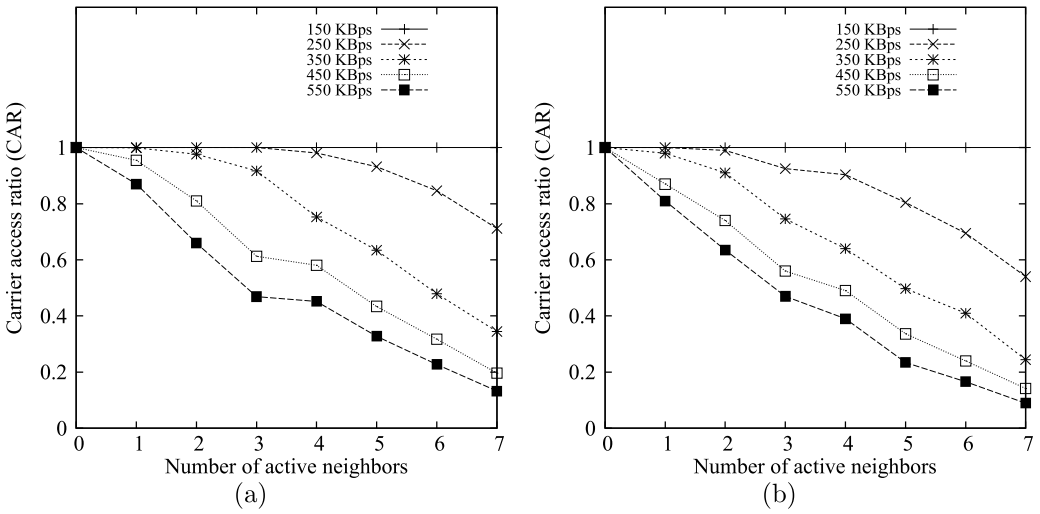

Figure 4.3: Variation of CAR (a) without RTS/CTS, (b) with RTS/CTS.

the variation of the CAR in a test link with respect to the distance from an active neighbor for different loads of the active neighbor. The figure also shows that with the chosen parameters, the carrier sensing range (CSR) is 155 meters[1].

When multiple active neighbors are involved, the CAR depends on a complex interaction of carrier sensing, back-offs, and transmission activities from all contending nodes, whose number vary from one node to another. Consequently, we attempt to determine the effect of the number of active neighbors on CAR from simulation experiments. We consider the test link $14 \rightarrow 15$ in a network of 30 nodes that are placed in a uniform grid as shown in Figure 4.2 and determine the variation of CAR in the test link with increasing number of active neighbors (i.e. by incrementally activating transmissions from nodes 7, 8, 9, 13, 19, 20 and 21). The results, depicted in Figure 4.3 (a) for the case where RTS/CTS packets are disabled, indicate that the CAR is not noticably affected by the active neighbors for loads lower than 150 KBps, but it drops significantly and non-linearly at higher loads, especially for higher number of active neighbors.

Figure 4.3 (b) shows the same results when the RTS/CTS is enabled. The CAR

[1]The fact that the transmission range and CSR turns out to be equal here is coincidental. Our analysis is quite general and is applicable even when they are different.

in presence of RTS/CTS is lower than without RTS/CTS, which is reasonable, since data packets are transmitted (i.e. the channel accessed) only when the channel is clear at both the sender and receiver node locations.

4.2.2 Transmission Delay

The transmission delay in 802.11 channels depends on a number of components, of which the queuing and access delays are significant. The queuing delay Q_d is the property of the transmitting router, which is the time that a packet has to wait in its transmission queue before it actually reaches the head of the queue and starts contending for the channel. Q_d is directly related to the length of the queue and the arrival rate of the packets entering in the queue. On the other hand, the access delay Q_a is the time that a packet at the head of the transmission queue has to wait before the contention in the channel is resolved by CSMA/CA and the packet gets access to the channel and starts transmission. The sum of the average queuing and access delays, referred to as total delay t_d, is an important factor affecting the quality of a communication link. Again, we consider the test link $14 \rightarrow 15$ and obtain the variation of the total delay in the test link with different number of active neighbors. When the RTS/CTS packets are disabled, the delay of the test link $14 \rightarrow 15$ is found to fit a quadratic polynomial:

$$T_d(n_a) = An_a^2 + Bn_a + C \tag{4.1}$$

where n_a is the number of active neighbors of the sender and A, B and C are the best fit coefficients that depend on the offered load. Simulations were run at several different offered loads, and the best-fit coefficients were found to be $A = -3.57 \times 10^{-7}$, $B = 4.814 \times 10^{-6}$, and $C = 0.001443$ for 5 KBps; $A = 1.88 \times 10^{-6}$, $B = 9.54 \times 10^{-6}$, and $C = 0.00146$ for 35 KBps; and $A = -7.023 \times 10^{-7}$, $B = 5.25 \times 10^{-5}$ and $C = 0.001425$ for 65 KBps. Delays obtained from simulations and the best fit curves described above

are shown in Figure 4.4(a), which validates the quadratic approximation.

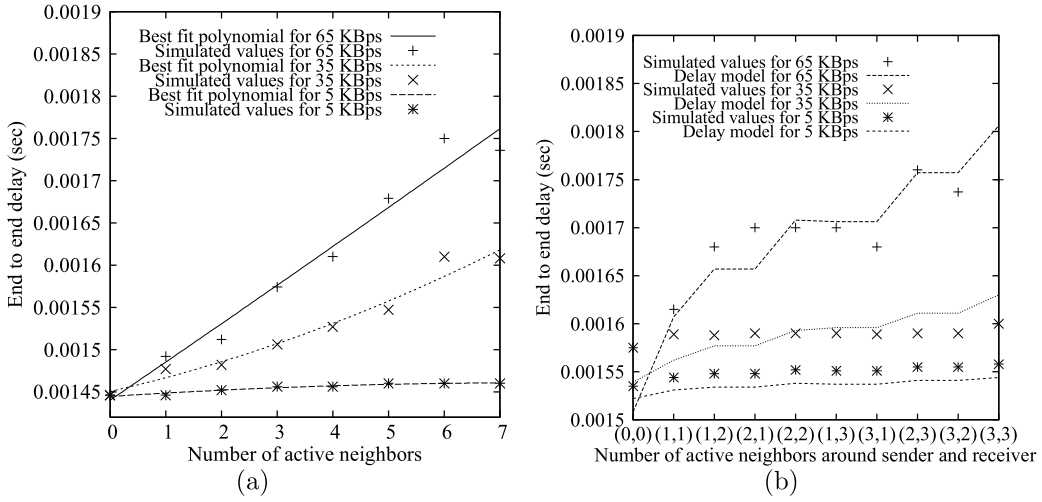

Figure 4.4: Variation of delay (a) with number of active neighbors of sender without RTS/CTS, (b) with number of active neighbors of sender and receiver with RTS/CTS.

If we enable RTS/CTS packets, then the time for a packet to reach the destination depends on the active neighbors of the sender (n_a) as well that of the receiver (which we denote by n_b) since a data packet is not transmitted unless the receiver has access to the channel to send the CTS. The total delay can be expressed as:

$$\begin{aligned} T_d^{RTS/CTS}(n_a, n_b) &= T_{CA\_sender} + T_{RTS} + SIFS + T_{CA\_recv} \\ &+ T_{CTS} + SIFS + T_{Data\_Tx} \end{aligned} \tag{4.2}$$

where T_{RTS} and T_{CTS} are the transmission times of RTS and CTS packets, respectively, which can be calculated from their sizes (assumed to be 20 bytes and 14 bytes, respectively), and SIFS is the short interframe spacing length, which is taken as $16\mu s$. T_{CA_sender} is the time for the sender to get access to the channel, which, from the previous section, is expressed as $T_{CA\_sender} = An_a^2 + Bn_a$. T_{Data_Tx} is the data transmission delay, which is equal to C. Similarly, the channel access delay at the receiver $T_{CA\_recv} = An_b^2 + Bn_b$. Then the expression for the total delay $T_d^{RTS/CTS}(n_a, n_b)$

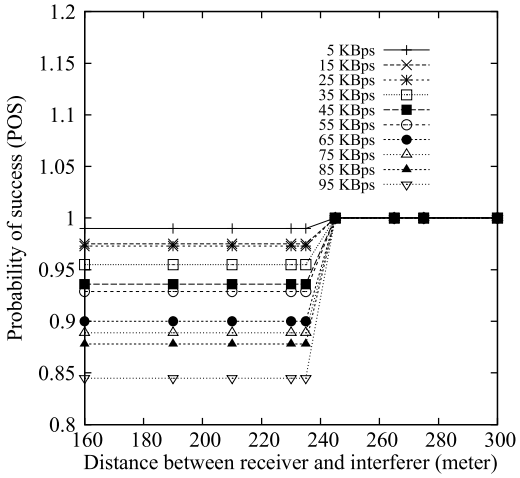

Figure 4.5: Variation of POS with respect to distance from an interferer.

in the presence of RTS and CTS can be written as:

$$T_d^{RTS/CTS}(n_a, n_b) = A(n_a^2 + n_b^2) + B(n_a + n_b) + 1.0324C + 0.000032 \quad (4.3)$$

We validate this model using simulations by evaluating the total delay with varying number of active neighbors. These results are shown in Figure 4.4 (b), where the sample point (i, j) on the x-axis implies that $n_a = i$ and $n_b = j$.

4.2.3 Probability of Success

We now evaluate the probability of successful reception of a transmitted packet on the test link. Since the POS (defined as the fraction of the transmitted data packets that are received successfully) is very different for the cases when RTS, CTS, and ACK packets are disabled and when they are enabled, we consider these two cases separately.

POS with RTS/CTS Disabled: With RTS/CTS packets disabled, the POS is only dependent on the probability of successful reception of the data packet at the receiver. A data packet is received correctly if its signal to interference-plus-noise ratio (SINR) does not fall below the minimum SINR threshold at the receiver at any time during the reception of the packet. When the receiver has only one interfering node,

a packet transmission can be unsuccessful if the distance of the interferer is smaller than a limit, which is often termed as the *interfering range*. In Figure 4.5, we depict the variation of the POS in the test link 14 $\rightarrow$ 15 with RTS/CTS turned off, with respect to the distance from an interfering node from the receiver. The figure shows that for the chosen parameters, the interfering range is 235m. When an interferer is within this range, the POS depends on the load, which determines the probability that a transmission from the interferer overlaps with the test packet. Note that if the transmissions from multiple interferers overlap, the aggregate interference will increase, thereby causing the interfering range to increase. However, that probability is usually low unless the offered load is very high. For the rest of this chapter, we assume the grid spacing to be 150 meters, with which a receiver can have up to 5 interferers.

Generally, a link in a wireless network comes under the influence of a number of interferers whose transmissions may be dependent or independent of one another. *Independent interferers* are those whose transmissions are not in any way affected by one another, i.e. each node's transmissions occur independently of those from the others. So the combined interference from a set of independent interferers can be calculated easily. On the other hand, if the transmissions of any interfering node is in some way dependent on transmissions from other nodes that are also located within the interfering range of the test node, then the combined interference is more difficult to model. We term such nodes *dependent interferers*, which is addressed in Appendix A.

If S is the transmitter and D is the receiver in a test link, then the POS of the link $S \rightarrow D$ in the presence of a set of N independent interferers I with transmitted load L (L is given by CAR$\times$offered load) can be written as:

$$P_S(I) = \prod_{k=1}^{N} P_S(i_k) \tag{4.4}$$

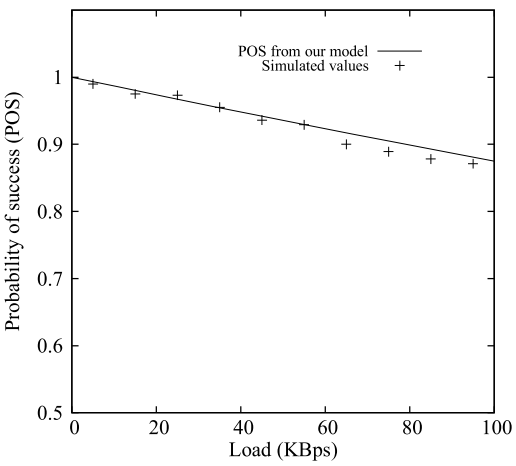

Figure 4.6: Experimentally obtained POS versus load in presence of 1 interferer.

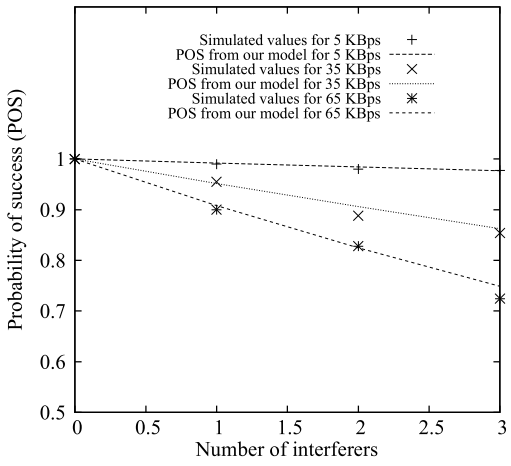

Figure 4.7: POS versus number of interferers of D: model and simulation results

where $I = \{i_1, i_2, \ldots, i_N\}$ is the set of N interferers of D and $P_S(i_k)$ is the probability of success of the test link when i_k is transmitting[2]. We assume that the length of data packet is $DLEN$ (in bits) and all the nodes generate packets based on a Poisson process. B is the bandwidth of the channels in bits/seconds or bytes/seconds and λ is the arrival rate of the data packets. In order to evaluate the POS using the above expression, we note that for any given load, the POS in the presence of a single interferer with the RTS/CTS disabled is given as:

$$\begin{aligned} P_S(i_k) &= \text{P}(i_k \text{ does not send DATA in vulnerable period} \\ &\quad \left(\tfrac{2\times DLEN}{B}\right) \text{ of S}) = e^{\frac{-2\times\lambda\times DLEN}{B}} \end{aligned} \tag{4.5}$$

The simulation results and the analytical results from equation (4.4) are shown in Figure 4.6. As expected, the POS decreases consistently with increasing load, which is due to increasing amount of interference from transmitting nodes.

It must be noted that although the set I can be estimated by the set of nodes that are located within the interfering range of the receiver, some additional factors

[2]Note that $P_S(i_k) = 1 - P_t(i_k)$, where $P_t(i_k)$ is the probability that a transmission from interferer i_k overlaps with the test packet from S and depends on the transmitted load L.

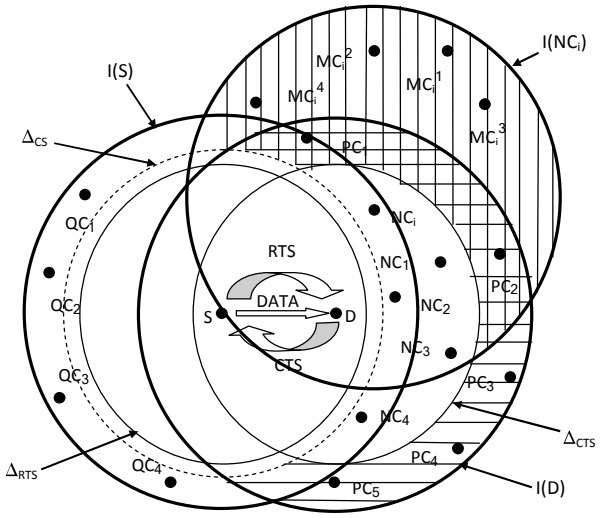

Figure 4.8: Effect of interferers in presence of RTS/CTS for test link $S \rightarrow D$

affect the accuracy of equation (4.4). For instance, wireless propagation can be highly non-isotropic because of shadowing, multipath reflections, and other long term fading effects. This can make it difficult to estimate the actual interference from a source from its distance from the receiver. However, because of the threshold effect of the interference from any source, we find that using the interfering range to identify interferers is generally acceptable. This issue needs additional considerations if RTS/CTS and ACK packets are assumed, which is discussed later.

To validate the POS model in equation (4.4), we compare results obtained from equation (4.4) with those obtained from simulations in Figure 4.7, where all the nodes have the same load, and hence, the same $P_S(i_k)$ for all i_k. The actual POS values obtained from simulations closely match the values obtained from the model. This confirms our claim that the POS of a test link for a given load can be approximately estimated from the number of active neighbors of the transmitter and the number of interferers of the receiver using the models developed above.

POS with RTS/CTS and ACK Enabled: When the RTS/CTS option is enabled, a data packet is only transmitted when the RTS/CTS exchange is successful, i.e. the channel is found to be clear both at the transmitting and receiving nodes.

However, the transmitted data packet can still be lost due to interference caused to the data packet or the ACK packet. Here, we analyze the possible events that can cause these transmission failures, which are explained with the help of Figure 4.8. In the figure, $S \rightarrow D$ represents the test link, Δ_{RTS} and Δ_{CTS} denote the regions where the RTS and CTS packets for the test link can be received, and Δ_{CS} denotes the area around S where nodes can sense the transmission from S. For any node i, $I(i)$ denotes the area from where a transmission from any node $j \in I(i)$ can interfere with a packet being received at i. Our approach is to explore various cases where events can lead to the loss of the DATA or the ACK packet, both of which can cause the data transmission from $S \rightarrow D$ to be unsuccessful. For each of these cases, we evaluate the factors that affect the POS, as outlined below:

★ Case-1: The transmitted data packet is unsuccessful due to interference from nodes that are within the interference range of the receiver but outside its transmissions range, i.e. range of reception of the CTS packet. These nodes are marked as PC_i in Figure 4.8, of which we assume p nodes are sending and r nodes are receiving. Since both events can generate interfering packets, we consider the probability of success of the test data packet in the presence of both these events. Note that the sending nodes can interfere by transmissions of either RTS or data packets. However, since the length of the RTS packet is much smaller than that of data packets, its effect on the POS of the data packet at D will be much smaller, and so we only consider the interference of data packet transmissions from the p sending nodes among PC_i. In the absence of any other interferer that can affect the reception of the test data

packet, the effect of a single interfering node among PC_i can be evaluated as follows.

$$
\begin{aligned}
&\text{P(DATA is received successfully | DATA is transmitted)} \\
&= \text{P(DATA is received successfully | RTS is received successfully at } D) \\
&= \frac{\text{P(DATA and RTS are received successfully)}}{\text{P(RTS is received successfully at } D)} \\
&= \frac{\text{P}(PC_i \text{ does not send DATA in vulnerable period } (\frac{2\times DLEN}{B}) \text{ of S})}{\text{P}(PC_i \text{ does not send DATA in vulnerable period } (\frac{DLEN}{B}) \text{ of } S)} \\
&= \frac{e^{\frac{-2\times\lambda\times DLEN}{B}}}{e^{\frac{-\lambda\times DLEN}{B}}} = e^{\frac{-\lambda\times DLEN}{B}}
\end{aligned}
$$

For p independent senders $(PC_1, PC_2, ..., PC_p)$ in this region, the probability of success of the DATA packet is given by $e^{\frac{-\lambda\times DLEN\times p}{B}}$.

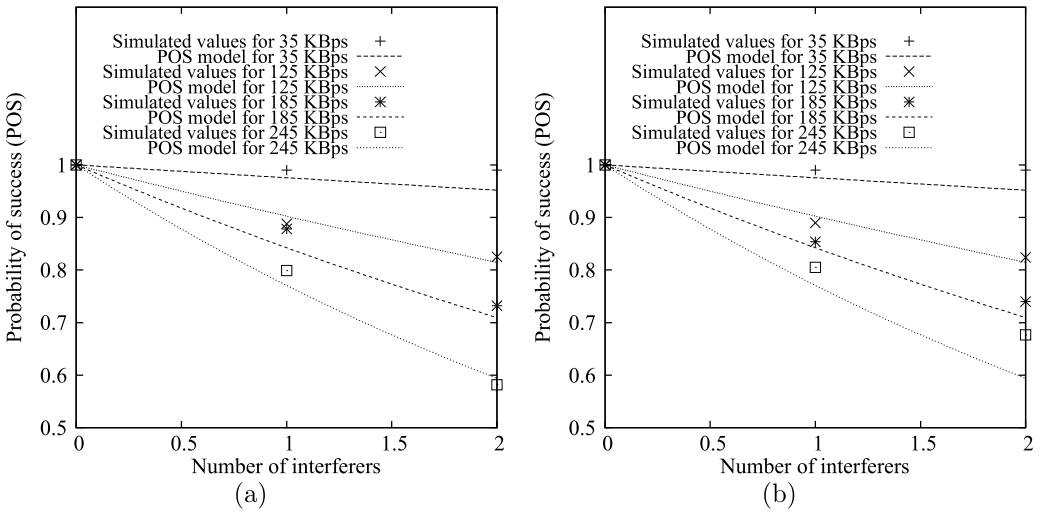

Figure 4.9: POS with (a) number of sending nodes among PC_i (p), (b) with number of receiving nodes among PC_i (r).

The receiving nodes among PC_i can interfere by the transmission of CTS packets during the transmission of the test DATA packet; thus the probability of success in the presence of r such nodes is $e^{\frac{-\lambda\times DLEN\times r}{B}}$.

To validate these models, we perform simulations to study the effect of p senders among PC_i and r receivers among PC_i independently. These are depicted in Figures 4.9 (a) and 4.9 (b), respectively, which show that our models are reasonably

accurate.

★ Case-2: The test data packet is unsuccessful due to interference from nodes that are within the transmission range of D but fail to receive the CTS packet. A node located in the Δ_{CTS} that is outside the Δ_{CS} of S (marked as NC_i in Figure 4.8) may not receive the CTS from D correctly due to an overlapping transmission from MC_j^i (refer to Figure 4.8). The probability of this event is $1 - e^{\frac{-\lambda \times DLEN}{B}}$, which is the probability that MC_i^j transmits in the vulnerable period ($\frac{DLEN}{B}$) of the CTS transmission from D [3]. In general, if there are m such interferers among MC_i^j, then the probability that the CTS is not received by NC_i is $1 - \prod_{i=1}^{m} e^{\frac{-\lambda \times DLEN}{B}} = 1 - e^{\frac{-\lambda \times DLEN \times m}{B}}$.

The probability that NC_i, having failed to receive the CTS from D, interferes with the reception of the DATA packet at D is then given by $(1 - e^{\frac{-\lambda \times DLEN}{B}})$, which is the probability that an RTS transmission from NC_i overlaps with the test DATA packet at D. Consequently, the probability that the DATA transmission from S to D is successful in the presence of unsuccessful reception of the CTS packet at NC_i is given by $1 - (1 - e^{\frac{-\lambda \times DLEN}{B}})(1 - e^{\frac{-\lambda \times DLEN \times m}{B}})$. If there are n such nodes $(NC_1, NC_2, \cdots, NC_n)$, then the DATA transmission will be successful with a probability of $\prod_{i=1}^{n} 1 - (1 - e^{\frac{-\lambda \times DLEN}{B}})(1 - e^{\frac{-\lambda \times DLEN \times m}{B}})$.

To validate the above POS model, we perform simulations by first varying n keeping $m = 1$, i.e. assuming that each of NC_i, $i = 1, 2, \cdots, n$, has one interferer MC_i^j only. These results are compared with the proposed POS model in Figure 4.10 (a). Figure 4.10 (b) depicts the results where the number of interferers for each NC_i is doubled, i.e. $m = 2$. These results are in close agreement with our POS model.

★ Case-3: The transmitted ACK packet is unsuccessful due to interference from nodes that are within the interfering range of S. This interference can be caused by a transmitted RTS or DATA packet. A node in this region may send an RTS packet during the transmission of the ACK packet on the test link, if it has missed

[3] As before, we ignore the effect of interference of the smaller RTS and CTS packets in favor of a data packet from MC_i^j, since those probabilities are comparatively smaller.

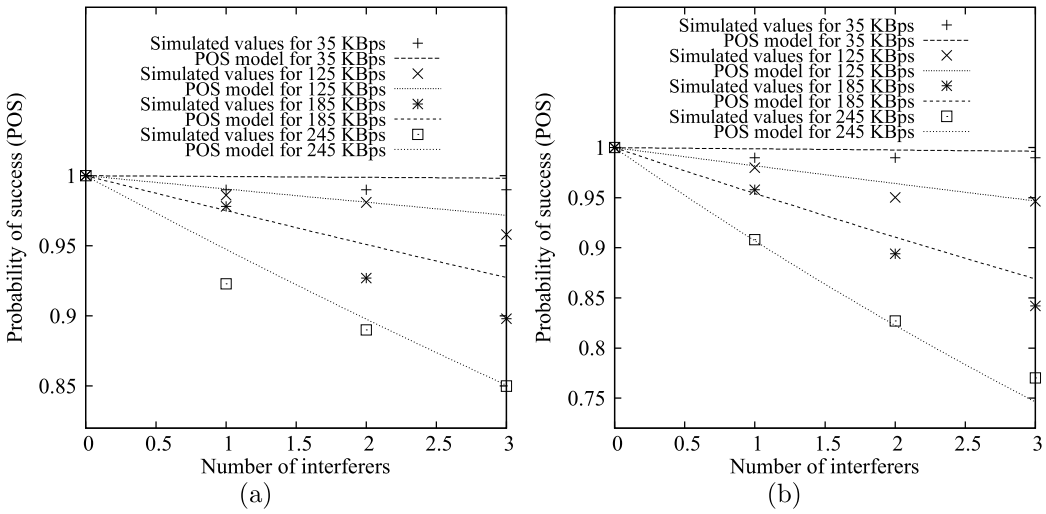

Figure 4.10: POS with number of active nodes among NC_i (n) (a) with $m = 1$, (b) with $m = 2$.

the RTS packet from S. But as the packet sizes of both ACK and RTS are very small in comparison to a DATA packet, the vulnerable period is also small. So, the probability of collision of an RTS and ACK is negligible and we ignore this possibility.

We next consider the possibility of interference of a data transmission from a node located within the interference range of S on the ACK being received at S. In particular, we are interested in the interference from the nodes marked as QC_i in Figure 4.8. Now, the transmission of an ACK packet from D to S implies that the corresponding RTS/CTS exchange was successful, which implies that the nodes QC_i, $i = 1, 2, \cdots$, did not transmit during the vulnerable period of the CTS transmission. These nodes would be unsuccessful in exchanging RTS/CTS packets during the following period of DATA transmission from S. Consequently, after successful completion of the DATA transmission from S, the only packets that can be transmitted from a node QC_i that can interfere with the reception of the ACK packet at S are RTS or CTS and not DATA, which results in a small probability of overlap. Hence, we can ignore the effect of this case as well.

By taking into account all the factors described above, the probability of success

of a transmitted data packet using the RTS/CTS handshake is given by

$$POS = \left\{ \prod_{i=1}^{n} 1 - \left(1 - e^{\frac{-\lambda \times DLEN}{B}}\right)\left(1 - e^{\frac{-\lambda \times DLEN \times m}{B}}\right) \right\} \times e^{\frac{-\lambda \times DLEN \times q}{B}} \times e^{\frac{-\lambda \times DLEN \times r}{B}} \quad (4.6)$$

It must be noted that some additional factors affect the POS and hence, the accuracy of equation (4.6). Firstly, equation (4.6) is based on the assumption that all interferers in case-1 transmit independently of interferers in case-2 and case-3. But this is not exactly true as there are dependencies among these interferers. The number of interferers whose transmissions are independent of each other is often hard to obtain. Secondly, in equation (4.6) we assume that the arrival rate of all the interferers are same. However, the rate of transmissions of DATA packets depends on successful reception of CTS at the sender, which depends on the nodes that interfere with it. Again these interferers depends on other interferers as well. Thus, obtaining an accurate estimate of the POS becomes intractable. Nevertheless, our model gives a good estimate of the POS for a test link considering the various measurable parameters in a static multihop wireless network, such as the number of interferers m, n, p, and r in different scenarios.

4.2.4 Route Quality Metric

We now apply the above models of the estimated POS and delay of a test link to define an end-to-end route quality metric. We consider that the end-to-end POS of a multi-hop route is given as the product of the POS of every individual link on the route and the end-to-end delay is given as the sum of the individual link delays. Consequently, based on the objective of maximizing the end-to-end POS and minimizing the end-to-end delay, we define the route quality $Q(r)$ metric for route r

of length v operating at load L as follows:

$$\begin{aligned} Q(r) &= \frac{\prod_{f=1}^{v} P_S(I_f)}{\sum_{f=1}^{v} T_d(n_{af})} \text{ without RTS/CTS} \\ &= \frac{\prod_{f=1}^{v} P_S(I_f)}{\sum_{f=1}^{v} T_d(n_{af}, n_{bf})} \text{ with RTS/CTS} \end{aligned} \tag{4.7}$$

Here, f is a link on the route from source to destination , $P_S(I_f)$ is the POS of link f, I_f is the set of interferers, and $T_d(n_{af})$ is the delay experienced by a packet with n_{af} active neighbors at the sender. Similarly, $T_d(n_{af}, n_{bf})$ is the delay with n_{af} and n_{bf} active neighbors at the sender and the receiver end respectively.

4.3 Interference and Delay Aware Routing

In this section we describe the proposed quality based routing protocol IDAR that uses the quality metric derived in the previous section. IDAR is a reactive routing protocol that tries to select routes with the highest ratio of the end-to-end POS and delay based on parameters collected and conveyed by RREQ packets. We present two versions of IDAR, which differ in the contents of the propagating RREQ packets and how the quality metric is calculated. These are described in detail below:

★ IDAR-v1: Protocol functionality of our proposed routing protocol IDAR-v1 can be divided into the following different phases.

- Route Discovery: When the source does not have a route to the destination, it broadcasts a route request packet (RREQ) to its neighbors. In addition to many other fields, the RREQ contains a *RREQ ID*, the destination address, the source address, the number of active neighbors of the sender (A), the accumulated POS on the current route (P_S), the accumulated delay in the current route (T_d), and a timestamp. These quantities A, P_S, T_d and the timestamp are initialized at the source to the number of active neighbors of the source, $P_S = 1$, $T_d = 0$, and timestamp = the time when the RREQ packet was generated. Every intermediate node updates the accumulated POS and delay based on

the number of active neighbors of the previous node and its active interferers before forwarding it. The *RREQ ID* combined with the source address uniquely identifies a route request. This is required to ensure that the intermediate nodes rebroadcast a route request only once in order to avoid broadcast storms. If any intermediate node receives a RREQ more than once, it just discards it. All intermediate nodes do the same thing until the RREQ reaches the destination. The timestamp is used to reduce unnecessary flooding of RREQ packets throughout the network.

- Route Selection: For every RREQ packet, the destination calculates the quality metric $Q = \frac{P_S}{T_d}$. The destination waits for the first N packets (which is ten in our case) and forwards a route reply packet (RREP) back on the route that has the highest Q value. All the intermediate nodes forward the RREP back to the source and update their routing table entry. The source then starts sending the data packets via this route.

- Route Maintenance: If a routing table entry is not used for along time, that entry is erased. This is required as the network scenario changes with time, thus after a long time if a source need a route to the gateway, it has to start a route discovery to get a good quality route.

In IDAR-v1, the intermediate nodes are required to calculate the POS and delay, for which the nodes must know its active neighbors and interferers. One way to achieve this is for the gateway to forward this information to all nodes at periodic intervals, which causes additional overhead.

★ IDAR-v2: In order to avoid the overhead problem mentioned above, we propose another version of the IDAR routing protocol, named IDAR-v2 and the different phases are described as follows.

- Route Discovery: Here, instead of carrying A, P_S and T_d as in IDAR-v1, the

RREQ simply carries the sequence of nodes that it has traversed. Rest of the route discovery procedure is similar to IDAR-v1.

- Route Selection: The destination (gateway) uses the node location and neighborhood information to calculate the end-to-end POS and delay, and hence the Q for each route. In addition to solving the problem of providing all nodes with node location information, IDAR-v2 also calculates the route quality more accurately because it can use global location information to determine dependent and independent interferers based on the information conveyed by each RREQ packet.

- Route Maintenance: Route maintenance is the same as for IDAR-v1.

But the disadvantage of this scheme is that as the intermediate routers have to append its own IDs, the size of the RREQ packet gets larger as it propagates along the network, which can be a problem for large networks.

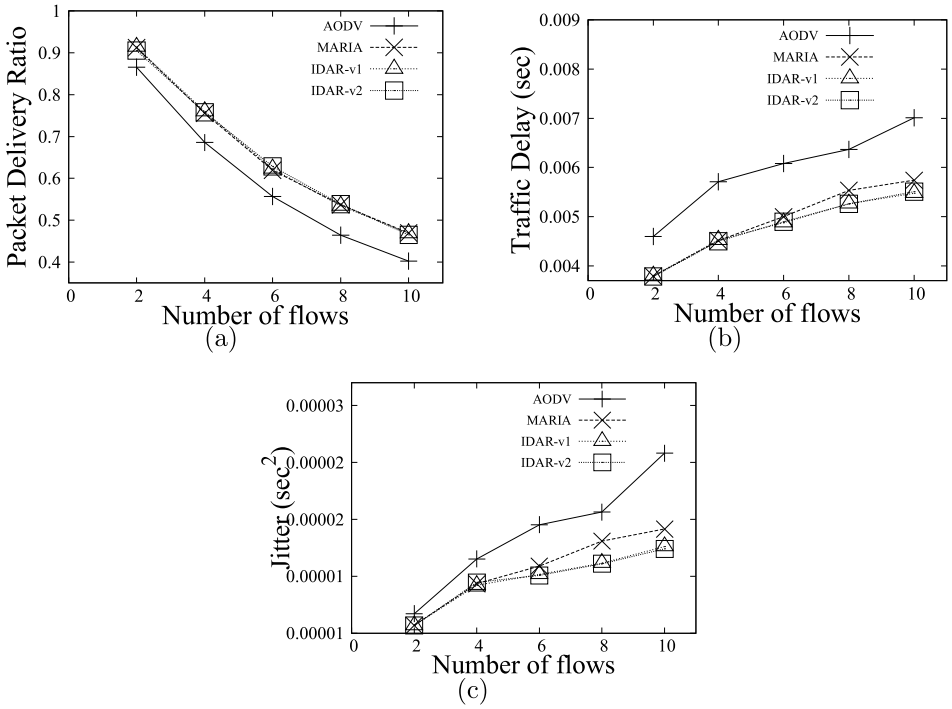

Figure 4.11: Comparison of (a) packet delivery ratio (b) delay (c) jitter

4.4 Performance Evaluation of IDAR

We perform extensive performance evaluations to determine the effectiveness of the proposed route quality metric and the IDAR routing schemes using *network simulator–2 (ns2)* [50]. The parameters used in the simulations are listed in Table 4.1. The quality of the routes were determined by obtaining the average UDP end to end packet delivery ratio and delay using *ns-2* and comparing them with a traditional shortest-path reactive routing protocol (AODV) and the quality based routing scheme MARIA [22].

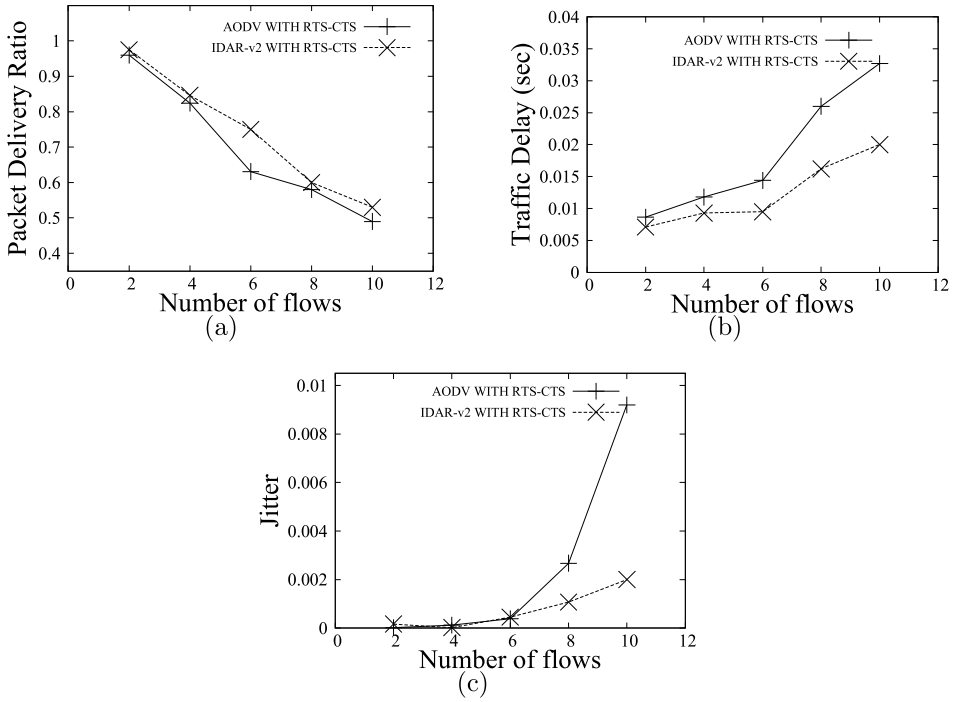

Figure 4.12: Comparison of (a) packet delivery ratio (b) delay (c) jitter

We next present the packet delivery ratio, delay and jitter performance of the proposed IDAR routing protocol in a general simulation scenario. We consider the same grid network as shown in Figure 4.2, and consider the case where all nodes are communicating with a common destination, node 29 (representing the Internet gateway). The sources are selected randomly. Each flow runs UDP with a transmission rate of 65 KBps. Each flow is alive for 200 seconds and the average delivery

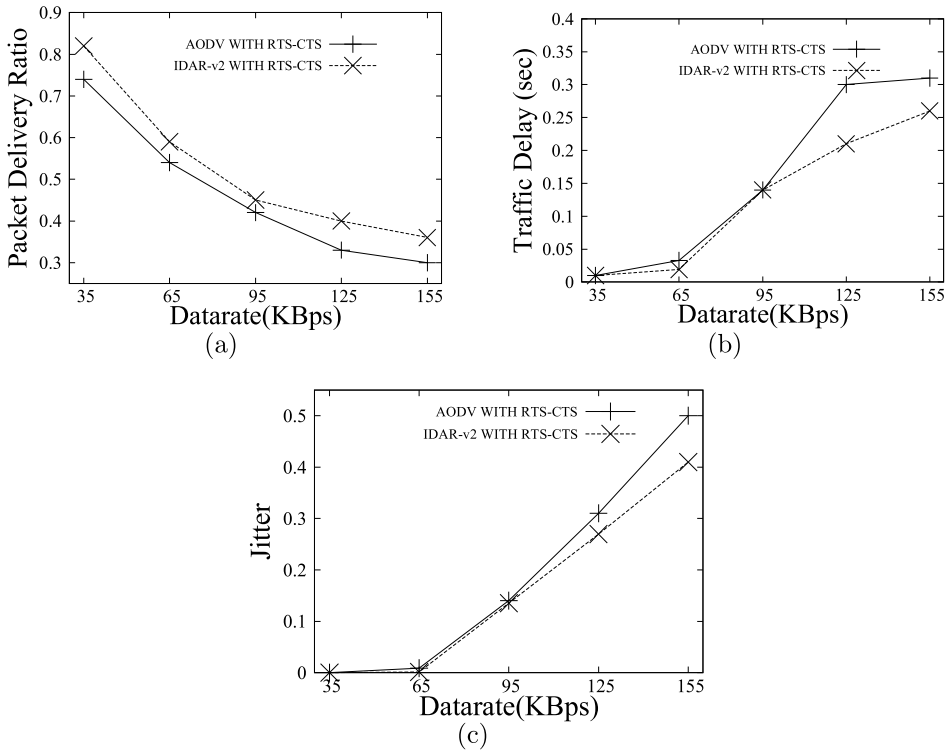

Figure 4.13: Comparison of (a) packet delivery ratio (b) delay (c) jitter

ratio, delay, and jitter of the data flows are averaged over 10 runs for four different routing protocols: AODV, MARIA, IDAR-v1, and IDAR-v2. Jitter is measured by the variance of the delay obtained from multiple simulations. The results, obtained with RTS/CTS and ACK disabled, are shown in Figure 4.11. It is observed that both IDAR-v1 and IDAR-v2 provide significantly better performance than AODV in terms of average delivery ratio, delay, and jitter. While MARIA gives almost same delivery ratio as IDAR-v2, IDAR-v2 provides a significant improvement in delay and jitter over MARIA. The reason is that MARIA only chooses the route based on higher residual bandwidth i.e. lesser interference, without considering the delay. However, delay is an important parameter for determining quality in many applications.

We next present the performance of *IDAR-v2* with RTS/CTS while varying the number of flows. Figure 4.12 shows the comparison of average delivery ratio, delay and jitter of AODV and *IDAR-v2* with RTS/CTS when the transmission rate is set to

65 KBps. It is observed that *IDAR-v2* with RTS/CTS gives higher delivery ratio and lower delay and jitter than AODV. In Figure 4.13, we fix the number of flows to 10, and vary the data rate. The results show that *IDAR-v2* gives better delivery ratio, delay, and jitter than AODV at all data rates. This is because of the ability of IDAR to choose higher quality routes than shortest routes to gateways. From Figure 4.13 we can observe that for lower load the improvement of delay and jitter in IDAR over AODV is not very significant, but for higher load, the difference is significant. Thus our proposed scheme is more efficient in heavy loads.

4.5 Discussions

In this chapter, we develop a route quality metric for wireless mesh networks that can be applied to improve the packet delivery and delay performance of multi-hop communications. We propose a routing protocol that applies this metric and evaluate its performance in multihop wireless networks. The proposed quality metric is developed using offline measurements and validated from simulations. The proposed quality aware routing scheme is extended to a WOBAN model that involves multiple gateway nodes, requiring anycast routing, in Chapter 5. Our final goal is to extend this quality aware routing on a WOBAN architecture that is characterized by multiple gateways and the mesh routers are equipped with multiple radio-interfaces that reduce the co-channel interferences and contention to improve the overall network performance, which is discussed in Chapter 6.

CHAPTER 5: ANYCASTING BASED ROUTING PROTOCOL IN MULTI-GATEWAY WOBAN

We now address the anycasting problem by considering a multi-gateway WOBAN where the wireless access network can connect to the fiber backbone through one of several gateways. Here, the problem is to determine the optimum gateway selection by considering the options for routing in the wireless mesh network to the candidate gateways to maximize the overall quality of all active traffic flows in the network. Multi-gateway WOBANs with anycast routing has several features that can be utilized for improving the quality of service of wireless connections. Firstly, multiple gateways provide redundancy, which help in reducing congestion on any single gateway. In addition, the possibility for cooperative selection of gateways for all active users and their corresponding routes enables better utilization of resources in the network. However, this leads to a joint gateway selection and routing problem, which is computationally hard. In addition, the network parameters may vary with time, which increases the complexity of the problem. For instance, as illustrated in Fig-

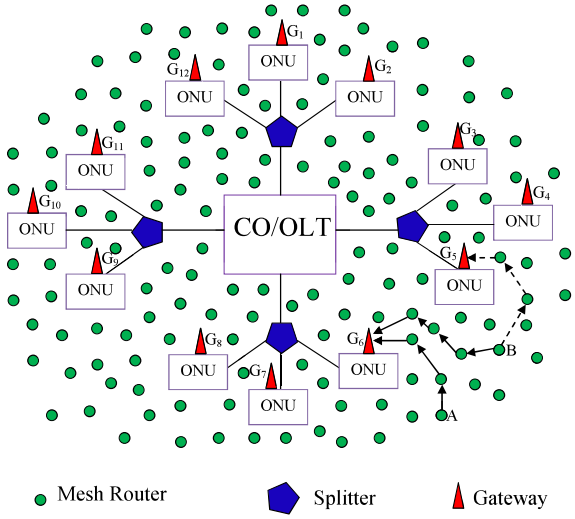

Figure 5.1: WOBAN with multiple gateways.

ure. 5.1, an user B may be initially connected to G_6, which provides the best quality of service among a number of available gateway nodes in the absence of any other active node in its vicinity. However, if user A becomes active after B is connected, it may be necessary to switch B to G_5 and connect A to G_6 so that the two active routes do not interfere with each other and the overall performance is optimized. Such decisions depend on a number of parameters that affect the quality, which are evaluated at different locations and times, making the optimization difficult.

We consider a centralized approach to address this issue, where it is assumed that the gateway nodes are connected by an infrastructured network such as an optical fiber network, and collaborate with each other for determining the optimum gateway and route selections for all active nodes in the network. Our problem of anycast based routing can be described as follows: consider a scenario with n sources $\{S_1, S_2, ..., S_n\}$ and a group of m gateways $\{G_1, G_2, ..., G_m\}$ where $1 \leq m \leq n$. The optimum gateway selection problem is to assign the n sources to m gateways so that the aggregate quality of all routes is maximized. This problem can be formulated as a $0-1$ *integer programming problem* as follows:

$$Maximize \sum_{i=1}^{n} \sum_{j=1}^{m} Q_{S_iG_j} X_{S_iG_j} \tag{5.1}$$

subject to

$$\sum_{j=1}^{m} X_{S_iG_j} = 1, \quad (1 \leq i \leq n) \tag{5.2}$$

$$X_{S_iG_j} = 0 \text{ or } 1 \ (1 \leq i \leq n) \ (1 \leq j \leq m) \tag{5.3}$$

where $Q_{S_iG_j}$ is the quality of the best route between S_i and G_j and $X_{S_iG_j}$ is a binary variable used for gateway selection: if the best gateway chosen for S_i is G_j, then $X_{S_iG_j}$ =1; otherwise $X_{S_iG_j}$ =0. Constraint (2) states that S_i can transmit all its packets to one gateway only.

5.1 Time Complexity of Optimal Gateway Selection

The problem of optimal gateway selection is a complex optimization problem. The complexity of this problem can be proven to be *NP-hard*. We prove this using reductions from the *3-PARTITION* problem. The *3-PARTITION* problem is to decide whether a given multiset of integers can be partitioned into triples that all have the same sum. More precisely, given $\{a_1, a_2, ..., a_{3p}\}$ integers, does there exist a partition $\{A_1, A_2, ..., A_p\}$ of $\{1, 2, ..., 3p\}$ such that $\mid A_i \mid$=3 for $i = 1, ..., p$ and $\sum_{j \in A_i} a_j = \sum_{j \in A_k} a_j$, for any $1 \leq i, k \leq p$.

From an instance of *3-PARTITION*, we construct an instance of optimal gateway selection problem as follows: Choose $n = 3p$, $m = p$, $\sum_{i=1}^{n} x_{S_i G_j} = 3$ for each i and set q_{ij}=a_j, $j = 1, 2, ..., n$; $i = 1, 2, ..., m$. Since *3-PARTITION* problem is *NP-complete*, from our reduction it follows that the optimal gateway selection problem is also *NP-hard*.

As the problem of optimal gateway selection is *NP-hard*, we propose two heuristics to solve this problem. Our solutions are centralized, where we assume that the set of gateway nodes communicate with each other through optical links and determine the optimum/sub-optimal routes for the network. We propose two versions of routing protocols named *Gateway Selection and Quality Aware Routing (GSQAR-v1)* and GSQAR-v2.

5.2 Gateway Selection and Quality Aware Routing-version 1

The proposed scheme is illustrated in Figure. 5.2, where we assume three sources S_1, S_2, S_3 and two gateways G_1, G_2 and the network is assumed to be a grid structure. Each small box represents a node and each box is assumed to be a unit square. We define *rect(S_i, G_j)* as the rectangular region whose diagonal is the line connecting S_i and G_j. The scheme follows the following steps:

- First, we consider costs associated with routing over each box, which are initialized to zero. For each source S_i and gateway G_j, the scheme chooses a route

inside *rect(S_i, G_j)*, which minimizes the cost. The route cost is entered in each box in this rectangular region, which is equal to the distance between S_i and G_j (distance is measured as the sum of horizontal and vertical distance in Figure. 5.2). Initially, each source considers routes to all gateways and marks the costs in the boxes. The costs for multiple gateways are superimposed on all boxes. For instance, in Figure. 5.2(a), all the boxes in the right of S_1 is set to 6, which is the distance between S_1 and G_1. Similarly, the boxes on the left of S_1 are assigned to 3. The column that consists of S_1 is assigned to 6+3=9 where two regions (*rect(S_1G_1)*) and (*rect(S_1G_2)*) overlap. Similar process is continued for S_2 (Figure 5.2(b)) and S_3 (Figure. 5.2(c)).

- Among all the boxes consisting of $\{S_1, S_2, ..., S_n\}$, the box with minimum cost is chosen first. Then path selection is based on traversing along neighboring boxes of minimum cost, i.e. comparing the costs of the boxes to the right/left-/up/down of the current box, until any gateway is reached. We cannot move to the boxes that have a cost of zero. The nodes that are visited to reach the gateway gives the route from source to the gateway. If we move up, we cannot move down again. The same rule applies in the down-up, left-right and right-left directions. If more than one box in left/right/up/down of the current box have minimum cost, the box that leads to the nearest gateway is selected. Once the route between any S_i and G_j is found, all the costs of boxes in *rect(S_i, G_k)* ($k \neq j$) are decremented by the distance between S_i and G_k. Next, all the unvisited boxes in *rect(S_i, G_j)* are decremented by the distance between S_i and G_j. Once the route from S_i is found, S_i is marked as a *visited_source*. For instance, in Figure. 5.2(d), the box consisting of S_2 is of minimum cost. So, we start with S_2 and follow the boxes with minimum cost until we reach gateway G_2. After that all the boxes in *rect(S_2, G_1)* are decremented by 7. All the unvisited boxes in *rect(S_2, G_2)* are also decremented by 6.

- After the route from a source S_i and gateway G_j is found, all the boxes that are in the interference range of any node in the new route are interfered. Thus we increment the cost of these boxes by the distance of S_i and G_j. In Figure. 5.2(d), all the boxes in the interference range of the new route are incremented by 6.

- Next, boxes consisting of *unvisited_sources* are searched and the box with the minimum cost is selected. Then the same technique is repeated until and unless all $\{S_1, S_2, ..., S_n\}$ get a route towards any gateway. This is depicted in Figure. 5.2(e) and Figure. 5.2(f).

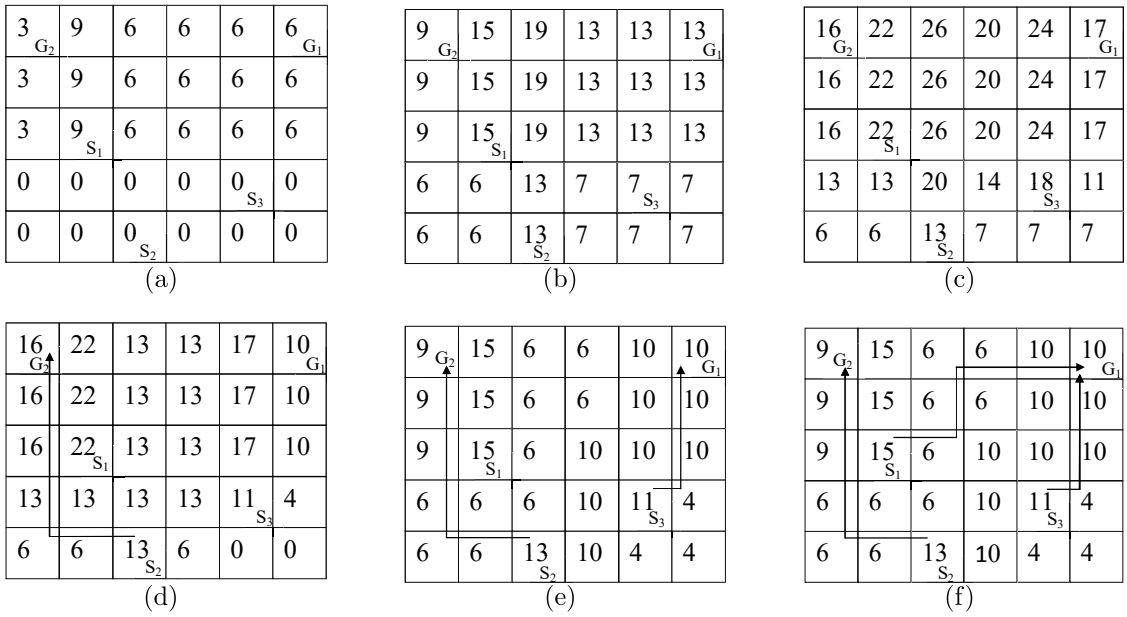

Figure 5.2: Proposed gateway selection scheme in grid environment.

The scheme is similar to how water flows from higher altitude to lower altitude. This is illustrated in Figure. 5.3 where Figure. 5.3(a), (b), (c) corresponds to Figure. 5.2(a), (b), (c) respectively. The values in the colorbars are proportional to the altitudes. The altitudes are nothing but the number in each blocks in Figure. 5.2(a), (b), (c) which are proportional to interference. Thus if we put some water in any source, it goes from high altitude to low altitude, thus high interference area to low interference

area. But the constraint is that if the water starts from S_i, then it should go in the area of $rect(S_i, G_j)$ for all $G_i \in G$. Another constraint is that the water cannot reverse it's direction, i.e. if it takes right once, it cannot take left and this is true for all directions. If there arise any situation when the water is in the lowest point and does not reach any gateway, then it choose the lowest altitude around it's neighboring areas (even if the neighboring areas are at higher altitude than it's current position) and reach the gateway.

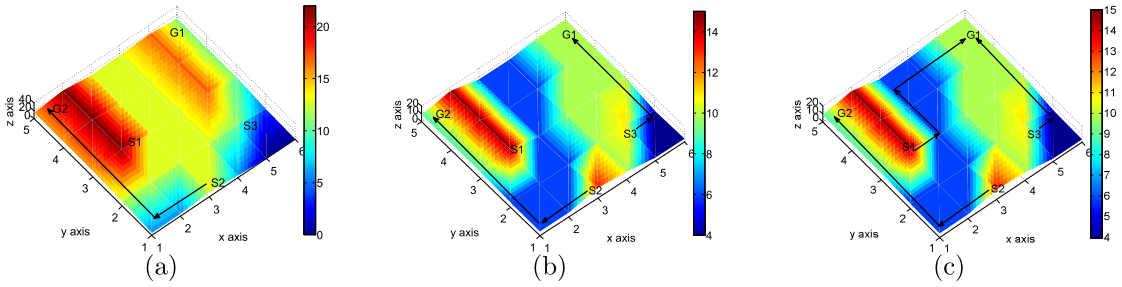

Figure 5.3: Proposed gateway selection scheme in grid environment.

The above scheme does not depend on the order of the flows. But in a real network, flows come one after another and that may create a problem. Let us assume in Figure. 5.2, S_3, S_1 and S_2 are activated in sequence. First S_3 chooses gateway G_1 and then S_1 chooses G_2. Next when S_2 becomes active, according to the scheme, S_1 should switch to G_1. But this switching degrades the network performance. For more number of sources the number of switching increases, thus making the scheme inefficient. To avoid this, the overall quality (the quality is calculated based on the quality metric from equation (4.7)) of all the routes before and after switching is calculated. *If the improvement after switching is significant*, only then the sources switch the gateways. The algorithm of gateway selection is depicted in Algorithm 2.

5.3 Gateway Selection and Quality Aware Routing-version 2

As GSQAR-v1 is difficult to implement for a very general network topology, we design another version of GSQAR for general networks. In this scheme, when a

Algorithm 2. Gateway selection scheme for GSQAR_v1

```
INPUT : G=set of gateways; S=set of sources; T=neighbor connectivity graph
OUTPUT : a set of paths from each source to one gateway
for each vertex v ∈ V do
    Draw a horizontal box around v
    Draw a vertical box around v
end for
for each vertex v ∈ V do
    cost(v)=0; put 0 in all the boxes
end for
S'=S
for each S_i ∈ S' do
    for each G_i ∈ G do
        d_ij=distance(S_i, G_j)
        cost_box(v)=cost_box(v)+d_ij
        Put cost_box(v) in all rectangular boxes in region [(S_ix, S_iy), (S_ix, G_jy), (G_jx, S_iy), (G_ix, G_jy)]
    end for
end for
Sort S' according to cost_box(S_i)
while not_empty(S') do
    while current_node ∉ G do
        n_i=minimum(S)
        Move to right, left, up or down based on which box has minimum cost
        if previous move is right/left/up/down respectively then
            Do not move left/right/down/up respectively
        end if
        if among right, left, up or down more than one boxes have minimum cost then
            Follow the path that leads to the nearest gateway
        end if
        Record the nodes in visited_node(n_i)
    end while
    S' = S'\n_i
end while
```

source becomes active (i.e. needs to connect to a gateway), it broadcasts a *RREQ* packet, which carries information about the route that it traces. This information is used by the gateway node to compute the route quality using equation (6.1) and neighborhood and activity information for all nodes involved in the route. For each source S_i, a gateway keeps the first N routes that it obtains from the arriving *RREQ* packets. These routes are called *candidate routes (CR)*. So, *CR*s from S_i to G_j can be written as $\{R^p_{S_iG_j}\}, p = 1, 2, ..., N$, where $R^p_{S_iG_j}$ is the route taken by the pth *RREQ* packet from S_i to G_j. The qualities of $R^p_{S_iG_j}$ are represented as $Q^p_{S_iG_j}$. Table 5.1(a) shows the *quality table (QT)* for an instance of three active sources and two gateways, where qualities of the best routes among the candidate routes for all source-gateway pairs are stored. So, $QT = \{Q_{S_iG_j}\} \quad \forall S_i \in S$ and $\forall G_j \in G$ where $Q_{S_iG_j} = max\{Q^p_{S_iG_j}\}, p = 1, 2, ..., N$ and the corresponding route is denoted as $R_{S_iG_j}$. So, gateway and route selection for the first source that becomes active is determined

by the highest $Q_{S_iG_j}$ in the QT corresponding to that source.

When a new source becomes active, the algorithm compares the average route quality for all active sources as obtained from the following two methods for gateway and route selection: (a) *Incremental method:* where all previously assigned routes are unchanged and gateway and route selection for the new source is performed based on the best $Q_{S_iG_j}$ value for the new source by considering *interflow interference* from existing routes, and (b) *Global method:* where the best set of gateways are calculated for all active sources together, assuming that existing routes can be switched to any other route in its *CR*. This gives a better solution, but not necessarily the globally optimum one. If the average quality using the *global* solution is greater than the *incremental* solution by a significant amount, then those selections are chosen. Else, the algorithm prefers the *incremental* solution, to avoid *frequent switching* (as frequent switching may lead to quality degradation). When more than one route have the same quality, the shortest route is selected.

We take an example to describe the process. Consider that S_1 and S_2 are active and connected to G_2 and G_1, respectively, when S_3 becomes active. Here, the *incremental* solution consists of $S_1 \rightarrow G_2$, $S_2 \rightarrow G_1$ and $S_3 \rightarrow G_i$, where $G_i \in \{G_1, G_2\}$ is the gateway corresponding to the highest entry for S_3 in QT assuming the interflow interference from $S_1 \rightarrow G_2$ and $S_2 \rightarrow G_1$. Let us assume that $Q_{S_1G_2} + Q_{S_2G_1} + Q_{S_3G_i} = Q^{inc}_{total}$.

The *global* solution is obtained as follows: the highest entry in the QT table constructed without any interflow interference (shown by $Q_{S_iG_j}$ in Table 5.1(a)) is selected first. Assume this entry is $S_1 \rightarrow G_2$. Next the quality of the candidate routes for the remaining sources (S_2, S_3) are recalculated by considering the *inter-flow interference* from $S_1 \rightarrow G_2$, as shown by $\dot{Q}_{S_iG_j}$ in Table 5.1(b). The highest quality among these entries is selected next, which in our example is $\dot{Q}_{S_3G_1}$. Consequently, S_3 is routed to G_1, as shown in Table 5.1(c). This procedure is repeated (recalculating the qualities of the candidate routes with existing interference of $S_1 \rightarrow G_2$ and $S_3 \rightarrow G_1$),

Table 5.1: Quality table

(a) Initially

	G_1	G_2
S_1	$Q_{S_1G_1}$	$Q_{S_1G_2}$
S_2	$Q_{S_2G_1}$	$Q_{S_2G_2}$
S_3	$Q_{S_3G_1}$	$Q_{S_3G_2}$

(b) After $S_1 \rightarrow G_2$ is selected

	G_1	G_2
S_1	$Q_{S_1G_1}$	$\mathbf{Q_{S_1G_2}}$
S_2	$\dot{Q}_{S_2G_1}$	$\dot{Q}_{S_2G_2}$
S_3	$\dot{Q}_{S_3G_1}$	$\dot{Q}_{S_3G_2}$

(c) After $S_3 \rightarrow G_1$ is selected

	G_1	G_2
S_1	$Q_{S_1G_1}$	$\mathbf{Q_{S_1G_2}}$
S_2	$\ddot{Q}_{S_2G_1}$	$\ddot{Q}_{S_2G_2}$
S_3	$\mathbf{\dot{Q}_{S_3G_1}}$	$\dot{Q}_{S_3G_2}$

(d) After $S_2 \rightarrow G_2$ is selected

	G_1	G_2
S_1	$Q_{S_1G_1}$	$\mathbf{Q_{S_1G_2}}$
S_2	$\ddot{Q}_{S_2G_1}$	$\mathbf{\ddot{Q}_{S_2G_2}}$
S_3	$\mathbf{\dot{Q}_{S_3G_1}}$	$\dot{Q}_{S_3G_2}$

for S_2 as shown in Table 5.1(d), which indicates the selection of $S_2 \rightarrow G_2$ in the last step. All selected entries in QT are indicated in larger font. Thus, the *global* method results in $S_1 \rightarrow G_2$, $S_2 \rightarrow G_2$, $S_3 \rightarrow G_1$, where the average quality is $Q^{glo}_{total} = Q_{S_1G_2} + Q_{S_2G_2} + Q_{S_3G_1}$. Now, if $Q^{glo}_{total} - Q^{inc}_{total} > \tau_Q$, where τ_Q is a predefined parameter, then the selection from the *global* method are selected, otherwise those from the *incremental* method are selected. The process can be repeated for additional sources. The algorithm is shown in Algorithm 3.

Algorithm 3. Gateway selection scheme for GSQAR_v2

INPUT : G=set of gateways; S=set of sources; All N routes carried by RREQ for each S_i to G_j, $RT^p_{S_iG_j}$ $\forall$ $S_i \in S, G_i \in G, p = 1, 2, ..., N$.
OUTPUT : A set of paths from each source to one gateway
Initialize chosen routes $AR = \phi$
Step 1: Calculate $Q_{S_iG_j} \forall S_i \in S, G_j \in G$, AR is the background traffic and store it in QT.
Step 2: Choose $Q_{S_pG_q} = max\{Q_{S_iG_j}\} \forall S_i \in S, G_j \in G$ from QT
if S_p is assigned to some other gateway $G_r \neq G_q$ and $Q^{glo}_{total} - Q^{inc}_{total} > \tau_Q$ **then**
  S_p is assigned to G_q; $AR = AR \cup RT_{S_pG_q}$; $S = S \setminus S_p$;
end if
Step 3:
if $S \neq \phi$ **then**
  go to Step 1
end if

5.4 GSQAR Routing Protocol

The proposed routing protocol GSQAR can be described as follows.

- Route Discovery: Route discovery is same as for IDAR.
- Route Selection: After getting the RREQ packets, the destinations (gateways)

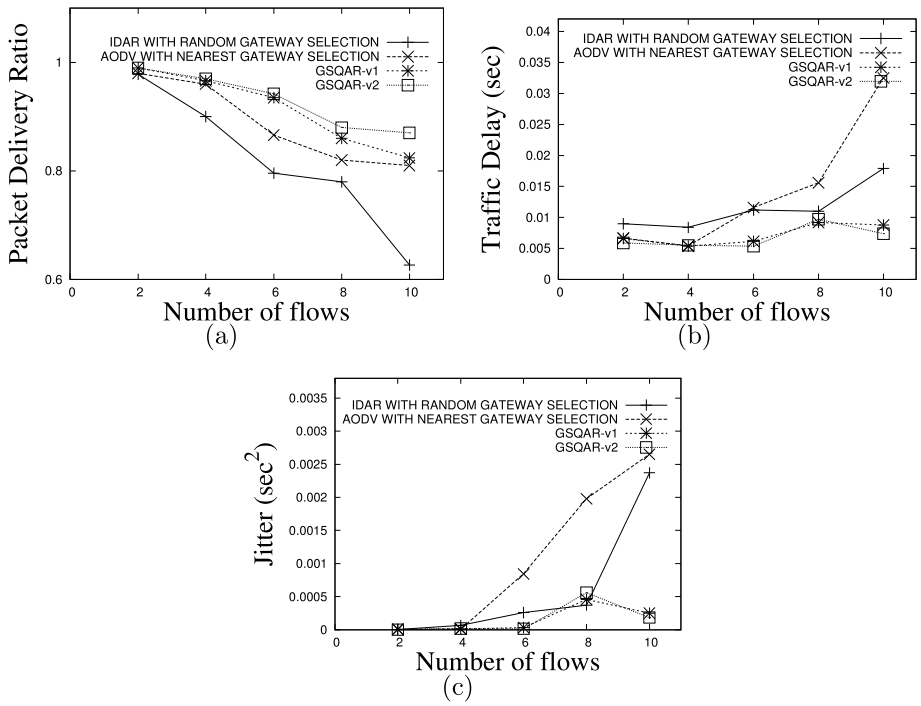

Figure 5.4: Comparison of (a) throughput (b) delay (c) jitter.

collaborate with each other to obtain the best gateway for each source by applying Algorithm 3. Then only the best gateway sends the RREP towards source, that consists of all the intermediate nodes from source to destination. All intermediate nodes update their routing table based on this RREP packet. When the source receives RREP, it starts transmitting DATA packets to the best gateway. When there is any route switching, the gateway informs the source about the switching. The source then route DATA packets based on that route only.

• Route Maintenance: Route maintenance is same as for IDAR.

5.5 Performance Evaluation of GSQAR

We now present the performance of the proposed *GSQAR* routing protocol and compare it with anycasting mechanisms employing other routing metrics and gateway selection policies. In particular, we consider *AODV based nearest gateway selection scheme*, which is a popular ad hoc routing protocol, and the *IDAR based random gateway gateway selection scheme* presented in [3]. We also compare the performance

of *GSQAR-v2* with *GSQAR-v1* presented in [6]. We use the *network simulator–2 (ns2)* [50] for all performance evaluations on a grid network consisting of 30 nodes. We choose two gateways and keep them fixed. The active sources are selected randomly, with each source generating *UDP* traffic with a transmission rate of 65 KBps for a period of 200 seconds. All results are averaged over 10 such simulations.

The performance is measured in terms of the average throughput, delay and jitter with different number of data flows, i.e. number of active sources. The results are shown in Figure. 5.4. It is observed that the two *GSQAR* schemes perform better than both *IDAR based random gateway selection scheme* and *AODV with nearest gateway selection scheme* in terms of throughput, delay, and jitter. This shows the benefits of anycasting for achieving the best overall quality. It is observed that *GSQAR-v2* provides higher throughput than *GSQAR-v1*, while the delay and jitter performances are similar for both the schemes.

Finally, we take a specific example to demonstrate the potential benefit of *GSQAR* over nearest gateway selection and random gateway selection. We consider the scenario shown in Figure. 5.5(a), where the sources, which are marked by shaded circles, are chosen to lie close to one another to increase the probability of contention for channel access. It is observed that when using the nearest gateway selection scheme, all sources choose the gateway 24, thereby causing heavy contention and interference that affects the throughput. On the other hand, *GSQAR* chooses gateways intelligently to give better performance. The results are shown in Figure. 5.5(b)-(e). Figure. 5.5(c)-(e) again show the superiority of *GSQAR* over nearest gateway and random gateway selection schemes in terms of throughput, delay and jitter. Figure. 5.5(b) confirms the fact that even if a large number of packets in *GSQAR* do not choose the nearest gateway, the throughput, delay and jitter performance are still far better than nearest gateway selection scheme.

5.6 Discussions

In this chapter, we develop a quality aware anycast routing protocol *GSQAR*, which uses a quality metric that is built on offline measurements of characteristics of data packet transmissions in a multihop network. Simulation experiments demonstrate that *GSQAR* is effective in improving both the throughput and delay performance in mutlihop environments in comparison to schemes using nearest or random gateway selection with shortest path routing. In Chapter 6, we extend our proposed quality qware anycast routing approach to incorporate multiple channels with multiple radios for each mesh router to reduce co-channel interference as well as channel contention.

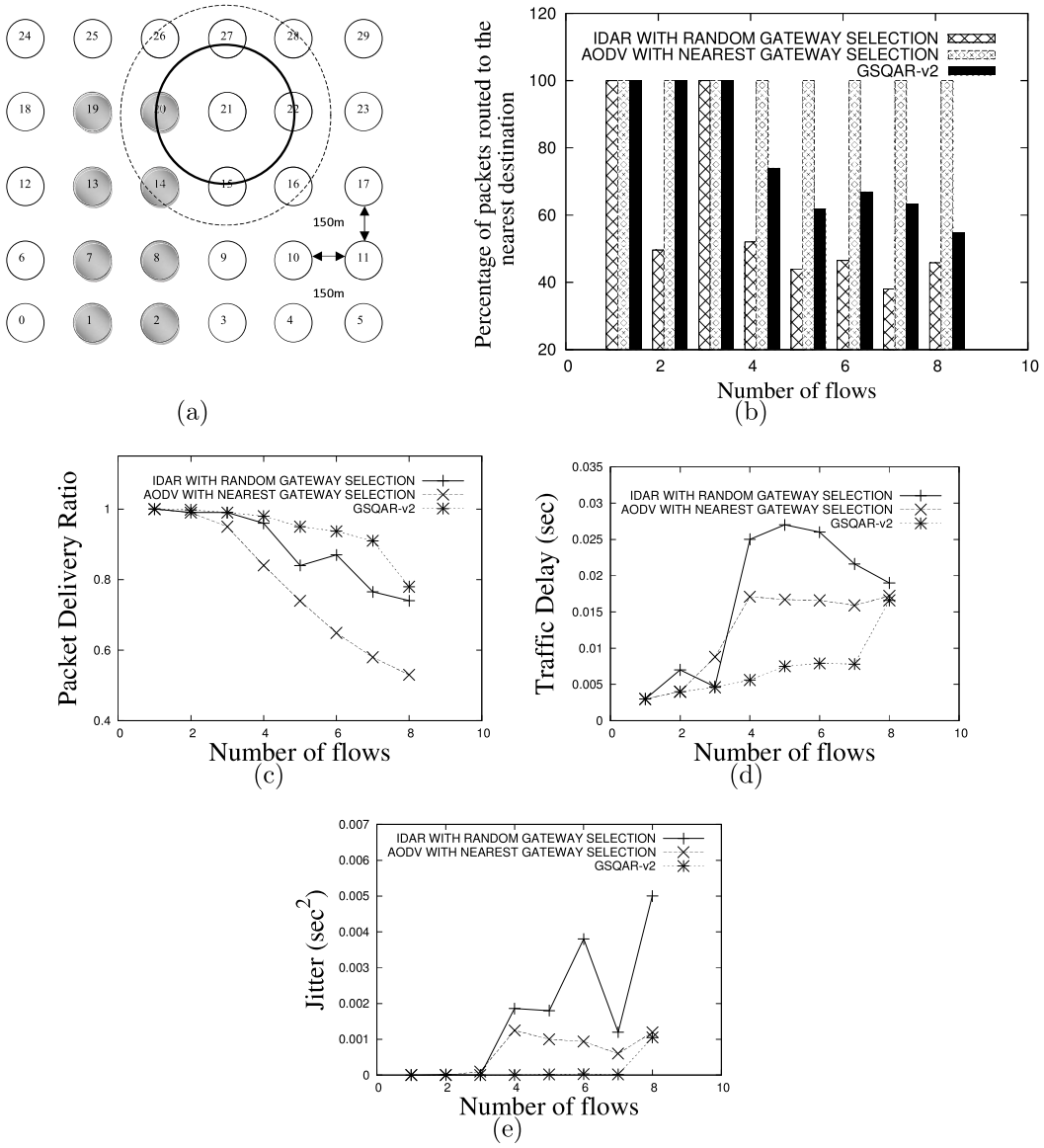

Figure 5.5: (a) Simulation scenario, 19, 20, 13, 14, 7, 8, 1, 2 are activated in sequence, 24 and 29 are gateways, interference and transmission range are dotted and dark circle respectively. (b) Comparison of percentage of packets routed to the nearest gateway. (c) Throughput (d) delay (e) jitter.

CHAPTER 6: JOINT ROUTING AND CHANNEL SELECTION IN MULTI-CHANNEL MULTI-GATEWAY WOBAN

In this chapter, we consider WOBANs that are equipped with multiple wireless gateways, under the assumption that wireless routers have multiple radio interfaces, that are capable of operating on multiple channels. Having multiple wireless interfaces greatly reduces wireless interference and channel contention, which results in higher network throughput. We assume that the gateways are connected to some infrastructured network as in WOBAN so that they can collaborate with each other to select the routes for all sources and also the channel for each link in that route. For this the gateways need to know the positions of all mesh routers. In our scheme, the gateways wait for the first N RREQ packets from each source, track the route traversed by each RREQ packet, and sends a RREP packet through the route that maximizes the quality after channel assignment. For doing this, the gateways have to assign channels to all the routes and measure the quality. For multi-channel WOBAN, we define the route quality metric for route R of length v as follows:

$$Q(R) = \frac{\prod_{f=1}^{v} P_S(I_f)}{\sum_{f=1}^{v} T_d(n_{af}, n_{bf}) + \sum_{f=1}^{v} s_d \times y_f} \tag{6.1}$$

where, s_d is the switching delay for an interface to switch from one channel to another and y_f is a binary variable which is 1 when the interfaces of link f switch and 0 otherwise. For positive switching delay, this model prefers routes that avoid frequent switching of channels.

For channel assignment, we use conflict graph to model wireless interference. We first form the conflict graph (discussed in Section 6.1) and use a vertex coloring scheme (where colors represent channels) for channel assignment. From this point onwards we

use the word *channel* and *color* interchangeably. But as the vertex coloring problem is an *NP-complete* problem [52], we apply the *genetic algorithm* [53] to solve it, which has been successfully applied to several problems to avoid a brute-force-search. We propose a novel mechanism to reduce the number of vertices on which we apply the genetic algorithm, to reduce the convergence time. This is achieved by planarizing the conflict graph using *vertex deletion* (in Section 6.3), applying backtracking to color the planar subgraph (in Section 6.4) and then using the genetic algorithm on the vertices that are not part of planar subgraph and those that violate the interface constraint (in Section 6.5). The details of the scheme is described in the following sections.

6.1 Conflict Graph

Our approach for maximizing the quality metric through joint route and channel selection requires an effective representation of co-channel interference, which we model using the conflict graph. Consider a wireless mesh network where all routers have identical transmission ranges (denoted by R) and the interference range is denoted by $R' \geq R$. For each link $i - j$ in the connectivity graph, the *conflict graph* [54] contains a vertex. There exists an edge between two nodes (say, $A - B$ and $C - D$) in the conflict graph if the corresponding links interfere in the connectivity graph. A transmission from A to B is successful if no other node located R' from B transmits at the same time. In the presence of RTS/CTS, it is additionally required that all nodes located within R' from A refrain from transmission. Thus, there is an edge between $A - B$ and $C - D$ in the conflict graph if either A or B are located within distance R' from C or D. Figure 6.1 shows an example illustrating this model.

Hence, if there is a link between two vertices in the conflict graph, then those two vertices interfere each other, thus we have to assign different channels to these two vertices (vertices in the conflict graph are links in the connectivity graph). This is similar to the vertex coloring problem, i.e. no two vertices in the conflict graph

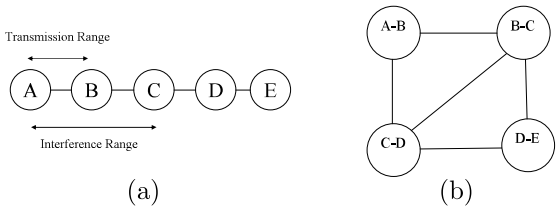

Figure 6.1: (a) Connectivity graph and (b) Conflict graph.

having a link have the same color. More precisely, if $G = (V, E)$ be an undirected graph with n vertices then a coloring of G is a mapping $\pi : V \rightarrow C$ such that for any two vertices x and y if $(x, y) \in E$, then $\pi(x) \neq \pi(y)$. So, we can formulate the channel assignment problem as a vertex coloring problem.

6.2 Planar Graph and the Four Color Theorem

In graph theory, a *planar graph* is a graph that can be embedded in a plane, i.e. it can be drawn on a plane in such a way that its edges intersect only at their endpoints [55]. On the other hand, graphs that are not planar are called *non-planar graphs*. According to *four color theorem* all planar graphs are four colorable. Thus, if we can get the planar subgraph of the conflict graph, we can color that subgraph with four colors.

6.3 Vertex Deletion to Get the Planar Subgraph

We use *vertex deletion* to get the planar subgraph of the conflict graph. The Boyer and Myrvold planarity test [55] is used to check whether a graph is planar or not in linear time. First the planarity of the conflict graph G is checked. If it is non-planar, the vertex with the highest degree is removed from G and placed in *genetic-colored-list (GCL)*, and then the planarity condition is checked again on the remaining graph (line 3-6 in Algorithm 4). This vertex deletion process is repeated until the remaining graph becomes planar. At the end of this process, GCL consists of the removed vertices, all the other vertices are stored in *fixed-colored-list (FCL)*. Thus, the subgraph consists of FCL and their edges is planar.

Algorithm 4. Function Vertex Deletion (Input graph G)

```
1: GCL = FCL = NULL
2: Sort v_i ∈ G in decreasing order of vertex degree
3: while G ≠ PLANAR do
4:     G = G \ v_i, v_i is of maximum degree in G
5:     GCL = GCL ∪ v_i
6: end while
7: FCL = G
8: return GCL and FCL
```

6.4 Algorithm for Coloring the Planar Subgraph

Let $\tilde{G}$ be the planar subgraph that consists of vertices in FCL and their corresponding edges. Now, according to the *Four Color Theorem*, $\tilde{G}$ can be colored with 4 colors. So, we propose an algorithm (line 4 - line 23 in Algorithm 5) based on *backtracking* to color $\tilde{G}$. This is explained with the help of Figure 6.2, where the graph in Figure 6.2(a) is the planar subgraph and Figure 6.2(b) shows it's backtracking tree. Let us assume that at first all the vertices can use RED, BLUE, GREEN and BLACK that are indexed as 1, 2, 3, 4 respectively in the *Color* array in Algorithm 5. In Algorithm 5, the nodes in FCL are denoted as $\{v_1, v_2, ..., v_n\}$. We start with vertex A and color it RED. So, all the neighbors of A cannot use RED. Thus B can use only BLUE, GREEN and BLACK. In this way if we proceed and if C, D, E and F are colored with RED, BLUE, GREEN and BLACK respectively, then there is no color left for E. Thus we need to backtrack and color D, E and F with GREEN, BLUE and GREEN respectively, and then G is colored with BLACK. This process of backtracking is guaranteed to give a 4-coloring to $\tilde{G}$. After coloring the subgraph $\tilde{G}$ in this fashion, if the number of channels used (C_u) in any node in the connectivity graph is more than the number of interfaces (I), then the interface constraint is violated. Thus, for each node in the connectivity graph, we check the interface constraint and if this constraint is violated, $C_u - I$ links (vertices in conflict graph) around that node are selected randomly and added to GCL (line 24). Then the GCL is passed to the *genetic algorithm* (line 25).

Even if the worst case complexity of backtracking is exponential with the number

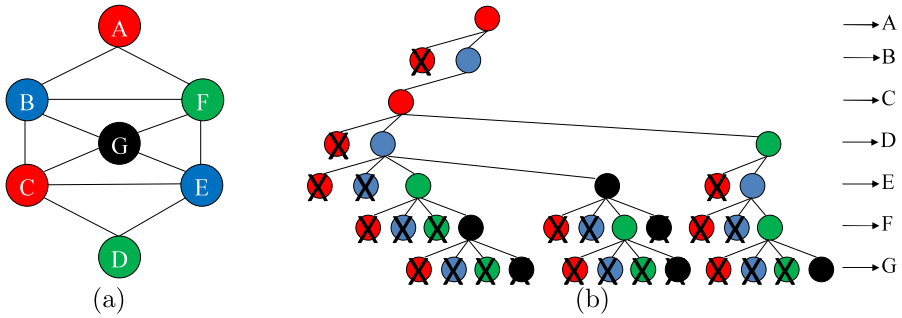

Figure 6.2: (a) A planar graph and (b) Backtracking tree of graph.

of nodes in the conflict graph, as all the nodes have only 4 colors, the complexity is not that high. At the same time as there are a number of solutions for a vertex coloring problem, we do not need to explore the whole tree. As an example, if we explore the whole search tree of n vertices, we need to explore $1 + 4 + 4^2 + ... + 4^{n-1}$ $= \frac{4^n-1}{3}$ nodes. At the same time we get a large number of solutions. For instance, a *tree* and a *cycle* of n vertices can be colored in $t(t-1)^{n-1}$ and $(t-1)^n + (-1)^n(t-1)$ ways respectively, with t colors [56]. Thus, the number of solutions with 4 colors for a tree and a cycle are 4.3^{n-1} and $3^n + 3.(-1)^n$, respectively. As a conflict graph is composed of trees and cycles, the search tree will have a very large number of solutions. Hence, for getting one solution, we need to search a small fraction of the whole search tree. Let us consider the effectiveness of this backtracking strategy to reduce the convergence time of the genetic algorithm, which is to be performed on the vertices in GCL. As mentioned in [57], the number of vertex deletions required to make the non-planar graph $K_{m,n}$ planar is given by $\min\{m, n\} - 2$. Hence, for $m = n = 100$, the number of vertex deletions is 98. Thus FCL consists of 102 vertices, whereas GCL consists of only 98 vertices instead of 200. Consequently, in this case we can reduce the length of GCL by around 50% which results in reduced convergence time of the genetic algorithm. It must be noted that in the worst case (when the conflict graph is a complete graph), almost all the vertices are in the GCL,

but in reality, conflict graphs are hardly complete graphs. Thus on an average, our scheme is able to reduce the convergence time of the genetic algorithm.

6.5 Genetic Algorithm for Channel Selection

Genetic algorithms are probabilistic techniques that mimic the natural evolutionary process. A genetic algorithm maintains a population of candidate solutions. This has the potential to better explore the search space. Each candidate solution in the population is encoded into a structure called the *chromosome*. To each chromosome, a value called *fitness value* is assigned, which represents the quality of the candidate solution. The process of assigning fitness values to chromosomes is called *evaluation*. A selection process simulates the *survival of the fittest* paradigm from nature. Better-fitted chromosomes have higher chances of surviving to the next generation. The number of chromosome per generation is constant.

As in natural life, offspring chromosomes are obtained from parent chromosomes. One possibility is for two parents to exchange encoded information and thus creating two new offsprings; this process is called *crossover*. Another possibility is to alter the encoded information in a chromosome obtaining a slightly different new chromosome; this process is known as *mutation*. Some other chromosomes simply survive unaltered, while others die off. Mutation and crossover are referred to as *genetic operators*.

- Genetic Representation: Let U is the number of vertices in GCL. Let us define a chromosome as a vector $(c_1, c_2, ..., c_U)$, where $c_i \in S_C$ is the channel/color assigned to vertex i. As an example, if $U = 6$ then chromosome 314252 means vertices $1, 2, 3, 4, 5, 6$ are assigned to channels $3, 1, 4, 2, 5, 2$ respectively. We assume that there are M chromosomes in a *mating pool*. The fitness value of each chromosome is the overall network quality based on the channel assignment from each chromosome. For all vertices in the GCL, initially we assign random channels in between 1 and C and make M chromosomes so that the interface constraint is satisfied.

- Selection Process: Selection is the process of choosing individual chromosomes

to participate in reproduction. After getting the initial M chromosomes in the mating pool, the fitness values of all the chromosomes are calculated based on the quality metric. We use the well known *elitism* selection process, where the $M_e < M$ best chromosomes (as determined from their fitness evaluations) are placed directly into the next generation. This guarantees the preservation of the M_e best chromosomes at each generation. Note that the elitist chromosomes in the original population are also eligible for selection and subsequent recombination. Next, $M - M_e$ parents are selected based on *roulette wheel* selection process. So, better chromosomes have higher chances to be selected. These $M - M_e$ parents take part in crossover and mutation.

• Crossover and Mutation Process: Crossover is designed to propagate and exchange information between two parent chromosomes and the result is two child chromosomes. We use two point crossover and the two crossing points are selected randomly between 1 and U. Usually, high values are chosen for the crossover probability ($90\% - 100\%$), we assume a value of 100% in our simulations. After a crossover, if the child chromosomes do not satisfy the interface constraint, some channels are merged randomly to meet the constraint. One example of crossover is shown in Figure 6.3(a).

The mutation process is performed for each new generation after crossover. In this process two random numbers are generated between 1 and U and the colors of these two vertices are interchanged. Generally mutation probability is pretty low, we assume a value of 1% in our simulations. An example of mutation process is shown in Figure 6.3(b) where the colors of vertex 1 and 6 are exchanged.

The algorithm stops when the best solution does not improve significantly for a fixed number of consecutive iterations or a large predefined number of iterations is reached. When the stopping criterion is reached, the algorithm chooses the chromosome/solution with the highest fitness value. This process is repeated for all the

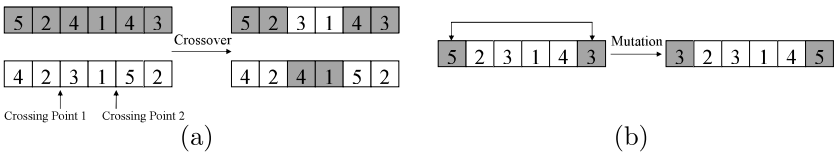

Figure 6.3: (a) Two-point crossover and (b) Mutation.

candidate routes, and the route with highest fitness value/quality is selected.

We now calculate the reduction of the convergence time of the genetic algorithm achieved from our scheme. As mentioned in [58], the probability that the genetic algorithm converges at generation t of chromosome length l is given by

$$P(t,l) = \left[1 - \frac{6p_0(1-p_0)}{M}\left(1 - \frac{2}{M}\right)^t\right]^l \tag{6.2}$$

where p_0 is the initial frequency of the allele and M is the population size (*mating pool* size). Now for an example, if we assume $M = 1000$ and $p_0 = 0.5$, then to get 90% probability of convergence ($P(t,l) = 0.9$) for a 200 bit chromosome ($l = 200$), the algorithm takes 522 generations to converge, but if we can reduce the chromosome length by 50% ($l = 100$) it takes 176 generations to converge. This shows a significant amount of reduction in convergence time.

6.6 Complexity of JRCA

The *average* case complexity of JRCA is discussed as follows:

• Conflict graph formation: If there are m edges in the connectivity graph, i.e. m vertices in the conflict graph then for any two of the m vertices we need to check whether they are in the interfere each other or not. Thus the conflict graph formation takes $O(m^2)$ time.

• Vertex deletion: Next we need to calculate the complexity of vertex deletion. First we need to sort m vertices based on their degree, this sorting takes $O(mlog_2m)$ time. After that for $O(m)$ vertices, we need to check whether the deletion of that

Algorithm 5. Algorithm for finding the color assignment

```
INPUT : Simple undirected graph G and the set of channels
OUTPUT : Color assignment of G
Vertex Deletion (G)
All_nodes_colored = false
v_i = v_1
Color(v_1) = 0
while All_nodes_colored == false do
    while Color(v_i) < 4 do
        if All_nodes_colored == true then
            break
        end if
        Color(v_i) = Color(v_i) + 1
        if ValidColor(Color(v_i), v_i) == true then
            if v_i == v_n then
                All_nodes_colored = true
            else
                v_i = v_{i+1}
                Color(v_i) = 0
            end if
        end if
    end while
    v_i = v_{i-1}
end while
GCL = GCL ∪ (vertices violating interface-constraint)
Perform Genetic-Algorithm(GCL)
return G with vertex coloring
```

vertex makes the remaining graph planar or not. Checking of the planarity condition takes $O(m)$ time based on Boyer-Myrvold planarity test [55]. Thus the total complexity of vertex deletion takes $O(mlog_2m + m^2) = O(m^2)$ time.

• Backtracking: The next stage is backtracking that takes $\sum_{L=0}^{n} 2^{-\frac{L}{2}} k^L 2^{-\frac{L^2}{k}}$ in the average case based on [59] where k is the number of colors. As in our case $k = 4$, the backtracking takes $O\left(\sum_{L=0}^{n} 2^{-\frac{L^2-20L}{8}}\right)$ times on average.

• Genetic algorithm: At last we need to calculate the average complexity of genetic algorithm. First let us calculate the number of generations the genetic algorithm takes to converge. If the expected number of generations is $E[i]$ then from equation (6.2), we get $E[i] = \sum_{t=1}^{\infty} tP(t, l)$. In each generation, it performs crossover and mutation that takes $O(U^2)$ and $O(U)$ time respectively, where U is the number of vertices in GCL. This the average time complexity of genetic algorithm is given by $E[i]O(U^2)$.

Thus the average complexity of JRCA is given by $O(m^2)+O(m^2)+O\left(\sum_{L=0}^{n} 2^{-\frac{L^2-20L}{8}}\right)+ E[i]O(U^2) = O(m^2) + O\left(\sum_{L=0}^{n} 2^{-\frac{L^2-20L}{8}}\right) + E[i]O(U^2)$.

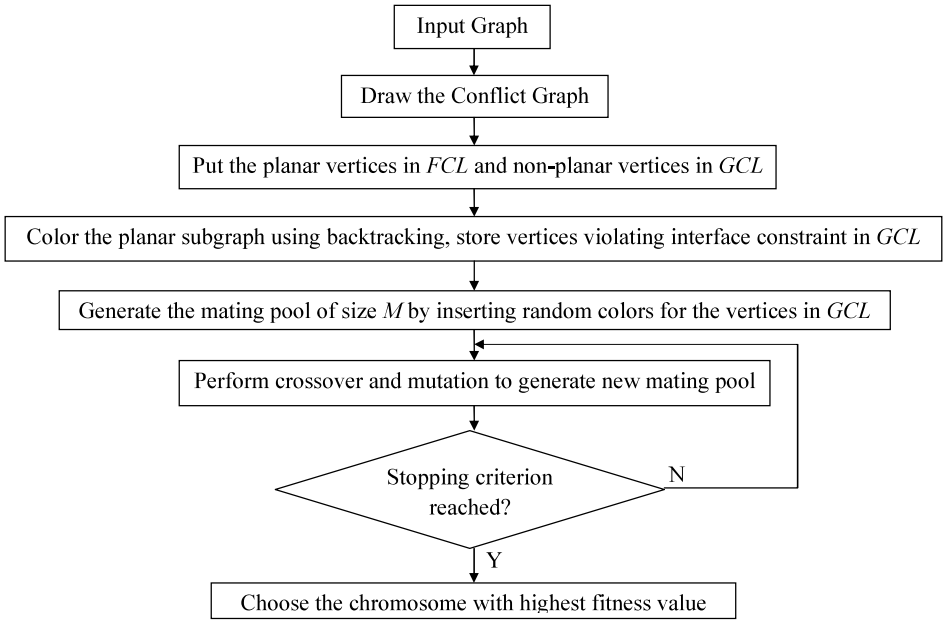

Figure 6.4: Joint route and channel assignment (JRCA) scheme.

6.7 JRCA Routing Protocol

Protocol functionality of our proposed routing protocol JRCA can be divided into the following different phases.

• Route Discovery: When the source does not have a route to the destination, it broadcasts a route request packet (RREQ) to its neighbors. In addition to many other fields, the RREQ contains a RREQ ID, the destination address, the source address, the number of active neighbors of the sender (A), the sequence of nodes that it has traversed and a timestamp. The RREQ ID combined with the source address uniquely identifies a route request. This is required to ensure that the intermediate nodes rebroadcast a route request only once in order to avoid broadcast storms. If any intermediate node receives a RREQ more than once, it just discards it. All intermediate nodes do the same thing until the RREQ reaches the destination. The timestamp is used to reduce unnecessary flooding of RREQ packets throughout the network.

• Route Selection: The destinations (gateways) wait for the first ten RREQ packet,

run *backtracking* and *genetic algorithm* on all the routes carried by the RREQ packets, collaborate with each other and choose routes and channels that maximizes route quality Q. For calculating Q, gateways use the node location and neighborhood information of the nodes. After choosing the route with highest Q, the gateway that receives the best route (carried of RREQ) forwards a route reply packet (RREP) back on the same route. All the intermediate nodes forward the RREP back to the source, perform channel switching if required and update their routing table entry. The source then starts sending the data packets via this route. The *default channel* is used for the transmissions of RREQ and RREP packets.

• Route Maintenance: If a routing table entry is not used for along time, that entry is erased. This is required as the network scenario changes with time, thus after a long time if a source need a route to the gateway, it has to start a route discovery to get a good quality route.

The overall scheme of joint route and channel selection (JRCA) is depicted in Figure 6.4.

6.8 Performance Evaluation of JRCA

We next present the performance of the proposed JRCA routing protocol in comparison to single channel and random channel selection schemes. We use the *network simulator–2 (ns2)* [50] to measure the performance of different protocols, with substantial modifications in physical and mac layer. Mainly we model the cumulative interference calculation in *ns-2* and also include the physical carrier sensing based on cumulative received power at the transmitter. The *DataCapture* is also modeled in our improved *ns-2* version. Next we extend *ns-2* to support multi-channel multi-interface simulation as described in [51]. For our performance evaluations, we consider a grid network consisting of 30 nodes placed in a uniform grid. We choose two gateways and keep them fixed. The sources are selected randomly. Each flow runs UDP and is alive for 200 seconds. We have averaged the results over 5 such simulations. The

parameters used in the simulations are listed in Table 6.1.

Table 6.1: Simulation environment

Parameter	**Values used**	**Parameter**	**Values used**
Max node queue length	200	Data packets size	1000 bytes
Propagation Model	Two Ray Ground	Traffic Generation	Exponential
Transmitter & Receiver antenna gain	0 dB	Transmit power	20 dBm
Noise floor	-101 dBm	SINRDatacapture	10 dB
Bandwidth	6 Mbps	PowerMonitor Threshold	-86.77 dBm
Basicrate	1 Mbps	Datarate	6 Mbps

The performance is measured in terms of the average throughput, delivery ratio, delay and jitter of the data flows using the single channel scheme, random channel selection scheme and JRCA. The results are shown in Figure 6.5-Figure 6.7.

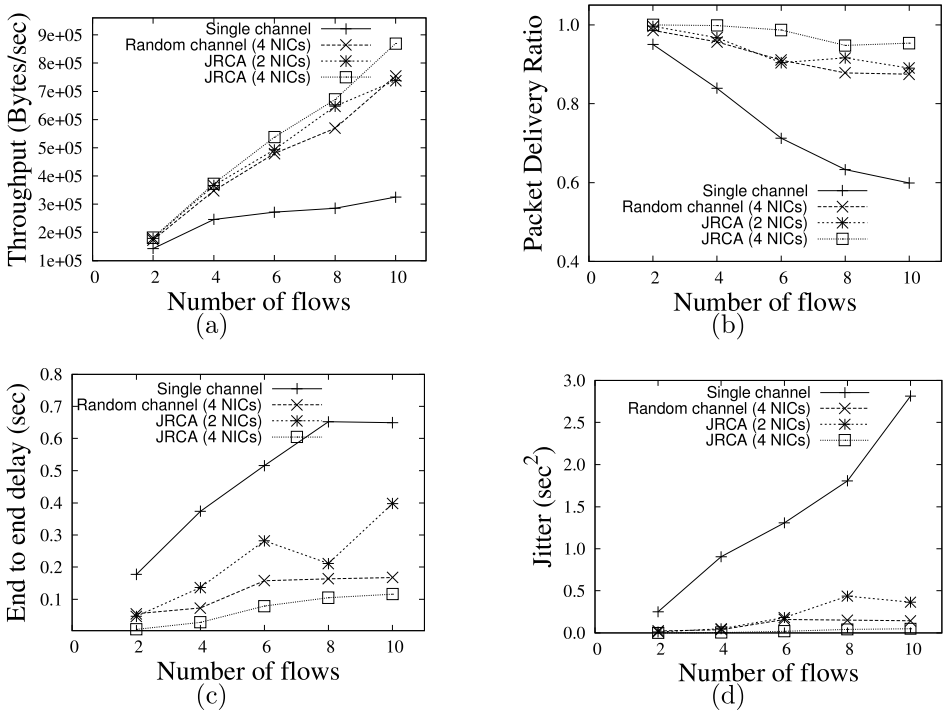

Figure 6.5: Comparison of (a) throughput b) delivery ratio (c) delay (d) jitter with different number of flows.

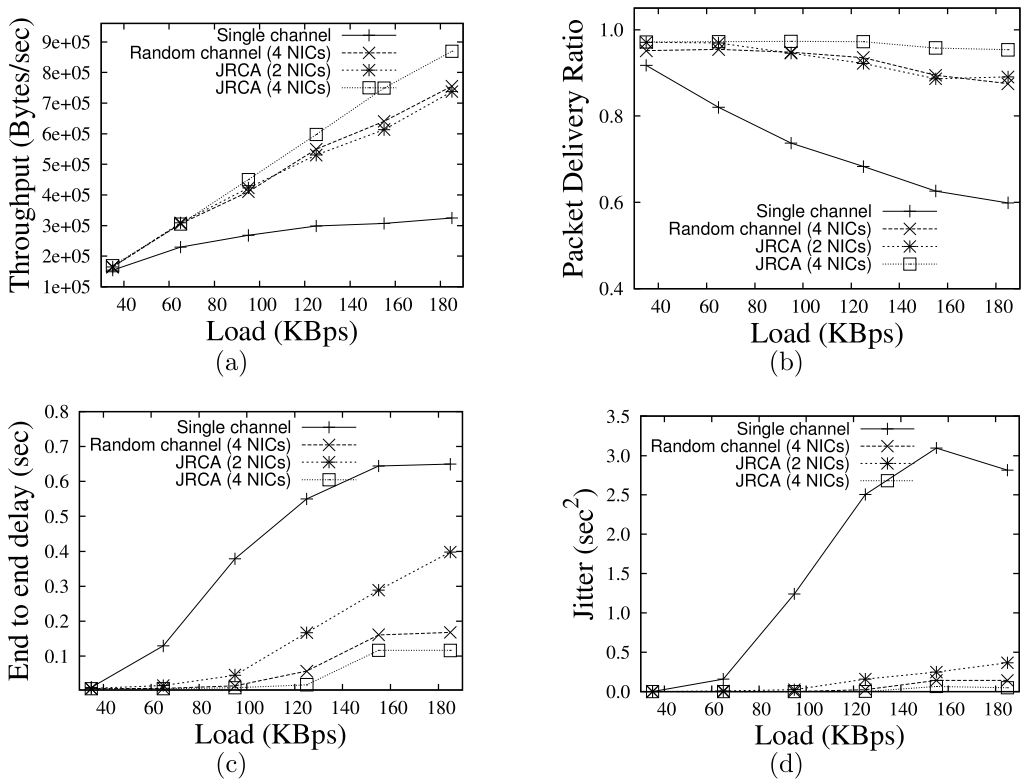

Figure 6.6: Comparison of (a) throughput b) delivery ratio (c) delay (d) jitter with different loads.

6.8.1 Comparison with Different Number of Flows

First we compare the performance of different schemes (shown in Figure 6.5) with different number of flows. We select the transmission rate of 185 KBps for these set of graphs. From Figure 6.5, we can observe that JRCA performs significantly better than single channel scheme in terms of throughput, delivery ratio, delay and jitter. The improvement in delivery ratio is because of reduced interference due to the utilization of multiple channels, whereas the reduction in delay and jitter is mainly due to reduction in channel access delay because of using multiple channels in neighbouring transmitting nodes. This reduction in interference and channel access delay results in significant improvement in the throughput. We vary the number of network interface cards (NICs) and as expected the increase in NICs result in increase in throughput and delivery ratio and decrease in delay and jitter. Also

in comparison to random channel selection scheme, JRCA gives better performance because of choosing channels intelligently.

6.8.2 Comparison with Different Loads

Figure 6.6 shows the performance of throughput, delay and jitter with variation in loads for both single and multiple channel schemes. The number of channels in these set of figures is 12 and 10 sources are chosen randomly. Here also we observe the significant improvement in throughput, delivery ratio, delay and jitter in case of JRCA than the single channel scheme and random channel selection scheme.

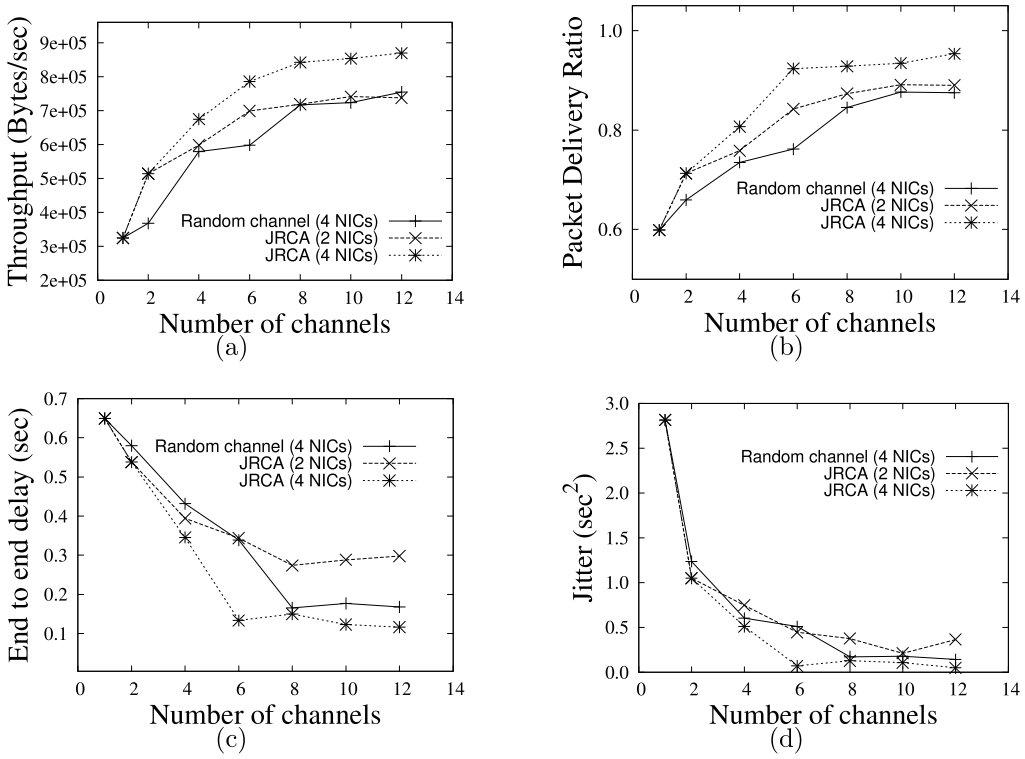

Figure 6.7: Comparison of (a) throughput (b) delivery ratio (c) delay (d) jitter with different number of channels.

6.8.3 Comparison with Different Number of Channels

The variation of throughput, delay and jitter with different number of channels are shown in Figure 6.7. For these set of figures, we set the transmission rate to 185 KBps and 10 sources are activated. As expected, the higher number of NICs gives

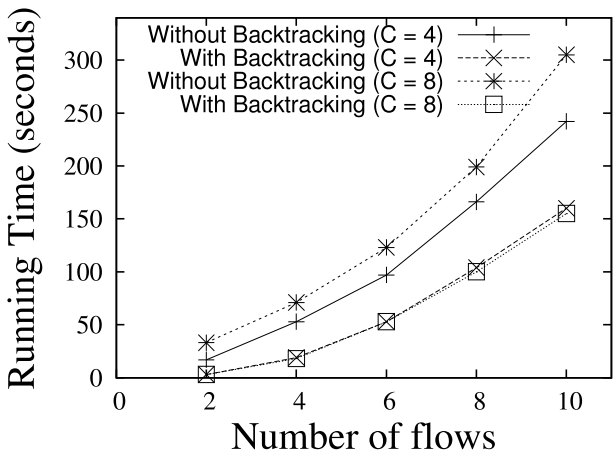

Figure 6.8: Comparison of running time.

more improvement in terms of throughput, delivery ratio, delay and jitter because of it's ability reduce channel conflict in neighbouring and interfering links.

6.8.4 Comparison of Running Time.

As mentioned earlier, for channel assignment, we use genetic algorithm on a subgraph of the whole conflict graph to reduce convergence time. To validate this, we compare our scheme with the scheme that uses genetic algorithm on all the vertices of the conflict graph, in an Intel Core2 Duo processor, running at 2 GHz. The result is shown in Figure 6.8, that confirms our claim that using backtracking on the planar subgraph and genetic algorithm on the remaining vertices of the conflict graph reduces the convergence time by a good factor. Also from Figure 6.8 we can observe that as we increase the number of channels from 4 to 8, the running time increases a little bit. This is because, as the number of channels increases, the diversity of chromosomes increases, that results in increased convergence time.

6.9 Discussions

In this chapter, we address our joint routing and channel assignment scheme in multi-channel wireless mesh networks, where each router is equipped with multiple radios. We develop a backtracking and genetic algorithm based channel selection scheme for solving this problem. For route selection, we propose a novel quality

based routing metric based on probability of success and delay. Using simulations in ns-2, we demonstrate the effectiveness of our routing and channel selection scheme in improving the network throughput, delivery ratio, delay and jitter.

CHAPTER 7: PERFORMANCE ANALYSIS OF IEEE 802.11 DISTRIBUTED COORDINATION FUNCTION IN PRESENCE OF HIDDEN STATIONS UNDER NON-SATURATED CONDITIONS WITH INFINITE BUFFER IN RADIO-OVER-FIBER WIRELESS LANS

In this chapter we present an analytical model to evaluate the performance of the IEEE 802.11 Distributed Coordination Function (DCF) in radio-over-fiber (RoF) wireless LANs. *Radio over fiber* technology has attracted significant attention in recent times as a promising approach for providing improved wireless coverage at a low cost in broadband access networks. RoF utilizes high bandwidth optical links to distribute radio frequency (RF) signals from a central unit to remote antenna units (RAU) that may be distributed over a wide region. Figure 7.1 illustrates the basic architecture of a typical RoF network. For the downlink, the electrical signal generated by an *access point (AP)* is converted to optical (E/O conversion) and sent through the optical link to the corresponding RAU. At the antenna, this is converted into a radio signal and transmitted to the wireless nodes. The reverse happens for the uplink where the RF signals from wireless nodes are converted into optical (E/O conversion) at the antenna and sent over the optical link to the central unit, where it is converted back to electrical signal.

Using RoF for wireless coverage has numerous advantages. In RoF networks, all complex and expensive equipment, such as those required for modulation and switching, are located at the central unit. The only functions carried out at the RAUs are the RF amplifications and optical to electrical conversion and vice versa. This enables the RAUs to be simpler and less expensive, which reduces the overall installation and maintenance costs. The large bandwidth and low attenuation of optical fiber offers high capacity for transmitting radio signals. Also, including optical

fibers reduce problems related to interference, as optical fiber cables are insensitive to electromagnetic radiations. In addition, this simpler RAU with low-complexity

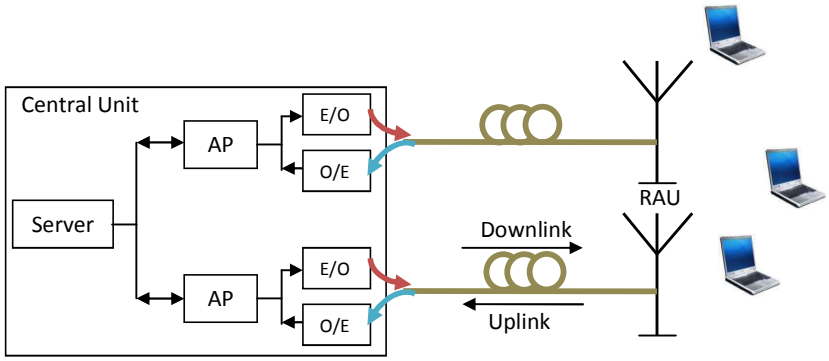

Figure 7.1: Block diagram of a radio-over-fiber network.

equipment results in reduced power consumption.

Although each AP in an RoF network can use the same channel access protocol as in other wireless LANs, the addition of the fiber link between the AP and the RAU introduces additional factors that affect the performance of the medium access control (MAC) protocol. In this chapter, we analyze the performance of the IEEE 802.11 DCF in RoF networks under non-saturated traffic conditions for both the basic and the optional RTS/CTS access mechanisms. Our analysis takes into account the effects of transmissions from contending nodes, i.e. nodes contending to gain access to the channel at the same time as the source node, as well as that of hidden terminals, which might disrupt the reception of a packet if they commence transmission at any time during the receiver's vulnerable period. In addition, as opposed to other existing literature on the analysis of DCF performance, we assume large buffer sizes, which is a more realistic assumption for accurate computation of the total delay (MAC plus queuing delay). Moreover, we consider the effect of the fiber length, which adds an extra propagation delay and poses a challenge to the system design of IEEE 802.11.

7.1 Related work

A significant amount of work has been reported on the performance analysis of 802.11 systems. The pioneering work by Bianchi in [60] presents a two-dimensional Markov chain model that effectively captures the performance of IEEE 802.11 DCF under saturated traffic conditions. However, it does not consider the effect of hidden stations. The authors of [61] extend Bianchi's model to obtain the performance under non-saturated traffic conditions, without capturing the effects of hidden nodes. The throughput performance with hidden nodes under saturated traffic condition with RTS/CTS is presented in [62], whereas in [63] the authors discussed the effects of hidden terminals in non-saturated traffic conditions to measure the throughput performance. The delay performance in 802.11 DCF is also well researched. In [64] [65] the delay performance in the presence of only contending stations and saturated traffic conditions are presented. In [66], the authors propose a model based on Bianchi's model to calculate delay in presence of hidden stations and in non-saturated traffic condition. All of the above literature consider short buffer sizes, which does not capture the effect of queuing delay properly. The impact of large buffer is considered in [67] where the authors model the throughput and total delay in absence of hidden stations. The saturated throughput performance of DCF in RoF is addressed in [68] in the absence of hidden nodes, where the effect of buffering is ignored as well.

In this chapter, our main contribution is as follows. First, we extend the model in [61], [63], [67] to include the effect of hidden stations with infinite buffer in the basic IEEE 802.11 DCF and that using RTS/CTS for radio-over-fiber wireless networks. We also evaluate the total delay, which includes the queuing delay. We validate our analytical model by using simulations in *ns-2*. Finally, we address the effect of fiber propagation delay on network throughput and probability of collision. To the best of our knowledge, this is the first work that addresses the performance evaluation of IEEE 802.11 MAC in presence of hidden stations with large buffer and nonsaturated

condition in RoF networks.

7.2 Modeling of IEEE 802.11 DCF in RoF Wireless LANs

In this section we present the analytical model of the IEEE 802.11 DCF in RoF wireless LANs, taking into account non-saturated traffic conditions, the effects of contending and hidden stations, infinite buffers and fiber propagation delay.

7.2.1 Modeling of Nonsaturated Stations

According to the IEEE 802.11 standard, the contention window, also called the backoff window, increases exponentially from a minimum size W_0 to the maximum size W_{max} as follows:

$$\begin{aligned} W_i &= 2^i W_0 \quad 0 \leq i \leq m \\ &= 2^m W_0 = W_{max} \quad i > m \end{aligned} \tag{7.1}$$

Here m is the backoff stage at which the contention window reaches the maximum value W_{max}, where it remains in successive stages as well. In [60], Bianchi presents a Markov model to describe this backoff window size where each station is modeled by a pair of integers (i, k). The back-off stage i starts at 0 at the first attempt to transmit a packet and is increased by 1 every time a transmission attempt results in a collision, up to a maximum value of m. It is reset after a successful transmission. The counter k is initially chosen uniformly between $[0, W_i - 1]$, where $W_i = 2^i W_0$ is the range of the counter. The counter is decremented when the medium is idle. The station transmits when $k = 0$.

The above model was extended to address nonsaturated traffic conditions in [61] and [67]. The authors assume a constant probability q of at least one packet arriving during the average slot time on the medium. They also assume the following terms: the probability that a packet is available to the MAC immediately after a successful transmission, denoted by r; the probability of collision, denoted by p; and the prob-

ability of transmission in a randomly chosen slot, denoted by τ. Our analysis is based on a similar approach; however, we also consider the effect of large buffer and fiber propagation delay. In this subsection, we first analyze the effect n contending stations (i.e. no hidden station).

Following the derivations presented in [61] and [67], the packet transmission probability τ in a generic slot time can be written as:

$$\tau = \frac{1}{\eta(1-r)}\left(\frac{q^2 W_0}{(1-p)(1-(1-q)^{W_0})} - rq(1-p)\right) \tag{7.2}$$

where η can be found by:

$$\begin{aligned}\eta \;=\; & (1-q) + \frac{q^2 W_0(W_0+1)}{2(1-(1-q)^{W_0})} + \\ & \frac{q(W_0+1)}{2(1-r)}\Big(\frac{q^2 r W_0}{1-(1-q)^{W_0}} + qp(1-r) - qr(1-p)^2\Big) \\ & + \frac{p}{2(1-r)(1-p)}\Big(\frac{q^2 W_0}{1-(1-q)^{W_0}} - rq(1-p)^2\Big) \times \\ & \Big(2W_0\frac{1-p-p(2p)^{m-1}}{1-2p} + 1\Big)\end{aligned} \tag{7.3}$$

Note that τ depends on the values of p, q, and r. The probability of collisions p is equal to the probability that at least one of the $n-1$ remaining stations transmit in that slot. Thus

$$p = 1 - (1-\tau)^{n-1} \tag{7.4}$$

We assume that packets are generated in each node according to a Poisson arrival process with exponentially distributed inter-packet arrival times with rate λ_g. When an infinite buffer size is considered, the collided packets will be retransmitted. Consequently, the rate at which packets arrive in the queue is given by

$$\lambda = \lambda_g + \lambda_g p + \lambda_g p^2 + ... = \frac{\lambda_g}{1-p} \tag{7.5}$$

With these, the probability of a packet arrival in a slot can be expressed as

$$q = 1 - e^{-\lambda T} \tag{7.6}$$

Here, T is the average slot time, which can either be empty, include a successful transmission, or have a collision. These can occur with probabilities $1 - P_{tr}$, $P_{tr}P_s$ and $P_{tr}(1-P_s)$ respectively, where P_{tr} represents the probability that there is at least one transmission in a time slot and P_s denotes the probability of success. Hence,

$$T = (1 - P_{tr})\sigma + P_{tr}P_sT_s + P_{tr}(1 - P_s)T_c \tag{7.7}$$

where σ is the duration of an empty time slot, T_s is the average time the channel is sensed busy because of a successful transmission, T_c is the average time the channel is sensed busy by each station during a collision. The expressions of T_s and T_c are presented in the next subsection.

Also, P_{tr} can be written as:

$$P_{tr} = 1 - (1 - \tau)^n \tag{7.8}$$

The probability of success P_s is given by the probability that exactly one station transmits, conditioned on the fact that there is at least one transmission in the channel, i.e.,

$$P_s = \frac{\binom{n}{1}\tau(1-\tau)^{n-1}}{P_{tr}} = \frac{n\tau(1-\tau)^{n-1}}{1-(1-\tau)^n} \tag{7.9}$$

As mentioned earlier, r is the steady state probability that a M/G/1 queue has a packet awaiting in it's buffer after a service time, thus r can be written as

$$r = \min(1, \lambda_g E[d]) \tag{7.10}$$

where $E[d]$ is the *access delay*, which is defined as the time interval between the instant when the packet reaches the head of the transmission queue and begins contending for the channel, and the time when the packet is successfully received at the destination station. Thus $E[d]$ consists of backoff time to get access to the channel and time for successful transmission of that packet, i.e.

$$\begin{aligned} E[d] &= \bar{T}_B + T_s \\ &= \frac{T\left(W_0 \frac{1-p-2^m p^{m+1}}{1-2p} - 1\right)}{2(1-p)} + \frac{p}{1-p} T_c + T_s \end{aligned} \tag{7.11}$$

where $\bar{T}_B$ is the average backoff time (calculation is shown in Appendix B).

The nonlinear equations (7.2)-(7.11) must be solved together. To calculate the throughput, we observe that during an average slot period T, a station transmits a successful packet with a probability of $P_s P_{tr}$. Hence, for a packet payload of $E[P]$, the throughput (number of bits in unit time) is represented as

$$S = \frac{P_s P_{tr} E[P]}{T} \tag{7.12}$$

To calculate the total delay (including the queuing delay) of a packet, we assume an M/G/1 queue model with arrival rate of λ and service time $E[d]$. Thus the total delay of a packet is given by

$$T_d = E[d] + \frac{\lambda E[d^2]}{(1-\rho)} \tag{7.13}$$

where ρ is given by $\rho = \lambda E[d]$. From [64], we can get $E[d^2]$ as

$$\begin{aligned} E[d^2] &= Var\{\bar{T}_B + T_s\} = Var\{\bar{T}_B\} \\ &= \left[\frac{T(W_0\gamma - 1)}{2} + T_c\right]^2 \frac{p}{(1-p)^2} \end{aligned} \tag{7.14}$$

where

$$\gamma = \frac{[2p'^2 - 4p' + 1 - m(-1 + 2p')p'][2p]^m + 2p'^2}{(-1 + 2p'^2)} \tag{7.15}$$

and $p' = 1 - p$. The delay can be calculated using equation (7.13) as long as $\rho \leq 1$, while $\rho > 1$ the queue becomes unstable, equation (7.13) does not capture this effect.

7.2.2 Modeling Hidden Stations in the 802.11 Basic Access Scheme

In the basic access scheme, T_s and T_c can be expressed as

$$\begin{aligned} T_s &= DIFS + H + E[P] + F + SIFS + T_{ACK} + F \\ T_c &= DIFS + H + E[P] + F \end{aligned} \tag{7.16}$$

where DIFS, SIFS are the interframe spacing length, H and T_{ACK} are the length of the header and the acknowledgement packet and F is the fiber propagation delay (discussed in section 7.2.4). Now let us assume that there are c contending stations and h hidden stations. Hence, here the total number of stations is $n = c + h$. In this situation a packet from a contending station is successful if

- None of the remaining contending stations transmit in the same slot. This happens with a probability of $(1 - \tau)^{c-1}$.

- No hidden stations transmit during the vulnerable period of the whole DATA transmission. The vulnerable period of the whole transmission is given by $V = 2T_s$, thus the probability that h hidden stations do not transmit in the vulnerable period of the DATA transmission is given by $e^{-h\lambda_g V} = (1-q)^{hk(1-p)}$, where k is the approximate number of slot durations in $2T_s$), i.e. $k = \frac{V}{T} = \frac{2T_s}{T}$.

Hence, here p, P_{tr} and P_s can be written as:

$$p = 1-(1-\tau)^{c-1}(1-q)^{hk(1-p)} \tag{7.17}$$

$$P_{tr} = 1-(1-\tau)^{c} \tag{7.18}$$

$$P_s = \frac{c\tau(1-\tau)^{c-1}(1-q)^{hk(1-p)}}{1-(1-\tau)^{c}} \tag{7.19}$$

Similar to [63], assuming $T_s = \alpha\sigma$, $T_c = \beta\sigma$ and $V = \gamma\sigma$, and using the values of T_s and T_c from equation (7.16) in (7.7), and $T = \frac{V}{k}$, we get

$$P_{tr}[1-\beta+(\beta-\alpha)P_s] = 1-\frac{\gamma}{k} \tag{7.20}$$

Since $P_sP_{tr} = c\tau(1-p)$ in (7.20), we get

$$\frac{\gamma}{k} = 1+P_{tr}(\beta-1)+c\tau(1-p)(\alpha-\beta) \tag{7.21}$$

Finally, after rearranging (7.21), we get

$$k = \frac{\gamma}{1+(1-(1-\tau)^{c}))(\beta-1)+c\tau(1-p)(\alpha-\beta)} \tag{7.22}$$

The values of p, P_{tr} and P_s obtained from the above value of k can be used to determine the network parameters as done before.

7.2.3 Modeling Hidden Stations in 802.11 with RTS/CTS

In the presence of RTS/CTS, T_s can be written as

$$\begin{aligned} T_s = {} & DIFS + T_{RTS} + F + SIFS + T_{CTS} + F + SIFS \\ & + H + E[P] + F + SIFS + T_{ACK} + F \end{aligned} \tag{7.23}$$

where T_{RTS} and T_{CTS} are the length of the RTS and CTS packet respectively. The expression of T_c is more complicated. Among the contending stations, some stations that are in the transmission range of the intended transmitter (say A) can receive the RTS/CTS, while others cannot. Let us assume that L_1 is the area that covers station A's transmission range and L_2 is the area that covers the carrier sensing range of A, excluding L_1. If a station X is placed in L_1, then after receiving the RTS from X, A stays silent for a duration $T_{c_1} = T_s$ even if transmission from X results in a collision. On the other hand, if X is placed in L_2, station A waits for a shorter amount of time $T_{c_2} = DIFS + T_{RTS}$ in case of a failed RTS transmission. Thus the collision duration T_c can be written as $T_c = P_{L_1} T_{c_1} + P_{L_2} T_{c_2}$, where P_{L_1} and P_{L_2} are the probabilities that X is placed in L_1 and L_2.

Among the hidden stations, some stations that are within the transmission range of the intended receiver (D) receive the CTS whereas stations that are outside the transmission range of D cannot. Stations that are in the transmission range of D only collide with the RTS from A (assuming CTS transmissions to these hidden stations are successful). Thus for these stations, the vulnerable period is $V_1 = T_s + T_{RTS} + SIFS$, whereas for others (that are outside the transmission range of D) the vulnerable period is $V_2 = 2T_s$. Thus the average vulnerable period is $V = P_1 V_1 + P_2 V_2$, where P_1 and P_2 are the probability that a hidden station is in the transmission range of D or not. Thus, using the expressions of new T_s, T_c and V, we can calculate other parameters as done in previous subsections.

7.2.4 Effect of Fiber Propagation Delay

In RoF networks there is a fiber propagation delay between the central unit and the remote antenna, given by $F = \frac{L \text{ meter}}{2\times10^8 \text{ meter/secs}}$, where L is the fiber length. For pure wireless networks, $F = 0$. The ACK and CTS timeouts put a constraint on the maximum fiber length L. The transmitter should receive an ACK from the receiver within the ACK timeout ($SIFS + T_{ACK}$ + maximum propagation delay M). Thus

the following condition should be satisfied

$$\begin{aligned} & SIFS + T_{ACK} + 2F \leq ACK_{TO} \\ & \Rightarrow F < \frac{ACK_{TO} - SIFS - T_{ACK}}{2} = \frac{M}{2} \\ & \Rightarrow L < \frac{2 \times 10^8 (ACK_{TO} - SIFS - T_{ACK})}{2} = M \times 10^8 \end{aligned} \tag{7.24}$$

Similarly, if RTS/CTS is used, in order for the transmitter to receive the CTS before the CTS timeout ($SIFS + T_{CTS} + M$)

$$\begin{aligned} & F < \frac{CTS_{TO} - SIFS - T_{CTS}}{2} = \frac{M}{2} \\ & \Rightarrow L < \frac{2 \times 10^8 (CTS_{TO} - SIFS - T_{CTS})}{2} = M \times 10^8 \end{aligned} \tag{7.25}$$

In equations(7.24) and (7.25), ACK_{TO} and CTS_{TO} denote ACK timeout and CTS timeouts, respectively. Note that there will be no packet transmissions if equations (7.24) and (7.25) are not satisfied, and consequently, the throughput will be zero under those conditions.

7.3 Results and Analysis

The accuracy of the model presented above is verified by simulations using the *network simulator–2 (ns2)*. For the ease of implementation, we assume the *transmission range* to be the same as the *carrier sensing range*. Thus $P_{L_1} = P_2 = 1$ and $P_{L_2} = P_1 = 0$. All stations generate packets using Poisson process and the interface queues at each nodes can store a maximum size of 2000 packets (unless otherwise mentioned). The parameters used in the simulations are listed in Table 7.1. For all the figures in this section, the solid lines represent values obtained from analytical model and discrete points represent values from simulations. In all the figures we keep the number of colliding stations as 4 and vary the number of hidden stations denoted as h. Unless specifically mentioned, the fiber length is kept to 500 meters for

the simulations.

Table 7.1: Simulation environment

Parameter	Values used	Parameter	Values used	Parameter	Values used
W_{min}	15	CTS	112 bits	RTS	160 bits
W_{max}	1023	Slot Time	9 μs	Payload Length	1000 Bytes
SIFS	16 μs	ACK	112 bits	Channel bit rate	6 Mbps
Header Duration	20 μs	DIFS	34 μs	Max propagation delay	10 μs

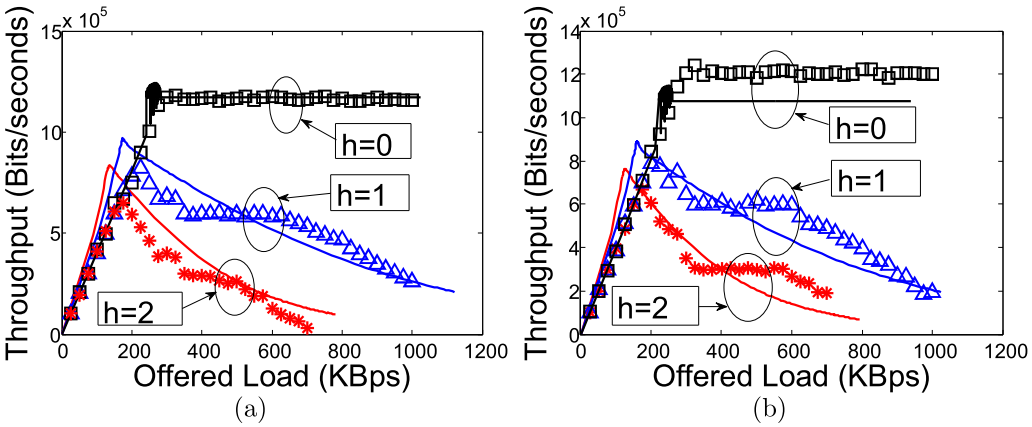

Figure 7.2: Individual throughput of contending stations with different offered load (a) Basic access mechanism, (b) RTS/CTS access mechanism.

7.3.1 Effect of Hidden Stations

Figure 7.2 shows the variations of the throughputs with offered load for both the basic and RTS/CTS access mechanisms. From this figure we can observe that our analytical results match the simulation results closely. Also we can observe that at first the throughput starts increasing till it reaches a *saturation point*. After this point, in absence of hidden stations, throughput does not change with further increase in offered load. However in the presence of hidden stations, the throughput starts decreasing after the saturation point. This decrease in throughput is mainly because of the interference from the hidden stations at high load and due to multiple retransmissions.

Figure 7.3 and 7.4 show the variation of the probability of collision and access

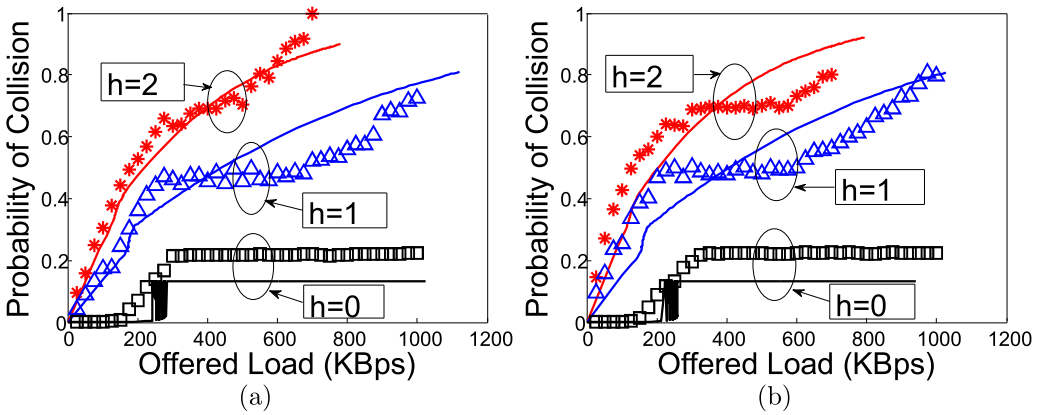

Figure 7.3: Probability of collision of contending stations with different offered load (a) Basic access mechanism, (b) RTS/CTS access mechanism.

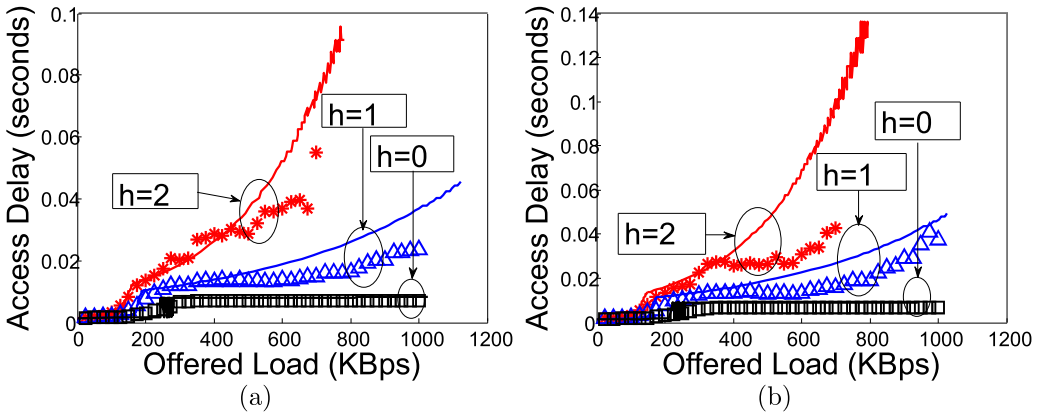

Figure 7.4: Access delay of contending stations with different offered load (a) Basic access mechanism, (b) RTS/CTS access mechanism.

delay respectively, with increasing load and different number of hidden stations. It is observed that with no hidden stations, the probability of collision and access delay get saturated after a certain offered load, while in the presence of hidden stations these parameters increase with offered load due to multiple collisions and retransmissions due to the hidden stations.

In Figure 7.5, we vary the offered load and compare the total delay (queuing plus access delay) of both basic and RTS/CTS access methods and compare with those obtained using our analytical model. As mentioned in section 7.2.1, our model is valid until $\rho \geq 1$, beyond which the queue is unstable and thus our model cannot capture

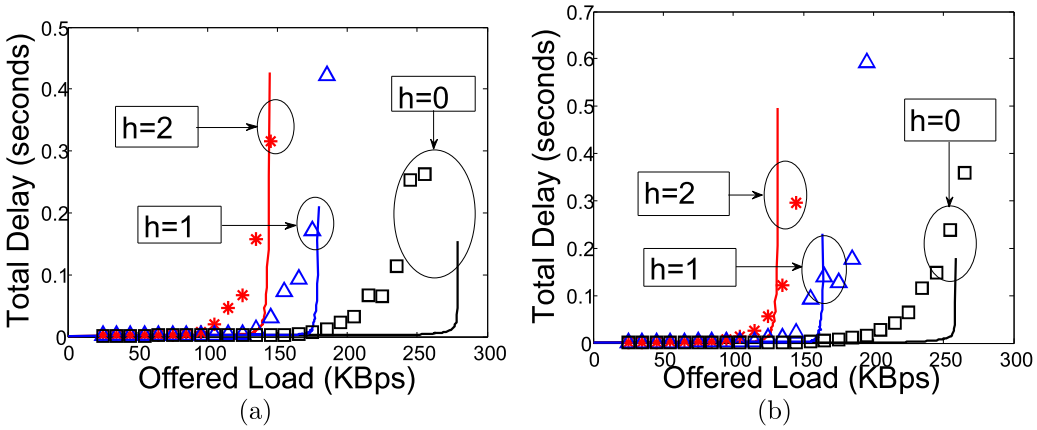

Figure 7.5: Total delay of contending stations with different offered load (a) Basic access mechanism, (b) RTS/CTS access mechanism.

that effect.

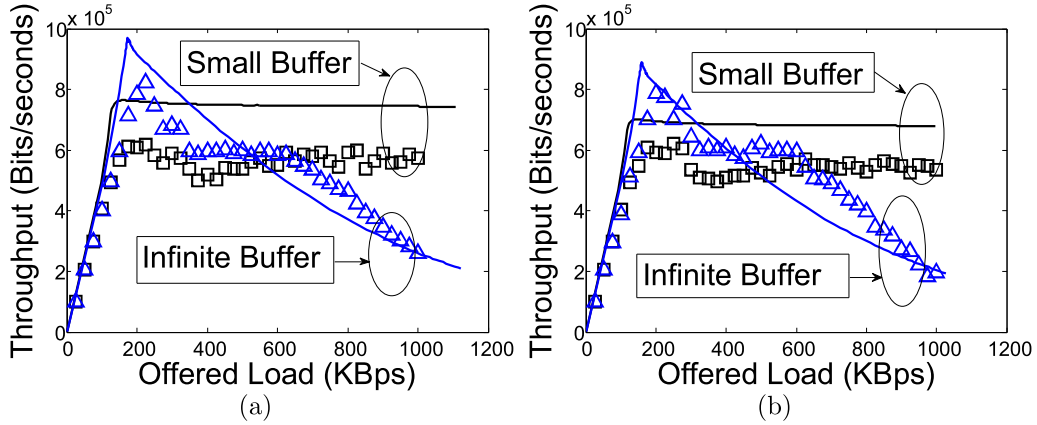

Figure 7.6: Individual throughput of contending stations with different offered load (a) Basic access mechanism, (b) RTS/CTS access mechanism.

7.3.2 Effect of Small and Large Buffers

Figure 7.6, 7.7 and 7.8 show the variations of throughput, probability of collision and access delay with different offered load for small buffer (maximum queue length of 2 for simulation) and infinite buffer (maximum queue length of 2000 for simulation), with the number of contending and hidden stations being 4 and 1 respectively. The results for the small buffer model is based on the model presented in [63]. We observe that after certain offered load, the throughput, probability of collisions, and access

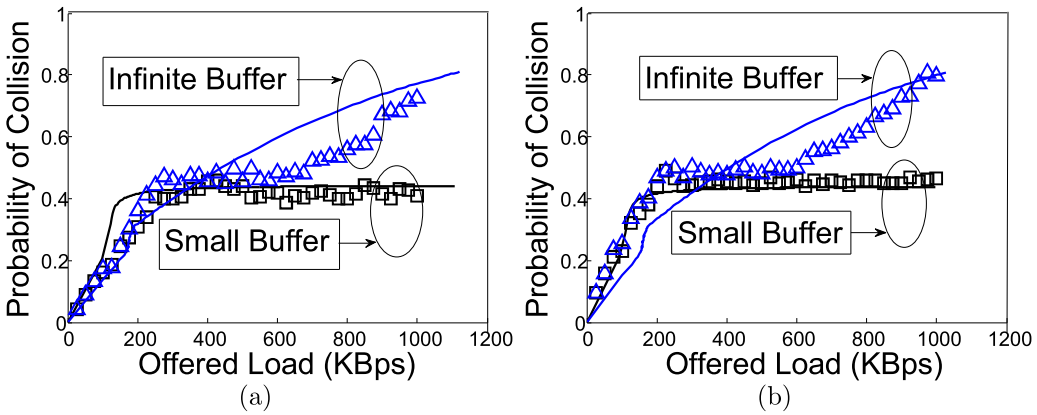

Figure 7.7: Probability of Collision of contending stations with different offered load (a) Basic access mechanism, (b) RTS/CTS access mechanism.

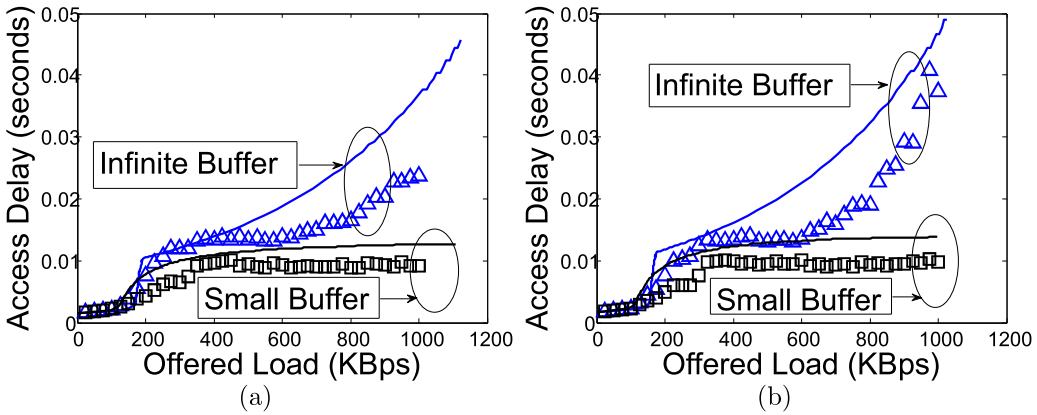

Figure 7.8: Access Delay of contending stations with different offered load (a) Basic access mechanism, (b) RTS/CTS access mechanism.

delay get saturated for small buffer. This is because after a certain offered load, for small buffer, the interface queue always has a packet to transmit, causing the network parameters to be unaffected by increasing load. But for infinite buffer size, collisions, contention and retransmissions continue to increase even after the saturation point, causing the throughput to decrease, while increasing the probability of collision and access delay.

7.3.3 Effect of Fiber Length

Figure 7.9 shows the variation of throughput with different fiber length for both access mechanisms at an offered load of 400 KBps. It is observed that if the fiber

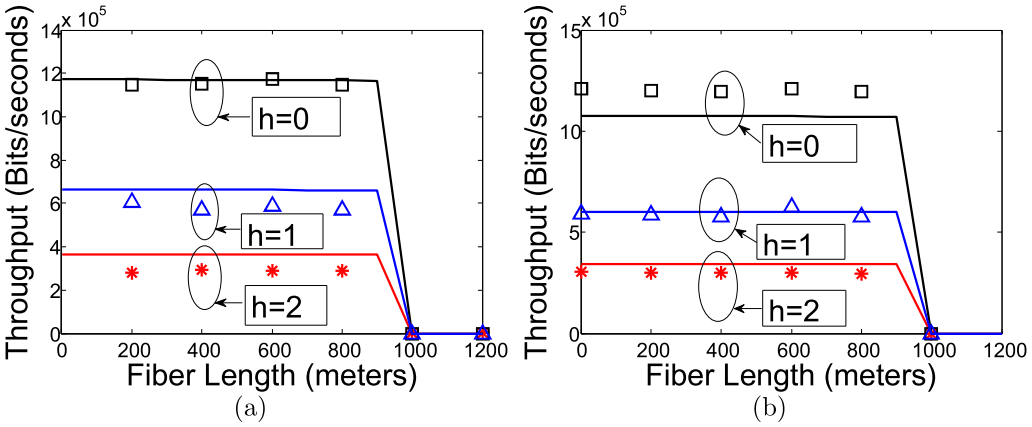

Figure 7.9: Individual throughput of contending stations with different fiber length (a) Basic access mechanism, (b) RTS/CTS access mechanism.

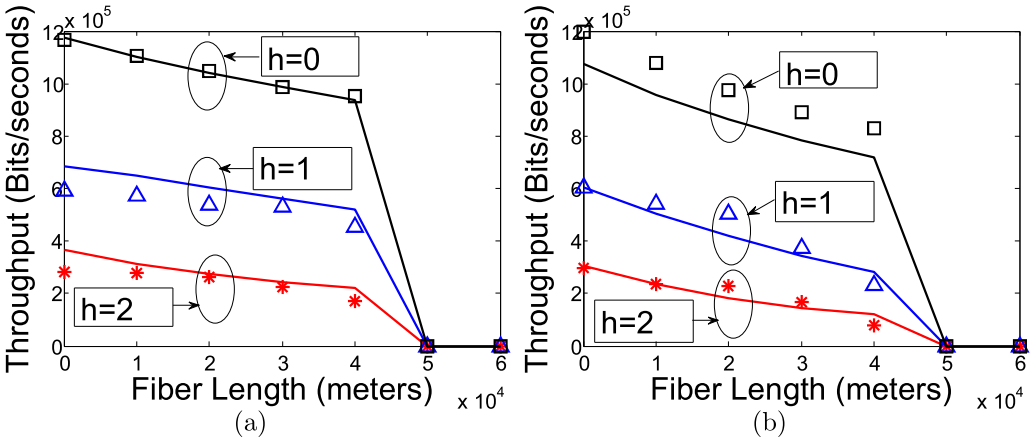

Figure 7.10: Individual throughput of contending stations with different fiber length (a) Basic access mechanism, (b) RTS/CTS access mechanism.

length crosses a maximum limit (for $M = 10$ μs, $L < 1000$ meters from equation (7.24) and (7.25)), the throughput drops down because of the timeouts. But until that point is reached, the throughput does not change significantly with the fiber length as the propagation delay is insignificant (fiber length $<$ 1000 meters).

To determine the effect of long fiber propagation delays, we change the maximum propagation delay M to 500 μs, shown in Figure 7.10. Thus timeouts occur at a fiber length of 50000 meters; however, until then the throughput drops with the fiber length. This is due to the higher contention from the contending stations and higher

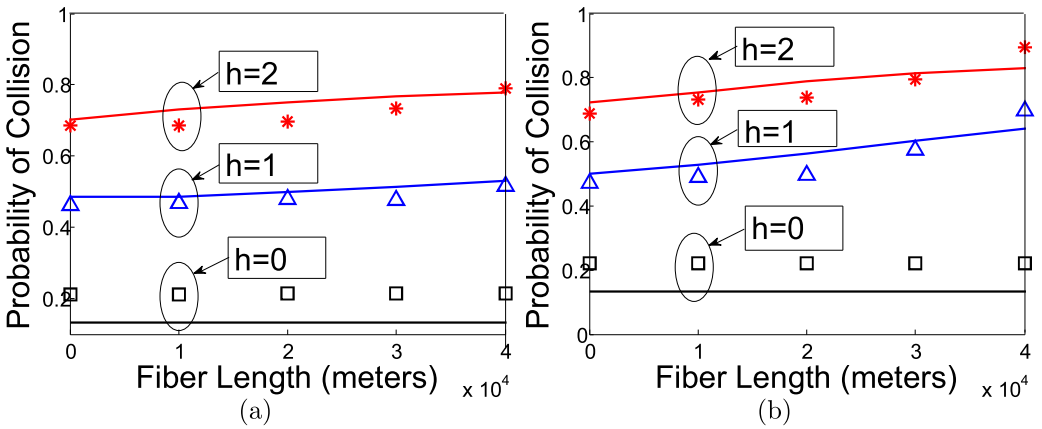

Figure 7.11: Probability of collision of contending stations with different fiber length (a) Basic access mechanism, (b) RTS/CTS access mechanism.

collision from hidden stations due to increase in vulnerable period because of extra fiber propagation delay. To observe the effect of fiber delay on probability of collision, we vary the fiber length from 0 to 4000 meters and the effect is shown in Figure 7.11. It is observed that in the absence of hidden stations, probability of collisions is hardly affected by the fiber delay. However, the situation is different in the presence of hidden stations because of the increase in vulnerable period.

7.4 Discussions

In this chapter, we derive an analytical model to calculate necessary network parameters of a packet for the basic and RTS/CTS access methods in IEEE 802.11 DCF under non-saturation condition in presence of hidden stations for radio-over-fiber LANs. We show the effect of hidden stations and buffer size on different network parameters like throughput, probability of collision, access delay etc. We also investigate the effect of fiber propagation delay on throughput and probability of collision. The accuracy of our analytical model is also confirmed with extensive simulations.

CHAPTER 8: ROUTING AND CROSS-LAYER ADAPTATION ISSUES IN WIRELESS SENSOR NETWORKS

Wireless sensor networks consists of small, inexpensive devices with hardware for sensing and a radio for communicating with others. They are self-organized ad-hoc networks capable of sensing, gathering, processing and forwarding different physical parameters in a multi-hop fashion towards the sink. They offer a flexible, self-adaptable, low-cost solution to the problem of event monitoring or structural monitoring especially in places with limited accessibility. Since batteries are difficult to replace, the popular approach for achieving long term operations in wireless sensor networks (WSNs) is by utilizing harvested energy from renewable resources, such as sunlight, vibration, heat etc. However, renewable energy can have wide spatial and temporal variations due to natural (e.g. weather) and location specific factors (e.g. exposure to sunlight) that can be difficult to predict prior to deployment. Consequently, rechargeable wireless sensor networks must have mechanisms to dynamically adapt their energy consumption based on estimated energy resources.

We assume a data gathering WSN where all sensor nodes periodically sense some physical parameters and forward these datas to the sink, which forms a data collection tree rooted at the sink. Also nodes send periodic beacon messages for exchanging different controlling parameters among themselves. In large scale WSNs that do not use transmission scheduling, synchronous sleep and wake cycles are difficult to implement. In such a network to conserve energy, nodes use low-power listening (LPL) [69], [70] where a node periodically checks (polls) the wireless channel for an incoming packet. If there is no transmission on the channel, it switches off the radio until the next poll. Otherwise it stays on to receive the incoming packet. In LPL, the sender prepends the message with a preamble that is long enough to span the complete

length of the poll interval to ensure that the receiving node observes it regardless of when it wakes up. Because of this long preamble length (for both beacons and data packets), the effect of *overhearing* becomes costly. The mechanism of LPL is shown in Figure 8.1.

In such scenarios, we propose two cross-layer adaptation schemes to reduce the effect of overhearing, especially on the nodes that are critically resource constrained. The first approach is to use multiple orthogonal channels to form a multi-channel collection tree, which divides the network traffic among different channels and reduce the effects of overhearing. Our second approach is to adapt the radio transmit power along with careful route selection to avoid overhearing on nodes that are challenged in terms of their remaining energy resources. Note that these physical layer properties, such as channel selection and radio power control need to be carefully tied with route selection to maintain perpetual network operations.

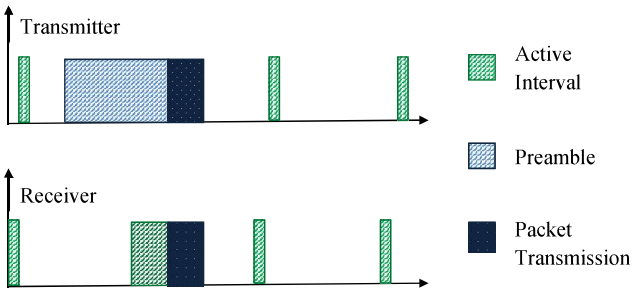

Figure 8.1: Low power listening.

8.1 Motivation Behind Building Distributed Channel Selection in WSNs

Radio transmissions as well as receptions are the critical energy-consuming tasks in typical low-powered wireless sensor nodes. For instance, the MICAz nodes draw about $20mA$ of current while transmitting and receiving, whereas it draws about 20 μA in idle mode and $1\mu A$ in sleep mode. Hence, a key aspect of designing energy-efficient wireless sensor nodes is to minimize the radio active periods, allowing the node to sleep as long as possible. Popular energy efficient wireless sensor networking protocols such as *XMesh* [1] employs low-power (LP) operation by letting nodes duty

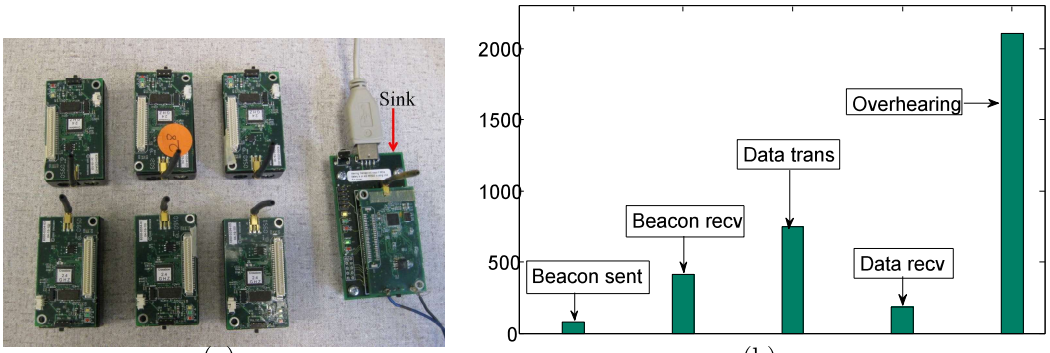

Figure 8.2: Experimental setup (a) to assess the activities of the radio (b) of a wireless sensor node performing data collection.

cycle in their sleep modes for brief periods of time to detect possible radio activity and wake up when needed. While this principle extends the battery life (lifetime) of the nodes considerably, a key factor that leads to energy wastage is *overhearing*, i.e. receiving packets that are intended for other nodes in the neighborhood. The traditional mechanism used for avoiding overhearing is transmission scheduling, which requires time synchronization that we assume is absent in the WSNs.

The effect of overhearing is illustrated in Figure 8.2, which depicts an experiment using six MICAz motes and a sink. The network is programmed with the *collection tree protocol (CTP)* [71] application where each node transmits periodic data packets comprising of sensor observations with an interval of 10 seconds and routing packets (beacons) with an interval that varies between 128 and 512000 milliseconds. The network uses the beacons to build link quality based least-cost routes from all nodes to the sink. All nodes use an extremely low transmit power of -28.5 dBm and apply the *LowPowerListening* scheme [69] with a wake-up interval of 125 milliseconds. We run this experiment for 10 minutes and record the total number of beacons and data packets sent/received throughout the network as well as the network wide overhearing. The results, shown in Figure 8.2(b), indicate that even with sleep cycles, overhearing is a dominating factor in the energy consumption in the nodes. Consequently, a

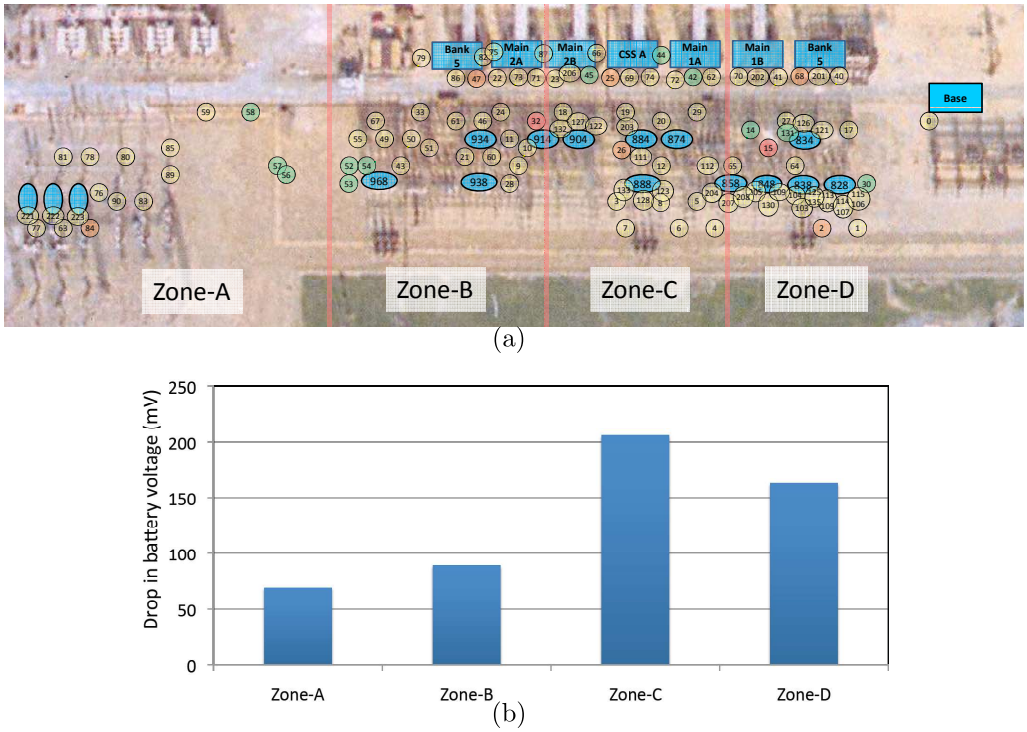

Figure 8.3: Illustration of the layout (a) of *ParadiseNet* [1], a 122-node WSN deployed for equipment health monitoring from a power substation, and the average battery usage of nodes in different geographical zones over a period of five months (b). *ParadiseNet* uses a single-channel link quality based routing protocol.

mechanism to optimally distribute the network traffic over multiple channels would lead to reduction in overhearing and significant improvement in the lifetime of the network.

In addition to reducing overhearing, a second consideration for improving the network lifetime is to address the effect of *differential battery drainage* among the nodes. This is motivated by experimental observations from a WSN testbed that was developed by the UNC Charlotte researchers for health monitoring of high-power equipment in a power substation in Figure 8.3. The WSN, called *PradiseNet* [72], consists of 122 wireless sensor nodes that were deployed in 1000 $\times$ 400 feet area, and uses a link-quality based routing protocol. Figure 8.3(a) depicts the location of nodes in *ParadiseNet* and Figure 8.3(b) depicts the average drops in the battery levels in the four regions of the network over a period of five months of operation.

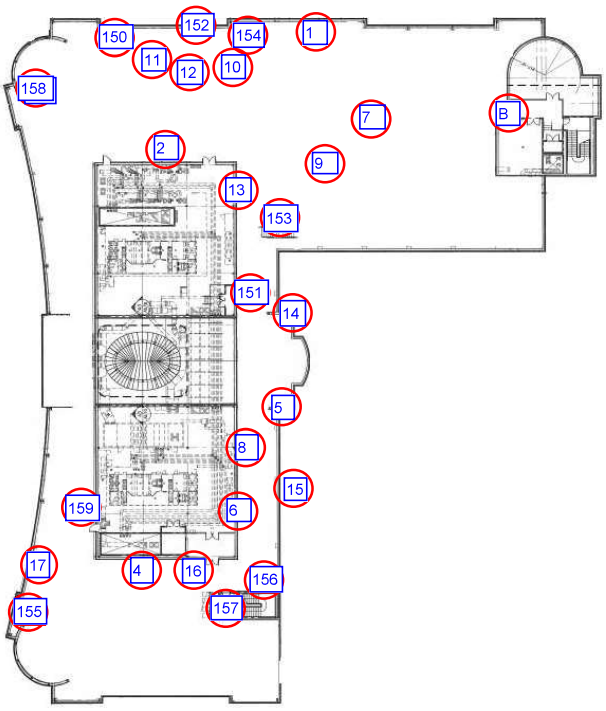

Figure 8.4: A MICAz wireless sensor network testbed *EPIC-RoofNet*.

It can be observed that while nodes closer to the base station generally have higher voltage drops, Zone-C has the highest drop. This is basically due to the fact that sensor nodes in Zone C are responsible for forwarding most of the packets from Zone A and Zone B. In addition, nodes from Zone C also experience higher amount of overhearing traffic. This type of energy imbalance ultimately results in, nodes in Zone C dying earlier than the ones in other zones which will collectively result in network partitioning and decrease in the lifetime of the network. Consequently, it is important that in addition to addressing the overhearing problem, the routing and channel selection scheme should balance the energy consumption in the nodes so that the network lifetime is maximized.

8.2 Motivation behind Transmit Power Adaptation Scheme for WSNs

Development of effective solutions for energy harvesting from renewable resources is gaining increasing importance for achieving long term reliable operations of wireless sensor networks. This includes energy from sunlight, vibrations, heat, magnetic field,

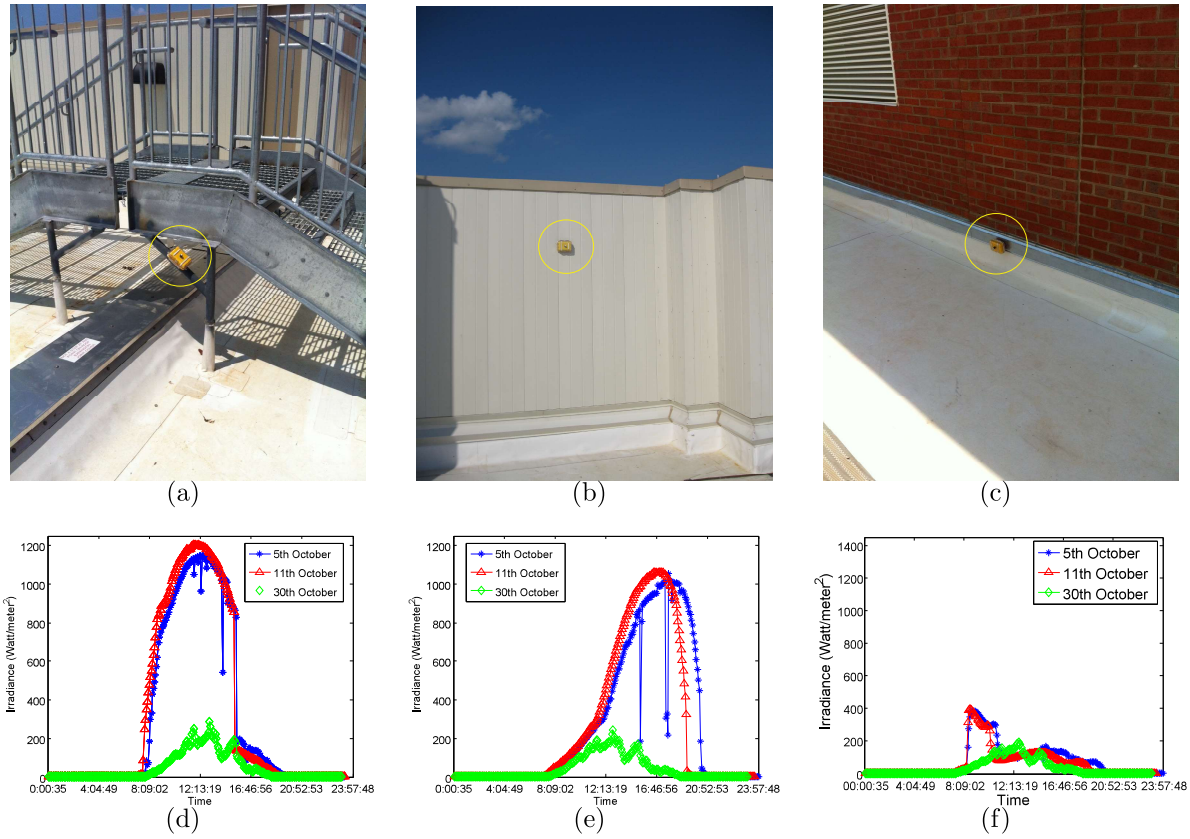

Figure 8.5: Samples of nodes deployed in *EPIC-RoofNet* (a) Node 153 (b) Node 155 (c) Node 159. Irradiance measurement of (d) node 153 (e) node 155 and (f) node 159 for two sunny days (5th and 11th October, 2012) and a cloudy day (30th October, 2012). Node 159 is kept in the shaded region, whereas 153 and 155 gets sunlight most of the time.

and others. All these sources produce spatial and temporal variations. A large scale WSN may comprise many sensor nodes placed somewhat randomly geographically, e.g. for environmental or structural monitoring applications. Random node placement may locate some nodes in shadows and others in extended sunlight. Nodes have different orientations, affecting the irradiance collected by the solar panels. Changes of weather and sun orientation also change solar power intake over time. An illustration of such spatio-temporal variations is shown in Figure 8.5, which depicts solar irradiance measurements obtained from an experimental testbed (shown in Figure 8.4) of MICAz motes equipped with pyranometers deployed at the UNC-Charlotte campus.

The figure shows the irradiance values recorded at three nodes from three different days, illustrating high variations in solar irradiance over both time and space.

Thus the objective of designing the power control and routing scheme is to adapt the energy consumption in the nodes that are critically resource constrained, by *controlling their corresponding overhearing traffic*. In the absence of such adaption, nodes that are in the shadowed region will deplete all their energy faster, which can result in unbalanced lifetimes of the nodes.

8.3 Overview of Research on WSNs

Tree based routing in sensor networks is well-researched. Two very popular such scheme in the context of this dissertation is Xmesh (in Tinyos 1.x) and CTP (in Tinyos 2.x). These are tree based collection protocols whose main objectives are to provide best effort anycast datagram communication to one of the collection root nodes in the network. At the start of the network some of the nodes advertise themselves as the root nodes or sink nodes. The rest of the nodes use the root advertisements to connect to the collection tree. When a node collects any physical parameter, it is sent up the tree. As there can be multiple root nodes in the network, the data is delivered to one with the minimum cost. These are *address free protocols*, so a node does not send the packet to a particular node but chooses its next hop based on a routing cost. The sink always broadcasts with cost = 0. Each node calculates its cost as the cost of its parent plus the cost of its link to the parent. This measure assumes that nodes use link-level acknowledgements and retransmissions. A node i chooses node j as its parent among all its neighbors if cost_{ij} + cost of j < cost_{ik} + cost of k $\forall k \neq j$. In this process a node chooses the route with the lowest cost to the sink. Xmesh and CTP are both designed for single channel WSNs, so overhearing plays a dominant role in reducing the network lifetime. In this dissertation, we consider using multiple channels and transmit power adaptation on top of these tree based routing schemes in an energy-efficient manner to reduce the effect of overhearing. Here we discuss the

current researches in these two areas separately.

★ Current research trends on multi-channel routing in WSNs: Multi-channel routing in wireless networks has received a lot of attention in recent times [42], [46], [36], [8]. However, most of the work published in this area either assume a multi-radio transceiver at each node or generate high control overhead for channel negotiation. Much of this work focuses on reducing the complexity of solving the joint channel selection and routing problem. These schemes are not suitable for WSNs where each sensor is typically equipped with single radio transceiver and has limited computational capabilities. In addition, overhead must be minimized since energy resources are at a premium. Some multi-channel MAC protocols for WSNs such as MMSN [73], TMMAC [74], MMAC [75] are designed for single radio interfaces per node. However, they require precise time synchronization, which is hard to obtain in WSNs.

Recently, some strategies for joint channel assignment and routing for WSNs were proposed in [76], [77], [78]. In [76], the authors propose a Tree-based multichannel protocol (TMCP) where the whole network is statically divided into a number of sink-rooted disjoint subtrees. Nodes residing on different trees are assigned different orthogonal channels. Thus the whole network is partitioned into multiple mutually exclusive single-channel subtrees that reduces the inter-tree interference.

Authors in [77] propose a control theory approach that selects channel dynamically to achieve load balancing among channels. All nodes in the network start on the same channel. When this channel becomes overloaded, some nodes migrate to other channels to spread the communication load across non-interfering frequencies. When a node needs to send messages to another on a different channel, it switches to the channel of the destination node to send the message.

In [78] authors use a game theory approach for assigning channels in WSNs with the total interference of the whole network as the social objective. By using both routing information and topology information, each autonomous agent, i.e., sensor

node chooses the channel that maximizes its payoff according to the channels chosen by the other players.

All of the above schemes mainly consider reducing network interference. Interference is proportional to packet size as well as packet interval. Generally in WSNs the packet size as well as packet interval are small, thus interference is usually not a primary performance factor. Also, some of the above approaches are either centralized or need the topology information that is not always possible to obtain in WSNs. As opposed to these contributions, here we address the problem of performing channel selection and routing together for improving the battery lifetime in WSNs. Furthermore, our goal is to achieve a distributed protocol that can be applied without time synchronization, and requires a single transceiver per node.

★ Current research trends on transmit power control in WSNs: A significant amount of works have been reported on transmit power control for WSNs. The basic ideas of these power control schemes [79], [80], [81], [82], [83] are to find the number of neighbors each node has and adjust the radio transmission power of each node so that the number of neighbors stays within desired range. In [79], the authors propose a power control scheme where a node maintains a list of neighbors whose signal strength are higher than some threshold, and it adjusts the radio transmission power if number of neighbors is outside the predetermined bound. Authors in [80] propose a similar scheme where a node determines its range by counting the number of nodes that acknowledge to its beacon messages.

In [81], the authors propose a scheme where each node ranks neighboring nodes in the order of their signal strengths and adjusts their radio transmission power so that it covers only a minimum number of neighbors with reasonable signal strength.

In PCBL scheme [82], each sensor node sends some packets with different power levels to measure the quality of the link. It then adjusts its radio transmission power for each destination node with the smallest possible value such that a minimum packet

reception ratio is achieved. The scheme also filters out the nodes that have too low reception ratio.

In ATPC [83], the authors propose a feedback based transmission power control scheme that dynamically measures link qualities over time. Each node broadcasts beacons at different transmission power levels, and its neighbours measure signal strength and a link-quality indicator corresponding to these beacons and send these values back by a notification packet. After the notification packet is received, the beaconing node determines the optimal transmission power level individually for each neighbor.

All of the above mentioned power control schemes are developed towards maintaining a reasonable link quality. On the other hand our objective is to adapt the transmit power to help reducing overhearing on the resource critical nodes, to enhance the overall network lifetime. None of these schemes address power control based on node specific requirements, which is a key objective of our work. Also, power control needs to be tied with routing as changing the link quality of a link results in changes in route selection. Also routes need to be adapted so that the overall network traffic avid going through the neighboring regions of the critically energy constrained nodes. Thus the power control problem should be considered jointly with routing, which is one of the contributions of this work.

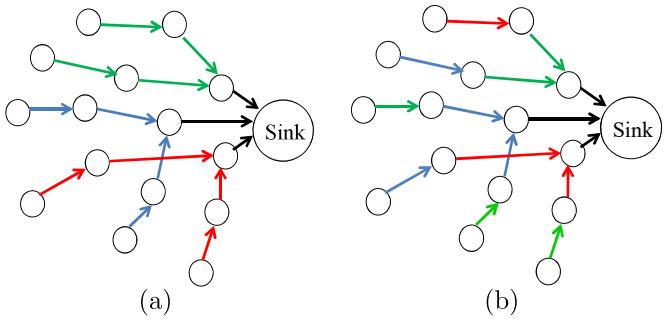

Figure 8.6: Channel assignment schemes (a) FCA, (b) RCA.

In the context of resource constrained wireless sensor networks, this dissertation

has three major contributions. First, we propose two types of multi-channel transmission schemes to reduce the effect of overhearing. In the first type, which we call *flow based channel assignment (FCA)*, k available channels are distributed over the nodes in the network, such that all nodes in a flow have the same channel. Nodes that are on the same channel form a subtree. Thus the scheme partitions the whole network into k vertex-disjoint subtrees as shown in Figure 8.6(a). The detailed description of FCA along with the simulation results is discussed in Chapter 9. Although this channel assignment scheme reduces the average overhearing, it does not allow the nodes to control their energy consumptions with respect to their varying energy resources, which is our goal for balancing the remaining lifetimes of the nodes and thereby maximizing the lifetime of the network. To achieve this, we propose a *receiver based channel assignment (RCA)* that works as follows. We define *receiver channel* as the channel on which a node receives packets. On the other hand *transmit channel* is the channel on which a node transmits, which is the receiver channel on its intended destination. The scheme is shown in Figure 8.6(b). In RCA, nodes monitor their receiver channels for incoming transmission by default. At the time of transmission, a node temporarily switches to a transmit channel and returns to its receiver channel after transmission. Essentially, RCA allows nodes to choose their transmit channels dynamically to balance the energy consumption of its neighbors so as to balance their residual battery capacities. Details on the implementation of RCA along with experimental results are reported in Chapter 10.

Second, we present a joint power control and routing scheme for rechargeable wireless sensor networks with an objective of enhancing the overall network lifetime. The proposed approach incorporates estimation of the minimum power levels for achieving reliable link quality and a routing metric that incorporates the effect of overhearing caused to nodes that are critically low in energy resources in addition to route quality. The detailed scheme is discussed in Chapter 11 along with the

performance evaluations.

Third, we also develop a mathematical model for network lifetime estimation under optimal transmit power control. This model is then extended to incorporate the benefits of multi-channel communications in improving the network lifetime. We also compare the two types of above mentioned channel selection schemes (FCA and RCA) using the optimal power control. The analytical model is presented in Chapter 12.

CHAPTER 9: FLOW BASED ENERGY AWARE ROUTING AND CHANNEL SELECTION SCHEMES FOR WSNS

In this chapter, we consider the problem of developing *flow-based*, energy aware channel selection and routing schemes for *data collecting* wireless sensor networks (WSNs). As discussed in the previous chapter, using multiple channels helps in reducing overhearing which results in increased network lifetime. Flow based channel selection schemes are defined by the schemes where all nodes in a flow have the same channels. As different flows are assigned to different channels, overhearing is avoided among the nodes that are part of different flows, which maximizes the overall network lifetime.

In *data collecting* wireless sensor networks, nodes follow a tree structure connecting the nodes to the sink. With a single channel, a node overhears all nodes that are in the receiving range of that node. To cope with this, we propose the idea of multi-channel tree. Let us define the nodes that are immediate neighbors of the sink as first-level nodes. Thus, for f first-level nodes, the multi-channel tree partitions the whole network in f vertex-disjoint subtrees all rooted at any of the f first-level nodes. All first-level nodes choose any of the k available channels and all their children transmit

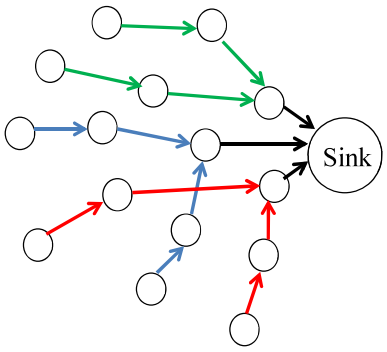

Figure 9.1: A multi-channel tree for WSNs.

on the same channel. The sink is tuned to a default channel and all the first-level nodes switch to that channel only when they want to transmit to the sink, otherwise they stay on their chosen channel. Figure 12.1 depicts a multi-channel tree where different channels are shown in different colors. This multi-channel scheme reduces overhearing and thus increases the battery life of the whole network. At the same time using multiple-channel reduces the interference as well as contention delay of the network.

9.1 Lifetime Calculation

We assume that each sensor node has finite electrical energy, which is determined by the capacity of the onboard battery. Based on the experimentally validated model [72], the current drawn in each node is calculated as follows:

$$\begin{aligned} \mathcal{I} &= \frac{I_{Bt}T_{Bt}}{T_B} + M.I_{Dt}T_{Dt} + N.\frac{I_{Br}T_{Br}}{T_B} + O.I_{Dr}T_{Dr} \\ &+ F.I_{Dt}T_{Dt} + \frac{I_sT_s}{T_D} + N_P.I_PT_P \end{aligned} \tag{9.1}$$

where I_x and T_x represent the current drawn and the duration, respectively, of the event x; and T_B represents the beacon interval. Transmission/reception of beacons is denoted by B_t/B_r, data transmit/receive is denoted by D_t/D_r and processing and sensing are denoted as P and S, respectively. O and F are the overhearing and forwarding rates, respectively, and N is the number of neighbors. M is the rate at which a node transmits its own packets. If there are no retransmissions, then $M = \frac{1}{T_D}$, where T_D is the data interval. N_P represents the number of times that a node wakes per second to check whether the channel is busy, and is set to 8 in our application. We assume that each node is able to estimate all the dynamic parameters that are used in equation (12.1), by periodic assessment of its overheard and forwarded traffic.

With this the lifetime of a mote can be calculated as $L = \frac{B}{\mathcal{I}}$ where B is the initial capacity of the battery. We define the lifetime of a network as the time until the first

node depletes it's energy, i.e. the *worst case network lifetime (WNL)*. Thus, the WNL can be expressed as $L = \min(L_1, L_2, ..., L_V)$ where $L_1, L_2, ..., L_V$ are the lifetime of the sensor nodes respectively.

9.2 Problem Formulation

Our objective is to maximize the worst case network lifetime L, subject to the following constraints:

• One parent constraint: This constraint states that each node has one parent. If N_i is the set of neighbors of i, then

$$\sum_{j=1}^{|N_i|} x_i^j = 1 \tag{9.2}$$

where x_i^j is a binary variable that is 1 when j is the parent of i and 0 otherwise.

• Directionality constraint: A child sends packets to only its parent, thus

$$x_i^j + x_j^i \leq 1 \tag{9.3}$$

• Connectivity constraint: Note that j is a parent of i if there is a connection between i and j in the connectivity graph, i.e.,

$$x_i^j \leq W_i^j \tag{9.4}$$

where W_i^j is 1 if j can be a parent of i and 0 otherwise.

• Flow constraint: The rate of flow at i, denoted by F_i is given by the rate at which node i generates packets plus the rate at which it's children send packets, i.e.,

$$F_i = c + \sum_{j=1}^{|N_i|} x_j^i F_j \tag{9.5}$$

where c is the rate at which each node sends packets.

• Overhearing constraint: The amount of overhearing traffic at node i, denoted by O_i is the total amount of traffic from all the nodes that are in the overhearing range of i and in the same channel of i, i.e.,

$$O_i = \sum_{j=1, j\neq i}^{|N_i|} Y_i^j F_j U_i^j \tag{9.6}$$

where Y_i^j is a binary variable that is 1 if i is in overhearing range of j and 0 otherwise and U_i^j is 1 if i and j are in the same channel and 0 otherwise. If C_i is the channel chosen by i, then U_i^j can be written as:

$$\begin{aligned} |C_i - C_j| &\leq M(1 - U_i^j) \\ 1 - U_i^j &\leq |C_i - C_j| \end{aligned} \tag{9.7}$$

where M is a very large number.

• Parent-child constraint: If j is the parent of i, then the channel of i is same as the channel of j, i.e.,

$$C_i = \sum_{j=1}^{|N_i|} C_j x_i^j \tag{9.8}$$

• Energy constraint: Also the total energy spent by node i cannot be more than the residual energy (B_i) of that node, i.e.,

$$\begin{aligned} L \quad & \left(\frac{I_{Bt} T_{Bt}}{T_B} + M.I_{Dt} T_{Dt} + N.\frac{I_{Br} T_{Br}}{T_B} + O.I_{Dr} T_{Dr} \right. \\ + \quad & \left. F.I_{Dt} T_{Dt} + \frac{I_s T_s}{T_D} + N_P.I_P T_P \right) \leq B_i \end{aligned} \tag{9.9}$$

• Critical node constraint: If we assume that there are some nodes named *critical nodes* that can support a maximum overhearing traffic and C_r is the set of these

nodes then

$$O_i \leq O_i^M \ \forall i \in C_r \tag{9.10}$$

where O_i^M is the maximum number of allowed overhearing rate for i.

• First-level node channel constraint: The first-level nodes choose any of the K available channels and Z_k^l is a binary variable that is 1 if first-level node k chooses channel l and 0 otherwise, than

$$\sum_{l=1}^{K} Z_k^l = 1 \ \forall k \in G \tag{9.11}$$

where G is the set of first-level nodes. Thus the channels chosen by the first-level nodes are given by

$$C_k = \sum_{l=1}^{K} l Z_k^l \ \forall k \in G \tag{9.12}$$

From constraints (9.2)-(9.12), we can observe that the problem is nonlinear. Next we calculate the complexity of this problem.

9.3 Complexity of Maximum-Lifetime Multi-Channel Routing Problem

We show that the maximum-lifetime routing problem is NP-complete using reduction from the *Degree constrained spanning tree problem* even if for single channel. Degree constrained spanning tree is a spanning tree where the maximum vertex degree is limited to a certain constant k. One instance of our problem is when all the nodes overhear each other. In that case, from equation (9.9) the worst case lifetime L is given by:

$$L = min \frac{B_i}{F_i + c} \forall i \tag{9.13}$$

as all the other terms are constants. In equation (9.13), c is a constant. If D_i is the degree of node i, then $D_i = F_i + 1$, thus $L = min \frac{B_i}{D_i + \mathcal{C}} \forall i$ for some constant $\mathcal{C}$.

Proof: First, it is clear that the maximum-lifetime multi-channel routing belongs

to NP, since given a tree, we can calculate the worst case lifetime of the network in polynomial time.

To show that the problem is NP-hard, we show that for a graph G has a spanning tree of maximum vertex degree of k if and only if G has a tree whose lifetime is greater than or equal to $\frac{1}{k+\mathcal{C}}$. We set $B_i = 1, \forall i \in G$.

Suppose G has a spanning tree T with a maximum vertex degree of k. Then it is straightforward that the lifetime of T is

$$L(T) = min\frac{B_i}{D_i(T) + \mathcal{C}} \geq \frac{1}{k + \mathcal{C}} \tag{9.14}$$

Similarly, if G has a spanning tree T with $L(T) \geq \frac{1}{k+\mathcal{C}}$, then we have $D_i(T) \leq k$, $i = 1...N$. Otherwise, if $D_j(T) > k + 1$ for some $j \in [1, N]$, then

$$L(T) \leq \frac{B_i}{D_j(T) + \mathcal{C}} \leq \frac{1}{k + 1 + \mathcal{C}} \tag{9.15}$$

which is contradictory.

Thus, we can reduce an instance of the degree constrained spanning tree problem to an instance of our maximum-lifetime routing problem. As the degree constrained spanning tree problem is NP-complete, the maximum-lifetime routing problem is NP-hard even for single channel.

As the single channel routing is a special case of multi-channel routing, thus the maximum-lifetime multi-channel routing is also NP-complete. In the light of NP-completeness, we propose some heuristics to solve this problem. We explore the solution of this problem by investigating three distributed schemes as well as one centralized scheme CRCA for route and channel selection which are explained in the following sections.

9.4 Distributed Route and Channel Assignment Schemes For Sensor Networks

We now present the proposed distributed route and channel assignments schemes named DRCA-1, DRCA-2 and DRCA-3 as described below:

9.4.1 DRCA-1

We define the nodes that are immediate neighbors of sink as first-level nodes. Nodes that are neighbors of first-level nodes are termed as second-level nodes and so on. For all the distributed schemes, we assume that all nodes know the battery life of their neighbors, i.e. if there is any change in battery life, nodes broadcast *update* messages. Our DRCA-1 scheme can be explained by the following set of actions.

★ Battery state broadcast phase: At first all the nodes are on the same channel (say C). The sink first broadcasts the route request to all first-level nodes through C. All the first-level nodes go on random backoff based on their battery life and then choose the least used channel (out of K orthogonal channel) around their neighbors and broadcast L_{P_i} (L_{P_i} is the estimated battery lifetime of P_i) and chosen channel through C. We call these packets *battery broadcast (BB)* packets. BB packets have a field named *full* that is 0 if a node still can afford children, otherwise the full bit is set to 1. All first-level nodes choose sink as their parent.

★ Parent broadcast phase: All the second-level nodes, upon receiving the BB packet, check their own battery power and based on the battery status, they wait for a random backoff that is proportional to their battery life. This is expected to give preference to the nodes to select channel that have lower power. In the backoff period, all nodes overhear the channel and calculate the usage of each channel in their neighborhood. When the backoff timer expires, each second-level node chooses it's parent as follows. For any channel c, each node calculates $\mathcal{L}_c = \min\{L_i\}\ \forall\ i \in S_c$ where S_c is the set of neighbors that are in channel c. Then a node chooses the channel j such that $\mathcal{L}_j = \max\{\mathcal{L}_c\}\ \forall\ c$. After choosing the channel j, a node chooses a parent P_i with maximum $L_{P_i}, \forall P_i \in \mathcal{P}_j$ where $\mathcal{P}_j$ is the set of parents of that node with

channel j. This avoids making a less powered node their parent. Also the channels used by the less powered neighboring nodes are avoided. After choosing their parent, nodes broadcast *parent broadcast (PB)* packets that consist of the parent ID.

★ Parent confirmation phase: After receiving the parent broadcast packet from a child, the parent confirms by sending *parent confirmation packet*. The parent P_i calculates a new L_{P_i} and sends this in the parent confirmation packet. If some nodes have a strict constraint on maximum overhearing traffic (say a maximum of $\mathcal{N}$ packets/second) and it has n nodes that are overheard by it, then it informs all it's neighbors not to send more than $\frac{\mathcal{N}}{n}$ packets/sec in the parent confirmation packet. All its neighbors in the next parent confirmation phase do the same to their children. This process goes on until and unless one node is reached that cannot afford more children. Thus this node broadcasts with a BB packet with full bit set to 1, implying that it cannot take any more children. All the children avoid using that node as their parent if they have other options. If they do not have any other parent, then they connect to that node. If may happen that a node can afford few children (say 2) in their parent broadcast phase. Thus they broadcast BB packets with full = 0, but after getting 2 children, they immediately broadcast a BB packet with full = 1.

This process goes on until the last-level nodes are reached. The last-level nodes choose their parent, send the BB packets and after sometime all nodes switch to their chosen channels and start sending packets to their parents.

• Overhead analysis: Let us assume that there are $\mathbb{L}$ labels and number of nodes in level i is l_i, $\forall\ i \in (1, \mathbb{L})$. At first the sink sends a route request packet to all the first level nodes. This is followed by l_1 BB packets from the first level nodes, followed by l_2 parent broadcast packets from the second level nodes, followed by l_2 parent confirmation packets from the first level nodes. Thus the total overhead for the parent discovery of the second level nodes is given by $l_1 + 2l_2$. This process goes on until the last level nodes, where each of the $l_{\mathbb{L}}$ nodes broadcasts one BB packets.

Thus the total overhead of DRCA-2 is given by $1 + \sum_{i=1}^{\mathbb{L}-1}(l_i + 2l_{i+1}) + l_{\mathbb{L}}$. This calculation ignores the case when the maximum overhearing constraint of any node is violated, in this case some extra overhead should be taken into account. Also the overheads of the update messages are not considered in overhead calculation.

9.4.2 DRCA-2

In DRCA-1 the channel and parent selection is done level by level. In DRCA-2, nodes do not choose their parents level by level. Rather parent selection is done in increasing order of the individual nodes battery lifetime. The idea of DRCA-2 stems from the idea of how water flows from a point to another, avoiding the high altitude areas. The notion of this scheme is that there is some altitude associated with the critical nodes and the nodes that are overheard by the critical nodes. Thus all nodes try to avoid these set of nodes to reach the sink. With this, the scheme of DRCA-2 can be described as follows:

At first the sink sends a broadcast packet with hop-count = 0. Any node that receives the packet increments the hop-count and rebroadcasts it. In this way, all nodes are able to get the hop-count from the sink. Then each node goes on random backoff that is proportional to it's battery life. When this backoff timer expires, it starts discovering the routes. Each node i calculates a metric named priority as $p_i = c_1.b_i$ and notifies it's neighbors, where c_1 is a constant. In the expression of priority, b_i is the battery life of node i. $c_1 < 1$ for all critical nodes and their neighbors and equal to 1 for all other nodes. This makes sure that the critical nodes and their neighbors (nodes that are overheard by the critical nodes) gets less priority (more altitude) than others in relaying others traffics.

At first, all the first level nodes choose any channel similar to DRCA-1 and then all the nodes go on random backoff based on their battery status. This channel selection of the first level nodes is same for all the schemes. When a node's turn comes, it chooses a node among it's neighbors (whose hop-count is less than its own) with the

highest priority and sends a *parent notify (PN)* packet to that neighbor that consists of the neighbor ID. The neighbor does the same and this process goes on until the PN packet reaches the second level nodes. For any channel c, each second level node calculates $\mathcal{L}_c = \min\{L_i\}\ \forall\ i \in S_c$ where S_c is the set of neighbors that are in channel c. Then the node chooses the channel with $\max\{\mathcal{L}_c\}\ \forall\ c$ and then chooses a parent P_i with maximum $L_{P_i}, \forall P_i \in \mathcal{P}$ where $\mathcal{P}$ is the set of parents of that node with the same channel. The PN packet carries the IDs of the nodes that it visits. To ensure that the PN packet does not circulate in a loop, an intermediate node upon receiving the PN packet, chooses a parent that is not visited by the packet. This process goes on for all the nodes until and unless all the nodes get a route to the sink. When the PN packets traverse in the network, nodes that can overhear the packet, update their battery life with the new information.

• Overhead analysis: At first the sink sends a broadcast packet for determining the hop-count of all nodes from the sink. For a n node network, this requires an overhead of n. After that all the nodes except the first level nodes select their parents and send PN packets, which incurs a total overhead of $n - l_1$ (assuming that there are l_1 nodes in the first level) packets. Thus, totally DRCA-2 needs $2n - l_1$ packets as overhead of route and channel selection. We assume that all nodes broadcast their recent priority metric by sending the update messages, the overhead due to these updates are not taken in overhead calculation.

9.4.3 DRCA-3

In the above two schemes, each node chooses its route based on the informations from it's neighbors. The information from all the intermediate nodes in the route is not used in these two cases. DRCA-3 is a scheme that exploits the information from the intermediate nodes of a route at the cost of more overhead. This scheme is described using the following stages:

★ Route Discovery: At first all the nodes notify the sink about their battery

condition. The critical nodes also notify the sink of their neighbor's ID so that the sink knows the critical nodes and their neighbors. The sink first sorts the nodes according to their battery life and sends route discovery packets in increasing order of battery life. In the discovery packet, the sink includes the IDs of the critical nodes as well as the nodes that overhears the critical nodes. When the discovery packet travels through the network, it carries the sequence of node IDs that it traverses. Any intermediate node i calculates $a_i = \min(b_i, b_j)$, $\forall j$ in its neighborhood, where b_i is the battery life of node i. Discovery packet also has a field that carries $\mathcal{T} = \min_{i \in \text{route}} a_i$.

★ Route Reply: The destined node waits for the first N packets and stores the routes in it's cache as well as their corresponding $\mathcal{T}$ values. Let us define $\mathcal{T}_i$, $i \in (1, N)$ as the minimum battery life of the i-th discovery packet. Then it chooses the route with highest $\mathcal{T}_i$, $i \in (1, N)$ and sends reply through that route.

★ Route Accept: After getting the reply packet, the sink checks whether this route fulfills the overhearing constraint or not. If the overhearing constraint is fulfilled then the sink sends an acknowledgement message with the accept bit set to 1, otherwise it sends accept message with accept bit set to 0. All the intermediate nodes update their route cache if the accept bit is 1. All nodes that overhears this packet get informed about the number of active nodes and their amount of traffic and recalculate their battery life. If the accept bit is 0, the destined node again sends reply packet through the next best route. Note that when the accept bit is 1, all the intermediate nodes are termed as explored nodes as they can get their path towards the sink as well. Next the sink sends the discovery packets form the list of unexplored nodes based on their battery life and this process goes on until all the nodes are explored.

It should be noted that this process incurs a large overhead. Thus in our scheme we consider that the sink sends route discovery for K destinations at a time. When K is small, the route and channel selection is very good but the route overhead is high

and for large K, the route and channel selection is poor where the route overhead is low. Next, we derive the average number of route discovery phases that the sink has to go through before exploring the whole tree. Number of overheads is also calculated analytically.

• Overhead analysis: We assume that there are $\mathbb{L}$ labels and number of nodes in level i is l_i, $\forall\ i \in (1, \mathbb{L})$. At first all the nodes are unexplored. Let us denote $P_{l_i}^j$, V^j, $V_{l_i}^j$, NV^j and $NV_{l_i}^j$ are the probability of choosing any unexplored node in level i at phase j, the number of nodes explored at phase j, the number of i-th level nodes explored at phase j, the number of unexplored nodes of level i at phase j respectively. Now, at first all the nodes are unexplored, i.e. $V^0 = 0$, $V_{l_i}^0 = 0$, $\forall i \in (1, \mathbb{L})$, $NV^0 = n$ and $NV_{l_i}^0 = l_i$, $\forall i \in (1, \mathbb{L})$, thus, $P_{l_i}^0 = \frac{l_i}{\sum_{i=1}^{\mathbb{L}} l_i} = \frac{l_i}{n}$, $\forall i \in (1, \mathbb{L})$.

At the first phase a random node is chosen from the list of unexplored nodes. For simplicity, let us assume that all the nodes choose any of their previous level nodes to reach the sink. If any unexplored node of the i-th level is chosen, then the number of nodes explored at the first phase is i (at each level 1 node is explored). Thus, the number of explored nodes in first phase is $V^1 = \sum_{i=1}^{\mathbb{L}} i \times P_{l_i}^0 = \sum_{i=1}^{\mathbb{L}} \frac{i \times l_i}{n}$ and $V_{l_i}^1 = \frac{\sum_{j=i}^{\mathbb{L}} l_j}{n}$.

In general, at any phase k, if any unexplored node at i is chosen, then that node is explored with probability of 1. But for any previous level j ($j < i$), an unexplored node is explored with a probability of $\frac{NV_{l_j}^{k-1}}{l_j}$. Thus the number of nodes explored at phase k is $V^k = \sum_{i=1}^{\mathbb{L}} P_{l_i} \times \left(1 + \sum_{j=i-1}^{0} \frac{NV_{l_j}^{k-1}}{l_j}\right)$. The number of unexplored vertices at k-th phase is the difference between the number of unexplored nodes at $(k-1)$-th phase and the number of vertices explored at k-th phase, i.e. $NV^k = NV^{k-1} - V^{k-1}$. For the same reason, at each level $i \in (1, \mathbb{L})$, $NV_{l_i}^k = NV_{l_i}^{k-1} - V_{l_i}^{k-1}$. This process goes on until the number of explored nodes is less than n. As an example, if $l_1 = 20$, $l_2 = 30$, $l_3 = 40$, $l_4 = 50$ and $l_5 = 60$, we get the number of phases required is 114. Thus, if the sink sends $K = 10$ discovery packets at a time, then the number of times

the sink has to send discovery packets is 12.

At first all nodes need to send their battery state to the sink, we assume that it takes an overhead of a broadcast i.e. n packets. Next in the i-th phase, it needs a broadcast and one route reply and route accept packet. If all nodes are explored in $\mathcal{K}$ phases, the total overhead is given by $(\mathcal{K}+1)n + 2\sum_{i=1}^{\mathcal{K}} V^i$.

9.5 Centralized Route and Channel Assignment For Sensor Networks (CRCA)

In the distributed approach, nodes do not have the picture of the whole network, thus this distributed solution can be further made better if this solution is passed from to the sink or base station where it can refine the route and channel selection and send this information to the nodes. For this, the sink needs the neighboring informations of all the nodes as well as their battery states.

We use a *simulated annealing* based approach to solve this problem. Let us assume that there are n nodes $\{v_1, v_2, ..., v_n\}$ and $\mathcal{S}_{v_i}$ is the set of neighbors of v_i. We use simulated annealing so that the solution does not get stuck into the local optima. As

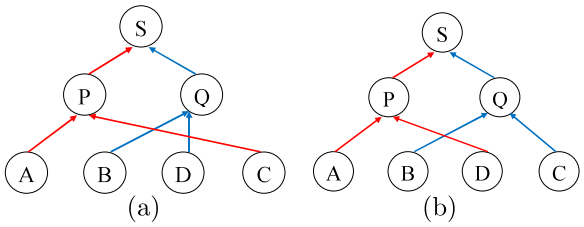

Figure 9.2: An example of (a) local optimal solution, (b) global optimal solution.

an example in Figure 9.2, let us assume that *(A, B)*, *(B, D)* and *(D, C)* can overhear each other. If nodes *A, B, C, D* choose their parents sequentially, and *A, C* choose *P* as their parent and *B* chooses *Q*, then *D* would choose *Q* as parent. Then the system is in a local optimum. In this solution, *B* and *D* will overhear. It should be observed that a better solution is to assign *A* and *D* to *P* and *B* and *C* to *Q*, which is also another optimum and gives better performance than the previous one. Next, we introduce a centralized route and channel selection scheme that comes out of this

local optimum with some probability.

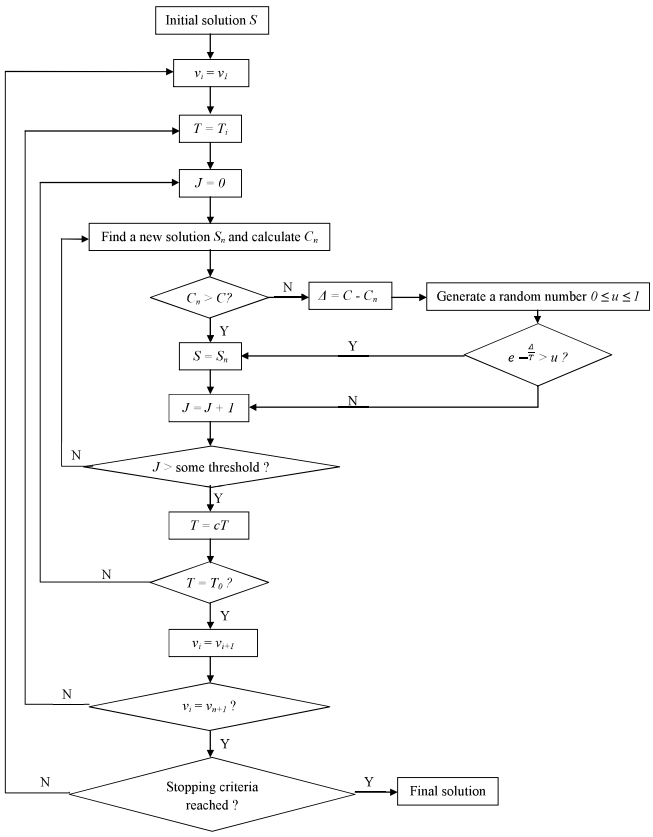

Figure 9.3: Our route and channel selection scheme using simulated annealing.

Our centralizaed route and channel selection (CRCA) scheme is shown in Figure 9.3. It takes the solution given by *DRCA* (or a random initial solution) and then tries to make it better iteratively. Each of the n nodes has a set of neighbors. In each iteration the leaf level nodes first choose their parents one by one and then the upper level nodes and so on. When a node's turn comes, it runs simulated annealing as shown in Figure 9.3. In simulated annealing there is a control parameter T that starts with a high temperature and then gradually reduces to a low temperature. For each T a node chooses a different parent and checks whether it reduces the cost or not. Here cost is defined as $\frac{1}{min(L_1,L_2,...,L_V)}$, thus our objective is to minimize the cost. If there is an improvement, the solution is accepted, otherwise the solution is accepted with a probability equal to $e^{-\frac{\Delta}{T}}$, where Δ is the difference between the pre-

vious cost and the new cost. This probabilistic acceptance avoids stucking into local optimum. Because of this probability, there is a possibility that C chooses Q and then D chooses P, i.e. the optimal solution. Also if the new solution does not satisfy equation (9.10), it is rejected. This process is iterated until a maximum number of iteration is reached or the nodes do not change parents for a predefined number of iterations.

9.6 Simulation Results

In this section, we present the performance of our proposed schemes as obtained from simulations. We consider one sink and 50 nodes in a grid topology of 450 meters $\times$ 500 meters as shown in Figure 9.4. The transmission as well as overhearing distance is 160 meters and interference range is 250 meters. The data interval (T_D) is assumed to be 60 seconds. The parameters used in the simulations are listed in Table 9.1.

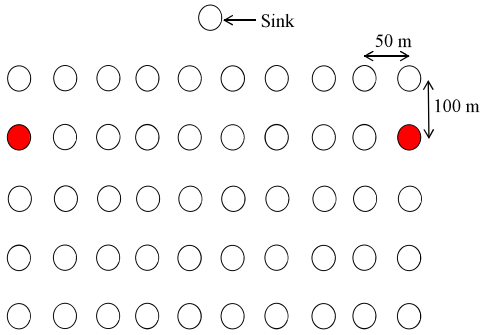

Figure 9.4: The simulation environment, the red nodes are two critical nodes.

Table 9.1: Simulation environment

Var	**Values**	**Var**	**Values**	**Var**	**Values**	**Var**	**Values**
I_{Rt}	20 mA	T_{Rt}	140 ms	I_{Rr}	20 mA	T_{Rr}	140 ms
I_{Dt}	20 mA	T_{Dt}	140 ms	I_{Dr}	20 mA	T_{Dr}	140 ms
I_P	8 mA	T_P	3 ms	I_S	7.5 mA	T_S	112 ms

★ Comparison of lifetime: We choose two critical nodes with an initial battery current of 500 mAhr and all other nodes have an initial battery current uniformly distributed between 1000-5000 mAhr. We vary the route update intervals and plot the

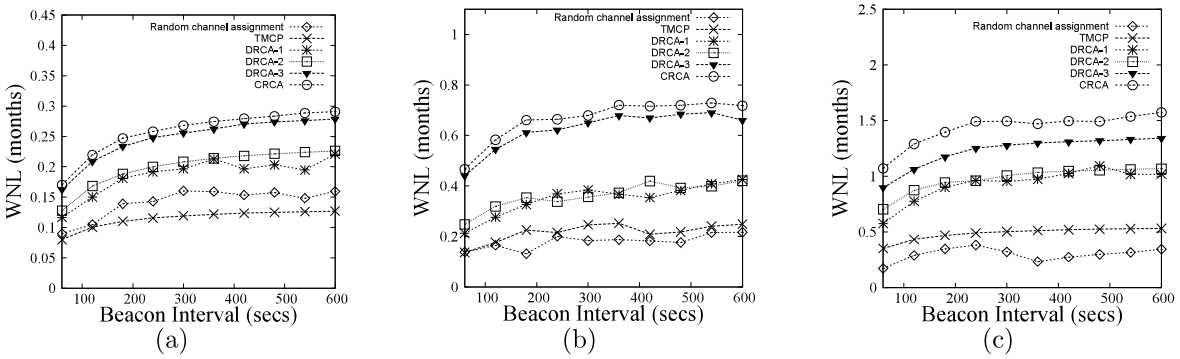

Figure 9.5: Comparison of lifetime when initial battery capacities are uniformly distributed for (a) 1 channel (b) 2 channels (c) 8 channels.

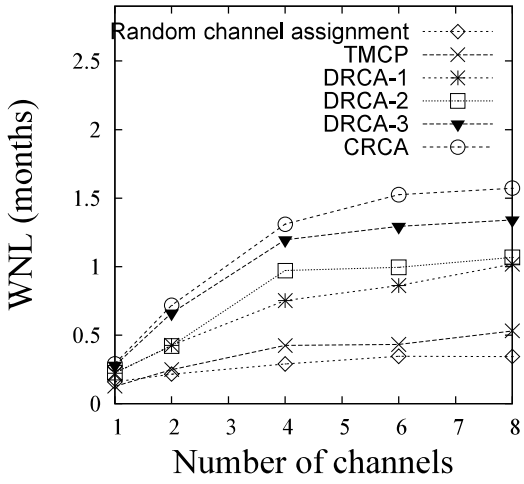

Figure 9.6: Comparison of lifetime when different number of channels.

variations of worst-case battery lifetime of the networks for all the proposed schemes in Figure 9.5. Besides that, we also compare our schemes with the random channel and route selection scheme and TMCP [76]. From Figure 9.5 we can observe that all our proposed schemes outperform the random channel and route selection scheme as well as TMCP. Among the proposed distributed approaches, DRCA-2 performs very similar to DRCA-1. Also we can observe that DRCA-3 (with $K = 1$) performs better than the other two. The drawback of DRCA-3 is that it incurs more overhead in terms of exchanging route discovery, reply and accept packets. While comparing DRCA-3 and CRCA we can observe that CRCA gives higher lifetime as the sink acts as a central agent to choose the routes with the global information of the networks.

★ Comparison with number of channels: Figure 9.6 shows the comparison of lifetime with the variation of number of channels for different schemes when the route update interval is 600 seconds. Similar to Figure 9.5, we can observe that DRCA-3 performs better than DRCA-1 and DRCA-2 over different number of channels and CRCA performs the best. Also we can observe that after 6 channels, the performance start getting saturated.

Table 9.2: Comparison of overhead

Initial Distribution of Battery	**DRCA-1**	**DRCA-2**	**DRCA-3 (K=1)**	**DRCA-3 (K=5)**	**DRCA-3 (K=10)**
Uniform	131	91	1416	406	289

★ Comparison of overhead: Table 9.2 shows the comparison of the routing overhead for different distributed schemes. These overheads are only the control messages that are to be exchanged throughout the network only at the time of routes and channel assignment. Thus the periodic route updates and data exchanges are not considered in these overhead calculations. From Table 9.2, we can observe that DRCA-3 has a much higher overhead compared to DRCA-1 and DRCA-2, but the performance of DRCA-3 is better compared to the other two. Thus DRCA-3 achieves better performance at the cost of high overheads.

★ Comparison of DRCA-3 for different K: Figure 9.7 shows the comparison of DRCA-3 with different values of K. From this figure, we can observe that the lifetime decreases with increase in K. As K increases, the route and channel updates are less frequent, which results in poor channel and route selection.

9.7 Discussions

In this chapter, we demonstrate the construction of data gathering tree in multi-channel wireless sensor networks. The problem turns out to be an NP-complete problem, which motivates the investigation of some distributed and centralized approximation schemes to solve this problem. Through simulations, we demonstrate

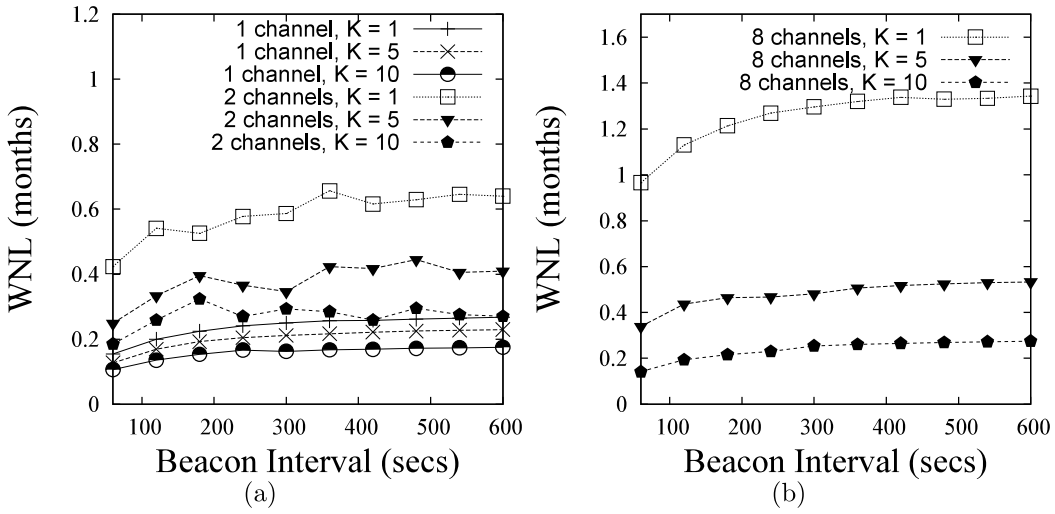

Figure 9.7: Comparison of lifetime when initial battery capacities are uniformly distributed for (a) DRCA-3, 1 and 2 channels (b) 8 channels.

the effectiveness of our proposed channel assignment and routing schemes compared to random channel and route selection and TMCP [76].

The above-mentioned schemes have the following limitations. First, in the above-mentioned schemes, nodes select the same channels as that of their parents. Hence, if the sink has n immediate neighbors and there are k channels where $k > n$, then at least $k - n$ channels will be unused, since there will be at most n sub-trees in the network. One improvement of these schemes is to let nodes on the same sub-tree to use multiple channels, thereby improving channel utilization. Second, in the proposed schemes, the parent and channel assignments are static. These do not change even with variations of congestion and link quality. These result in poor route quality that leads to higher packet loss, retransmissions, and overhearing. Moreover, the channel quality may vary over time, which requires a dynamic protocol. In Chapter 10, we address all these issues and develop a *dynamic routing and channel selection scheme* for WSNs based on some route quality metric. In the proposed research, nodes have their designated *receiver channel* for receiving their incoming packets. While transmitting, nodes switch to the receiver channel of their parents. The parent

selection is done dynamically in such a way that the overhearing is minimized to the nodes with lesser battery lifetime. By doing this, we achieve a much higher network lifetime by dynamically balancing the lifetimes of individual nodes.

CHAPTER 10: RECEIVER BASED DISTRIBUTED ROUTING AND CHANNEL SELECTION SCHEMES FOR WSNS

To overcome the limitations of the *flow based* channel assignment schemes, discussed in the previous chapter, we develop a *receiver based*, quality and battery-health aware *Distributed Routing and Channel Selection (DRCS)* scheme that dynamically chooses channels and routes to optimize network lifetime and performance. To do that, we assume a multi-channel transmission model where nodes can choose their own channels for reception, which they monitor by default, and any node wishing to transmit to another node needs to temporarily switch to the channel of the receiver for transmission. This leads to a multi-channel tree rooted at the sink, where individual links can be on different channels as determined by the receive channel of the corresponding receiver. The objective is to dynamically control the current consumptions of the nodes, by dynamically switching the parents and channels, so as to *equalize their remaining lifetimes* as estimated from their current battery capacity and usage.

In *data collecting* wireless sensor networks, the forwarding scheme follows a tree structure connecting the nodes to the sink. With a single channel, a node overhears all nodes that are in the receiving range of that node. Our first objective is to use a multi-channel tree so that the overhearing problem is reduced. In our scheme, the available channels are distributed among the nodes so that each node listens on its selected channel by default. For data transmissions and forwarding, each node temporarily switches to the channel of its parent and switches back to its designated channel when the transmission is completed. Selection of designated channels as well as parents are performed based on a battery health parameter H and a path metric that is calculated using a link quality parameter (ETX), as explained below.

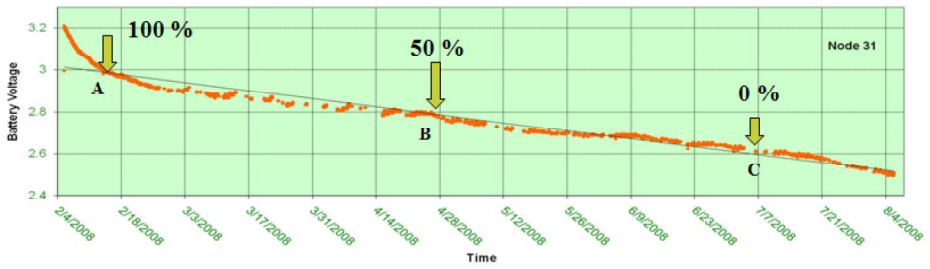

Figure 10.1: Battery discharge curve of a typical node in *Paradisenet*.

While channel selection builds a multi-channel tree that is the primary mechanism for overhearing reduction (see illustration in Figure 8.3(c), where different channels are shown in different colors), it also builds the framework for dynamic route and channel selection to achieve load balancing, which is designed to meet our second objective of lifetime equalization.

10.1 Preliminaries

We define the battery *health-metric* H of a node to represent its remaining battery lifetime, i.e. the estimated time until its battery is depleted under its currently estimated energy usage. We assume $H \propto \frac{B}{\mathcal{I}}$, where B is the remaining capacity of the battery and $\mathcal{I}$ represents the estimated current drawn at the node. Based on the experimentally validated model [72], the current drawn in each node is calculated as follows:

$$\begin{aligned} \mathcal{I} &= \frac{I_{Bt}T_{Bt}}{T_B} + M.I_{Dt}T_{Dt} + N.\frac{I_{Br}T_{Br}}{T_B} + O.I_{Dr}T_{Dr} \\ &+ F.I_{Dt}T_{Dt} + \frac{I_sT_s}{T_D} + N_P.I_PT_P \end{aligned} \tag{10.1}$$

where the parameters and variables used in equation (12.1) are discussed in Chapter 9. These dynamic parameters can be obtained by periodic assessment of a nodes overheard and forwarded traffic.

In this work, we assume that the battery capacity B is estimated from the battery voltage. We consider MICAz nodes, which operate in a voltage range of 2.7V to 3.3V

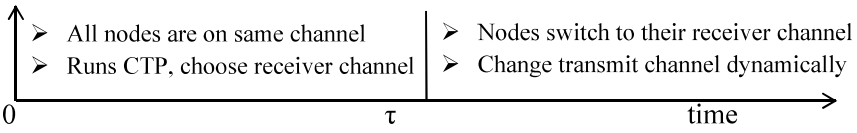

Figure 10.2: The proposed channel selection scheme in DRCS.

[84]. Experimental data from *ParadiseNet* indicates that the discharge curve for alkaline cells under typical usage (i.e. $< 1mA$ average current) is approximately linear within this range. This is illustrated in Figure 10.1. The actual battery voltage is related to the ADC reading as follows: $V_{bat} = \frac{1.223 \times 1024}{\text{ADC reading}}$. Thus, assuming that the capacity is 100% when the battery voltage is greater than or equal to 3V (ADC reading = 417 from MICAz voltage sensor), and 0% when it drops below 2.6V (ADC reading = 482), the battery capacity can be estimated as $B = \min\left(100, \frac{482 - \text{ADC reading}}{0.65}\right)$. Although this is not an accurate estimate, it provides a computationally simple assessment of the battery health[1].

To estimate the quality of a route, we use a path metric that is obtained as the sum of the *expected number of transmissions (ETX)* on each of its links, which is the same principle applied in CTP. An ETX for a link is the expected number of transmission attempts required to deliver a packet successfully over the link. In CTP, path selection is performed as follows. The sink always broadcasts a path metric = 0. A node i chooses node j as its parent among all its neighbors if ETX_{ij} + path vector of $j < \text{ETX}_{ik}$ + path vector of $k \; \forall k \neq j$. In this process a node chooses the route with the lowest path metric to the sink.

10.2 The Proposed DRCS Scheme

We now present the proposed distributed channel selection and routing scheme DRCS for single-radio WSNs that distributes transmission over multiple channels and tries to balance the remaining lifetimes of all nodes in the network. We define the *receiver channel* of a node to be its designated channel for receiving all incoming

[1] A more accurate method for estimating the battery capacity is currently being implemented, which is beyond the scope of this work.

packets. On the other hand, a *transmit channel* is the channel to which a node temporarily switches to transmit a packet, which is the receiver channel of its intended destination. According to DRCS, nodes select their receiver channels to enable distribution of traffic over multiple orthogonal channels. Nodes listen on their receiver channels by default, and hence overhearing is limited to neighboring transmissions on a node's receiver channel only. Transmit channels are chosen dynamically to prolong the lifetime of the *neighboring node with the worst battery health-metric*. Note that channel selection is tied to parent selection, which leads to route determination. Hence the proposed approach leads to a joint channel selection and routing in the WSNs.

As shown in Figure 10.2, the channel selection scheme in DRCS runs in two stages, which are described below. We assume that all nodes broadcast periodic beacon messages, which include their node ID, receiver channel, path metric and battery health-metric. This is performed at intervals called route-update interval (RUI), each time over a different channel that is chosen in a round-robin fashion.

★ First stage: In this stage, all nodes use a common default channel. Each node chooses a random backoff (this ensures that nodes choose channels one after another) and selects *the least used channel in its neighborhood* when the backoff timer expires. This channel becomes the node's receiver channel, which it announces to its neighbors via beacon packets. If there are multiple channels that are least used, the tie is broken by choosing a random channel among the channels that make the tie. All nodes store their neighbors as well as the neighbors' receiver channel information. After a certain time interval τ, the second stage begins. At the end of the first stage, all nodes select their receiver channels so as to minimize overlap in their neighborhoods, in a distributed fashion. Nodes also determine their path metrics to the sink by running CTP over the default channel.

★ Second stage: In the second stage, all nodes switch to their receiver channels.

In this stage, nodes dynamically perform parent selection, and consequently, their transmit channels, based on periodic assessments of the battery health and path metric parameters. This is done as follows. For any channel c, each node calculates $\mathcal{H}_c = \min\{H_i\}\ \forall\ i \in S_c$ where S_c is the set of neighbors that are in receiver channel c and H_i is the health metric of node i. In order to transmit to the sink, the common default channel is chosen, which is the receiver channel of the sink. For all other transmissions (i.e. for transmitting to nodes other than the sink) the transmitting node chooses a transmit channel c with a probability of $\frac{\mathcal{H}_c}{\mathcal{H}}.\frac{1}{e_c}$, where $\mathcal{H} = \sum \mathcal{H}_i\ \forall$ channel i in the node's neighborhood such that there is at least one neighbor that is in channel i and whose path metric is less than the node's path metric. e_c is the ETX of the link between a node and the neighbor in c that has the lowest path metric to the sink. The term $\frac{\mathcal{H}_c}{\mathcal{H}}$ ensures that the receiver channel of the node with the worst health-metric is chosen with the lowest probability. This mechanism *minimizes the overhearing for the neighboring nodes with low health-metrics.* The term $\frac{1}{e_c}$ represents the probability that the packets sent by a node are received successfully by its parent if channel c is chosen. After choosing the transmit channel, a node chooses the parent among all its neighbors on c that has the best path metric to the sink. Nodes choose transmit channels as well as their parents at intervals of RUI.

The routing and channel selection scheme should ensure that new nodes that are added to the network at any time are able to get connected to the network and send informations to the sink. In our proposed scheme, this is ensured by sending the beacon messages in different channels in rotation. Hence, a new node is always able to receive beacons from its neighbors and get connected, irrespective of its choice of the receiver channel.

10.3 Characteristics of DRCS

The proposed routing and channel selection scheme takes into account a number of factors that are explained as follows:

★ Battery state of individual nodes: The battery state of a node is taken into account by the term B. If the battery condition of any node deteriorates, the value of its health-metric will drop. This will result in a lower probability of selection of that node's channel by its neighboring nodes for DATA transmission.

★ Load balancing between nodes: If a node's load increases, its $\mathcal{I}$ will increase, causing its health-metric to decrease. This will cause that node's channel to be chosen with lower probability in the next RUI. Also after choosing the transmit channel, a parent is chosen based on the lowest path metric. Thus, if a parent is overloaded, the value of its path metric will increase, resulting in other nodes to avoid selecting that node.

★ Load balancing between channels: If a channel is overused, the forwarding and overhearing traffic on that channel will increase. This will decrease the health-metric of the nodes in that channel. Thus, that channel is avoided in the next RUIs with higher probability.

★ Route quality: The value of the path metric quantifies the quality of a route. The route quality is important as bad routes result in higher retransmissions, which reduce the network lifetime.

★ Channel quality: DRCS favors selection of channels with better quality, i.e. lower interference, as follows. A high level of channel interference will result in higher number of retransmissions and overhearing on that channel, causing the health-metrics of the nodes on that channel to reduce. Moreover, it will increase the e_c for that channel. Consequently, the corresponding channel will be chosen with lower probability in the next RUIs.

The proposed scheme does not incur any additional control overhead other than periodic beacon updates. Also, to avoid *idle listening*, nodes use low-power listening where they sleep most of the time and wake up in periodic intervals. If they sense some channel activity, they remain on. Otherwise, they go back to sleep to conserve energy.

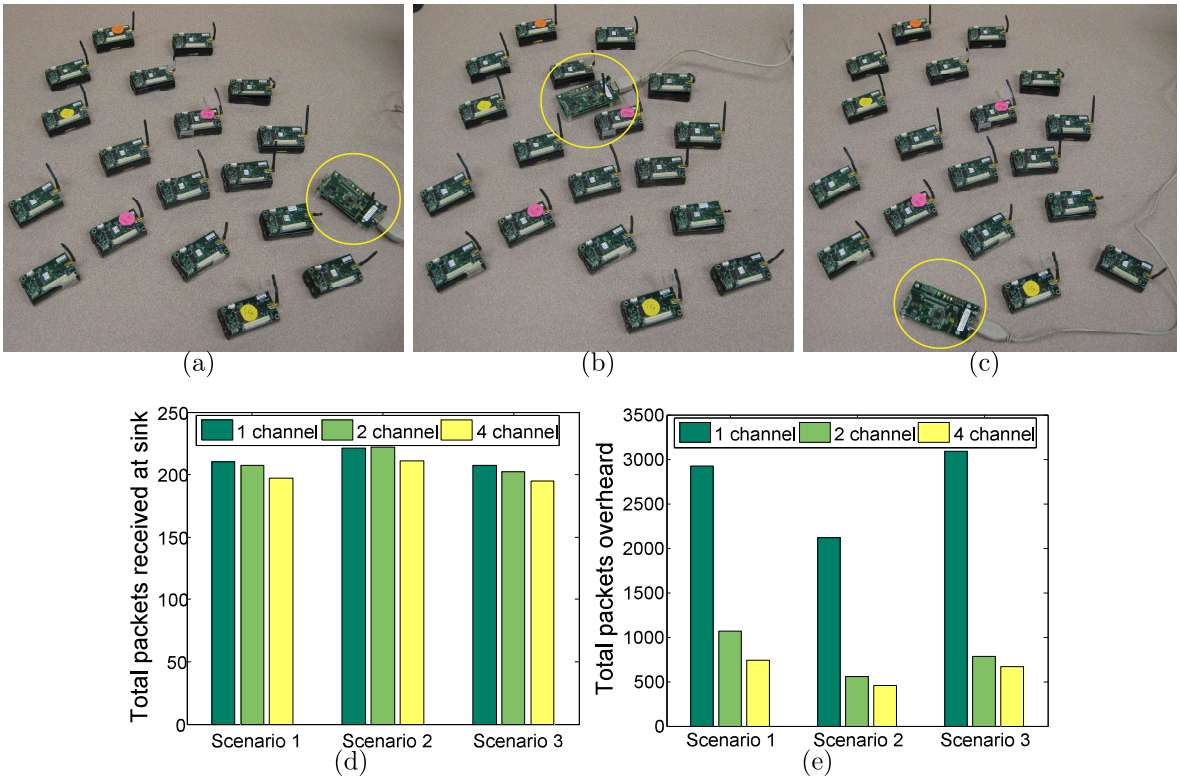

Figure 10.3: Experimental deployment scenarios with sink locations marked by yellow circles: 1 (a), 2 (b), and 3 (c); and comparison of the number of packets delivered at the sink (d) and the total packets overheard (e), with 1, 2, and 4 channels.

Problems such as routing loop detection and repairing are tackled similar to CTP. One possible drawback of DRCS is the possibility of frequent channel switching which happens when the receive and transmit channels of a node are different. Channel switching introduces time delays as well as additional power consumption in the nodes, which has been ignored in this work. Our experimental results demonstrate that in data collection applications with low data rates, the channel switching delay does not affect the delivery ratio significantly. However, for high data rate applications, frequent channel switching may result in some data loss as well as additional energy consumption.

10.4 Performance Evaluation

This section presents evaluation results of DRCS that are obtained from and experimental testbed as well as from simulations. We first demonstrate that our

proposed multi-channel scheme effectively reduces overhearing using an experimental testbed comprising of 18 MICAz motes. The experimental tests also demonstrate the effectiveness of the dynamic channel selection scheme based on individual node's battery health metrics. To show the performance of our scheme in a larger network, we implement this scheme in the *Castalia* simulator [85] on a 150-node network. Finally, we compare the performance of DRCS with a well-known tree-based multi-channel scheme TMCP. Parameters used for experiments and simulations are listed in Table 10.1.

Table 10.1: Simulation environment

Var	**Values**	**Var**	**Values**	**Var**	**Values**	**Var**	**Values**
I_{Bt}	20 mA	T_{Bt}	140 ms	I_{Br}	20 mA	T_{Br}	140 ms
I_{Dt}	20 mA	T_{Dt}	140 ms	I_{Dr}	20 mA	T_{Dr}	140 ms
I_P	8 mA	T_P	3 ms	I_S	7.5 mA	T_S	112 ms

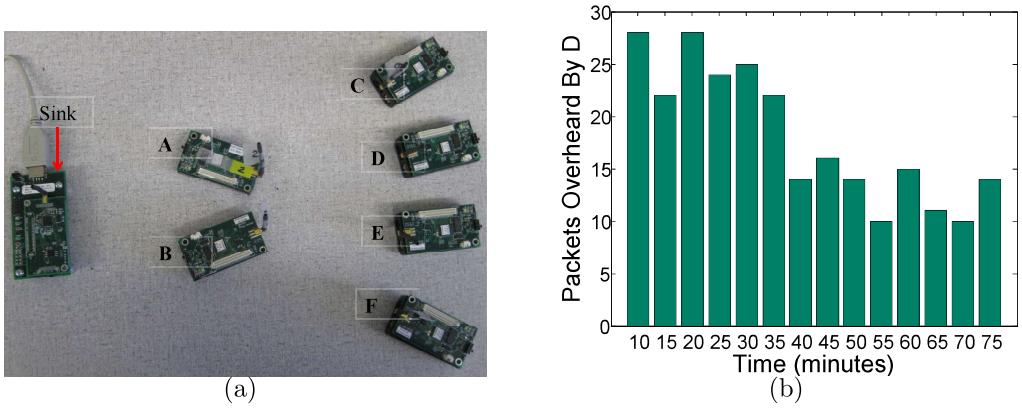

(a) (b)

Figure 10.4: Experiment to evaluate the effectiveness of dynamic transmit channel selection.

10.4.1 Evaluation in an experimental testbed

We implement our proposed scheme DRCS in TinyOS using MICAz motes that use LowPowerListening with wake-up intervals of 125 milliseconds. The beacon interval, DATA interval and τ are chosen to be 30, 60 and 180 seconds respectively. The transmit power is chosen to be -28.5 dBm to enable experimentation in a small place.

We place 18 motes that periodically sense and forward sensor data to the sink using our proposed multi-channel routing scheme DRCS. We perform experiments using three difference scenarios, all having the same network topology but with different sink locations. These are shown in Figure 10.3(a)-(c). For ease of obtaining packet counts, we disable retransmissions in these experiments. The results obtained over a duration of 15 minutes are shown in Figure 10.3(d)-(e). It is observed that in all three scenarios, the number of packets received at the sink drops only marginally with increasing number of channels, even with no retransmissions. This implies that the packet delivery performance is not significantly affected by the channel switching delay in these data-rates. However, there is a significant reduction in the total number of overhearing packets by using 2 and 4 channels. This experiment demonstrates that DRCS can significantly reduce energy wastage due to overhearing without sacrificing the delivery performance.

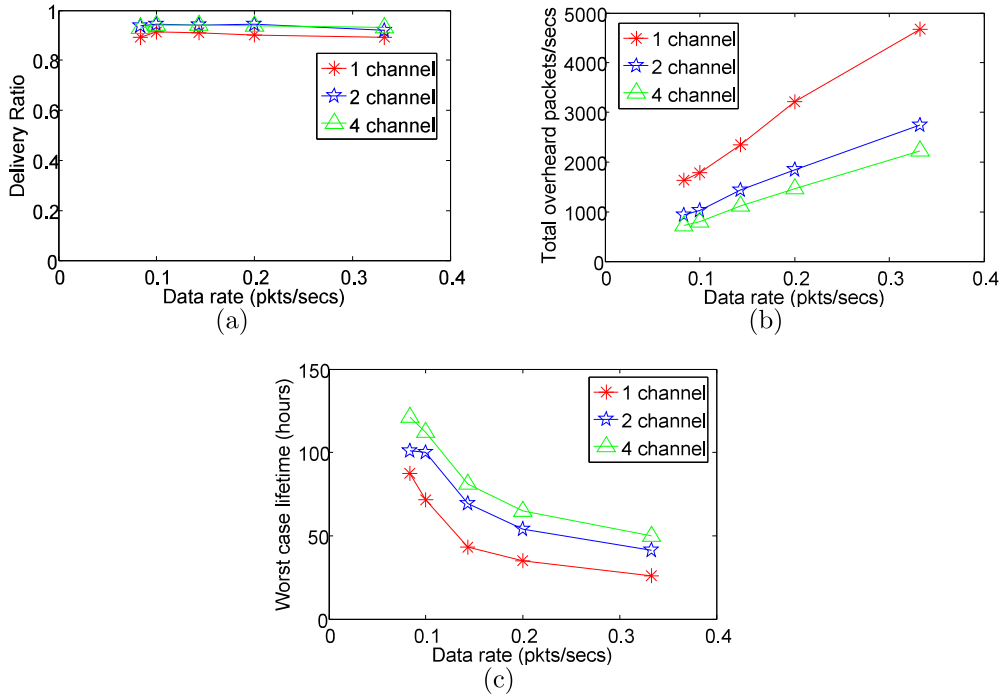

Figure 10.5: Comparison of (a) packet delivery ratio (b) network-wide packets overheard (c) worst case network lifetime with different data rates.

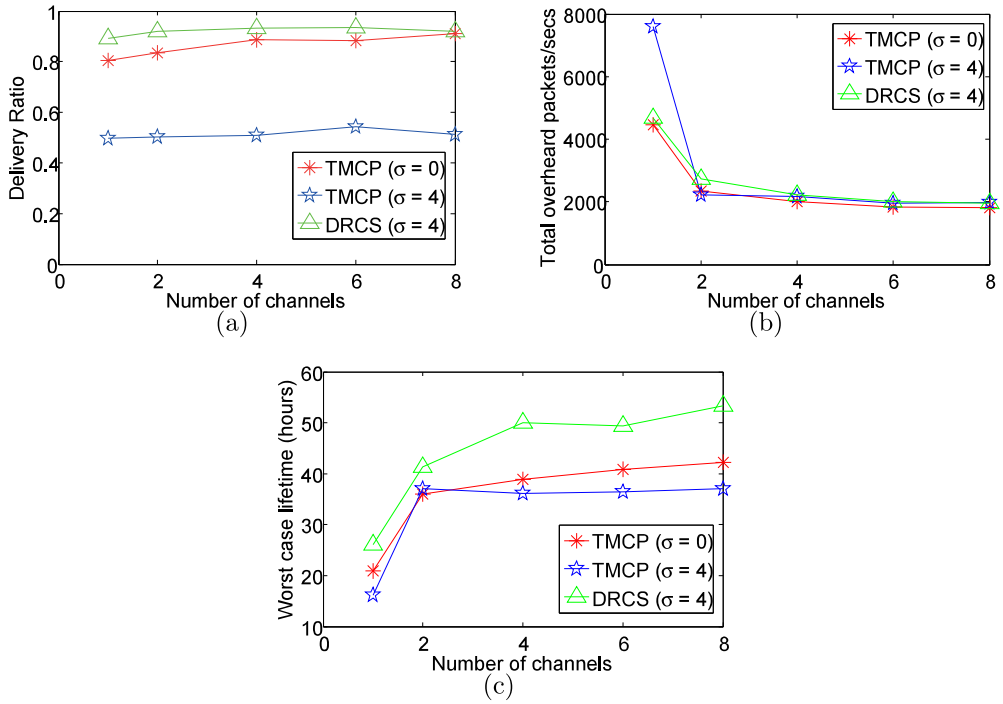

Figure 10.6: Comparison of (a) packet delivery ratio, (b) network-wide packets overheard (c) worst case network lifetime with different number of channels.

To show the effectiveness of the dynamic channel selection scheme, we set up a small network as shown in Figure 10.4(a), and monitor the variations of the number of packets overheard in a specific node when its battery voltage (and hence, its capacity B) is changed manually. Initially, the battery capacities of all nodes are made to be 100%. After 30 minutes, the battery voltage of node D is reduced manually using a voltage regulator to represent a battery capacity of 50%, keeping all others unchanged. In this experiment, we use only 2 channels and a data interval of 15 seconds. Figure 10.4(b) shows the variation of the number of packets overheard by D over time. Each bar on the x-axis shows the number of overheard packets by D over a duration 5 minutes. It can be observed that after 30 minutes the overhearing on node D starts reducing as all other nodes switch their transmit channels to avoid the receiver channel of D. This experiment demonstrates that our proposed scheme helps in reducing energy consumption at a node with bad health-metric, which can occur

due to deteriorating battery health.

10.4.2 Simulation Results

We conduct simulations to evaluate the performance of our proposed scheme in a larger network and to also evaluate the lifetime improvement achieved by DRCS. We consider a network of 150 nodes that are uniformly placed in an area of 200 × 200 meters. The transmission power is assumed to be 0 dBm. The initial battery capacities of the nodes are assumed to be uniformly (randomly) distributed between 75% to 100%. The capacity of a fresh battery (100% capacity) is assumed to be 5000mAH. The beacon interval is set to 30 seconds and the maximum retransmission count is set to 30. Each simulation is run for 500 seconds and all the results are averaged over five independent simulations.

★ Comparison with different datarates: Figure 10.5 shows the variation of the packet delivery ratios, overhearing counts and the *worst case network lifetime* with different number of channels and transmission rates. Note that the performance of DRCS using a single channel is essentially the same as that of CTP. The worst case network lifetime is defined as the time when the first node of the network dies. It is observed that the packet delivery ratio is above 90% for all cases. This is consistent with the findings from the experimental testbed, indicating that at these data rates, the packet delivery ratio is not significantly affected by the channel switching scheme employed in DRCS. However, overhearing is reduced by nearly 40% with 2 channels and by over 50% with 4 channels. This significantly reduces the average current consumption in the nodes and improves the network lifetime.

★ Comparison with TMCP [76]: Figure 10.6 shows the comparison of DRCS with another well-known tree based multi-channel routing scheme TMCP for different number of channels. We assume a communication range of 40 meters and an interference range that is 1.5 times of the communication range. Here, we set the data interval to 3 seconds. Figure 10.6 shows that DRCS generates a higher packet

delivery ratio in comparison to TMCP. This is due to several reasons. Firstly, TMCP uses a distance-based communication and interference model that does not effectively capture the link qualities, especially with a high channel variance σ^2. Secondly, DRCS uses channels more efficiently than TMCP. In TMCP nodes select the same channels as that of their parents. Hence, if the sink has n immediate neighbors and there are k channels where $k > n$, then at least $k - n$ channels will be unused, since there will be at most n sub-trees in the network. On the other hand, nodes on the same sub-tree in DRCS may use multiple channels, thereby improving channel utilization. Also in case of TMCP, the parent and channel assignments are static. These do not change even with variations of congestion and link quality. These result in poor route quality that leads to higher packet loss, retransmissions, and overhearing. Moreover, the channel quality may vary over time, which requires a dynamic protocol. It should be noted that the performance of DRCS and TMCP are similar in terms of the total reduction of overhearing with multiple channels. However, DRCS provides a much higher network lifetime that is achieved by dynamically balancing the lifetimes of individual nodes.

10.5 Discussions

In this chapter, we propose a scheme for building a multi-channel tree in data gathering wireless sensor networks for maximizing the network lifetime. The proposed scheme DRCS involves distributed channel selection to enable nodes to reduce overhearing, and dynamic parent selection for minimizing the load of nodes that have the worst expected lifetime. Through simulations and experiments, we demonstrate that DRCS significantly improves the network lifetime without sacrificing the packet delivery ratio. The proposed scheme has no additional overhead other than periodic beacon updates, which makes it suitable for implementations in real-life applications to prolong the network lifetime.

CHAPTER 11: POWER CONTROL AND ROUTING FOR RECHARGEABLE WIRELESS SENSOR NETWORKS

In this chapter, we propose a power control and routing scheme for rechargeable wireless sensor networks (WSNs) that are characterized by spatial and temporal variations of energy resources. Powering wireless sensor nodes with energy harvested from the environment, such as solar, mechanical, thermal, and others, is an effective approach for achieving longterm maintenance-free operation of WSNs. A key challenge for achieving reliable and uninterrupted operation of WSNs powered by such renewable energy sources is to adequately address the variability of the energy resources in these devices. Renewable energy such as solar can have wide spatial and temporal variations due to natural (e.g. weather) and location specific factors (e.g. exposure to sunlight) that can be difficult to predict prior to deployment. An illustration of such spatio-temporal variations is discussed in Chapter 8. Because of such variations of available solar irradiance, WSNs powered by solar energy can suffer from frequent and unpredictable node outages that can seriously affect the monitoring operations of the network. Similar problems also arise in WSNs that are powered by other forms of renewable energy resources. An effective approach for addressing this problem is to design network protocols and processing schemes that enable the nodes to dynamically adapt their energy consumption based on estimated energy resources [10], [86], [13], which is the main objective of this work.

We consider WSNs that are applied for environmental monitoring applications, typically using periodic transmissions of sensor observations to a centralized base station. For such data collection traffic, routing protocols such as the *Collection Tree Protocol (CTP)* [71] can be applied to achieve quality-aware routes from each node to the sink. Since network-wide time synchronization is difficult to achieve in

resource-constrained sensor nodes, the traditional approach for conserving energy in such networks, especially when the network size is large (i.e. over 100 nodes), is application of asynchronous duty-cycling of sleep and wake states of the radio, such low-power listen [69]. While this is effective in reducing the energy consumption by reducing the radio active times, asynchronous duty cycling typically requires the use of extensively long preambles to be sent with each packet, which leads to energy wastage from overhearing [87], [88]. In Chapter 8, we reported experimental assessment of the effect of overhearing in WSNs that apply asynchronous LPL under data collection traffic [86]. Results indicate that even with sleep cycles, overhearing is a dominating factor in the energy consumption in the nodes. Mechanisms such as interruption of reception of unnecessary packets based on information transmitted in the preamble [89], adaptive duty-cycling [90, 91] and others have been proposed to reduce the energy wasted from overhearing caused in such LPL and preamble sampling schemes.

In this work, we consider reducing overhearing by reducing the neighborhood size using transmission power control as well as through route adaptations. Although a significant amount of work has been reported on power control for WSNs, most of it has been directed towards reducing interference effects for improving the communication performance in the network [83], [92]. Here, our objective is apply power control to achieve energy conservation by *reducing overhearing*. The main challenge for achieving this goal is that the degree of overhearing at a node depends on the transmit power levels and traffic of its *neighbors*. Consequently, effective overhearing control requires *network wide* adaptations of transmit power levels as well the distribution of data traffic in the nodes as opposed to independent adaptations at the nodes. To address these issues we implement a cooperative *joint Power COntrol and Routing (PCOR)* scheme for rechargeable sensor networks that derives benefits from two approaches. First, PCOR applies a prediction model at each node to determine the extent by which it can reduce its power while maintaining acceptable probabil-

ity of success in data packet delivery to its parent. Secondly, PCOR incorporates a parameter into the routing metric that represents the level of overhearing caused by transmissions along candidate routes to nodes that have critically low energy resources.

11.1 Preliminaries

We consider a *data collecting* wireless sensor network where nodes follow a tree structure to forward data to the sink. There is no network wide time synchronization. It is assumed that the nodes apply asynchronous duty-cycling with uniform duty cycles to conserve energy. In such networks, a node overhears all transmissions within its receiving range, which causes wastage of energy. All nodes are powered by energy harvested from the environment such as solar, which results in random spatial and temporal variations of their energy resources. In PCOR, if a node has significantly lower energy resources compared to its neighbors (termed as an *energy-critical node*), its neighbors cooperatively reduce power to reduce overhearing on that node keeping the link quality within a reasonable range. This power control scheme is performed jointly with an adaptive routing scheme that helps in reducing the amount of overhearing to energy-critical nodes. The objective of the routing protocol is to divert traffic away from regions where energy-critical nodes are located, which in effect reduces overhearing on these nodes. PCOR achieves these objectives by applying a *statistical prediction model* to (i) measure the extent by which a node can reduce its transmit power while maintaining a reasonable link quality to its parent and (ii) the amount of overhearing caused to energy-critical nodes, which we discuss in section 11.2. Before going into the details on the proposed scheme in section 11.3, we discuss some related terms and ideas first.

We define the *battery health-metric* H of a node to represent its remaining battery lifetime, i.e. the estimated time until its battery is depleted under its currently estimated energy usage. We assume $H \propto \frac{B}{I}$, where B is the remaining capacity of the

battery and $\mathcal{I}$ represents the estimated current drawn at the node. The current drawn in each node is modeled similar to Chapter 9 as follows:

$$\begin{aligned} \mathcal{I} &= \frac{I_{Bt}T_{Bt}}{T_B} + M.I_{Dt}T_{Dt} + N.\frac{I_{Br}T_{Br}}{T_B} + O.I_{Dr}T_{Dr} \\ &+ F.I_{Dt}T_{Dt} + \frac{I_sT_s}{T_D} + N_P.I_PT_P \end{aligned} \tag{11.1}$$

Detailed of these parameters are discussed in Chapter 9, which can be estimated by periodic assessments of a nodes overheard and forwarded traffic.

We define a node to be energy-critical if its $H < \alpha.\mu_H$, where μ_H is the mean of its neighbors health metrics. Energy-critical are indicated by a variable called *critical node (CN)* that is set to 1. It then makes the POC $= \frac{\mu_H - H}{\mu_H}$. Otherwise, the node is considered as a good node and POC = 0 for all good nodes. The parameter POC is mainly used by an energy-critical node to inform its neighbors how much cooperation is required from them in conserving its energy. If a node's condition is very critical, it broadcasts a high POC, prompting its neighbors to reduce their transmit powers with high probability. The reverse happens when a node is less critical.

In addition to energy considerations, PCOR also tries to achieve a minimum quality of established routes. To estimate the quality of a route, we use a path metric that is obtained as the sum of the *expected number of transmissions (ETX)* on each of its links, which is the same principle applied in CTP. An ETX for a link is the expected number of transmission attempts required to deliver a packet successfully over the link. We define forward-ETX of a link as the ETX in the forward direction, i.e. from sender to the receiver. We also define min-ETX of a node as the path-ETX of the best quality route towards the sink.

11.2 Prediction Model for Power Control

We now develop a power control model that represents the relationship between a node's transmission power level and its forward link quality with a minimum number

of parameters. The model can also be applied to determine the level of overhearing caused by a node to a specific neighbor. The objective is to develop a mechanism for nodes to estimate the range of transmit power levels that can be used for cooperative overhearing control and quality-aware route selection. Note that overhearing is really a physical layer phenomenon; however, the amount of overhearing can be estimated from the number of received packets as observed at the network layer.

We observe that the packet delivery ratio (PDR) of a link under *log-normal shadowing* can be represented as follows.

$$\begin{aligned} PDR &= Prob\left[P_r(d) > \gamma\right] = Prob\left[P_t - P_l(d) > \gamma\right] \\ &= Prob\left[P_t - \overline{P_l(d)} + X_\sigma > \gamma\right] = Q\left(\tfrac{\gamma - P_t + \overline{P_l(d)}}{\sigma}\right) \end{aligned}$$

where P_t is the transmit power, $P_r(d)$ and $P_l(d)$ are the power received and path loss at distance d, γ is the threshold for minimum received signal level at the received. X_σ is a Gaussian random variable, used to model the shadowing effects that has a zero-mean and a standard deviation of σ.

Our proposed model comprises of a relationship between the packet delivery ration p and the transmit power t that is represented by only two parameters that can easily estimated from a sequence of transmission measurements between a transmitter and a receiver using a linear regression curve-fitting approach. The model is essentially a sigmoid function that effectively approximates the distribution of delivery ratio at different transmission power levels. By using extensive experimental results, we model this relationship as

$$p = \tfrac{1}{1+e^{-(a.t+b)}} \qquad \Rightarrow a.t + b = \ln\left(\tfrac{p}{1-p}\right) = P \text{ (say)}$$

A set of sigmoid curves that represent this model for different transmitter receiver pairs are shown in Figure 11.1. We formulate this predictive model in the following

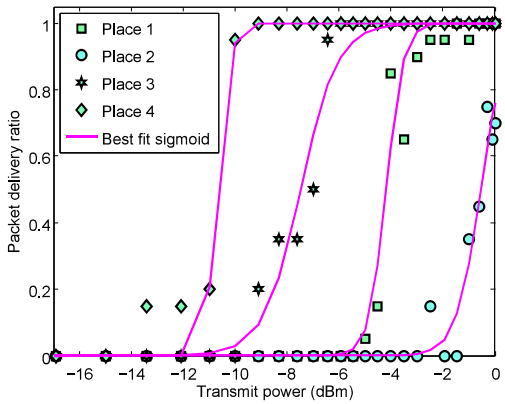

Figure 11.1: Sigmoid best fit curve of delivery ratio vs transmit power.

way, which uses two vectors $\mathbb{T}$ and $\mathbb{P}$. $\mathbb{T}$ contains all transmission power levels, thus $\mathbb{T} = \{t_1, t_2, ..., t_N\}$. The vector $\mathbb{P}$ contains all the $\ln\left(\frac{p}{1-p}\right)$ terms, i.e. $\mathbb{P} = \{P_1, P_2, ..., P_N\}$. Thus, expressing equation (11.2) in matrix form we get

$$\begin{bmatrix} t_1 & 1 \\ \vdots & \vdots \\ t_N & 1 \end{bmatrix} \begin{bmatrix} a \\ b \end{bmatrix} = \begin{bmatrix} P_1 \\ \vdots \\ P_N \end{bmatrix} \Rightarrow \begin{cases} a = \frac{\sum P_i . \sum t_i - m . \sum t_i . P_i}{\sum t_i . \sum t_i - m . \sum t_i^2} \\ \text{and} \\ b = \frac{\sum P_i - a . \sum t_i}{m} \end{cases}$$

Note that a and b can change with time, depending on link characteristics. The idea is for each node estimate these values and broadcast them using beacon messages. Beacons messages are sent with highest power so that all neighboring nodes can receive them.

Here we need to mention three points which are important corresponding to this prediction model. First, the accuracy of this prediction model increases with the number of data samples. Thus the prediction model is used only when a node gets enough confidence over a link, i.e. if it receives enough data packets covering a significant range of PDR values. Second, this prediction model is receiver-oriented as shown in Figure 11.2, i.e. the receiving node is able to estimate the coefficients (a, b) of a link when it receives or overhears packets transmitted by a sender in different

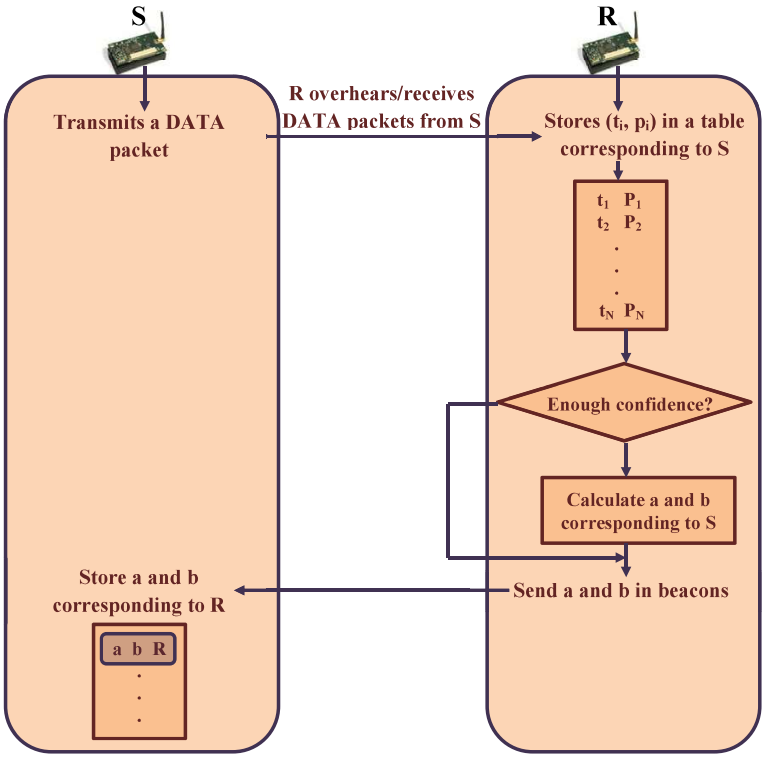

Figure 11.2: Receiver-oriented prediction model.

power levels The coefficients a and b are then broadcasted along with the sender ID with the beacon messages. If the receiver does not have enough confidence from its data samples, it simply broadcasts a and b with their default values. The transmitter uses this coefficients to predict the link quality to that receiver for any power level. Third, beacons are transmitted periodically with the highest transmit power. Note that in this scheme a node appends the coefficients and the neighbor ID corresponding to each neighbor in its beacon message. If a node has a large number of neighbors, this scheme increases the packet size. To restrict the beacon message size, in our scheme a node appends n (we assume n to 3) neighbor's ID and coefficients in each beacon. Thus the neighbor IDs as well as their coefficients are appended in a round-robin fashion, each time for n neighbors.

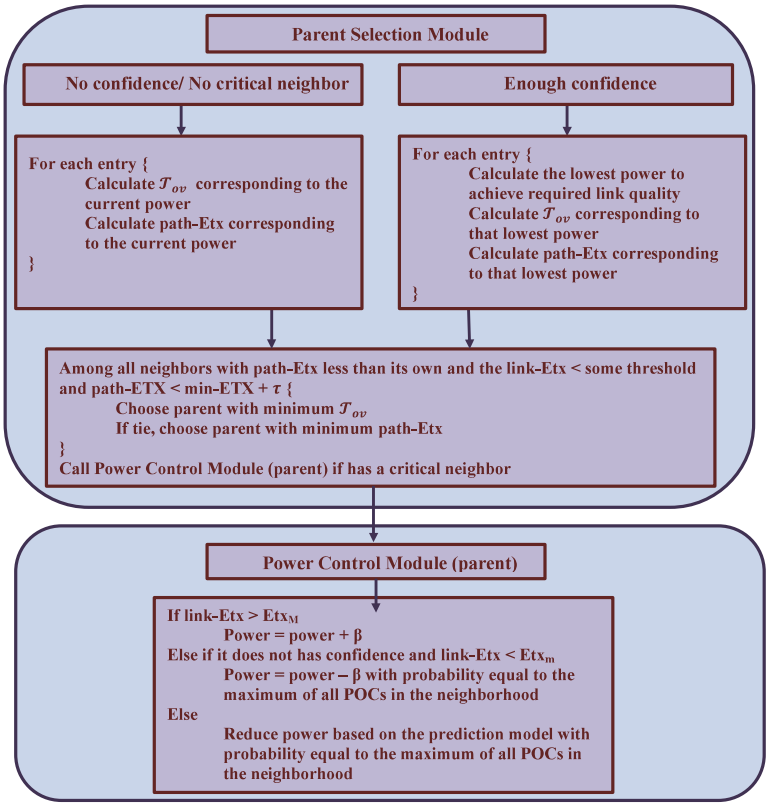

Figure 11.3: Proposed joint power control and route adaptation scheme.

11.3 The Proposed Cooperative Joint Power Control and Route Adaptation (PCOR) Scheme

We now present the proposed joint power control and routing scheme PCOR for WSNs that mainly tries to fulfill two objectives. First, it reduces overhearing on *energy-critical nodes*. This will extend the overall lifetime of the network. Second, routes are adapted dynamically and in a distributed fashion to avoid regions that have energy-critical nodes, which reduces forwarding and overhearing rates on the nodes that have critically low energy resources. All nodes periodically determine their parents as well as transmit powers based on their neighboring link qualities and their neighbors health metrics. We assume that all nodes broadcast periodic beacon messages, which include their node ID, its ETX value, CN (which is 1 if a node is critical and 0 otherwise), and the POC. Besides that a beacon message includes n neighbor IDs, their corresponding coefficients and the current forward-ETX (ETX_F)

of the link from its neighbor to itself, as well as its current transmit power level. For the sake of simplicity, we explain the power control and parent selection separately as follows. Although power control and parent selection are described separately, these are done jointly as explained later.

★ Power control: If there are no energy-critical nodes in the network, then it works the same as CTP. The parent is selected as the neighbor with lowest ETX and is done periodically. The power adaptation does not take place in this case. When a node becomes critical, it broadcasts its beacon message with CN = 1. Any node that receives a beacon with CN = 1 adapts its transmit power level to its parent as follows:

• Reduce transmit power in steps: If it only knows the default values of the coefficients a, b for the forward link to its parent, it reduces its transmission power in steps, i.e. by β, with probability = POC of its critical neighbor, if its link-ETX is less than some threshold ETX_m and its current transmit power is more than a minimum level. If it receives beacon messages from multiple critical nodes, the power is reduced with probability equal to the maximum of all POCs of the critical nodes. This results in reduced overhearing on the critical nodes.

• Reduce transmit power using the prediction model: If the node is aware of the estimated (non-default) values of the parameters (a, b) for the link with its parent, it uses the prediction model to reduce its power. In that case the node uses transmit power t such that t is the minimum transmit power of achieve a delivery ratio greater than some threshold required to maintain a minimum link quality.

• Increase power: A node starts increasing power in steps of β if (i) the link-ETX to its parent goes beyond a threshold ETX_M, or (ii) its $\mathbb{R}$ consecutive transmissions to its parent fail. For our performance evaluations, we assume $\mathbb{R}$ to be 10.

★ Parent selection: As the change in transmit power affects the ETX, adapting transmit power may result a node to adapt its route, i.e. parent selection as well.

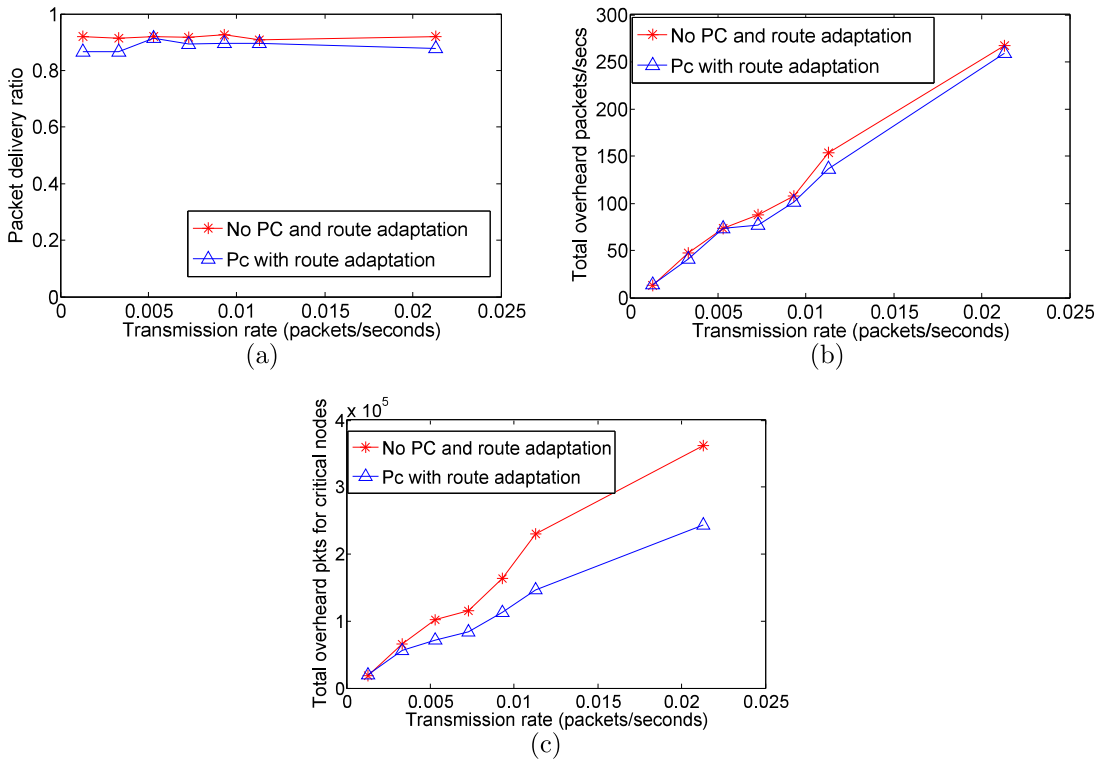

Figure 11.4: Comparison of (a) packet delivery ratio (b) network-wide packets overheard (c) packets overheard by the critical nodes with different rates.

Hence, our scheme effectively ties routing with power control. If a node is not a direct neighbor of a critical node, it does not adapt its transmit power; but it may still select a parent such that the chosen route avoids the neighboring regions of the critical nodes. This is implemented by a route metric $\mathcal{T}_{ov}$, which represents the total overhearing caused by all transmissions along the route to energy-critical nodes. $\mathcal{T}_{ov}$ is computed as follows. Let $\mathcal{N}_{ov}$ of a node represent the rate of its packets that are overheard by its worst critical neighbor, i.e. $\mathcal{N}_{ov} = F.p_{ov}$, where p_{ov} is the probability that packets transmitted by the node are overheard by its most energy-critical neighbor. p_{ov} is basically the packet delivery ratio which can be measured (i) from the prediction model corresponding to any power level, if estimated (non-default) values of the coefficients are known or (ii) from ETX_F if the coefficients are their default values.

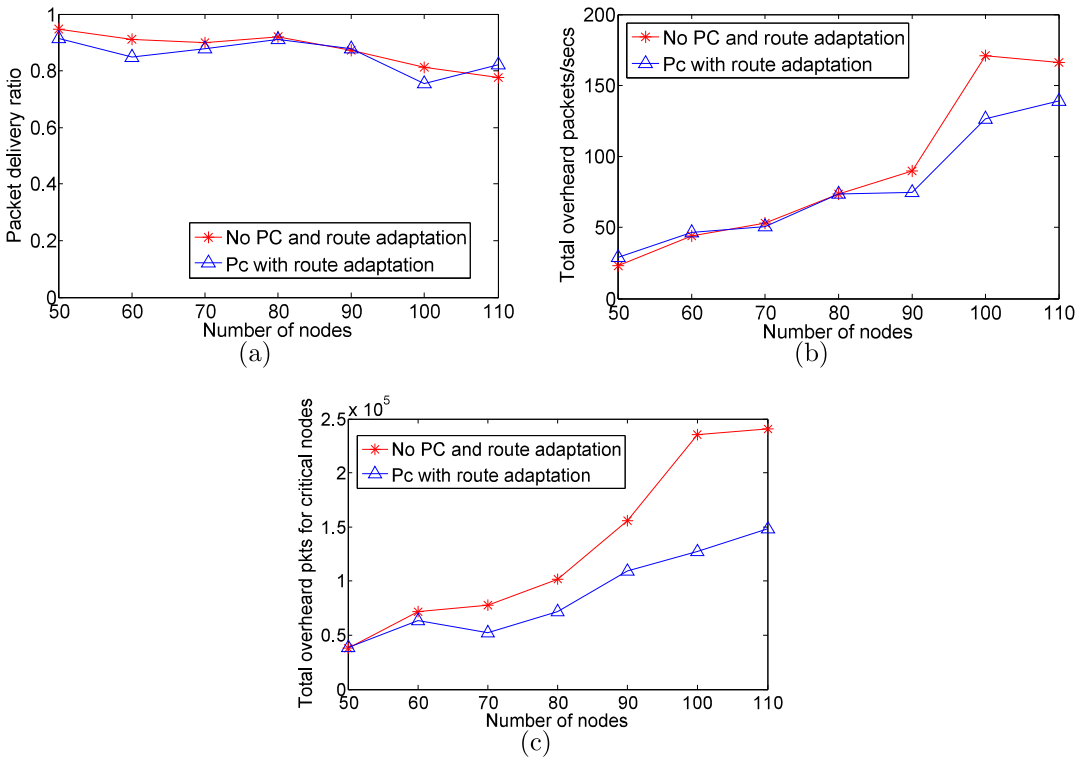

Figure 11.5: Comparison of (a) packet delivery ratio (b) network-wide packets overheard (c) packets overheard by the critical nodes with different node density.

The sink broadcasts beacons with $\mathcal{T}_{ov} = 0$. The value of the routing metric from node i to the sink is represented as $\mathcal{T}_{ov}^{i}$, and the value of the routing metric for node j if it selects node i as its parent is $\mathcal{T}_{ov}^{ij}$, which is given as the $\mathcal{T}_{ov}^{i}$ broadcasted by i plus its own $\mathcal{N}_{ov}$. For each entry i in its neighbor table, a node j calculates the minimum transmit power t_{ij} required to achieve a minimum link quality from the prediction model if the non-default coefficients are known. Otherwise it considers its current transmit power level t_c. It also calculates its $\mathcal{N}_{ov}^{ij}$, which is its $\mathcal{N}_{ov}$ corresponding to the transmit power (t_{ij} or t_c) and record the metric $\mathcal{T}_{ov}^{ij}$ which is the sum of that $\mathcal{N}_{ov}^{ij}$ and the $\mathcal{T}_{ov}^{i}$ sent by neighbor i. Also it calculates the link-ETX and path-ETX based on that transmit power. It then chooses the entry corresponding to the minimum $\mathcal{T}_{ov}^{ij}$ $\forall$ i among the neighbors that have (i) an ETX less than its own (to avoid routing loop) and (ii) a reasonable link-ETX (to avoid links with very poor quality) and (iii)

the path-ETX $< \tau +$ min-ETX (to avoid routes that have very low quality than the best quality route), as its parent. For our performance evaluations we assume τ to be 0.5. The $\mathcal{T}_{ov}^{ik}$ corresponding to its parent entry k is then broadcasted using the beacon messages. In case of a tie, it chooses the parent that gives least path-ETX. Thus a route with minimum $\mathcal{T}_{ov}$ is the route that overhears the critical nodes with least probability and the route with minimum path-ETX gives the route with minimum cost. While choosing its parent k in this process, the node j determines its transmit power (t_{kj} or t_c) as well, which fulfills our objective of *joint* power control and route adaptation to avoid overhearing on the critical nodes. This transmit power and parent selection go on periodically.

The design for our joint power control and route adaptation scheme is depicted in Figure 11.3. The proposed scheme does not incur any additional control overhead other than periodic beacon updates. Problems such as routing loop detection and repairing are tackled similar to CTP.

11.4 Performance Evaluation

This section presents evaluation results of PCOR from experiments on a real testbed as well as from simulations. We implement the proposed scheme in the Castalia simulator [85] to demonstrate its effects on large network. We also demonstrate that our proposed multi-channel scheme effectively reduces overhearing on the critical nodes using an experimental testbed comprising of 25 MICAz motes.

11.4.1 Simulations

We simulate our joint power control and routine scheme in the *Castalia* simulator where nodes are placed in grid structure in an area of 100×100 meters. We have chosen 10% nodes to be critical nodes that has lesser capacities as well as receive lesser amount of sunlight compared to others. In this way we try to imitate an actual spatial nature of an outdoor environment. The beacon interval varies between 5 seconds to 50 seconds similar to *Trickle* algorithm used in CTP. The maximum retransmission

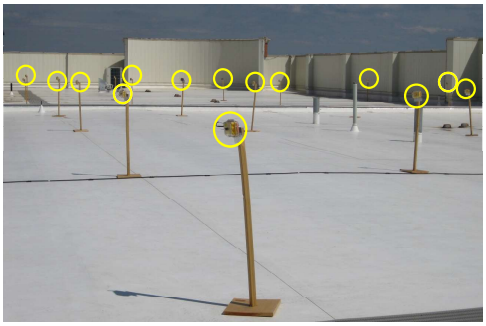

Figure 11.6: A 25-node wireless sensor network testbed.

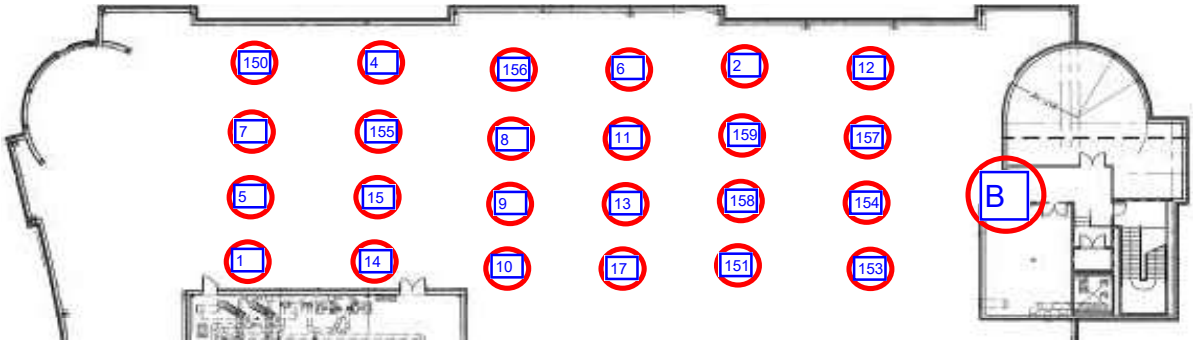

Figure 11.7: The map of the wireless sensor network testbed. Node 1 and Node 156 are made to be resource critical nodes.

count is set to 3. Routes are updated in every 8 seconds. At first transmit power is controlled periodically in every 5 minutes. When a node receives confidence for using the sigmoid model, the transmit power is updated along with the route updates. Each simulation is run for around four hours. Parameters used for experiments are listed in Table 11.1.

Table 11.1: Parameters used

Var	**Values**	**Var**	**Values**	**Var**	**Values**	**Var**	**Values**
I_{Bt}	20 mA	T_{Bt}	140 ms	I_{Br}	20 mA	T_{Br}	140 ms
I_{Dt}	20 mA	T_{Dt}	140 ms	I_{Dr}	20 mA	T_{Dr}	140 ms
I_P	20 mA	T_P	3 ms	I_S	7.5 mA	T_S	112 ms

★ Comparison with different rates: Figure 11.4 shows the variation of the packet delivery ratios, overhearing counts for all the nodes as well as for the critical nodes with different transmission rates, where 80 nodes are placed in a grid. It is observed

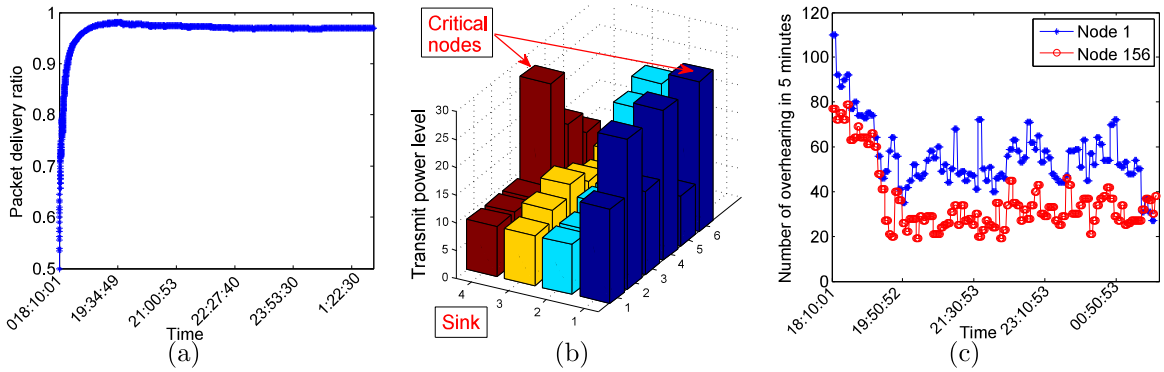

Figure 11.8: (a) Overall packet delivery ratio to the sink over time. (b) Transmit power levels of different nodes, power level 27 corresponds to -1 dBm and power level 9 corresponds to -13.4 dBm. (c) Number of packets overheard by the two critical nodes over time.

that the packet delivery ratio is above 90% for all cases. However, overhearing is reduced by nearly 20-25% for the critical nodes when the transmit power is controlled with route adaptation. This clearly shows the effectiveness of our proposed scheme in reducing overhearing on the critical node without significantly affecting the overall packet delivery ratio.

★ Comparison with different node density: Figure 11.5 shows the variation of the packet delivery ratios, overhearing counts for all the nodes as well as for the critical nodes. where the number of nodes are varied from 50 to 110. From this figure also we can observe that with different node densities, the overhearing on the critical nodes are reduced by a significant amount, which validates the effectiveness of our proposed transmit power control and route adaptation scheme.

In both set of graphs we can observe that the overall overhearing is sometimes more and sometimes less compared to the scheme without power control. The reduction in overall overhearing results from reduced transmit power and reduced overhearing on the critical nodes. On the other hand, the increase in overhearing occurs because of more retransmissions due to reduced transmit power and because of taking de-routes to avoid traffic through the regions that are under shadows. But our main objective is

to reduce overhearing on critical nodes, even if overall overhearing increase to reduce the effect of spatial variations of energy availability and consumptions.

11.4.2 Experimental Tests:

We implement our proposed scheme PCOR in TinyOS in an experimental testbed comprising of 25 MICAz sensor nodes as shown in Figure 11.6. Figure 11.7 shows the map of the testbed. The motes periodically sense and forward sensor data to the sink using our proposed power control and route adaptation scheme. The beacon interval is adaptively varied between 525 milliseconds and 1 minute. The DATA interval is chosen to be 1 minute. The transmit power is varied between -1 dBm to -13.4 dBm. We place two critical nodes whose energy availability is assumed to be significantly lower compared to others. The maximum number of retransmissions is set to 5. ETX_m and ETX_M are set to be 1.5 and 2, respectively.

The results obtained over a duration of six hours are shown in Figure 11.8(a)-(c). All nodes start with the maximum power level of -1 dBm and then gradually reduce power and adapt routes to avoid overhearing caused to the energy-critical nodes. Figure 11.8(b) shows the transmit power levels of different nodes after six hours, which shows that most of the nodes significantly reduce their transmit power. At the same time we can see some variations in transmit power levels, which comes from the spatial variations of the route and channel qualities. Figure 11.8(c) shows the variation of overhearing with time for the critical nodes which clearly shows the reduction in overhearing on the critical node due to power control and route adaptation done by the other nodes. These results demonstrate that PCOR significantly reduces energy wastage due to overhearing on the energy-critical nodes without affecting the packet delivery ratio significantly (Figure 11.8(a)).

11.5 Discussions

In this chapter, we propose a distributed scheme for controlling transmit power and adapting routes dynamically in a data gathering rechargeable wireless sensor net-

works for maximizing the network lifetime. Through simulations and experimental evaluations, we demonstrate that our proposed scheme significantly reduces overhearing on the critical nodes. The proposed scheme has no additional overhead other than periodic beacon updates, which makes it suitable for implementations in real-life applications to prolong the network lifetime.

CHAPTER 12: LIFETIME OF ASYNCHRONOUS WIRELESS SENSOR NETWORKS WITH MULTIPLE CHANNELS AND POWER CONTROL

In this chapter, we present a mathematical model of network lifetime under dynamic channel selection and power control for reducing the effect of overhearing in asynchronous sensor networks. The issue of energy conservation and lifetime optimization is critical for reliable long-term operations of wireless sensor networks (WSNs). It is well known that the radio transceiver typically dominates the energy consumption in wireless sensor nodes. The most effective strategy for conserving the energy consumed by the transceiver is duty-cycling between sleep and wake periods, which has been adapted in a large number MAC protocols proposed for WSNs. The key challenge for applying duty-cycling is synchronization of the wake periods between a transmitter and a receiver. If the nodes are time synchronized, then network-wide or local scheduling policies can be applied that can enable nodes to synchronize their wake periods during transmission/reception and go back to sleep at other times. However, challenges in achieving network-wide time synchronization and latency in multi-hop transmissions caused by such synchronized scheduling principles are concerns with this approach. An alternative is asynchronous duty-cycling, where all nodes wake up briefly at periodic intervals of time to check for activity and only remain awake if some activity is detected. Otherwise, the nodes return to their energy-conserving sleep states. Generally, a lengthy preamble is used for each transmitted packet so that the receiving node is able to detect it during its brief wake time. This provides an effective solution for energy conservation in asynchronous WSNs especially under low data rates. Asynchronous duty cycling has been applied to a number of Low Power Listening (LPL) and preamble sampling MAC protocols [93, 94]. One of the key problems with this approach is that it leads to energy wastage

from *overhearing*, since unintended neighbors need to receive an entire packet before knowing the destination. Possible solutions to this overhearing problem include mechanisms for providing additional information in the preamble to enable neighbors to interrupt the reception of long preambles when not needed [89], adaptive duty-cycling (EA-ALPL, ASLEEP) [90, 91] and others. Despite these developments, overhearing remains to be a dominating factor in the energy consumption in asynchronous WSNs, especially under high node density and large network sizes.

To alleviate the problem of overhearing in such asynchronous WSNs, we propose two approaches. The first is the use of multiple orthogonal channels to reduce the number of co-channel transmissions in a node's neighborhood. Multi-channel operation is supported by typical WSN platforms such as MICAz and Telos, which is typically applied for reducing interference. In Chapter 9 and Chapter 10, we presented the benefits of using a multi-channel routing schemes by which nodes perform dynamic channel selection to reduce overhearing based on the energy constraints of its neighbors. Secondly, we consider distributed transmit power control [13] presented in Chapter 11, that is also an effective mechanism for controlling the effect of overhearing. Our objective is to apply channel selection and power control to adapt the energy consumption in the nodes in order to balance their remaining battery lifetimes, which effectively maximizes the network lifetime.

In this chapter, we analyze the network lifetime mainly in two steps. First, we develop a mathematical model to evaluate the network lifetime of single-channel wireless sensor networks under optimal power control. This is derived under a node energy consumption model that assumes asynchronous LPL and a data collection traffic using a link-quality based routing protocol, such as collection tree protocol (CTP) [71]. We first calculate the optimal transmission range of the nodes so that the overall current consumption is minimized. We then apply this result to calculate the network lifetime assuming that all nodes apply transmit power to achieve this optimal

transmission range. Our objective is to determine the effect of transmission power control on the lifetime of the network that is primarily affected by energy consumed in transmissions, receiving, and overhearing. Secondly, we extend the network lifetime calculation to consider multi-channel operation where nodes are assumed to dynamically select channels with optimal power control to balance the nodes remaining lifetimes.

12.1 System Model

We assume a data gathering WSN where all sensor nodes periodically sense some physical parameters and forward them to the sink. Nodes broadcast periodic beacons to exchange various control parameters. We assume that nodes are not time synchronized and they apply the basic LPL principle to conserve energy [69, 70]. We assume that the sender prepends each message with a preamble that is long enough to span the complete length of a sleep-wake cycle to ensure that the receiving node detects it regardless of when it wakes up[1]. Because of this long preamble length (for both beacons and data packets), the effect of overhearing becomes costly. We assume that nodes apply a distributed power control mechanism to reduce the effect of overhearing.

To further reduce the energy consumption and extend the lifetime of the network, we propose two multi-channel transmission schemes. In the first scheme, which we call *flow based channel assignment (FCA)*, we assume that k channels are uniformly distributed over the nodes in the network. Nodes that are on the same channel form a subtree. Thus the scheme partitions the whole network into k vertex-disjoint subtrees as shown in Figure 12.1(a). Although this channel assignment scheme reduces the average overhearing, it does not allow the nodes to control their energy consumption with respect to their *varying energy resources*, which is our goal for *balancing the remaining lifetimes* of the nodes and thereby maximizing the lifetime of the network.

[1]In this work, we do not consider mechanisms for nodes to interrupt unintended receptions using special information transmitted within the preamble, for simplicity.

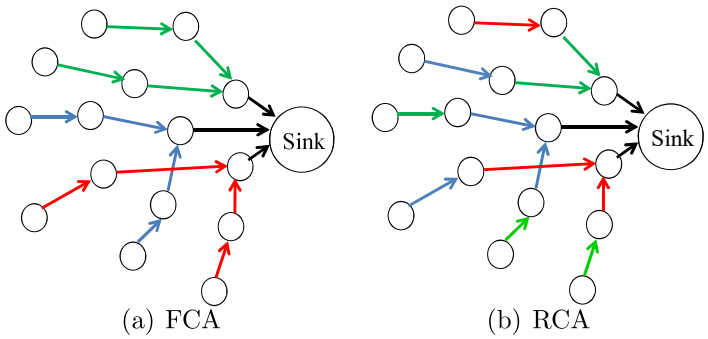

(a) FCA (b) RCA

Figure 12.1: Proposed data collection trees with multiple channels. Each color represents a different channel.

To achieve this, we propose a *receiver based channel assignment (RCA)* that works as follows. We define *receiver channel* as the channel on which a node receives packets. On the other hand *transmit channel* is the channel on which a node transmits, which is the receiver channel on its intended destination. The scheme is shown in Figure 12.1(b). In RCA, nodes monitor their receiver channels for incoming transmission by default. At the time of transmission, a node temporarily switches to a transmit channel and returns to its receiver channel after transmission. Essentially, RCA allows nodes to choose their transmit channels dynamically to balance the energy consumption of its neighbors so as to balance their residual battery capacities. Details on the implementation of RCA along with experimental results are reported in [86]. Here we develop a mathematical model to analyze the network lifetime.

12.2 Optimal Transmission Range Calculation

We first consider single channel operation, where the estimated current consumption of a node is represented similar to Chapter 9 as:

$$\begin{aligned} \mathcal{I} &= \frac{I_{Bt}T_{Bt}}{T_B} + M.I_{Dt}T_{Dt} + S.\frac{I_{Br}T_{Br}}{T_B} + O.I_{Dr}T_{Dr} \\ &+ F.I_{Dt}T_{Dt} + R.I_{Dr}T_{Dr} + \frac{I_sT_s}{T_D} + P.I_pT_p \end{aligned} \tag{12.1}$$

Let us assume that the current drawn by the receiver electronics in the receiving

mode is $I_{Dr} = \alpha_{12}$. In transmit mode, the current drawn is dependent on the transmit power. Assuming that optimal power control is applied, to transmit a packet over a distance d with a path loss exponent of n, the current drawn is

$$I_{Dt} = \alpha_{11} + \alpha_3 d^n \tag{12.2}$$

where α_{11} is the current consumed by the transmitter electronics, α_3 accounts for current dissipation in the transmit op-amp. The duration of a packet transmission and reception is proportional to the packet length. We assume that both the data packets and the beacon packets are of same length, thus $T_{Dt} = T_{Dr} = T_{Bt} = T_{Br} = T_l$. [2] Thus, the current consumed by a relay node that receives a packet and transmits it d meters onward is,

$$I_{relay}(d) = (\alpha_{11} + \alpha_3 d^n + \alpha_{12}) .T_l \tag{12.3}$$

With a node density (i.e. number of nodes in an unit area) of ρ is the node density the expected number of nodes that overhear the transmission is given by $\pi.d^2\rho - 2$, where we deduct 2 to remove the transmitter and the receiver from consideration of overhearing. Thus the current consumed for overhearing while transmitting a packet is given by $I_{ov} = (\pi.d^2\rho - 2) .\alpha_{12}.T_l$.

We first calculate the total current consumed in the network to transmit a packet from A to B with $K-1$ relays between them as shown in Figure 12.2(a). The distance between A and B is D. Thus the total current (sum of currents in all nodes) consumed is given by

$$I_T(D) = \sum_{i=1}^{K} (I_{relay}(d_i) + I_{ov}(d_i)) = \sum_{i=1}^{K} I_R(d_i) \tag{12.4}$$

[2]This is based on the assumption that with low-power operation, the packet size is primarily determined by the long preamble.

where

$$\begin{aligned} I_R(d_i) &= I_{relay}(d_i) + I_{ov}(d_i) \\ &= (\alpha_{11} - \alpha_{12} + \alpha_3 d_i^n + \pi.d_i^2\rho.\alpha_{12}).T_l \\ &= (\alpha_1 + \alpha_2 d_i^2 + \alpha_3 d_i^n).T_l \end{aligned} \tag{12.5}$$

★ Theorem 1: *Given D and K, $I_T(D)$ is minimized when all hop-distances are equal to $\frac{D}{K}$.*

Proof. The proof is obtained similar to that presented in [95]. Note that $I_R(d)$ is strictly convex as $\frac{d^2 I_R}{dt^2} > 0$. Thus from *Jensen's inequality*, we can write

$$\begin{aligned} I_R\left(\frac{\sum_{i=1}^{K} d_i}{K}\right) &\leq \frac{\sum_{i=1}^{K} I_R(d_i)}{K} \\ \Rightarrow K.I_R\left(\frac{D}{K}\right) &\leq \sum_{i=1}^{K} I_R(d_i) \quad \Rightarrow K.I_R\left(\frac{D}{K}\right) \leq I_T(D) \end{aligned} \tag{12.6}$$

which completes the proof. □

Thus, the minimum energy consumption for sending a packet to a distance D using K hops is given by $I_T(D) = \left(\alpha_1 K + \alpha_2.K.\left(\frac{D}{K}\right)^2 + \alpha_3.K.\left(\frac{D}{K}\right)^n\right).T_l$. This is minimized when $\alpha_1 - \alpha_2.\left(\frac{D}{K}\right)^2 + (n-1)\alpha_3.\left(\frac{D}{K}\right)^n = 0$. If K_{opt} is the optimal value of K, then the corresponding distance, termed as the *characteristic distance*, is $d_m = \frac{D}{K_{opt}}$. Replacing d_m in the previous equation, we get

$$\alpha_1 - \alpha_2.d_m^2 + (n-1)\alpha_3.d_m^n = 0 \tag{12.7}$$

By solving this equation 12.7, we get d_m in terms of α_1, α_2, α_3, n. Note that d_m is independent of D.

Another fact that needs to be considered while calculating the transmission range is network connectivity. In general to ensure connectivity with a high probability,

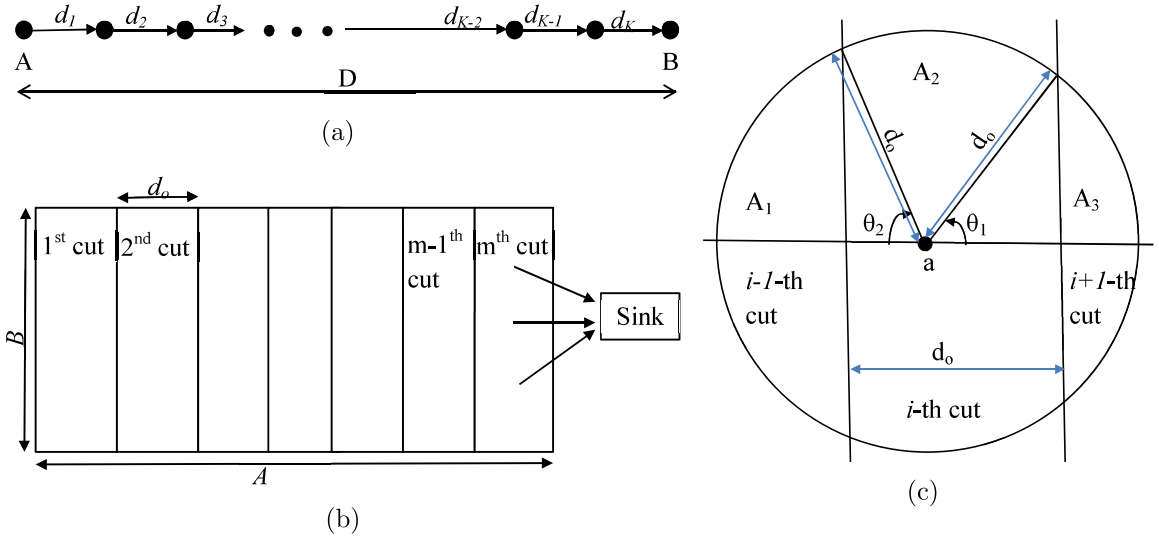

Figure 12.2: (a) Introducing $K-1$ relay between A and B. (b) A sensor network with N nodes in a field of A×B, (c) Calculating overhearing at the i-th cut.

there should be at least $\mathbb{K}$ nodes in the area of $\pi.r^2$, where r is the transmission range[3], i.e.

$$\pi.r^2.\rho \geq \mathbb{K} \Rightarrow r \geq \sqrt{\frac{\mathbb{K}}{\pi.\rho}} \tag{12.8}$$

Thus the optimal transmission range is $d_o = \max\{d_m, r^{min}\}$ where $r^{min} = \sqrt{\frac{\mathbb{K}}{\pi.\rho}}$. We consider the special case where the nodes from A to B have the same hop-distances (according to Theorem 1), $\mathbb{K} = 3$.

★ Theorem 2: *If the maximum current drawn by a radio to transmit at its maximum transmit power is I_t^{max} and the current drawn in the receive mode is I_r, then $d_o = r^{min}$ as long as the $I_t^{max} < (\mathbb{K}+1).I_r$.*

Proof. Let us assume that I^h and I^{h+1} are the overall current consumption when there are h and $h+1$ hops present in between A and B. Also $r_i = \frac{D}{i}$ is the transmission range when there are i hops in between A and B. To preserve the connectivity with

[3]Such as to ensure 1-connectivity in a homogeneous network of N nodes with a probability of atleast p, $\pi.r^2\rho \geq$ -ln $\left(1-p^{\frac{1}{N}}\right)$ [96].

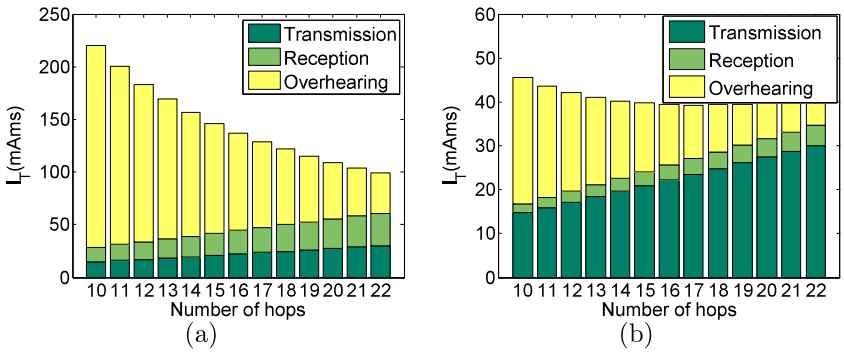

Figure 12.3: Variation of I_T with K when $D = 200$ meters and $\rho = 0.0125$ nodes/meters^2 for MICA2 motes (a) with typical value of $I_r = 10$ mA, and (b) with a fictitious value of $I_r = 1.5$ mA.

some high probability, $\pi.r_i^2.\rho \geq \mathbb{K}\ \forall\ i$. Then,

$$\begin{aligned} I^h &= \left(I_t^h + (\pi.r_h^2.\rho - 2).I_r + I_r\right).h.T_l \\ I^{h+1} &= \left(I_t^{h+1} + (\pi.r_{h+1}^2.\rho - 2).I_r + I_r\right).(h+1).T_l \\ \Delta^I &= I^h - I^{h+1} = \Delta^T + \Delta^R \end{aligned}$$

where

$$\begin{aligned} \Delta^T &= I_t^h.h.T_l - I_t^{h+1}.(h+1).T_l \\ &= \left(I_t^h - I_t^{h+1}\right).h.T_l - I_t^{h+1}.T_l \\ \Delta^R &= \left((\pi.r_h^2.\rho - 1).h - \left(\pi.r_{h+1}^2.\rho - 1\right).(h+1)\right).I_r.T_l \\ &= \left(\left(\pi.\left(\tfrac{D}{h}\right)^2.\rho - 1\right).h - \left(\pi.\left(\tfrac{D}{h+1}\right)^2.\rho - 1\right).(h+1)\right).I_r.T_l \\ &= \left(\tfrac{\pi.D^2.\rho}{h.(h+1)} + 1\right).I_r.T_l \\ &> \left(\tfrac{\pi.D^2.\rho}{(h+1)^2} + 1\right).I_r.T_l = \left(\pi.r_{h+1}^2.\rho + 1\right).I_r.T_l \\ &> (\mathbb{K}+1).I_r.T_l \end{aligned} \tag{12.9}$$

When $\Delta^T \geq 0$ then $\Delta^I > 0$. When $\Delta^T < 0$ then $\Delta^T = \left(I_t^h - I_t^{h+1}\right).h.T_l - I_t^{h+1}.T_l > -I_t^{h+1}.T_l > -I_t^{max}.T_l$ as $I_t^h > I_t^{h+1}$. Thus $\Delta^I = \Delta^T + \Delta^R > \left(-I_t^{max} + (\mathbb{K}+1).I_r\right)T_l$ which is positive if $I_t^{max} < (\mathbb{K}+1).I_r$. This concludes that if $I_t^{max} < (\mathbb{K}+1).I_r$, $I^h > I^{h+1}$ i.e. increasing the number of hops results in reduced current consumption as long as $r \geq \sqrt{\frac{\mathbb{K}}{\pi.\rho}}$. At $r = \sqrt{\frac{\mathbb{K}}{\pi.\rho}}$, the current consumption is minimized, i.e. $d_o = r^{min}$. □

For typical radio transceivers used in sensor networks such as CC1000 (used by MICA2 motes) and CC2420 (used by MICAz motes), $I_t^{max} < 4.I_r$ (obtained under the special case of $\mathbb{K} = 3$). For instance, for CC1000 radios $I_t^{max} = 27$ mA and $I_r = 10$ mA whereas for CC2420 radios $I_t^{max} = 17.4$ mA and $I_r = 19.7$ mA. Hence, it is always good to use the minimum power that is sufficient to preserve the network connectivity and required quality with these radios. Figure 12.3(a) shows the variation of I_T with the number of hops, for MICA2 motes. The maximum number of hops occurs when the distance between each node is r_{min}. It is observed that for smaller number of hops, overhearing dominates due to high transmission range. With the increase in number of hops, overhearing starts reducing whereas consumptions due to reception and transmission increase as the number of relays increases.

Note that for transceivers with $I_t^{max} > (\mathbb{K}+1).I_r$, d_0 has to be calculated as $\max\{d_m, r^{min}\}$. An example of the case when $I_t^{max} > (\mathbb{K}+1).I_r$ is shown in Figure 12.3(b), where a non-realistic low value of $I_r = 1.5mA$ is assumed with all the other parameters considered to be the same as of MICA2 mote.

12.3 Network Lifetime Calculation

We now calculate the upper limit of the lifetime of a network of N sensor nodes that are uniformly distributed in an area of $A \times B$. Consider that the network area is divided into rectangular areas (called *cuts*) of width d_o as shown in Figure 12.2(a). A node in any cut forwards its packets to a node that is located in the cut to its immediate right. We first consider single channel operation and calculate the energy

consumption in each cut under the assumptions that each node generates b packets/seconds and the beacon rate is B beacons/seconds. The total number of cuts is $m = \frac{A}{d_o}$, with cuts numbered in increasing order from left to right. We assume that the nodes in any cut convey the traffic of the nodes in their left cuts. Thus, nodes in the first cut transmits b packets/seconds, the nodes in the second cut on average transmit $2b$ packets/seconds (their own b packets/seconds + packets generated by the first cut). So, the nodes in the i-th cut on average transmit ib packets/seconds. Thus the expected energy consumed for different actions under our assumptions in the i-th cut can be written as:

$$\mathcal{I}^i_{Dt} = ib\left(\alpha_{11} + \alpha_3 d_o^n\right).T_l \qquad \mathcal{I}^i_{Dr} = (i-1)b\alpha_{12}.T_l$$

$$\mathcal{I}^i_{Bt} = B\left(\alpha_{11} + \alpha_3 d_o^n\right).T_l \qquad \mathcal{I}^i_{Br} = \left(\pi.d_o^2\rho - 1\right)B\alpha_{12}.T_l$$

Now let us calculate the expected overhearing in the i-th cut with the help of Figure 12.2(b). Let us consider a point a and draw a circle with radius d_o. Thus if we place a node at a, that node overhears all traffic that are forwarded by the nodes that are inside this circle. Nodes that are in A_1, A_2 and A_3 transmit at $(i-1)b$, ib and $(i+1)b$ packets/seconds. The areas of A_1, A_3 and A_2 can be written as $d_o^2\left(\theta_2 - \sin\theta_2\cos\theta_2\right)$, $d_o^2\left(\theta_1 - \sin\theta_1\cos\theta_1\right)$ and $\pi.d_o^2 - A1 - A2$ respectively. Thus the

expected number of packets that a node at a overhears in a second is given by:

$$\begin{aligned} ov_i &= E[A_1](i-1)b\rho + (E[A_2]\rho - 1)ib \\ &\quad + E[A_3](i+1)b\rho \text{ for } i < m \\ &= E[A_1](i-1)b\rho + (E[A_2]\rho - 1)ib \text{ for } i = m \\ E[A_1] &= \frac{2}{\pi}\int_0^{\frac{\pi}{2}} d_o^2\left(\theta_2 - \sin\theta_2\cos\theta_2\right).d\theta_2 \\ E[A_3] &= \frac{2}{\pi}\int_0^{\frac{\pi}{2}} d_o^2\left(\theta_1 - \sin\theta_2\cos\theta_1\right).d\theta_1 \\ E[A_2] &= \pi.d_0^2 - E[A_1] - E[A_2] \end{aligned} \tag{12.10}$$

Then

$$\begin{aligned} \mathcal{I}_{ov}^i &= \frac{2bi\alpha_{12}.T_l\left(\pi.d_0^2.\rho - 1\right)}{\pi} \text{ for } i < m \\ &= \frac{2bm\alpha_{12}.T_l\left(\pi.d_0^2.\rho - 1\right)}{\pi} \\ &\quad - \frac{2b\alpha_{12}.T_l\rho.d_0^2(m+1)\left(\frac{\pi^2}{8} - \frac{1}{2}\right)}{\pi} \text{ for } i = m \end{aligned} \tag{12.11}$$

Thus the total current consumption for the nodes in the i-th cut is

$$\mathcal{I}^i = \mathcal{I}_{Dt}^i + \mathcal{I}_{Dr}^i + \mathcal{I}_{Bt}^i + \mathcal{I}_{Br}^i + \mathcal{I}_{ov}^i + \mathcal{I}_S^i + \mathcal{I}_P^i \tag{12.12}$$

12.3.1 Expected Lifetime for Identical Battery Capacities

We define the initial battery capacity of each node by e_0 and τ is the cut-off capacity, beyond that the sensor mote does not work. Then the expected lifetime of any node in the i-th cut L_i can be written as $L_i = \frac{e_0 - \tau}{\mathcal{I}^i}$. For any $i < m$, it can be shown that $L_i < L_{i-1}$. Now let us compare L_i for $i = m-1$ and $i = m$. Clearly, $\mathcal{I}_{Dt}^m > \mathcal{I}_{Dt}^{m-1}$ and $\mathcal{I}_{Dr}^m > \mathcal{I}_{Dr}^{m-1}$. But $\mathcal{I}_{ov}^m$ can be greater or less than $\mathcal{I}_{ov}^{m-1}$ based on the values of different parameters. This is because, nodes in the $(m-1)$-th cut overhear

from transmissions from both $(m-2)$-th cut and m-th cut, whereas nodes in the m-th cut overhear only from transmissions from $(m-1)$-th cut. Thus L_i is minimum when $i = m$ or $i = m-1$.

12.3.2 Expected Lifetime for Different Battery Capacities

In practice, if nothing is done to balance the energy consumption at the nodes, nodes deplete batteries non-uniformly. Consequently, the battery capacities of the nodes at any time are expected to be different. To represent this effect, we model the battery capacity of the nodes at any instant of time to be independent and identically distributed Gaussian random variables with mean μ and standard deviation σ. Define the remaining capacity of any node k in the i-th cut at time t_j to be $e_{ki}(t_j)$. If at a time instance t_0, $e_{ki}(t_0) \sim \mathcal{N}(\mu, \sigma^2)$, the probability that the remaining capacity of a node in the i-th cut is greater than τ at time $t_j = t_0 + \Delta t$ is

$$\begin{aligned} p_i &= P[e_{ki}(t_j) > \tau] = P[e_{ki}(t_0) - \mathcal{I}^i.\Delta t > \tau] \\ &= P[e_{ki}(t_0) > \tau + \mathcal{I}^i.\Delta t] = Q\left(\tfrac{\tau + \mathcal{I}^i.\Delta t - \mu}{\sigma}\right) \end{aligned} \tag{12.13}$$

Thus expected number of nodes at time t_j in the i-th cut whose capacity is greater then τ is given by $\sum_{x=1}^{\mathbb{N}} x.\binom{\mathbb{N}}{x}.p_i^x.(1-p_i)^{\mathbb{N}-x}$, where $\mathbb{N} = \frac{N}{m}$ is the number of nodes in each cut. If we assume that the lifetime of the cut is the time till f fraction of the nodes stay alive then

$$\sum_{x=1}^{\mathbb{N}} x.\binom{\mathbb{N}}{x}.p_i^x.(1-p_i)^{\mathbb{N}-x} = f.\mathbb{N} \tag{12.14}$$

By solving equation (12.14) we find the expected lifetime of any cut i. To illustrate the results, we take an example with 100 nodes that are uniformly distributed in an area of 200×200 meter^2. The parameters used for the results are listed in Table 12.1. Nodes are assumed to transmit data packets as well as beacons once a minute. We consider two cases: where the initial battery capacities of all nodes are same and

equal to 5000 mAHr, and where the battery capacities are normally distributed with mean of 5000 mAHr and standard deviation of 1000 mAHr[4]. For the case of non-uniform battery capacities, the expected lifetime is calculated as the time till the 75% of nodes in a cut survive. Each node transmits a packet and a beacon in every minute. τ is assumed to be 0. The results, depicted in Figure 12.4 depict that the lifetimes are lower with unequal battery capacities. Also, with these set of parameters, the $(m-1)$-th cut has the lowest lifetime for both cases.

Table 12.1: Different Parameters for MICA2

Var	**Values**	**Var**	**Values**	**Var**	**Values**	**Var**	**Values**
I_{Br}	10 mA	T_{Br}	140 ms	I_{Dr}	10 mA	T_{Dr}	140 ms
I_P	10 mA	T_P	3 ms	I_S	7.5 mA	T_S	112 ms

Var	**Values**	**Var**	**Values**
I_{Bt}, I_{Dt}	26.7 mA (10 dBm), 20 mA (8 dBm) 16.8 mA (7 dBm), 14.8 mA (5 dBm) 13.8 mA (4 dBm), 12.8 mA (2 dBm) 11.8 mA (1 dBm), 9.7 mA (-2 dBm)	T_{Bt}, T_{Dt}	140 ms

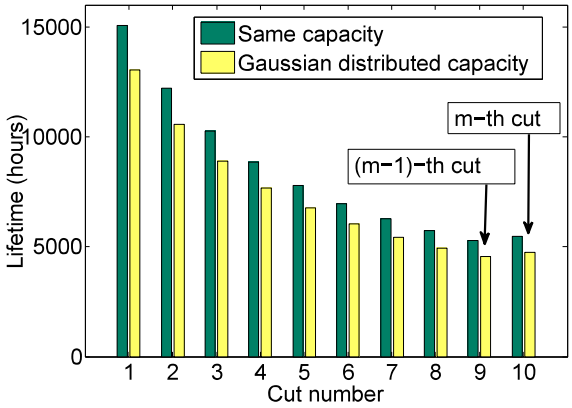

Figure 12.4: Expected lifetime in each cut.

12.3.3 Expected Lifetime for Flow Based Channel Assignment

Now consider the case where there are k orthogonal channels, that helps in reducing overhearing. We consider the effect of overhearing in presence of multiple

[4]This is the capacity of batteries that we used in an experimental deployment [72].

channels using the *vertex coloring problem.* [5] For any greedy algorithm, the worst case chromatic number is $\delta + 1$, where δ is the maximum vertex degree of a graph. In our case of uniform node distribution, the average vertex degree (which is basically the maximum degree in our case) $\delta = \pi.d_o^2.\rho - 1$.

To analyze this case, we find the average overhearing at a node using the concepts of vertex coloring. First we assume that the network is represented as a *regular graph* of degree δ. A regular graph is a graph where each vertex has the same degree. Now we assign k colors uniformly to the N vertices of this graph. We group all nodes of same color, and let S_i represent the set of nodes colored with the i-th color, where $1 \leq i \leq k$. Clearly, $|S_i| = \frac{N}{k}$ and we assume that N is divisible by k for simplicity. Then

$$\begin{aligned} & \text{Pr(An edge is an overhearing edge)} \\ = \; & \text{Pr(Nodes at the both ends of that edge are from the same color set)} \\ = \; & \frac{k.\binom{|S_i|}{2}}{\binom{N}{2}} \end{aligned} \tag{12.15}$$

As the total number of edges in the graph is $\frac{N.\delta}{2}$ then the expected number of overhearing edges is $q = \frac{N.\delta}{2}.\frac{k.\binom{|S_i|}{2}}{\binom{N}{2}} = \frac{N.\delta.(N-k)}{2.k.(N-1)}$. Thus each node has $\frac{2.q}{N} = \frac{\delta.(N-k)}{k.(N-1)}$ overhearers. Also the number of overhearers in unit area is $\rho_c = \frac{\delta.(N-k)}{\pi.d_0^2.k.(N-1)}$. Putting ρ_c in place of ρ in equation (12.11), we get a modified expression of $\mathcal{I}_{ov}^i$. By changing the expression of $\mathcal{I}_{ov}^i$, we get a new expression of $\mathcal{I}^i$ and L_i for network lifetime with multiple channels. Note that in case of FCA with multiple channels, d_0 is higher than that of single channel. This is because to preserve connectivity with some high probability, there should be atleast $\mathbb{K}$ nodes in the area of $\pi.d_0^2.\rho$ that have the same channel.

[5] Throughout this chapter we use the word *color* and *channel* interchangeably.

12.3.4 Expected Lifetime for Receiver Based Channel Assignment

For simplicity we assume that the forwarding and overhearing rate of a node is proportional to its battery health or remaining capacity at any instance. The residual capacity of node k in the i-th cut at time t_0 (when the network starts) is $e_{ki}(t_0) \sim \mathcal{N}(\mu, \sigma^2)$. Also as the forwarding and overhearing rate is proportional to its remaining capacity, then

$$\mathcal{I}_{Dt}^{ik}(t_j) = b_i(t_j).e_{ki}(t_j) \qquad \mathcal{I}_{ov}^{ik}(t_j) = c_i(t_j).e_{ki}(t_j)$$
$$\mathcal{I}^{ik}(t_j) = b_i(t_j).e_{ki}(t_j) + c_i(t_j).e_{ki}(t_j) + C$$

where $b_i(t_j)$ and $c_i(t_j)$ is the proportionality constant for nodes in the i-th cut at time instance t_j and C is the constant current consumption for other actions such as receptions, sensing etc. The k superscript is used to represent the k-th node. Clearly $b_i(t_j), c_i(t_j) < 1 \ \forall \ i$ and j. Then at any instance t_j,

$$\begin{aligned}
e_{ki}(t_j) &= e_{ki}(t_{j-1}) - \mathcal{I}^{ik}(t_j) \\
&= e_{ki}(t_{j-1}) - b_i(t_{j-1}).e_{ki}(t_{j-1}) \\
&\quad -c_i(t_{j-1}).e_{ki}(t_{j-1}) - C \\
&= (1 - b_i(t_{j-1}) - c_i(t_{j-1}))\, e_{ki}(t_{j-1}) - C \\
&= (1 - b_i(t_{j-2}) - c_i(t_{j-2})) \\
&\quad .(1 - b_i(t_{j-1}) - c_i(t_{j-1}))\, e_{ki}(t_{j-2}) \\
&\quad -(1 - b_i(t_{j-1}) - c_i(t_{j-1})).C - C = ... \\
&= \textstyle\prod_{l=0}^{j-1} (1 - b_i(t_l) - c_i(t_l))\, .e_{ki}(t_0) - \mathcal{C} \qquad (12.16)
\end{aligned}$$

where $\mathcal{C}$ is a constant. Thus $e_{ki}(t_j)$ is a Gaussian random variable with mean μ and standard deviation of $\sigma_j = \prod_{l=0}^{j-1}(1 - b_i(t_l) - c_i(t_l)).\sigma$. As j increases σ_j reduces and gradually approaches zero, i.e. the distribution approaches to a constant figure. This

means the residual capacity of all nodes becomes similar and all nodes in a cut die around the same time (i.e. the lifetime of nodes in the i-th cut approaches to $\frac{\mu-\tau}{I_i}$), which increases the worst case network lifetime.

For both FCA and RCA, we assume that the sink always stays in a designated channel. The nodes that are immediate neighbors to the sink switches to the channel of the sink temporarily while transmitting.

12.4 Results

We obtain numerical results of the network lifetime under different conditions using network parameters as used in the example described in section 12.3.2, unless it is mentioned otherwise. For all the following graphs, we assume $T_l = \frac{1}{P} + 15$ ms, thus for $P = 8$, $T_l = 140$ ms. Also $I_{Br} = I_{Dr} = \alpha_r = T_l$, i.e. considering that nodes overhear the whole preamble as well as the data or control packet. The data packets and beacons are transmitted once a minute. For Gaussian distributed battery capacities, we assume $\mu = 5000$ mAH with $\sigma = 1000$ mAHr. For the following set of graphs we consider two cases. For the first case α_r is assume to be 10 mA ($I_t^{max} < 4.I_r$) and for second case $\alpha_r = 1.5$ mA ($I_t^{max} > 4.I_r$).

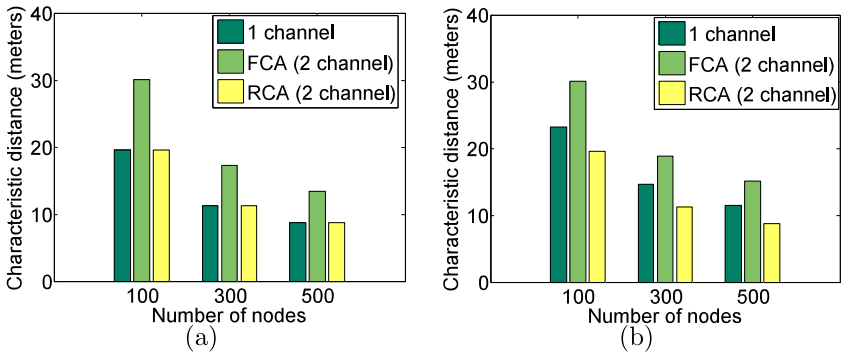

Figure 12.5: Characteristic distance with different number of nodes (a) $\alpha_r = 10$ mA and (b) $\alpha_r = 1.5$ mA.

Figure 12.5 shows the characteristic distance with different number of nodes. It can be observed that the characteristic distance starts reducing with increasing num-

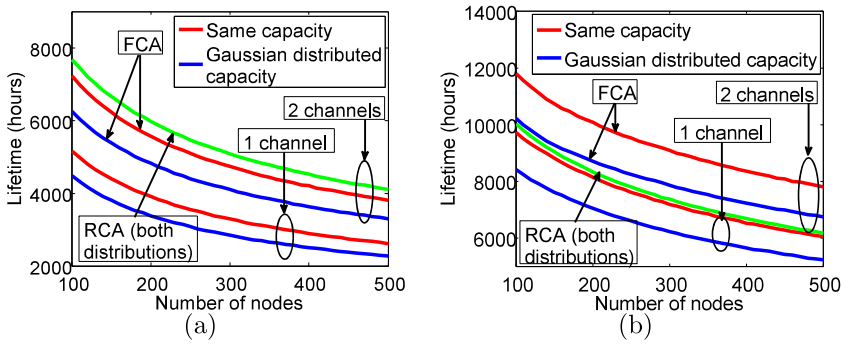

Figure 12.6: Expected network lifetime with different number of nodes (a) $\alpha_r = 10$ mA and (b) $\alpha_r = 1.5$ mA.

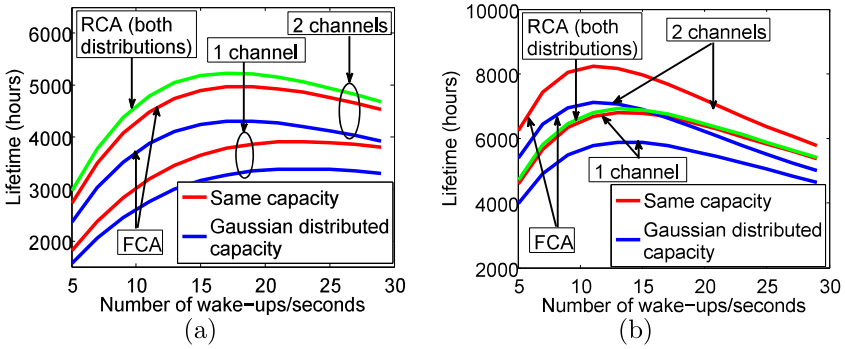

Figure 12.7: Expected network lifetime with different wake-up rates (a) $\alpha_r = 10$ mA and (b) $\alpha_r = 1.5$ mA.

ber of nodes because of higher overhearing caused by increasing node density. Also the characteristic distance is same for both single channel and RCA with 2 channels with $\alpha_r = 10$ mA. This is because when $\alpha_r = 10$ mA, the characteristic distance is effectively equal to the minimum distance required to maintain connectivity. In case of FCA, to preserve connectivity, there should be atleast $\mathbb{K}$ nodes on the same channel within its characteristic distance, which increases the characteristic distance. For $\alpha_r = 1.5$ mA, the characteristic distance is lowest in case of RCA with 2 channels. Also due to connectivity considerations, FCA gives higher characteristic distance.

Figure 12.6 shows the variation of lifetime for the $(m-1)$-th cut with the number of nodes. It can be observed that there is significant improvement in the lifetime with

2 channels in comparison to then single channel case. This is due to lower interference and overhearing. Also we can observe that when $\alpha_r = 10$ mA, RCA performs better than FCA, based on the assumption that all nodes in a cut die at the same time in RCA. This can be attributed to two reasons. First, to stay connected, d_0 in FCA is higher compared to that in RCA, which results in higher transmit power and higher overhearing. Also RCA balances the overhearing based on a nodes capacity, which results in more overall battery lifetime. Note that when $\alpha_r = 1.5$ mA, RCA performs poorly. This is because the characteristic distance for RCA decreases which results in more transmissions. In this case, the transmission current is the dominating factor in reducing the network lifetime.

Figure 12.7 shows the variation of lifetime for the $(m-1)$-th cut with wake-up frequencies. For this set of graphs we kept the number of nodes to be 500. As we can see from these graphs, the lifetime first starts to increase with increasing values of the wake-up frequency, due to a smaller preamble length. But after a certain point the lifetime starts reducing because of higher current consumption due to frequent wake-ups. Similar to the previous set of graphs, for $\alpha_r = 1.5$ mA, RCA performs poorly with 2 channels because of a higher number of transmission due to smaller d_0.

12.5 Discussions

The fundamental challenge of designing WSN protocols is to maximize the network lifetime. In this chapter, we analyze the battery lifetime of a WSN under data collection traffic and asynchronous duty-cycling. The current consumption in such networks can be optimized by applying transmission power control. This is applied to derive the maximum lifetime of the network. In addition, multi-channel operation with adaptive channel selection is considered as a mechanism to further reduce current consumption as well as to balance the remaining lifetimes of the nodes. Analysis of the network lifetime with multi-channel operation and optimal power control is presented.

CHAPTER 13: CONCLUSIONS AND FUTURE WORKS

In this dissertation, we addressed a number of routing problems in multihop wireless networks that require solutions involving one or more cross-layer adaptations for achieving the required performance objectives. Such problems are characterized by a high degree of computational complexity that require special considerations to formulate tractable design approaches. Our approach for the joint channel selection and routing problems in WOBANs include development of a novel quality aware routing metric that can be applied when global network parameters are available, which is a valid assumption in a WOBAN framework; and development of a joint channel selection and route selection based on this quality metric. The proposed channel selection and routing protocol can improve the network throughput up to three times with eight channels and four NICs, while reduces the traffic delay by six times, as demonstrated by our simulation results obtained from ns-2 implementations. In addition, we explore the problem of planning and setup of a WOBAN, i.e. the placement of ONUs across the network, and discuss their effects on network performance and cost optimization.

We also addressed a joint channel selection and routing problem in wireless sensor networks, where the key performance objective is to maximize the network lifetime that is depended on the energy consumption of the nodes. We explored two types of channel selection schemes that impose different design considerations for the joint routing and channel selection problem, named flow based and receiver based scheme, for building multi-channel trees in data gathering wireless sensor networks. The proposed flow based schemes involve distributed channel selection to enable nodes to reduce overhearing, whereas the receiver based scheme involves dynamic parent

and channel selection for minimizing the load of nodes that have the worst expected lifetime. Through extensive simulations and experiments, we demonstrate that our proposed channel selection schemes almost doubles the network lifetime with four channels, without sacrificing the packet delivery ratio.

We next consider a routing problem that involves adaptive routing to be addressed jointly with transmit power control in a data gathering rechargeable wireless sensor networks for maximizing the network lifetime. The proposed scheme performs quality aware route selection while reducing the energy consumption in sensor nodes that have low remaining battery life through cooperative and network-wide adaptations of transmit power levels and parent selection. Through simulations and experiments, we demonstrate that our proposed scheme significantly reduces overhearing on the critical nodes, without sacrificing the network performance significantly. Finally, we consider the problem of routing together with power control and channel selection, and develop an analytical model for evaluating the lifetime of WSNs under different conditions.

In the near future I would like to work on the following research aspects as described below.

★ Harvesting energy prediction and routing in WSNs: In future, we want to explore integration of different energy harvesting techniques (such as solar harvesting) with sensor networks to extend the network lifetime. As the availability of harvested energy varies over time and space, some prediction models for the available energy will be investigated. Also the data collection pattern should change depending on the spatio-temporal energy availability of solar power, which is one of our future considerations.

★ Exploring the use of supercapacitors in rechargeable WSNs: Rechargeable batteries (RBs), the traditional (and popular) choice for powering wireless devices suffer from a limited *cycle life*, which is the number of charge-discharge cycles, typically

from 200 to 1000. An alternative to RBs is to consider supercapacitors (SC) (capacitors with extremely high energy storage values in relatively small packages and extremely long cycle lives, on the order of millions of cycles) to temporarily store the harvested energy to route packets. The main limitation of SCs is the high leakage current especially when they are fully charged. Our future consideration is to use suitable recharging policies, forwarding and duty-cycle adaptation in SC-powered WSNs with the main objective of *minimizing the leakage current from the SCs*. This kind of scheme will be useful for applications that require long-term operation, such as those used for structural health monitoring of bridges, buildings, and other construction sites.

Other research plans include the following research topics.

★ Developing a beaconless collection tree protocol for WSNs: As mentioned earlier, sensor nodes are energy constrained tiny devices with limited battery capacity. Beacon transmissions and receptions wastes a lot of energy, which is crucial especially for the nodes with critically low battery capacity. Beacon transmissions are mainly used to maintain connectivity, estimate the route quality as well as exchanging some network parameters such as individual nodes remaining battery capacities etc. By the use of *overhearing*, these informations can be exchanged through data packets where all the necessary parameters needs to be appended into the data packets. One of my future research goal is to explore this technique that is expected to reduce the energy consumption in a network by a significant amount.

★ Adaptive duty-cycling for rechargeable WSNs: As mentioned in Chapter 12, in rechargeable wireless sensor networks, sensor nodes have wide variety of energy resources. This results in few of the sensor nodes to die early compared to others. Thus using adaptive duty cycling based on individual nodes energy resources will result in critically energy constrained nodes to increase their sleep periods based on their energy budget, resulting in more energy saving and increased overall network

lifetime.

★ Exploring the effect of cooperative diversity in WSNs: In general wireless networks, it has been observed that for a fixed outrage probability, cooperative relaying protocols offer a significant signal-to-noise ratio (SNR) gain compared to conventional relaying. This SNR gain can be exploited to decrease the transmit power level of the sensor nodes without degrading the error rate performance which can translate into network-wide energy saving and significant increase in network lifetime. However, this benefit requires a careful incorporation of cooperative relaying into the routing process to exploit the diversity gain, which is one of our future research interests.

★ Exploring the application of Game Theory in WSNs: Game theory is a mathematical method that describes the phenomenon of conflict and cooperation between intelligent rational decision-makers. In recent times, there has been significant interest on applications of Game theory to design of wireless sensor networks. One of my future considerations is to study how to incorporate Game theory such that sensor nodes behave as rational players to fulfill a common social objective, which is maximizing the network lifetime.

REFERENCES

[1] "Xmesh user manual, Crossbow technology," `http://www.xbow.com/Products`, 2007.

[2] A. Pal and A. Nasipuri, "Effects of optical network unit placement schemes for multi-channel hybrid wireless-optical broadband-access networks," in *IWON (accepted)*, 2013.

[3] A. Pal, S. Adimadhyam, and A. Nasipuri, "QoSBR: A quality based routing protocol for wireless mesh networks," in *ICDCN*, 2010, pp. 497–508.

[4] A. Pal and A. Nasipuri, "A quality based routing protocol for wireless mesh networks," *Pervasive and Mobile Computing*, vol. 7, no. 5, pp. 611–626, 2011.

[5] H. Lundgren, E. Nordström, and C. F. Tschudin, "The gray zone problem in ieee 802.11b based ad hoc networks," *Mobile Computing and Communications Review*, vol. 6, no. 3, pp. 104–105, 2002.

[6] A. Pal and A. Nasipuri, "A quality aware anycast routing protocol for wireless mesh networks," in *IEEE SoutheastCon*, 2010, pp. 451–454.

[7] A. Pal and A. Nasipuri, "GSQAR: A quality aware anycast routing protocol for wireless mesh networks," in *IEEE GLOBECOM*, 2010, pp. 1–5.

[8] A. Pal and A. Nasipuri, "JRCA: A joint routing and channel assignment scheme for wireless mesh networks," in *IEEE IPCCC*, 2011.

[9] A. Pal and A. Nasipuri, "Maximum-lifetime multi-channel routing in wireless sensor networks," in *Technical Report, The University of North Carolina at Charlotte, ECE Department*, 2012.

[10] A. Pal and A. Nasipuri, "A distributed channel selection scheme for multi-channel wireless sensor networks," in *MobiHoc*, 2012, pp. 263–264.

[11] A. Pal and A. Nasipuri, "DRCS: A distributed routing and channel selection scheme for multi-channel wireless sensor networks," in *IEEE PerSeNS*, 2013, pp. 602–608.

[12] A. Pal and A. Nasipuri, "Lifetime of asynchronous wireless sensor networks with multiple channels and power control," in *IEEE WCNC (In submission)*, 2014.

[13] A. Pal, B. Soibam, and A. Nasipuri, "A distributed power control and routing scheme for rechargeable sensor networks," in *IEEE SoutheastCon*, 2013.

[14] A. Pal and A. Nasipuri, "PCOR: A joint power control and routing scheme for rechargeable sensor networks," in *IEEE WCNC (In submission)*, 2014.

[15] S. Sarkar, B. Mukherjee, and S. Dixit, "Optimum placement of multiple optical network units (ONUs) in optical-wireless hybrid access networks," in *Optical Fiber Communications*, 2006.

[16] S. Sarkar, B. Mukherjee, and S. Dixit, "Towards global optimization of multiple ONUs placement in hybrid optical-wireless broadband access networks," in *COIN, Jeju, Korea*, 2006.

[17] S. Sarkar, B. Mukherjee, and S. Dixit, "A mixed integer programming model for optimum placement of base stations and optical network units in a hybrid wireless-optical broadband access network (WOBAN)," in *Wireless Communications and Networking Conference, Hong Kong*, 2007.

[18] R. Draves, J. Padhye, and B. Zill, "Routing in multi-radio, multi-hop wireless mesh networks," in *MOBICOM*, 2004, pp. 114–128.

[19] D. Passos, D. V. Teixeira, D. C. Muchaluat-saade, L. C. S. Magalhães, and C. V. N. Albuquerque, "Mesh network performance measurements," in *International Information and Telecommunication Technologies Symposium*, 2006.

[20] C. E. Koksal and H. Balakrishnan, "Quality-aware routing metrics for time-varying wireless mesh networks," *IEEE Journal on Selected Areas in Communications*, vol. 24, no. 11, pp. 1984–1994, 2006.

[21] A. P. Subramanian, M. M. Buddhikot, and S. Miller, "Interference aware routing in multi-radio wireless mesh networks," in *IEEE Workshop of Wireless Mesh Networks*, 2006, pp. 55–63.

[22] X. Cheng, P. Mohapatra, S.-J. Lee, and S. Banerjee, "Maria: Interference-aware admission control and qos routing in wireless mesh networks," in *ICC*, 2008, pp. 2865–2870.

[23] V. Kolar and N. B. Abu-Ghazaleh, "A multi-commodity flow approach for globally aware routing in multi-hop wireless networks," in *PerCom*, 2006, pp. 308–317.

[24] E. Carlson, H. Karl, A. Wolisz, and C. Prehofer, "Distributed allocation of time slots for real-time traffic in a wireless multi-hop network," 2004.

[25] L. Romdhani and C. Bonnet, "Cross-layer qos routing framework for wireless mesh networks," *International Conference on Wireless and Mobile Communications*, vol. 0, pp. 382–388, 2008.

[26] Z. Ke, L. Li, Q. Sun, and N. Chen, "A qos multicast routing algorithm for wireless mesh networks," in *SNPD (1)*, 2007, pp. 835–840.

[27] V. Kone, S. Das, B. Y. Zhao, and H. Zheng, "Quorum - quality of service in wireless mesh networks," *MONET*, vol. 12, no. 5-6, pp. 358–369, 2007.

[28] Q. Xue and A. Ganz, "Qos routing for mesh-based wireless lans," *IJWIN*, vol. 9, no. 3, pp. 179–190, 2002.

[29] C. H. Liu, K. K. Leung, and A. Gkelias, "A novel cross-layer qos routing algorithm for wireless mesh networks," in *Information Networking, 2008. ICOIN 2008. International Conference on*, 2008, pp. 1–5.

[30] S. Sarkar, H.-H. Yen, S. S. Dixit, and B. Mukherjee, "Dara: Delay-aware routing algorithm in a hybrid wireless-optical broadband access network (woban)," in *ICC*, 2007, pp. 2480–2484.

[31] A. A. Reaz, V. Ramamurthi, S. Sarkar, D. Ghosal, S. S. Dixit, and B. Mukherjee, "Cadar: An efficient routing algorithm for wireless-optical broadband access network," in *ICC*, 2008, pp. 5191–5195.

[32] L. Song and Z. bing Xia, "An anycast routing protocol for wireless mesh access network," *Information Engineering, International Conference on*, vol. 2, pp. 82–85, 2009.

[33] K. Sharif, L. Cao, Y. Wang, and T. A. Dahlberg, "A hybrid anycast routing protocol for load balancing in heterogeneous access networks," in *ICCCN*, 2008, pp. 99–104.

[34] S. Lakshmanan, R. Sivakumar, and K. Sundaresan, "Multi-gateway association in wireless mesh networks," *Ad Hoc Networks*, vol. 7, no. 3, pp. 622–637, 2009.

[35] D. Nandiraju, L. Santhanam, N. Nandiraju, and D. Agrawal, "Achieving load balancing in wireless mesh networks through multiple gateways," in *IEEE MASS*, 2006, pp. 807–812.

[36] M. K. Marina and S. R. Das, "A topology control approach for utilizing multiple channels in multi-radio wireless mesh networks," in *BROADNETS*, 2005, pp. 412–421.

[37] A. P. Subramanian, H. Gupta, S. R. Das, and J. Cao, "Minimum interference channel assignment in multiradio wireless mesh networks," *IEEE Transactions on Mobile Computing*, vol. 7, no. 12, pp. 1459–1473, 2008.

[38] A. K. Das, R. Vijayakumar, and S. Roy, "Static channel assignment in multi-radio multi-channel 802.11 wireless mesh networks: Issues, metrics and algorithms," in *GLOBECOM*, 2006.

[39] A. K. Das, H. M. K. Alazemi, R. Vijayakumar, and S. Roy, "Optimization models for fixed channel assignment in wireless mesh networks with multiple radios," in *In SECON*, 2005, pp. 463–474.

[40] M. Kodialam and T. Nandagopal, "Characterizing the capacity region in multi-radio multi-channel wireless mesh networks," in *in ACM MobiCom*. ACM Press, 2005, pp. 73–87.

[41] R. Koshy and L. Ruan, "A joint radio and channel assignment (JRCA) scheme for 802.11-based wireless mesh networks," in *GLOBECOM Workshops, 2009 IEEE*, December 2009, pp. 1–6.

[42] A. Raniwala, K. Gopalan, and T. cker Chiueh, "Centralized channel assignment and routing algorithms for multi-channel wireless mesh networks," *ACM Mobile Computing and Communications Review*, vol. 8, pp. 50–65, 2004.

[43] A. Raniwala and T. cker Chiueh, "Architecture and algorithms for an ieee 802.11-based multi-channel wireless mesh network," in *INFOCOM*, 2005, pp. 2223–2234.

[44] J. Chen, J. Jia, Y. Wen, D. Zhao, and J. Liu, "A genetic approach to channel assignment for multi-radio multi-channel wireless mesh networks," in *GEC Summit*, 2009, pp. 39–46.

[45] W. Fu, B. Xie, X. Wang, and D. P. Agrawal, "Flow-based channel assignment in channel constrained wireless mesh networks," in *ICCCN*, 2008, pp. 424–429.

[46] P. Kyasanur and N. H. Vaidya, "Routing and link-layer protocols for multi-channel multi-interface ad hoc wireless networks," *SIGMOBILE Mob. Comput. Commun. Rev.*, vol. 10, no. 1, pp. 31–43, 2006.

[47] K. N. Ramachandran, E. M. Belding, K. C. Almeroth, and M. M. Buddhikot, "Interference-aware channel assignment in multi-radio wireless mesh networks," in *INFOCOM 2006. 25th IEEE International Conference on Computer Communications. Proceedings*, 2006, pp. 1–12.

[48] D. Aloise, A. Deshpande, P. Hansen, and P. Popat, "NP-hardness of euclidean sum-of-squares clustering," *Mach. Learn.*, vol. 75, pp. 245–248, May 2009.

[49] P. Hansen and D. Aloise, "A survey on exact methods for minimum sum-of-squares clustering," `http://www.math.iit.edu/Buck65files/msscStLouis.pdf`.

[50] "The network simulator - ns-2 webpage," `http://www.isi.edu/nsnam/ns/`.

[51] "Multi-channel multi-interface simulation in ns2," `http://www.cse.msu.edu/ wangbo1/ns2/nshowto8.html`.

[52] M. Garey, *Computers and intractability - A guide to the theory of NP-completeness*, 1995.

[53] D. Whitley, "A genetic algorithm tutorial," *Statistics and Computing*, vol. 4, pp. 65–85, 1994.

[54] K. Jain, J. Padhye, V. N. Padmanabhan, and L. Qiu, "Impact of interference on multi-hop wireless network performance," in *MOBICOM*, 2003, pp. 66–80.

[55] J. M. Boyer and W. J. Myrvold, "On the cutting edge: Simplified O(n) planarity by edge addition," *Journal of Graph Algorithms and Applications*, vol. 8, pp. 241–273, 2004.

[56] T. Hubai, "The chromatic polynomial," Master's thesis, Eötvös Loránd University, 2009.

[57] L. Faria, C. M. H. de Figueiredo, S. Gravier, C. F. Mendonça, and J. Stolfi, "Non-planar vertex deletion: maximum degree thresholds for NP/Max SNP-hardness and a $\frac{3}{4}$-approximation for finding maximum planar induced subgraphs," *Electronic Notes in Discrete Mathematics*, vol. 18, pp. 121 – 126, 2004.

[58] S. J. Louis and G. J. E. Rawlins, "Predicting convergence time for genetic algorithms," in *Foundations of Genetic Algorithms 2*, 1992, pp. 141–161.

[59] S. Wilf, "Backtrack: an O(1) expected time algorithm for the graph coloring problem," in *In Information Processing Letters*, 1984.

[60] G. Bianchi, "Performance analysis of the ieee 802.11 distributed coordination function," *IEEE JOURNAL ON SELECTED AREAS IN COMMUNICATIONS*, vol. 18, no. 3, pp. 535–547, 2000.

[61] D. Malone, K. Duffy, and D. Leith, "Modeling the 802.11 distributed coordination function in nonsaturated heterogeneous conditions," *IEEE/ACM Trans. Netw.*, vol. 15, pp. 159–172, February 2007.

[62] T.-C. Hou, L.-F. Tsao, and H.-C. Liu, "Analyzing the throughput of IEEE 802.11 DCF scheme with hidden nodes," in *Vehicular Technology Conference, 2003. IEEE VTC*, 2003, pp. 2870 – 2874.

[63] O. Ekici and A. Yongaçoglu, "Modeling hidden terminals in IEEE 802.11 networks," in *PIMRC*, 2008, pp. 1–5.

[64] M. M. Carvalho and J. J. Garcia-Luna-Aceves, "Delay analysis of ieee 802.11 in single-hop networks," in *ICNP*, 2003, pp. 146–155.

[65] P. Chatzimisios, A. C. Boucouvalas, and V. Vitsas, "Packet delay analysis of IEEE 802.11 MAC protocol," *Electronics Letters*, vol. 39, pp. 1358 – 1359, 2003.

[66] F.-Y. Hung and I. Marsic, "Access delay analysis of IEEE 802.11 DCF in the presence of hidden stations," in *GLOBECOM*, 2007, pp. 2541–2545.

[67] K. Duffy and A. J. Ganesh, "Modeling the impact of buffering on 802.11," *IEEE Communications Letters*, vol. 11, pp. 219–221, 2007.

[68] B. Kalantari-Sabet, M. Mjeku, N. J. Gomes, and J. E. Mitchell, "Performance impairments in single-mode radio-over-fiber systems due to mac constraints," *J. Lightwave Technol.*, vol. 26, no. 15, pp. 2540–2548, Aug 2008.

[69] D. Moss, J. Hui, and K. Klues, "Low Power Listening, Core Working Group, TEP 105."

[70] M. T. Hansen, B. Kusy, R. Jurdak, and K. Langendoen, "Autosync: Automatic duty-cycle control for synchronous low-power listening," in *SECON*, 2012, pp. 139–147.

[71] O. Gnawali, R. Fonseca, K. Jamieson, D. Moss, and P. Levis, "Collection tree protocol," in *SenSys*, 2009, pp. 1–14.

[72] A. Nasipuri, R. Cox, J. Conrad, L. V. der Zel, B. Rodriguez, and R. McKosky, "Design considerations for a large-scale wireless sensor network for substation monitoring," in *LCN*, 2010, pp. 866–873.

[73] G. Zhou, C. Huang, T. Yan, T. He, J. A. Stankovic, and T. F. Abdelzaher, "MMSN: Multi-frequency media access control for wireless sensor networks," in *INFOCOM*, 2006.

[74] J. Zhang, G. Zhou, C. Huang, S. H. Son, and J. A. Stankovic, "TMMAC: An energy efficient multi-channel mac protocol for ad hoc networks," in *ICC*, 2007, pp. 3554–3561.

[75] X. Chen, P. Han, Q.-S. He, S. liang Tu, and Z. long Chen, "A multi-channel mac protocol for wireless sensor networks," in *CIT*, 2006.

[76] Y. Wu, J. A. Stankovic, T. He, and S. Lin, "Realistic and efficient multi-channel communications in wireless sensor networks," in *INFOCOM*, 2008, pp. 1193–1201.

[77] H. K. Le, D. Henriksson, and T. F. Abdelzaher, "A control theory approach to throughput optimization in multi-channel collection sensor networks," in *IPSN*, 2007, pp. 31–40.

[78] Q. Yu, J. Chen, Y. Fan, X. Shen, and Y. Sun, "Multi-channel assignment in wireless sensor networks: A game theoretic approach," in *INFOCOM*, 2010, pp. 1127–1135.

[79] R. Ramanathan and R. Hain, "Topology control of multihop wireless networks using transmit power adjustment," in *INFOCOM*, 2000, pp. 404–413.

[80] M. Kubisch, H. Karl, A. Wolisz, L. C. Zhong, and J. M. Rabaey, "Distributed algorithms for transmission power control in wireless sensor networks," in *WCNC*, 2003, pp. 558–563.

[81] T. A. ElBatt, S. V. Krishnamurthy, D. Connors, and S. K. Dao, "Power management for throughput enhancement in wireless ad-hoc networks," in *ICC*, 2000, pp. 1506–1513.

[82] D. Son, B. Krishnamachari, and J. S. Heidemann, "Experimental study of the effects of transmission power control and blacklisting in wireless sensor networks," in *SECON*, 2004, pp. 289–298.

[83] S. Lin, J. Zhang, G. Zhou, L. Gu, J. A. Stankovic, and T. He, "ATPC: adaptive transmission power control for wireless sensor networks," in *SenSys*, 2006, pp. 223–236.

[84] "MIB/MPR user manual," `http://www.xbow.com`.

[85] "Castalia: A Simulator for WSN," `http://castalia.npc.nicta.com.au/`.

[86] A. Pal and A. Nasipuri, "DRCS: A distributed routing and channel selection scheme for multi-channel wireless sensor networks," in *IEEE PerSeNS*, 2013, pp. 602–608.

[87] P. Basu and J. Redi, "Effect of overhearing transmissions on energy efficiency in dense sensor networks," in *IPSN*, 2004, pp. 196–204.

[88] W. Ye, J. S. Heidemann, and D. Estrin, "An energy-efficient mac protocol for wireless sensor networks," in *INFOCOM*, 2002.

[89] D. Moss and P. Levis, "BoX-MACs: Exploiting Physical and Link Layer Boundaries in Low-Power Networking," 2008.

[90] R. Jurdak, P. Baldi, and C. V. Lopes, "Adaptive low power listening for wireless sensor networks," *IEEE Trans. Mob. Comput.*, vol. 6, no. 8, pp. 988–1004, 2007.

[91] G. Anastasi, M. Conti, and M. D. Francesco, "Extending the lifetime of wireless sensor networks through adaptive sleep," *IEEE Trans. Industrial Informatics*, vol. 5, no. 3, pp. 351–365, 2009.

[92] Y. Fu, M. Sha, G. Hackmann, and C. Lu, "Practical control of transmission power for wireless sensor networks," in *ICNP*, 2012.

[93] J. L. Hill and D. E. Culler, "Mica: A wireless platform for deeply embedded networks," *IEEE Micro*, vol. 22, no. 6, pp. 12–24, 2002.

[94] A. El-Hoiydi, "Aloha with preamble sampling for sporadic traffic in ad hoc wireless sensor networks," in *ICC*, 2002, pp. 3418–3423.

[95] M. Bhardwaj, T. Garnett, and A. P. Chandrakasan, "Upper bounds on the lifetime of sensor networks," in *ICC*, 2001, pp. 785–790.

[96] C. Bettstetter, "On the minimum node degree and connectivity of a wireless multihop network," in *MobiHoc*, 2002, pp. 80–91.

APPENDIX A: DEPENDENT INTERFERERS AND PROBABILITY OF SUCCESS

In this section we address the issue of independence of transmissions from interferers in the set I. We show with an example that not all nodes located within the interference range of a test receiver cannot transmit independently. For instance, consider Figure A.1, where the test link $S \rightarrow D$ has seven active interferers, nodes 1, 2, 3, 4, 5, 6 and 7. Now, with the RTS/CTS option disabled, we can observe that when 1, 2, 6 and 7 transmit neither of 3, 4 and 5 transmit as they all can sense the transmissions of either 1 or 2 or 6 or 7. Thus, we say that the maximum number of independent interferers of D is four (1, 2, 6 and 7). Now, if we construct a graph where the vertices are the interfering nodes of D and there is an edge between two vertices if they are in the carrier sensing range of each others then the maximum number of independent interferers is the *maximum independent set (MIS)* of this graph.

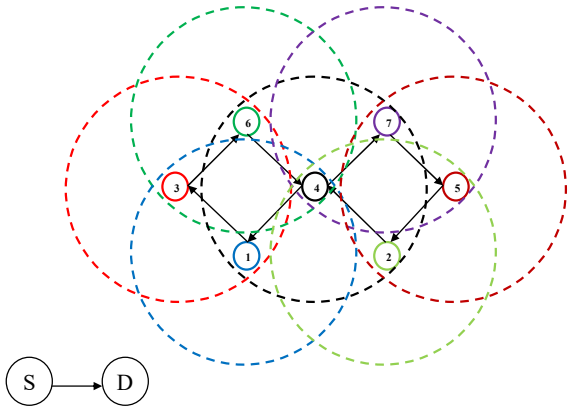

Figure A.1: Effect of dependent interferers on test link $S \rightarrow D$.

Suppose we want to solve the *maximum independent set (MIS)* problem. An independent set is a set of vertices in a graph such that no two vertices in the set are adjacent. A MIS is just an independent set containing the largest possible number of vertices. Maximum independent set is a well-known NP-complete problem. Let us assume a graph $G = (V, E)$, where V is the set of vertices and E is the set of edges. Let us also assume that there are n vertices $v_1, v_2, ..., v_n$ in V. For any two

vertices v_i and v_j, $v_i - v_j \in E$ if v_j is in the carrier sensing range of v_i and vice versa. Let $S^{max} \subset V$ is the MIS. For any $v_i \in V$, we define a binary variable x_{v_i} such that $x_{v_i} = 1$ if $v_i \in S^{max}$; otherwise $x_{v_i} = 0$. Thus the MIS problem can be written as in *Integer Linear Programming (ILP)* as follows:

$$Maximize \sum_{i=1}^{n} x_{v_i} \tag{A.1}$$

subject to

$$x_{v_i} + x_{v_j} \leq 1 \ (1 \leq i, j \leq n), (x_{v_i} - x_{v_j} \in E) \tag{A.2}$$

$$x_{v_i} \in \{0, 1\} \ (1 \leq i \leq n) \tag{A.3}$$

The first constraint states that no two adjacent vertices can be in S^{max} together. The second constraint states that x_{v_i} is binary.

Next we consider two different cases to calculate the POS in presence of dependent interferers.

Case 1: Let us first consider the case where all the interferers are within the carrier sensing range of each others, that is |MIS| = 1. Let us also define all the queues of the interferers as *interfering queues* and the server (channel) while serving these interferers are termed as *interfering server*. Thus for |MIS| = 1 all the N interferers make a M/D/1 queuing system with arrival rate of $N\lambda$. Thus the probability that the test link packet is successful is the probability that the interfering server is idle (say I is the idle time of the server) for at least the whole packet transmission time ($\frac{DLEN}{B}$). Now a queuing system always passes through alternating cycles of busy period and idle period as shown in Figure A.2. If δt is the interarrival time of packets and R is the residual time (time that the server takes to finish transmitting the previous

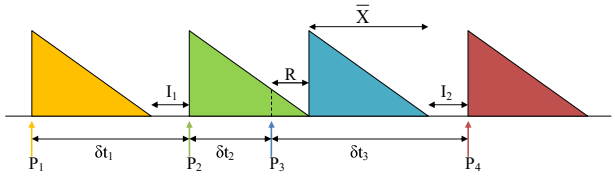

Figure A.2: Interarrival time (δt), residual time (R), service time ($\bar{X}$) and Idle periods (I) of a queuing system.

packet), then idle time I can be written as

$$\begin{aligned} I &= \delta t - R - \bar{X} \text{ if } \delta t > R + \bar{X} \\ &= 0 \text{ otherwise} \end{aligned} \tag{A.4}$$

$$\begin{aligned} &\text{Then } P[I > \tfrac{DLEN}{B}] \\ &= P[\delta t - R - \bar{X} > \tfrac{DLEN}{B}] \text{ if } \delta t > R + \bar{X} \\ &= 0 \text{ otherwise} \\ &= P[\delta t > R + \bar{X}] \times P[\delta t - R - \bar{X} > \tfrac{DLEN}{B} | \delta t > R + \bar{X}] \\ &= P[\delta t > R + \bar{X}] \times \tfrac{P[\delta t > \frac{DLEN}{B} + R + \bar{X} \text{ AND } \delta t > R + \bar{X}]}{P[\delta t > R + \bar{X}]} \\ &= P[\delta t > \tfrac{DLEN}{B} + R + \bar{X}] \end{aligned} \tag{A.5}$$

Thus POS can be written as

$$\begin{aligned} POS &= P[I > \frac{DLEN}{B}] = P[\delta t > \frac{DLEN}{B} + R + \bar{X}] \\ &= P[\delta t > 2\bar{X} + R] = e^{-N\lambda(2\bar{X}+R)} \\ &= e^{-N\lambda(2\bar{X} + \frac{N\lambda\bar{X}^2}{2})} = e^{-2N^e\lambda\bar{X}} \end{aligned} \tag{A.6}$$

where $N^e = N + \frac{\lambda\bar{X}N^2}{4}$ is the effective number of interferers, $R = \frac{\lambda\bar{X}^2}{2}$ and $\bar{X} = \frac{DLEN}{B}$.

We validate our analytical model by considering different combinations of interferers and compare with the simulation results which is shown in Figure A.4. *Case 2:* Now let us consider the case where not all interferers are in the carrier sensing ranges

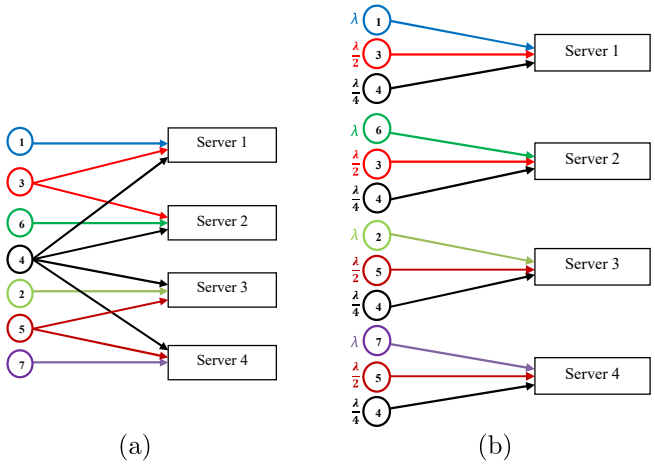

Figure A.3: (a) Queuing diagram (b) Our approximation.

of each other and they are not independent as well. One such scenario is depicted in Figure A.3(a) which is based on Figure A.1. In Figure A.1, 1 cannot transmit when 3 or 4 transmit, thus in Figure A.3(a) we show that 1 has to share the channel (server 1) with 3 and 4. Similarly, 6, 2 and 7 have to share the channel with (3, 4), (5, 4) and (5, 4) respectively.

Now, imagine the scenario where only 1, 2, 6 and 7 are active. This scenario can be modeled with 4 interfering servers each one gives service to λ packets/sec. Next, if 3, 4 and 5 come in picture, each one of 1, 2, 6 and 7 has to share their server (channel) with some of the nodes among 3, 4 and 5. In this scenario, as 3 shares the channel with 1 and 6, for approximation, we divide the load of 3 in two interfering servers with $\frac{\lambda}{2}$ packets/sec each in Figure A.3(b). Similarly 4 shares the channel with 1, 6, 2 and 7, thus the load of 4 is divided among the 4 interfering servers and the load of 5 is divided among server 3 and server 4. Then we calculate the POS as the probability that all interfering servers are idle for more than $\frac{DLEN}{B}$ period. In general if I_i is the idle time of server i then

$$POS = \prod_{i=1}^{S^{max}} P[I_i > \frac{DLEN}{B}] = \prod_{i=1}^{S^{max}} e^{-\lambda_i(2\bar{X}+\frac{\lambda_i \bar{X}^2}{2})}$$

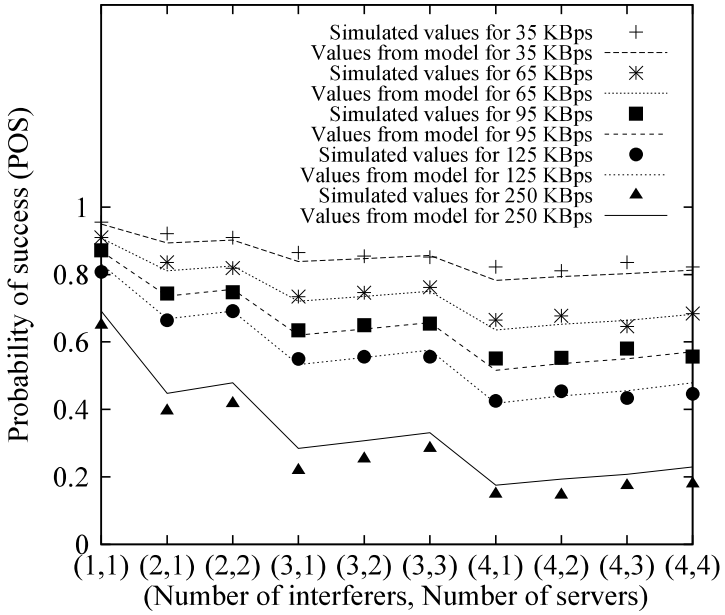

Figure A.4: POS in presence of dependent interferers around D: model and simulation results.

$$= \quad e^{-2N^e\lambda\bar{X}} \tag{A.7}$$

where λ_i is the total arrival rate in server i and $N^e = N + \frac{\bar{X}\sum{\lambda_i}^2}{4\lambda}$. This is to be noted that MIS is a NP-complete problem and the solution that we mention is just an approximation algorithm.

APPENDIX B: CALCULATION OF AVERAGE BACKOFF TIME FOR RADIO-OVER-FIBER WIRELESS LANS

Let us assume that $\bar{T}_B^i$ is the average backoff time at the i-th backoff stage, then

$$\begin{aligned} \bar{T}_B^i &= T\sum_{j=0}^{W_i-1} P\{U_i = j\}j = T\sum_{j=0}^{W_i-1}\frac{j}{W_i} \\ &= \frac{T(W_i-1)}{2} \end{aligned} \tag{B.1}$$

where U_i is a random variable with discrete uniform distribution. Now let us assume that the packet is transmitted successfully at the end of the k-th backoff slot. Then the backoff time is given by

$$\bar{T}_B(k) = \sum_{i=1}^{k}\bar{T}_B^i + (k-1)T_c \tag{B.2}$$

Let K is the discrete random variable of the number of backoff stages a station has to go through before transmitting a successful packet. Then the probability a packet takes k attempts is $Pr[K=k] = (1-p)p^{k-1}$. Then the average time spent for backoff $\bar{T}_B$ can be given by

$$\begin{aligned} \bar{T}_B &= E\{\bar{T}_B(k)\} = \textstyle\sum_{k=1}^{\infty}\bar{T}_B(k)P\{K=k\} \\ &= \textstyle\sum_{k=1}^{\infty}\left[\left(\sum_{i=1}^{k}\bar{T}_B^i\right) + (k-1)T_c\right]p^{k-1}(1-p) \\ &= \textstyle\sum_{k=1}^{\infty}\left[\left(\sum_{i=1}^{k}\frac{T(W_i-1)}{2}\right) + (k-1)T_c\right]p^{k-1}(1-p) \\ &= \textstyle\sum_{k=1}^{\infty}\left(\sum_{i=1}^{k}\frac{TW_i}{2}\right)p^{k-1}(1-p) - \frac{T}{2(1-p)} + \frac{p}{1-p}T_c \\ &= \frac{T\left(W_0\left[\frac{1-p-2^m p^{m+1}}{1-2p}\right]-1\right)}{2(1-p)} + \frac{p}{1-p}T_c \end{aligned}$$

APPENDIX C: THEORETICAL ANALYSIS OF THE DRCS SCHEME

In this chapter we give a detailed theoretical analysis of the DRCS scheme which shows that DRCS indeed results in reduced variances of the worst node's healths in each channel which ultimately results in network lifetime maximization. Let us consider the scenario where node A has n neighbors. We assume that the routes and transmit channels are chosen periodically with an interval of Δt. Next we calculate the variance of healths of the worst neighbors in each channel and calculate their variances at two time instance t and $t + \Delta t$, based on our proposed scheme.

If $Q = f(x, y)$ then the variance of Q can be approximated by

$$\sigma_Q^2 \approx \sigma_x^2 . \left(\frac{\partial Q}{\partial x}\right)^2 + \sigma_y^2 . \left(\frac{\partial Q}{\partial y}\right)^2 + 2. \left(\frac{\partial Q}{\partial x}\right) \left(\frac{\partial Q}{\partial y}\right) \sigma_{xy} \tag{C.1}$$

where σ_x^2, σ_y^2 are the variances of x and y respectively and σ_{xy} is the covariance of x and y. Thus if $Q = \frac{u}{v}$ then

$$\sigma_Q^2 = \frac{\mu_v^2 . \sigma_u^2 + \mu_u^2 . \sigma_v^2 - 2 . \mu_u . \mu_v . \sigma_{uv}}{\mu_v^4} \tag{C.2}$$

In the t-th time period, the health of the worst neighbor in the i-th channel is $\mathcal{H}_i(t) = \frac{B_i}{(O_i + C_i)\Delta t}$ where B_i is the residual capacity for node i and O_i is the overhearing traffic that nodes in the i-th channel experience from A in time period t. C_i is the current consumption for any event other than overhearing from A. We assume that the mean and variance of $B = \{B_i\}$, $O = \{O_i\}$ and $C = \{C_i\}$ are $\{\mu_B, \mu_O, \mu_C\}$ and $\{\sigma_B^2, \sigma_O^2, \sigma_C^2\}$ respectively. Assume that $Y(t) = \{O_i + C_i\}$, so $\sigma_{Y(t)}^2 = \sigma_O^2 + \sigma_C^2$. Then the variance of healths of worst neighbors in each channel at time t is $\sigma^2(t) = \frac{\mu_B^2 . \sigma_{Y(t)}^2 + \mu_{Y(t)}^2 . \sigma_B^2}{\mu_{Y(t)}^4}$ as the covariance $\sigma_{RY(t)} = 0$.

Now we find the variance of healths at time $t + \Delta t$. At time instance $t + \Delta t$, the channel i is chosen with a probability of $p_i = \frac{\mathcal{H}_i}{\mathcal{H}} = \frac{B_i}{(O_i + C_i).\mathcal{H}}$ where $\mathcal{H} = \sum \mathcal{H}_i$ of

all channels. If node A chooses channel c, then all neighbors that are in channel c overhears the transmissions. Let us assume that these neighbors consume K unit of current in unit time for overhearing from A. Then the health of the worst neighbor in the i-th channel at time $t+\Delta t$ is $\mathcal{H}_i(t+\Delta t) = \frac{B_i}{(p_i.K.\Delta t + C_i)\Delta t} = \frac{B_i}{\left(\frac{B_i.K.\Delta t}{(O_i+C_i).\mathcal{H}} + C_i\right)\Delta t}$. We assume that $R(t+\Delta t) = \{B_i\}$ and $Y(t+\Delta t) = \left\{\left(\frac{B_i.K.\Delta t}{(O_i+C_i).\mathcal{H}} + C_i\right)\Delta t\right\}$. This is clear that $\mu_Y(t) = \mu_Y(t+\Delta t)$ and $\mu_O = E[S] = \mu_S$ where $S = \left\{\frac{B_i.K.\Delta t}{\mathcal{H}(O_i+C_i)}\right\}$. Now let us first calculate the variance of $Y(t+\Delta t)$ as follows

$$\begin{aligned}
\sigma^2_{Y(t+\Delta t)} &= \sigma^2_C + \sigma^2_S + 2.\sigma_{CS} \\
&< \sigma^2_C + \sigma^2_S \text{ as covariance is negative} \\
&= \sigma^2_C + E[S^2] - \mu^2_S = \sigma^2_C + E[S^2] - \mu^2_O \\
&= \sigma^2_C + \sigma^2_O + E[S^2] - E[O^2] \qquad \text{(C.3)}
\end{aligned}$$

Then $\sigma^2_{Y(t+\Delta t)} < \sigma^2_{Y(t)}$ if

$$E[S^2] < E[O^2] \rightarrow \Delta t < \sqrt{\frac{E[O^2]}{E[T^2]}}.\frac{K}{\mathcal{H}} \text{ where } T = \left\{\frac{B_i}{O_i+C_i}\right\} \qquad \text{(C.4)}$$

When $\sigma^2_{Y(t+\Delta t)} < \sigma^2_{Y(t)}$

$$\begin{aligned}
&\sigma^2(t+\Delta t) \\
&= \frac{\mu^2_B.\sigma^2_{Y(t+\Delta t)} + \mu^2_{Y(t+\Delta t)}.\sigma^2_B - 2.\mu_B.\mu_{Y(t+\Delta t)}.\sigma_{R,Y(t+\Delta t)}}{\mu^4_{Y(t+\Delta t)}} \\
&< \frac{\mu^2_B.\sigma^2_{Y(t+\Delta t)} + \mu^2_{Y(t+\Delta t)}.\sigma^2_B}{\mu^4_{Y(t+\Delta t)}} \text{ as covariance is positive} \\
&= \frac{\mu^2_B.\sigma^2_{Y(t+\Delta t)} + \mu^2_{Y(t)}.\sigma^2_B}{\mu^4_{Y(t)}} \\
&< \frac{\mu^2_B.\sigma^2_{Y(t)} + \mu^2_{Y(t)}.\sigma^2_B}{\mu^4_{Y(t)}} < \sigma^2(t)
\end{aligned} \qquad \text{(C.5)}$$

Thus in the proposed scheme each node tries to reduce the variances of healths of the worst nodes in each channel in its neighborhood when the time interval Δt is small. As the variances become smaller in each interval, the healths become similar i.e. the nodes will die at the same time which increases the overall network lifetime.

PUBLICATIONS

1. **Amitangshu Pal** and Asis Nasipuri, "PCOR: A Joint Power Control and Routing Scheme for Rechargeable Sensor Networks". Submitted In *IEEE WCNC 2014*.

2. **Amitangshu Pal** and Asis Nasipuri, "Lifetime of Asynchronous Wireless Sensor Networks with Multiple Channels and Power Control". Submitted In *IEEE WCNC 2014*.

3. **Amitangshu Pal** and Asis Nasipuri, "Effects of Optical Network Unit Placement Schemes for Multi-Channel Hybrid Wireless-Optical Broadband-Access Networks", Accepted In *IWON 2013*, Atlanta, GA, USA.

4. **Amitangshu Pal** and Asis Nasipuri, "DRCS: A Distributed Routing and Channel Selection Scheme for Multi-Channel Wireless Sensor Networks", In *IEEE PerSeNS 2013*, pp. 602-608, San Diego, California, USA.

5. **Amitangshu Pal**, Anthony Harris, Jason Anderson, Asis Nasipuri, Robert Cox, and James Conrad, "EPIC-RoofNet: An Experimental Testbed for Solar-powered Wireless Sensor Networks", Technical report, The University of North Carolina at Charlotte, ECE Department, July 2013.

6. **Amitangshu Pal**, Bonee Soibam and Asis Nasipuri, "A Distributed Power Control and Routing Scheme for Rechargeable Sensor Networks", In *IEEE SoutheastCon 2013*, Jacksonville, Florida, USA.

7. Ndubueze Chuku, **Amitangshu Pal** and Asis Nasipuri, "An RSSI Based Localization Scheme for Wireless Sensor Networks to Mitigate Shadowing Effects", In *IEEE SoutheastCon 2013*, Jacksonville, Florida, USA.

8. **Amitangshu Pal** and Asis Nasipuri, "A Distributed Channel Selection Scheme for Multi-Channel Wireless Sensor Networks", In *Proc. ACM MobiHoc 2012*, pp. 263-264, Hilton Head Island, SC, USA.

9. **Amitangshu Pal** and Asis Nasipuri, "Maximum-lifetime multi-channel routing in wireless sensor networks", Technical report, The University of North Carolina at Charlotte, ECE Department, September 2012.

10. **Amitangshu Pal** and Asis Nasipuri, "JRCA: A Joint Routing and Channel Assignment Scheme for Wireless Mesh Networks", In *Proc. IEEE IPCCC 2011*, Orlando, Florida, USA.

11. **Amitangshu Pal** and Asis Nasipuri, "Performance Analysis of IEEE 802.11 Distributed Coordination Function in Presence of Hidden Stations under Non-saturated Conditions with Infinite Buffer in Radio-over-Fiber Wireless LANs", In *Proc. IEEE LANMAN 2011*, Chapel Hill, NC, USA.

12. **Amitangshu Pal** and Asis Nasipuri, "A Quality Based Routing Protocol for Wireless Mesh Networks", *Elsevier Pervasive and Mobile Computing*, Vol. 7, No. 5, pp 611-626, 2011.

13. **Amitangshu Pal** and Asis Nasipuri, "GSQAR: A Quality Aware Anycast Routing Protocol for Wireless Mesh Networks", In *Proc. IEEE Globecom 2010*, Miami, Florida, USA.

14. **Amitangshu Pal** and Asis Nasipuri, "A Quality Aware Anycast Routing Protocol for Wireless Mesh Networks", In *Proc. IEEE SoutheastCon 2010*, pp. 451-454, Charlotte, NC, USA.

15. **Amitangshu Pal**, Sandeep Adimadhyam and Asis Nasipuri, "QoSBR: A Quality Based Routing Protocol for Wireless Mesh Networks", In *Proc. ICDCN 2010*, pp. 497-508, Kolkata, India.